WAVE PROPAGATION IN NONLINEAR PERIODIC STRUCTURES

A Dissertation
Presented to
The Academic Faculty

by

Raj K. Narisetti

In Partial Fulfillment
of the Requirements for the Degree
Doctor of Philosophy in the
School of Aerospace Engineering

Georgia Institute of Technology
December, 2010.

WAVE PROPAGATION IN NONLINEAR PERIODIC STRUCTURES

Approved by:

Dr. Massimo Ruzzene, Advisor
School of Aerospace Engineering
Georgia Institute of Technology

Dr. Aldo A. Ferri
School of Mechanical Engineering
Georgia Institute of Technology

Dr. Michael J. Leamy, Co-advisor
School of Mechanical Engineering
Georgia Institute of Technology

Dr. Timothy C. Lieuwen
School of Aerospace Engineering
Georgia Institute of Technology

Dr. Olivier A. Bauchau
School of Aerospace Engineering
Georgia Institute of Technology

Date Approved: 12-02-2010

To my beautiful fiancé, Harini

and especially to my family

ACKNOWLEDGEMENTS

I would like to express my deepest appreciation to my advisor, Dr. Massimo Ruzzene for guiding, supporting and encouraging me throughout the doctoral study, which is my greatest academic achievement. I would like to thank him for his unconditional availability and scientific inputs for every step in the research. Without his guidance and persistent help this dissertation would not have been possible. I am grateful for his efforts in providing me with opportunities to present and participate at various conferences where I gained great scientific exposure and knowledge.

I am also exceedingly grateful to Dr. Michael Leamy for his immeasurable support and technical guidance towards the research. His research inputs and advice throughout my graduate school have made this work possible. I deeply appreciate his time and patience for numerous technical discussions which led to accomplish major milestones in my research. I would also like to thank Dr. Erian Armanios who first motivated me to pursue doctoral study after my masters.

I would like to deeply thank my dad, Mr. Devaraja Kumar Narisetti for his support, patience and love during the strenuous graduate school and without him I would have never been here in the first place. I am very grateful to my family, my mother Surapaneni Santhi Sree, my brother Taran Kumar Narisetti and my grandmother Kanyakumari Narisetti for their unconditional love and encouragement. The next dearest person whom I owe my achievements is my fiancé, Harini Kondamudi, whose emotional support and love throughout my graduate life made me get through the difficult times.

I would also like to thank my best friends Sharath Gudla, Varun Nare, Srikanth Goruganthu, Praveen Pasupuleti, Jaiprakash Nanna, Suneel Reddy and Dr. Irfan Khan for their support and help in many ways throughout my graduate life. I am thankful to my pal Dr. Vishwanath Natarajan with whom I had many technical and research discussions

during recent years. I also would like to express my thanks to labmates Matteo Sinesi, Dr. Giorgio Calanni, Ritu Marpu, Maria Chierichetti, Filippo Casadei, Dr. James Ayers, Akash Dixit, Luca Airoldi and Dr. Samer Tawfik with whom I had memorable times during the doctoral study.

Finally, I am grateful to all the Thesis committee members Dr. Aldo Ferri, Dr. Olivier Bauchau and Dr. Tim Lieuwen for their time and insightful thoughts which were invaluable for the completion of this thesis.

TABLE OF CONTENTS

LIST OF TABLES

LIST OF FIGURES

SUMMARY

A periodic structure consists of spatially repeating unit cells. From man-made multi-span bridges to naturally occurring atomic lattices, periodic structures are ubiquitous. The periodicity can be exploited to generate frequency bands within which elastic wave propagation is impeded. A limitation to the linear periodic structure is that the filtering properties depend only on the structural design and periodicity which implies that the dispersion characteristics are fixed unless the overall structure or the periodicity is altered.

The current research focuses on wave propagation in nonlinear periodic structures to explore tunability in filtering properties such as bandgaps, cut-off frequencies and response directionality. The first part of the research documents amplitude-dependent dispersion properties of weakly nonlinear periodic media through a general perturbation approach. The perturbation approach allows closed-form estimation of the effects of weak nonlinearities on wave propagation. Variation in bandstructure and bandgaps lead to tunable filtering and directional behavior. The latter is due to anisotropy in nonlinear interaction that generates low response regions, or "dead zones," within the structure.

The general perturbation approach developed has also been applied to evaluate dispersion in a complex nonlinear periodic structure which is discretized using Finite Elements. The second part of the research focuses on wave dispersion in strongly nonlinear periodic structures which includes pre-compressed granular media as an example. Plane wave dispersion is studied through the harmonic balance method and it is shown that the cut-off frequencies and bandgaps vary significantly with wave amplitude. Acoustic wave beaming phenomenon is also observed in pre-compressed two-dimensional hexagonally packed granular media. Numerical simulations of wave

propagation in finite lattices also demonstrated amplitude-dependent bandstructures and directional behavior so far observed.

CHAPTER I

INTRODUCTION

1.1 OVERVIEW

The present research focuses on the wave propagation in nonlinear periodic structures to explore tunable filtering properties. The following section first introduces the periodic structures along with some definitions and examples. Next, the filtering properties such as bandgaps, propagation and attenuation properties are described along with the literature review on the analysis and applications of periodic structures based on linear models. Wave filtering properties of periodic structures enable them to act as mechanical band-pass filters, vibration isolators, wave-guides and resonators. Although a number of interesting wave properties are exhibited by linear periodic media, the existence of complex wave phenomenon such as solitary wave, discrete breathers, wave localization motivated the study of wave propagation in nonlinear periodic media. The present research classifies the nonlinear periodic structures into *weakly* and *strongly* nonlinear based on the strength of nonlinearity. Next, the literature review and the analysis of weakly nonlinear periodic structures followed by the background study and properties of strongly nonlinear periodic media are presented. Research studies on tunable periodic structures are also mentioned and the motivations for the present research are detailed. Research objectives and the contributions of the present work to the existing knowledge on wave propagation in nonlinear periodic media are highlighted and finally, the chapter concludes with the organization of the present research.

1.2 PERIODIC STRUCTURES

A periodic structure consists of a number of identical structural elements, also termed as periodic elements, which are joined together end-to-end and/or side-to-side to form the whole structure. Periodic structures can be man-made and can exist naturally at a wide range of length-scales. Examples range from the lumped parameter systems with discrete masses such as atomic lattices of pure crystals in which atoms are held together by inter-atomic elastic forces to the engineering structures such as multi-storey buildings, stiffened plates and shells, multi-span bridges, multi-layer composites, etc… (Figure 1).

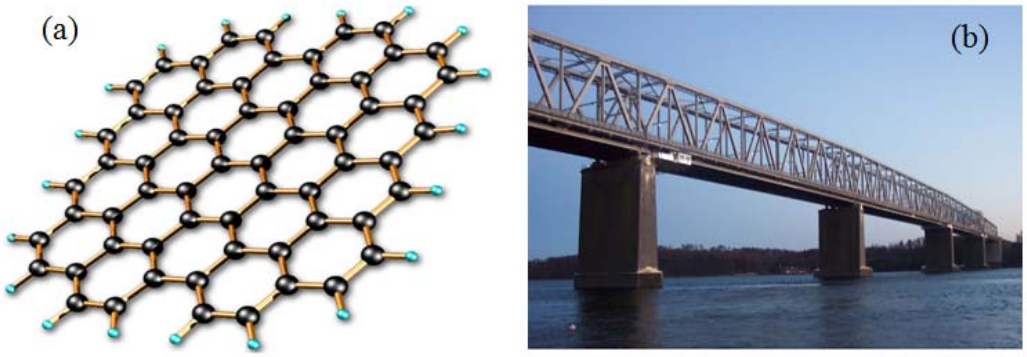

Figure 1: (a) Graphene sheet - A two dimensional hexagonal periodic lattice at molecular level (b) Truss bridge - A periodic structure at macro level

Throughout the life of the structure, a wide range and variety of time-dependent forces acting on these structures generate vibrations whose levels should be controlled to prevent any catastrophic damage. For some applications, response amplitude can be an important criterion but for others, it can be energy transmission from source to the point of interest. Depending on the design of the unit cell, structural periodicity can be exploited to generate frequency bands in which elastic waves do not propagate through the structure thus enabling periodic structures to act as wave-guides, vibration isolators and resonators.

1.3 FILTERING PROPERTIES OF PERIODIC STRUCTURES

The structural design of the periodic element or the unit cell which forms the periodic structure determines the filtering properties exhibited by the structure. The frequency band in which the structure allows the waves to propagate is called *propagation zone* (PZ) and the frequency range within which the wave attenuates and propagation ceases to exist is defined as *attenuation zone* (AZ). The attenuation generated in AZ is not due to the presence of any dissipation in the structure but due to the internal reflection of waves caused by the periodicity. The frequency range between two PZs in which waves do not propagate can be termed as a *bandgap* [1]. Figure 2a shows a periodic structure formed by hollow metal tubes which exhibits a sonic band gap at a frequency 1.67 KHz as demonstrated by the sound attenuation diagram (Figure 2b) [2].

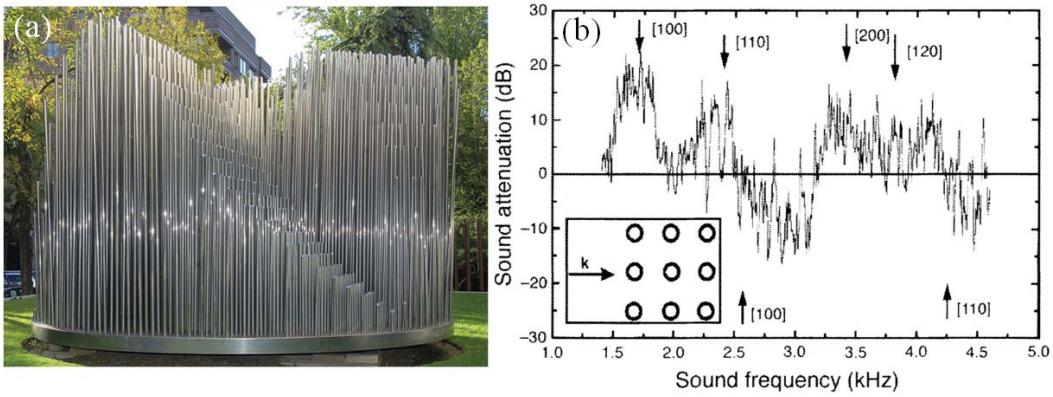

Figure 2: (a) Periodic structure formed by hollow metal tubes and air (b) Sound attenuation exhibited by structure as the first peak at 1.67 KHz corresponds to maximum attenuation of sound (sonic band gap) [2]

Lord Rayleigh first demonstrated the existence of such frequency bands in periodic structures in which the wave solutions do not exist [3]. Brillouin [1] detailed the historical background and motivation behind the study and analysis of wave propagation in periodic structures. References [4] and [5] provide a comprehensive study on the methods and techniques to investigate continuous periodic structures. As discussed

therein, a number of techniques exist for introducing bandgaps, such as strategically placed periodic inclusions and geometric discontinuities. Depending on the inclusions, geometry, and elastic properties, one can design for specific bandgaps [6]. Response to harmonic excitations determines the vibration characteristics of the structure and from a structural optimization standpoint, if there exists a control over mass distribution in a structure, a periodic structure forms the solution to an optimization problem where vibration transmission is minimal for a given frequency [7]. The periodicity and mass distribution is such that the frequency of vibration would fall into the bandgap of the formed periodic structure. Wave filtering properties such as bandgaps allow periodic structures to behave as acoustic filters, wave guides and resonators. For example, Figure 3 shows a z-shaped wave guide formed by a periodic structure. The rest of the structure without z-channel is designed such that the frequency of vibration falls into the bandgap but the same frequency is within the propagation zone of the structure which forms the z-channel. Hence, a wave guide allows the vibration energy to be transferred from one point to other depending on the design of the guide.

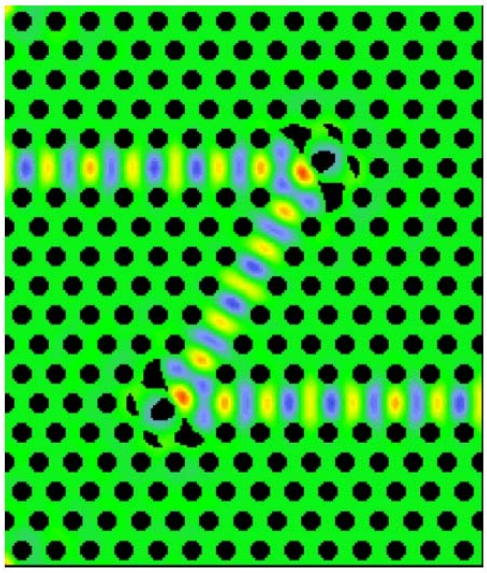

Figure 3: Wave propagation in a z-shaped wave guide formed by periodic structure

The current research on periodic structures focuses on the theoretical predictions and experimental estimation of bandgaps. The piling dimension also plays an important role in characterizing a periodic structure. A number of structures can be considered as one-dimensional [8]. Experimental and theoretical analysis of band gap in a string mass chain has been documented in [9] where authors apply normal-mode and pulse analysis to determine eigenfrequencies of the chain. Diez *et.al* [10] report experimental study of acoustic stopband in one-dimensional grating fabricated on an optical fiber. Closed form wave solutions using transfer matrix approach in finite one-dimensional *locally periodic* structures (structure where the periodic elements exist within a finite domain of the structure but do not repeat continuously to form the whole structure) has been reported in [11].

Analysis of wave propagation in two- and three-dimensional periodic structures is also documented by Brillouin [1]. There exist a number of techniques to study dispersion in two- and three-dimensional periodic structures such as finite elements (FEM) [12] in which authors utilize unit cell meshing and Bloch-Floquet boundary conditions. Other works e.g. Refs [13, 14] also have demonstrated the application of finite elements to predict wave propagation in periodic media. Other approximate methods such as Galerkin's method [15, 16] and computational techniques such as related Rayleigh theory [17], plane wave expansion [18] and multiple scattering method [19, 20] have also been applied to predict the gaps in elastic band structures. Apart from bandgaps, spatial filtering and wave directional properties are also important characteristics of periodic structures. For example, Ruzzene et al. [21] examine wave propagation in cellular structures and illustrated the wave beaming phenomenon, whereby propagation is limited to certain directions within the lattice. Similarly the spatial filtering of two dimensional, reticulated cellular structures such as triangular, square, hexagonal and Kagomé lattices is documented in [22]. Periodic inclusion of auxetic honeycomb structures are proposed as an effective way to generate impedance mismatch sufficient to stop the waves to

propagate in sandwich beams and plates in [23]. Kohrs and Petersson [24] document wave beaming in lightweight plates with truss-like cores with periodicity in one direction. Langley [25] studied the response of a linear two-dimensional periodic structure subject to point harmonic forcing using a spring mass model. Spring mass models provide a convenient setting for visualizing and modeling periodic structures which can easily include nonlinearities, damping and imperfections and the same time qualitatively capture wave phenomenon [26]. Low response regions or *dead zones* appear if the excitation frequency is within a frequency band, termed as *caustic band* [25]. The frequency range for caustics to appear depends on non-isotropic mass and stiffness properties. Caustics are responsible for wave beaming phenomenon as the vibratory response within a caustic band of a structure is in general characterized by the directions with very low response and directions with very high response. The associated low response regions suggest that the structure can be designed to act as a spatial filter through a combination of stop bands and wave directionality. Later, Langley and Bardell [27] investigated wave beaming phenomenon in a complex two-dimensional periodic structure, such as a beam grillage. The finite element method is employed to predict the response theoretically and the results are verified experimentally.

The aforementioned research on the wave propagation in periodic structures is primarily based on linear structural models. Although periodic structures under the assumption of linearity possess a range of interesting wave propagation properties, nonlinear periodic structures due to their inherent complexity may exhibit rich wave transmission properties which can be exploited for the design of novel devices based on the concept of periodic structure.

1.4 NONLINEAR PERIODIC STRUCTURES

A number of physical systems arising in different scientific areas such as optics, crystallography, chemistry and mechanics can be modeled as periodic chains. The

literature on wave propagation in nonlinear periodic media is sparse and as most of the structures are inherently nonlinear and it is important to investigate the effect of such nonlinearities on the wave propagation characteristics such as wave speed, cut-off frequencies etc… Depending on the strength of nonlinearity, the relevant literature can be classified as investigating *weakly* and *strongly* nonlinear periodic structures. Magnitude of nonlinearity plays an important role in determining the kind of solutions the structure would support. From the analysis standpoint, the approach to solving dispersion in weakly nonlinear systems can be significantly different from that of strongly nonlinear systems.

1.4.1 WEAKLY NONLINEAR PERIODIC STRUCTURES

A periodic structure can be inherently nonlinear due to the nature of interaction of a periodic element with its neighboring ones. In some cases, the nonlinear restoring forces are of an order of magnitude less than the linear restoring forces and the system can be formulated as a weakly nonlinear system. For example, a strongly nonlinear system such as simple pendulum acting under gravity can be modeled as a weakly nonlinear problem near the state of equilibrium [28]. Several perturbation techniques have been applied for predicting wave propagation in weakly nonlinear *continuous* systems, as detailed in standard texts on nonlinear vibration theory [28]. However, *discrete* nonlinear systems have received far less attention. In the engineering literature concerning the subject, most researchers replace the discrete system with a continuous one, implying that the studied wavelengths are much larger than the repeating periodic unit. Although this assumption is reasonable for studying lattice vibrations where the element length is far less than the wavelength, mechanical structures often are too large to be considered as a continuum. Vakakis and King [29] studied an infinite chain of mono-coupled nonlinear oscillators by invoking a continuum approximation and then employing a multiple-scales analytical technique. For waves in the attenuation zone, which are assumed to have synchronous motion, the concept of a “nonlinear normal mode” is applied to examine the response and

to show that the bounding frequencies are amplitude-dependent. Similar to the idea of linear mode, the concept of nonlinear normal mode (NNM) was first developed by Rosenberg [30] for conservative and symmetric nonlinearities. Later the concept was applied to study vibrations in nonlinear structural dynamical problems [31] and a comprehensive review of the research in this area is detailed by Vakakis [32].

Chakraborty and Mallik [33] applied a perturbation analysis to find the bounding frequencies for harmonic waves in a weakly nonlinear mono-atomic cubic chain. They showed that the limiting frequencies can be derived by studying a single nonlinear element. Interactions of harmonic waves in a semi-infinite chain, nonlinear modes, and natural frequencies of finite chain and cyclic chains were also presented. Other studies have employed analysis methods not requiring perturbation. For example, the "nonlinear mapping technique" has been used to determine the pass bands in a discrete chain of nonlinear Hamiltonian oscillators [34]. A nonlinear transformation matrix is found in terms of the amplitude and nonlinearity parameters, and a linear stability analysis of its period-q orbit Jacobian leads to the system dispersion relations. In another study [35], a one-dimensional periodic chain with attached nonlinear pendulums has been examined using an invariant manifold approach. The authors demonstrate that this weakly nonlinear periodic system contains an invariant manifold capturing slow dynamics, while fast dynamics appear as slow-manifold perturbations. For weak coupling, it is shown that nonlinear traveling and attenuating waves exist in this slow invariant manifold, allowing the wave dispersion to be approximated analytically. Localization and solitary wave phenomenon is also observed in weakly nonlinear periodic structures [36].

Filtering properties of a linear periodic chain with attached nonlinear damped oscillators have also been investigated using the harmonic balance method [37]. Bandgaps are generated around the resonant frequencies of the attached mass-damper systems. The researchers document low-frequency bandgaps which depend on displacement amplitude and nonlinearity.

1.4.2 STRONGLY NONLINEAR PERIODIC STRUCTURES

A number of physical systems such as Hertzian chains are strongly nonlinear periodic media and there exist a number of different wave phenomena such as solitary waves and solitons [38], response localization and other chaotic responses that are supported by strongly nonlinear periodic structures. Sievers and Takeno [39] report localization phenomenon occurring in a pure anharmonic lattice. The localized mode properties are shown to be equivalent to the localized mode of a defective harmonic lattice. Vakakis, King and Pearlstein [40] show that localization occurs in a periodic system with weakly coupled or strongly nonlinear oscillators. During localization, response is confined to a limited sub-domain while the remainder of the system domain oscillates with relatively low amplitudes. The authors also demonstrate that the localized modes are weak if the interaction is weak and the modes get stronger (high amplitude) if the nonlinear interaction is strong.

Strongly nonlinear periodic structures such as uncompressed granular media admit solitary wave propagation [41]. Daraio and Nesterenko et al. [42] demonstrated experimentally that one-dimensional nonlinear phononic crystals formed by chains of viscoelastic PTFE (polytetrafluoroethylene) as well as elastic (stainless-steel) beads exhibit significant wave speed tunability by varying the induced preload. Significant work has been reported in literature that demonstrates unique wave transmission properties and the response of two-dimensional strongly nonlinear periodic lattices. For example, Alejandro [43] demonstrated light beam localization and trapping in nonlinear two-dimensional periodic waveguide via defect modes. Similarly, Feng and Kawahara [44] report the properties of spatial localization (discrete breathers) in two dimensional nonlinear structures modeled as FPU (Fermi-Pasta-Ulam) and DNLS (Discrete NonLinear Schrödinger) lattices. Sreelatha and Joseph [45] have shown solitary wave solutions existing in a two-dimensional nonlinear lattice characterized by weak quadratic and cubic stiffness properties. W. Duan et al. [46] report dispersion of harmonic wave in

a continuous nonlinear two-dimensional lattice. Using a Taylor series expansion and a simple perturbation in displacement, they obtain dispersion relations as well as coupled Korteweg de Vries (KdV) equations. For a symmetric case, three different solitons are shown to exist and dispersion properties resulting from various inter-mass potentials such as Toda, Morse and LJ are investigated. It is evident that a nonlinear periodic structure depending on its physical and structural properties is capable of supporting multiple wave solutions, but the present thesis focuses on analyzing the influence of nonlinearity and wave amplitude on the dispersion properties of plane waves in a periodic structure.

1.5 TUNABLE PERIODIC STRUCTURES

A major limitation of a linear periodic structure is that the filtering properties depend only on the structural design and the periodicity which implies that the dispersion characteristics are fixed unless the overall structure or the periodicity is altered. For example, Goffaux and Vigneron [47] controlled phononic bandgaps by altering the geometry of the system. A particular case of a set of parallel solid square-section columns distributed in air on a square lattice is considered and it is shown that the rotation of the columns altered the bandstructure by modifying bandgap widths. Yeh [48] demonstrated tunable bandgaps by application of electrorheological material, defined as the material whose physical properties depend on the applied electric field. Therefore by varying the applied electric field, the phononic crystal exhibited tunability in the bandgaps. Robillard *et.al* [49] applied magnetostrictive materials to achieve contactless control over phononic bandgaps by varying the applied magnetic field. The authors demonstrated a transmission switch as an example application based on the tunability in filtering properties of the magneto-elastic periodic structure. In the research mentioned above, the physical parameters of the periodic structure have been modified through external sources of control such as application of magnetic or electric fields to achieve tunability in bandstructure. One of the major motivations behind the present research is to explore if

tunability of dispersion properties can be achieved through the influence of nonlinearity in periodic structures.

1.6 MOTIVATIONS

- ◊ One of the major motivations of the research is to examine the wave propagation in a periodic structure whose dynamics are governed by nonlinear force interaction. The effect of nonlinearities could play an important role in determining the wave propagation characteristics.
- ◊ To explore the dependence of wave amplitude on the dispersion properties: Depending on how the force interaction varies according to the element displacement the wave propagation properties could significantly be affected by the wave amplitude.
- ◊ By exploiting the influence of nonlinear dynamics on propagation characteristics, is it possible to affect the filtering properties of a periodic structure such as controlling bandgaps and cutoff frequencies.
- ◊ With the influence of nonlinearities and wave amplitude, would it also be possible to explore tunable response of periodic structure and achieve control over wave directional behavior and focusing capabilities?

1.7 RESEARCH OBJECTIVES

Given the motivations above, the objectives of the thesis are:

1) To evaluate the influence of nonlinearity and wave amplitude on the dispersion properties
2) To examine the effect of nonlinearity on the bandstructures exhibited by the periodic structures
3) To explore tunable filtering through bandgaps and response directionality

To accomplish the objectives, the work first employs analytical methods such as perturbation analysis and harmonic balance methods to treat nonlinear systems in obtaining approximate closed-form dispersion relationships. Next, numerical analysis is followed to validate the analytical predictions using numerical integration techniques.

1.8 RESEARCH CONTRIBUTIONS

Achievement of the objectives mentioned above led to the following original contributions in this work:

- ◊ A novel perturbation methodology which handles an infinite set of difference equations eliminating the need to replace discrete setting with continuous one;
- ◊ An asymptotic approach to analyze the wave propagation in discrete weakly nonlinear periodic structures which allows for a solution of higher-order dispersion relationships;
- ◊ Determination of closed form analytical expressions of dispersion relations for weakly nonlinear periodic lattices;
- ◊ Prediction of amplitude-dependent bandgaps and tunable wave directional behavior in two-dimensional nonlinear periodic structures;
- ◊ Demonstrating significant shift in cut-off frequencies with respect to the wave amplitude exhibited by strongly nonlinear granular chains using harmonic balance method;
- ◊ Acoustic wave beaming phenomenon in two-dimensional hexagonal granular packing;

1.9 ORGANIZATION OF THE WORK

Analytical tools such as linear dispersion analysis, perturbation approach and harmonic balance technique to evaluate the dispersion in nonlinear periodic lattices is presented in Chapter 2. The chapter introduces a general arrangement of the nonlinear periodic

structure for which the analytical tools can be applied. Using a general perturbation approach, Chapter 3 details the dispersion properties of the one-dimensional weakly nonlinear chains. The analysis is extended to propose the application to conceptual devices exploiting depicting tunable filtering properties. Chapter 4 documents the dispersion analysis of two-dimensional weakly nonlinear lattices. Band structures of some example lattices are detailed and group-velocity analysis is presented to predict amplitude-dependent wave directionality. The response of finite nonlinear lattice is also evaluated through numerical integration of equations of motion to validate the analytical predictions. Chapter 5 presents the application of perturbation approach to a more complex weakly nonlinear periodic structure which is discretized using Finite Elements to predict amplitude dependent band diagrams. Chapter 6 details the application of the harmonic balance method to evaluate the dispersion of strongly nonlinear periodic structures. The chapter focuses on both one-dimensional and two-dimensional granular media in which the nonlinearity is due to the geometry of contacting granules. Future work and opportunities for subsequent research are proposed in Chapter 7.

CHAPTER II

DISPERSION ANALYSIS OF PERIODIC STRUCTURES

2.1 OVERVIEW

The present chapter details the analytical tools necessary to predict the dispersion in periodic lattices. First, the geometry of a general two-dimensional periodic lattice is described. Linear dispersion analysis is presented next and some of the tools presented in this section are utilized to analyze nonlinear problem. A perturbation approach to predict the dispersion in weakly nonlinear periodic structures is detailed. Next, the harmonic balance method is presented to estimate dispersion in strongly nonlinear periodic structures along with an algorithm for numerical implementation.

2.2 GEOMETRY DESCRIPTION

Consider a two-dimensional (2D) lattice consisting of the periodic arrangement of identical unit cells assembled to cover a portion of the x_1, x_2 plane. In this work, the unit cells feature lumped masses interacting through linear restoring forces. The analysis approach presented in what follows however applies to a general domain discretized through a Finite Element scheme, whose behavior is described in terms of mass and stiffness matrices, and of vectors of interaction forces. Although a 2D formulation is presented in the analysis, the theory can be easily applied to 1D system as a particular case.

The periodicity of the lattice is defined by the primitive lattice vectors $\mathbf{a}_1$ and $\mathbf{a}_2$ which form the basis for the periodic lattice. The position of the i^{th} mass of the unit cell at location n_1, n_2 can be expressed as follows,

$$\mathbf{r}_{n_1,n_2}^{(i)} = \mathbf{r}_i + \mathbf{r}_{n_1,n_2}, \tag{2.1}$$

where $\mathbf{r}_{n_1,n_2}^{(i)}, \mathbf{r}_i$ respectively define the location of the mass in the global coordinate system x_1, x_2, and in a local frame of reference on the cell under consideration (Figure 4)). Local and global coordinates are related by the vector,

$$\mathbf{r}_{\boldsymbol{n_1,n_2}} = n_1\mathbf{a_1} + n_2\mathbf{a_2} \tag{2.2}$$

which defines the location of the unit cell through the integer pair n_1, n_2. In here and in the following the notation utilizes lower case, bold letters for vectors, and capitalized bold letter for matrices.

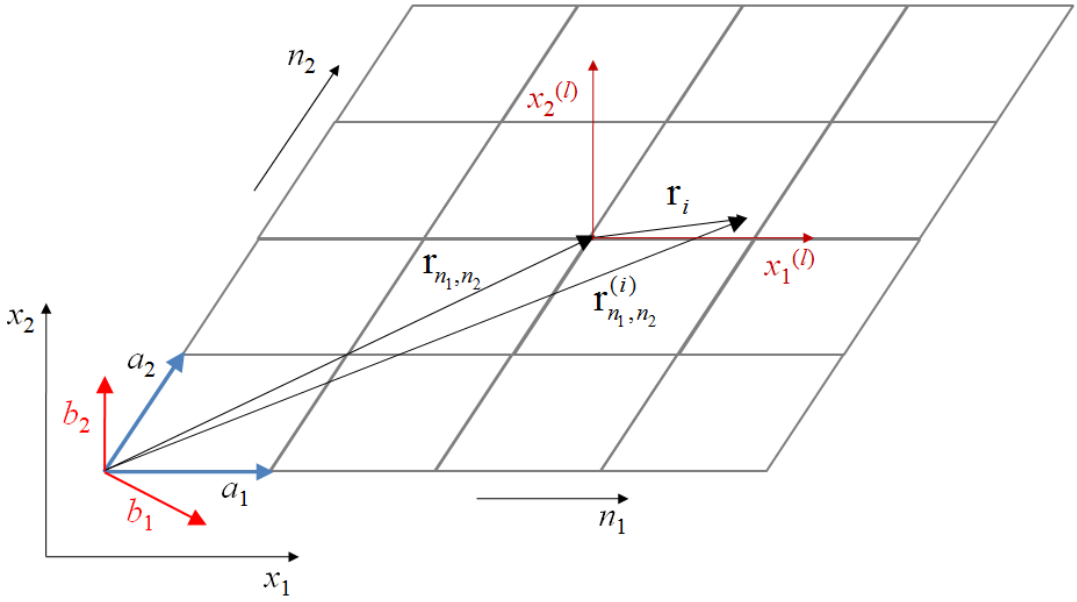

Figure 4: Schematic of a generalized two-dimensional periodic structure and considered system of reference.

Let **k** denote the wave vector [1] which can be expressed in the reciprocal basis,

$$\mathbf{k} = \mu_1\mathbf{b_1} + \mu_2\mathbf{b_2}, \tag{2.3}$$

where $\mathbf{b}_1, \mathbf{b}_2$ define the unit cell of the reciprocal lattice, and are given by,

$$\mathbf{b_1} = \frac{\mathbf{1}}{\boldsymbol{a}}(\mathbf{a_2} \times \mathbf{e});\ \mathbf{b_2} = \frac{\mathbf{1}}{\boldsymbol{a}}(\mathbf{e} \times \mathbf{a_1}), \tag{2.4}$$

with $a = \|\mathbf{a}_1 \times \mathbf{a}_2\|$, and $\mathbf{e} = \frac{1}{a}(\mathbf{a}_1 \times \mathbf{a}_2)$. The definitions of the reciprocal lattice vectors imply that

$$\mathbf{a}_i \cdot \mathbf{b}_j = \delta_{ij}, \quad i,j = 1,2, \tag{2.5}$$

where δ is the Kronecker delta.

2.3 EQUATIONS OF MOTION FOR UNIT CELL

The dynamic behavior of the cell is described by the vector of generalized displacements $\mathbf{u}_{n_1,n_2} = [u_1\, u_2\, u_3\, \ldots\, u_{N-1}\, u_N]^{\mathrm{T}}$. Without loss of generality, it is assumed that the unit cell contains N masses each having a single degree of freedom. To analyze the dispersion in a periodic structure, the dynamics of a unit cell is sufficient to capture the behavior of the whole structure. Equations of motion representing the dynamics of the unit cell are obtained by considering a nine-cell assembly as shown in Figure 5.

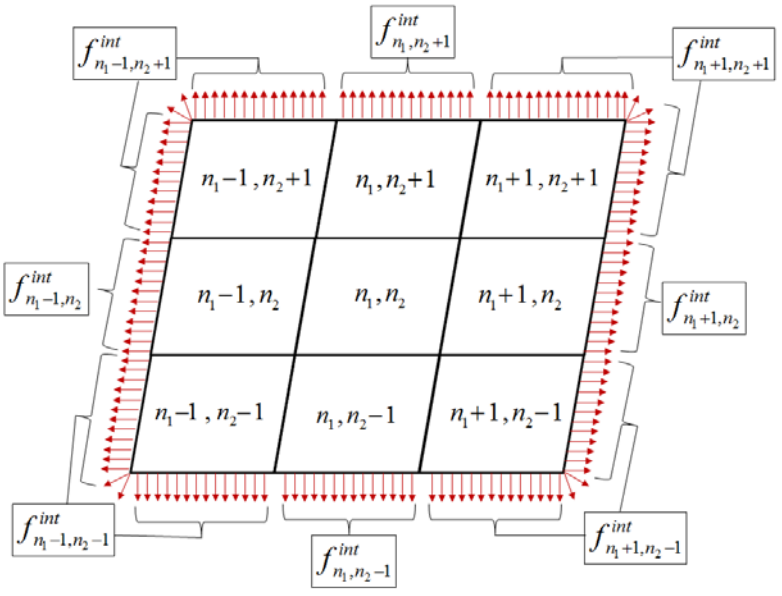

Figure 5: A schematic describing a 9-cell assembly of periodic elements separated from the whole structure along with internal forces on the boundary

Let $\widehat{\mathbf{M}}$ and $\widehat{\mathbf{K}}$ denote the mass and stiffness matrices of the 9-cell assembly, $\hat{\boldsymbol{f}}^{int}$ as shown in Figure 5 denotes the internal force on the boundary of the 9-cell assembly due to its separation from the whole structure and let $\hat{\boldsymbol{f}}^{ext}$ represent the external forcing on the whole assembly (not shown in Figure 5). Let $\hat{\boldsymbol{u}}$ denote a vector containing all the generalized coordinated representing the 9-cell assembly, then the equations of motion representing the discretized model of 9-cell assembly can be written as,

$$\widehat{\mathbf{M}}\frac{d^2\hat{\boldsymbol{u}}}{dt^2} + \widehat{\mathbf{K}}\hat{\boldsymbol{u}} = \hat{\boldsymbol{f}}^{int} + \hat{\boldsymbol{f}}^{ext}. \tag{2.6}$$

Equation (2.6) represents the equations of motion governing the behavior of the generalized coordinates of the 9-cell assembly. To analyze wave propagation, one needs to arrive at the equations of motion representing the dynamics of unit cell n_1, n_2 capturing all the force interactions within the unit cell and with the neighboring cells. This is accomplished by further discretizing and identifying the generalized coordinates in the displacement vector $\hat{\boldsymbol{u}}$. The displacement vector $\hat{\boldsymbol{u}}$ can be written as,

$$\hat{\boldsymbol{u}} = \begin{bmatrix} \mathbf{u}_{n_1-1,n_2-1} \\ \mathbf{u}_{n_1,n_2-1} \\ \mathbf{u}_{n_1+1,n_2-1} \\ \mathbf{u}_{n_1-1,n_2} \\ \mathbf{u}_{n_1,n_2} \\ \mathbf{u}_{n_1+1,n_2} \\ \mathbf{u}_{n_1-1,n_2+1} \\ \mathbf{u}_{n_1,n_2+1} \\ \mathbf{u}_{n_1+1,n_2+1} \end{bmatrix}. \tag{2.7}$$

Note that the internal force as shown in Figure 5 can be expressed as,

$$\hat{\boldsymbol{f}}^{int} = \begin{bmatrix} \boldsymbol{f}^{int}_{n_1-1,n_2-1} \\ \boldsymbol{f}^{int}_{n_1,n_2-1} \\ \vdots \\ \mathbf{0} \\ \vdots \\ \boldsymbol{f}^{int}_{n_1,n_2+1} \\ \boldsymbol{f}^{int}_{n_1+1,n_2+1} \end{bmatrix}. \tag{2.8}$$

where $\boldsymbol{f}_{n_1,n_2}^{int} = \mathbf{0}$ implying that the internal forces on the unit cell at n_1, n_2 are zero due to the fact that these forces cancel out. The mass matrix $\widehat{\mathbf{M}} \in \mathbb{R}^{9N \times 9N}$, with N denoting the degrees of freedom of the unit cell. For a lumped mass model, the mass matrix $\widehat{\mathbf{M}}$ can be expressed in a 9×9 block diagonal matrix form where each block is a sub-matrix of dimensions $N \times N$ described by Eq.(2.9).

$$\widehat{\mathbf{M}} = \begin{bmatrix} \mathbf{M}^{-1,-1} & & & & & & & & \\ & \mathbf{M}^{0,-1} & & & & \mathbf{0} & & & \\ & & \ddots & & & & & & \\ & & & \mathbf{M}^{0,0} & & & & & \\ & & & & \ddots & & & & \\ & \mathbf{0} & & & & \mathbf{M}^{1,0} & & & \\ & & & & & & \mathbf{M}^{1,1} & & \end{bmatrix}. \tag{2.9}$$

The stiffness matrix $\widehat{\mathbf{K}}$ can also be partitioned into 9×9 block diagonal matrix in a similar way to the mass matrix and can be expressed in the following way,

$$\widehat{\mathbf{K}} = \begin{bmatrix} \mathbf{K}_1^{-1,-1} & \mathbf{K}_1^{0,-1} & \mathbf{0} & \mathbf{K}_1^{-1,0} & \mathbf{K}_1^{0,0} & \mathbf{0} & \mathbf{0} & \mathbf{0} & \mathbf{0} \\ \mathbf{K}_2^{-1,-1} & \mathbf{K}_2^{0,-1} & \mathbf{K}_2^{1,-1} & \mathbf{K}_2^{-1,0} & \mathbf{K}_2^{0,0} & \mathbf{K}_2^{1,0} & \mathbf{0} & \mathbf{0} & \mathbf{0} \\ \vdots & \vdots & \vdots & \vdots & \vdots & \vdots & \vdots & \vdots & \vdots \\ \mathbf{K}_5^{-1,-1} & \mathbf{K}_5^{0,-1} & \mathbf{K}_5^{1,-1} & \mathbf{K}_5^{-1,0} & \mathbf{K}_5^{0,0} & \mathbf{K}_5^{1,0} & \mathbf{K}_5^{-1,1} & \mathbf{K}_5^{0,1} & \mathbf{K}_5^{1,1} \\ \vdots & \vdots & \vdots & \vdots & \vdots & \vdots & \vdots & \vdots & \vdots \\ \mathbf{0} & \mathbf{0} & \mathbf{0} & \mathbf{0} & \mathbf{K}_9^{0,0} & \mathbf{K}_9^{1,0} & \mathbf{0} & \mathbf{K}_9^{0,1} & \mathbf{K}_9^{1,1} \end{bmatrix} \tag{2.10}$$

$$\hat{\boldsymbol{f}}^{\boldsymbol{ext}} = \begin{bmatrix} \boldsymbol{f}_{n_1-1,n_2-1}^{ext} \\ \boldsymbol{f}_{n_1,n_2-1}^{ext} \\ \vdots \\ \boldsymbol{f}_{n_1,n_2}^{ext} \\ \vdots \\ \boldsymbol{f}_{n_1,n_2+1}^{ext} \\ \boldsymbol{f}_{n_1+1,n_2+1}^{ext} \end{bmatrix}. \tag{2.11}$$

The external force vector can be partitioned as 9×1 block vector where each element is a sub-vector of dimensions $N \times 1$ as shown in Eq. (2.11). A slight change in notation is

introduced: $\mathbf{M}^{(0,0)}$ and $\mathbf{K}_{\mathbf{5}}^{(\mathrm{p,q})}$ are replaced by $\mathbf{M}$ and $\mathbf{K}^{(\mathrm{p,q})}$ respectively $\forall\, p, q = -1,0,1$. Using Eqs. (2.8) - (2.11), the equations of motion for the unit cell n_1, n_2 which comprises of the generalized coordinates $\mathbf{u}_{n_1,n_2}$ can be written in a general and compact form as,

$$\mathbf{M}\frac{\mathbf{d^2u}_{n_1,n_2}}{\mathbf{dt^2}} + \sum_{\mathbf{p,q=-1,0,1}} \mathbf{K}^{(p,q)}\mathbf{u}_{n_1+p,n_2+q} = \mathbf{f}^{\mathrm{ext}}_{n_1,n_2}(\mathrm{t}), \tag{2.12}$$

The non-dimensional time $\tau = \omega t$ is introduced to transform Eq. (2.12) into,

$$\omega^2\mathbf{M}\frac{\boldsymbol{d^2\mathbf{u}}_{n_1,n_2}}{\boldsymbol{d\tau^2}} + \sum_{\mathbf{p,q=-1,0,1}} \mathbf{K}^{(p,q)}\mathbf{u}_{n_1+p,n_2+q} = \boldsymbol{f}^{ext}_{n_1,n_2}(\tau). \tag{2.13}$$

2.4 LINEAR DISPERSION ANALYSIS

Free wave motion in the lattice can be investigated through the solution of Eq. (2.13) in the absence of external forcing ($\boldsymbol{f}^{ext}_{n_1,n_2}(\tau) = 0$). The dispersion properties of the lattice are obtained by imposing a solution of the kind,

$$\mathbf{u}_{n_1,n_2}(\tau) = \mathbf{u}_0 e^{i\,\mathbf{k}\cdot\mathbf{r}_{n_1,n_2}} e^{i\,\tau}, \tag{2.14}$$

which implies the application of Bloch theorem for the considered periodic medium [1]. Substitution of Eq. (2.14) into Eq. (2.13) leads to the solution of wave modes supported by the considered lattice. Using Eqs. (2.2), (2.3) and (2.5) the following relation can be arrived at,

$$\mathbf{k}\cdot\mathbf{r}_{\boldsymbol{n_1,n_2}} = \mu_1 n_1 + \mu_2 n_2, \tag{2.15}$$

so that Eq. (2.14) can be rewritten as,

$$\mathbf{u}_{n_1,n_2}(\tau) = \mathbf{u_0}(\mathbf{k})\, \boldsymbol{e}^{\boldsymbol{i}\,(\mu_1 n_1 + \mu_2 n_2)} e^{i\,\tau}. \tag{2.16}$$

Equation (2.16) defines amplitude and phase relations for waves propagating from the cell at location n_1, n_2 to the cell at $n_1 \pm p, n_2 \pm q$, so that the following relation holds,

$$\mathbf{u}_{n_1\pm p,\, n_2\pm q}(\tau) = \mathbf{u_0}(\mathbf{k})\, e^{i\,(\mu_1(n_1\pm p)+\mu_2(n_2\pm q))} e^{i\,\tau} = \mathbf{u}_{n_1,n_2}(\tau) e^{i\,(\pm p\mu_1 \pm q\mu_2)}. \tag{2.17}$$

Equations (2.16) and (2.17) show that the wave vector $\mathbf{k} = \mu_1\mathbf{b}_1 + \mu_2\mathbf{b}_2$ in a 2D lattice is a periodic function in the reciprocal lattice, i.e. $\mathbf{k}' = \mathbf{k} + 2\pi(m_1\mathbf{b}_1 + m_2\mathbf{b}_2)$, m_1, m_2 being an integer pair. Hence, full representation of the dependency of the wave vector on frequency is obtained by investigating its variation over a single period. In a 2D lattice, the period corresponds to a region in the reciprocal lattice whose area equals the area of the reciprocal lattice's unit cell, known as first Brillouin zone [1]. Any symmetry in the first Brillouin zone can be utilized to identify a sub-region, known as irreducible Brillouin zone, which is the smallest frequency/wavenumber space necessary to determine wave dispersion for a given lattice. Chapter 4 demonstrates irreducible Brillouin zones for a square mono-atomic lattice, diatomic lattice and mono-atomic lattice with inclusion.

Bloch conditions as expressed by Eqs. (2.16) and (2.17), can be enforced in the equation of motion of the unit cell (Eq. (2.13)) to give,

$$\omega^2\mathbf{M}\frac{\boldsymbol{d^2}\mathbf{u}_{n_1,n_2}(\tau)}{\boldsymbol{d}\tau^2} + \left[\sum_{p,q=-1}^{+1}\mathbf{K}^{(p,q)} e^{i\,(\pm p\mu_1 \pm q\mu_2)}\right]\mathbf{u}_{n_1,n_2}(\tau) = \mathbf{0}, \tag{2.18}$$

Equation (2.18) is further simplified using Eq. (2.16) to give,

$$\left[-\omega^2\mathbf{M} + \sum_{p,q=-1}^{+1}\mathbf{K}^{(p,q)} e^{i\,(\pm p\mu_1 \pm q\mu_2)}\right]\mathbf{u}_0(\mathbf{k})\, e^{i\,(\mu_1 n_1+\mu_2 n_2)} e^{i\,\tau} = \mathbf{0}, \tag{2.19}$$

$$\left[-\omega^2\mathbf{M} + \widetilde{\mathbf{K}}(\mathbf{k})\right]\mathbf{u}_0(\mathbf{k}) = \mathbf{0}, \tag{2.20}$$

where

$$\widetilde{\mathbf{K}}(\mu_1,\mu_2) = \widetilde{\mathbf{K}}(\mathbf{k}) = \sum_{p,q=-1}^{+1}\mathbf{K}^{(p,q)}\, e^{i(\pm p\mu_1 \pm q\mu_2)}. \tag{2.21}$$

is denoted as the wavenumber-reduced stiffness matrix.

2.4.1 DISPERSION RELATIONS

Equation (2.20) represents an eigenvalue problem which defines the linear dispersion characteristics of the lattice. Typically, its solution is sought by imposing the wave vector

k and solving for the frequency ω which leads to *dispersion surfaces*. The wave vector is set to vary within the first Brillouin zone so that complete information of the frequency/wavenumber relation is obtained. Alternatively, it is common practice to impose the components of the wave vector along the boundary of the first Brioullin zone [1]. This leads to 2D diagrams, called band diagrams, which effectively represent the basic features of the dispersion properties of the lattice, while requiring reduced amounts of computations.

The *j*-th branch of the linear dispersion relations is defined by the variation of the *j*-th eigenvalue of Eq. (2.20) in terms of the wave vector components,

$$\omega_j = \omega_j(\mathbf{k}). \tag{2.22}$$

In the case of a 2D lattice, the dispersion relations are surfaces relating the frequency associated with the two components μ_1, μ_2 of the wave vector. The number of surfaces corresponding to a given pair μ_1, μ_2 is determined by the dimensions of the eigenvalue problem in Eq. (2.20), which correspond to the number of wave modes supported by the lattice. Mode polarization is described by the eigenvector $\mathbf{u}_{0,j}(\mathbf{k})$ or the *j*-th wave mode. In the remainder of the paper, it assumed that the notation $\mathbf{u}_{0,j}(\mathbf{k})$ denotes an eigenvector normalized to its highest component, so that,

$$max\{\mathbf{u}_{0,j}(\mathbf{k})\} = 1. \tag{2.23}$$

The wave modes, as eigenvector of Eq. (2.20), satisfy the following orthogonality conditions,

$$\mathbf{u}_{0,r}^{\mathrm{H}}(\mathbf{k})\mathbf{M}\,\mathbf{u}_{0,j}(\mathbf{k}) = m_r\delta_{rj}, \tag{2.24}$$

$$\mathbf{u}_{0,r}^{\mathrm{H}}(\mathbf{k})\tilde{\mathbf{K}}(\mathbf{k})\mathbf{u}_{0,j}(\mathbf{k}) = k_r\delta_{rj}, \tag{2.25}$$

where $\mathbf{u}_{0,r}^{\mathrm{H}}$ denotes the complex conjugate transpose or the hermitian of $\mathbf{u}_{0,r}$, δ_{rj} is the kronecker delta, while m_r and k_r are scalar parameters given by,

$$\mathbf{u}_{0,r}^{\mathrm{H}}(\mathbf{k})\mathbf{M}\mathbf{u}_{0,r}(\mathbf{k}) = m_r, \tag{2.26}$$

$$\mathbf{u}_{\mathbf{0},r}^{\mathrm{H}}(\mathbf{k})\widetilde{\mathbf{K}}(\mathbf{k})\mathbf{u}_{0,r}(\mathbf{k}) = k_r. \tag{2.27}$$

Substituting the j^{th} mode in Eq. (2.20) yields,

$$\left[-\omega_{0,j}^2\mathbf{M} + \widetilde{\mathbf{K}}(\mathbf{k})\right]\mathbf{u}_{0,j}(\mathbf{k}) = \mathbf{0}, \tag{2.28}$$

and premultiplying by $\mathbf{u}_{0,r}^{\mathrm{H}}(\mathbf{k})$ gives,

$$\left[-\omega_{0,j}^2\mathbf{u}_{0,r}^{\mathrm{H}}(\mathbf{k})\mathbf{M}\mathbf{u}_{0,j}(\mathbf{k}) + \mathbf{u}_{0,r}^{\mathrm{H}}(\mathbf{k})\widetilde{\mathbf{K}}(\mathbf{k})\mathbf{u}_{0,j}(\mathbf{k})\right] = \mathbf{0}. \tag{2.29}$$

For $r = j$, Eq. (2.29) reduces to

$$\omega_{0,j}^2 m_j - k_j = 0 \tag{2.30}$$

2.4.2 GROUP VELOCITY

The group velocity defines the way in which energy flows in the structure in response to an external perturbation. The group velocity is defined as the gradient of the dispersion surface [21, 50],

$$\boldsymbol{c}_g = \nabla\omega(\mathbf{k}). \tag{2.31}$$

The vector $\mathbf{k}$ can be expressed in the reciprocal lattice space or Cartesian space and the gradient of the scalar dispersion relation results in a group velocity vector expressed in the same space. The dispersion relations for a 2D lattice can be represented as surfaces defining the frequencies associated with an assigned pair of wave vector components μ_1, μ_2. Such surfaces can be represented as iso-frequency contours, which effectively visualize the group velocity as a vector perpendicular to each frequency contour for the considered μ_1, μ_2 pair [21, 51]. This representation is effective at identifying preferential directions of wave propagation, or the existence of "forbidden directions" along which waves do not propagate. Of particular interest is the existence of "caustics", which are identified as cusps in the group velocity distributions of the kind

observed in anisotropic media [51, 52]. Such caustics are associated with strong energy focusing of the propagating wave packets, resulting from the interference of the various wave components propagating in the lattice plane. The group velocity patterns exhibited by some example lattices at various frequencies are discussed in Chapter 4 and the existence of low response regions within the lattice structures is demonstrated.

2.5 DISPERSION IN WEAKLY NONLINEAR PERIODIC STRUCTURES: A PERTURBATION APPROACH

2.5.1 EQUATIONS OF MOTION

Considering the 2D configuration of the lattice, and the assumption that each cell interacts nonlinearly with the eight neighboring units, the equation of motion for the considered cell can be expressed as follows,

$$\sum_{p,q=-1,0,1}\left[\mathbf{M}^{(p,q)}\frac{d^2}{dt^2}\mathbf{u}_{n_1+p,n_2+q}+\mathbf{K}^{(p,q)}\mathbf{u}_{n_1+p,n_2+q}\right]+ \varepsilon\boldsymbol{f}_{\boldsymbol{NL}}\left(\mathbf{u}_{n_1\pm p,n_2\pm q}\right)=\boldsymbol{f}^{ext}_{n_1,n_2}(\mathrm{t}) \tag{2.32}$$

where $\boldsymbol{f}^{ext}_{n_1,n_2}$ is the vector of the generalized forces applied to the considered unit cell, while $\boldsymbol{f}_{\boldsymbol{NL}}\left(\mathbf{u}_{n_1\pm p,n_2\pm q}\right)$ defines the nonlinear interactions. In general, there exists nonlinear interaction within the degrees of freedom of unit cell. Also, the nonlinear interaction can exist among the degrees of freedom of the unit cell and the ones associated with neighboring cells. Therefore nonlinear force vector in Eq. (2.32) is expressed as a function of $\mathbf{u}_{n_1\pm p,n_2\pm q}\forall\, p,q=-1,0,1$ which captures the nonlinear interactions within the reference unit cell and also the ones among the reference unit cell and the neighboring cells. The parameter ε determines the magnitude of nonlinear interaction in comparison with linear interactions. If $\varepsilon \ll 1$ then the nonlinear interactions are weak in comparison with linear restoring forces. For simplicity, lumped-

mass discretization is assumed, and the non-dimensional time $\tau = \omega t$ is introduced to transform Eq. (2.32) into,

$$\omega^2 \mathbf{M} \frac{d^2 \mathbf{u}_{n_1,n_2}}{d\tau^2} + \left[\sum_{p,q=-1,0,1} \mathbf{K}^{(p,q)} \mathbf{u}_{n_1+p,n_2+q}\right] + \varepsilon \mathbf{f}_{\boldsymbol{NL}}\left(\mathbf{u}_{n_1\pm p,n_2\pm q}\right) = \boldsymbol{f}^{ext}_{n_1,n_2}(\tau). \tag{2.33}$$

2.5.2 PERTURBATION ANALYSIS

The present section details the perturbation method applied to solve for the dispersion in weakly nonlinear lattices ($\varepsilon \ll 1$). Equation (2.33) represents an open set of nonlinear difference equations and the solution procedure described here is different from traditional methods employed for weakly nonlinear systems.

The first step of the analysis involves the asymptotic expansion of displacement and frequency in a series form,

$$\mathbf{u}_{n_1,n_2} = \mathbf{u}^{(0)}_{n_1,n_2} + \varepsilon \mathbf{u}^{(1)}_{n_1,n_2} + O(\varepsilon^2), \tag{2.34}$$

$$\omega = \omega_0 + \varepsilon \omega_1 + O(\varepsilon^2), \tag{2.35}$$

The ordered equations are obtained by substituting Eqs. (2.34) and (2.35) into Eq. (2.33),

$$\varepsilon^0: \ \omega_0^2 \mathbf{M} \frac{d^2 \mathbf{u}^{(0)}_{n_1,n_2}}{d\tau^2} + \sum_{p,q=-1}^{+1} \mathbf{K}^{(p,q)} \mathbf{u}^{(0)}_{n_1+p,n_2+q} = \boldsymbol{f}^{ext}_{n_1,n_2}(\tau), \tag{2.36}$$

$$\varepsilon^1: \ \omega_0^2 \mathbf{M} \frac{d^2 \mathbf{u}^{(1)}_{n_1,n_2}}{d\tau^2} + \sum_{p,q=-1}^{+1} \mathbf{K}^{(p,q)} \mathbf{u}^{(1)}_{n_1+p,n_2+q} = -2\omega_0\omega_1 \mathbf{M} \frac{d^2 \mathbf{u}^{(0)}_{n_1,n_2}}{d\tau^2} - \boldsymbol{f}_{\boldsymbol{NL}}\left(\mathbf{u}^{(0)}_{n_1,n_2}, \mathbf{u}^{(0)}_{n_1\pm p,n_2\pm q}\right), \tag{2.37}$$

Analysis of the free wave motion is done by first obtaining the linear dispersion solution governed by ε^0 equation (Eq. (2.36)) in the absence of external forcing $\boldsymbol{f}^{ext}_{n_1,n_2}(\tau) = 0$ which follows exactly same procedure as outlined for the linear dispersion analysis. Identification of such modes and their substitution in the ε^1 equation (Eq. (2.37)) allows

evaluating the influence of nonlinearities on the wave propagation characteristics of the lattice.

2.5.3 NONLINEAR DISPERSION ESTIMATION THROUGH FIRST-ORDER CORRECTION

Nonlinear effects on dispersion are estimated through the substitution of the linear solution in the first order perturbation equation (Eq. (2.37)). The nonlinear correction to the dispersion properties are evaluated for each wave mode and corresponding frequency. Specifically, the following solution is imposed in Eq. (2.37),

$$\mathbf{u}^{(0)}(\tau) = \frac{A_0}{2}\mathbf{u}_{0,j}(\mathbf{k})e^{i\,\tau} + c.c., \tag{2.38}$$

where $c.c.$ denotes the complex conjugate, A_0 defines the wave amplitude and $\mathbf{u}_{0,j}(\mathbf{k})$ represents the normalized j-th complex wave mode for which the nonlinear correction needs to be evaluated for a specific wave vector $\mathbf{k}$ and corresponding frequency $\omega_{0,j}$. For simplicity and without loss of generality, Eq. (2.38) assumes that the study considers the reference cell at location $n_1 = n_2 = 0$, whose motion is denoted by the simplified notation $\mathbf{u}_{1,1}^{(0)} = \mathbf{u}^{(0)}$. Also in Eq. (2.38) such amplitude is determined by the initial conditions applied to the system, and their influence on the various wave modes. In the study of dispersion, $A_{0,j}$ is considered as a parameter, whose effect on dispersion needs to be investigated.

Assuming a solution of the kind described by Eq. (2.38), the first order equation (Eq. (2.37)) may be written as,

$$\begin{aligned}\omega_{0,j}^2\mathbf{M}\frac{d^2\mathbf{u}^{(1)}}{d\tau^2} + \sum_{p,q=-1}^{+1}\mathbf{K}^{(p,q)}\mathbf{u}_{p,q}^{(1)} = \\ \omega_{0,j}\omega_1 A_0\mathbf{M}\mathbf{u}_{0,j}(\mathbf{k})e^{i\,\tau} - \boldsymbol{f}_{\boldsymbol{NL}}\left(\mathbf{u}^{(0)}(\tau), \mathbf{u}_{\pm\mathbf{1},\pm\mathbf{1}}^{(0)}(\tau)\right).\end{aligned} \tag{2.39}$$

The nonlinear term $\boldsymbol{f}_{\boldsymbol{NL}}$ may be expressed as,

$$\boldsymbol{f_{NL}}\left(\mathbf{u}^{(\mathbf{0})}, \mathbf{u}^{(0)}_{\pm 1,\pm 1}\right) = \sum_{p,q=-1}^{+1} \boldsymbol{f_{NL}}\left(\mathbf{u}^{(0)}, \mathbf{u}^{(0)}_{p,q}\right) \tag{2.40}$$

where it is assumed that the same nonlinear interaction occurs among all unit cell neighbors, and that such interaction is solely a function of the degrees of freedom within the unit cell and in the neighboring cells. The displacement of neighboring cells can be expressed as,

$$\mathbf{u}^{(0)}_{p,q}(\tau) = \frac{A_0}{2}\left[\mathbf{u}_{0,j}(\mathbf{k})\, e^{i\,(p\mu_1 + q\mu_2)} e^{i\tau} + c.c.\right]. \tag{2.41}$$

Equations (2.38) and (2.41) show that both $\mathbf{u}^{(0)}(\tau)$ and $\mathbf{u}^{(0)}_{p,q}(\tau)$ are periodic functions in the variable $\tau \in [0\,, 2\pi]$. Hence, the function describing the nonlinear interactions is also periodic in τ, *i.e.*:

$$\boldsymbol{f}_{NL}\left(\mathbf{u}^{(0)}(\tau), \mathbf{u}^{(0)}_{p,q}(\tau)\right) = \boldsymbol{f}_{NL}\left(\mathbf{u}^{(0)}(\tau + 2\pi), \mathbf{u}^{(0)}_{p,q}(\tau + 2\pi)\right). \tag{2.42}$$

The nonlinear function of interaction $\boldsymbol{f}_{NL}$ is dependent on the magnitude of the wave amplitude A_0 and on the complex wave mode $\mathbf{u}_{0,j}(\mathbf{k})$, which is known and fixed at this stage of the analysis. Accordingly, $\boldsymbol{f}_{NL}$ can be expressed in terms of the variables,

$$\boldsymbol{f}_{NL} = \boldsymbol{f}_{NL}(A_0, \tau). \tag{2.43}$$

Given the periodicity of the nonlinear expression, it is convenient to expand it in a Fourier series in the form,

$$\boldsymbol{f}_{NL}(A_0, \tau) = \sum_{n=-\infty}^{+\infty} \boldsymbol{c}_n(A_0)\, e^{in\tau} \tag{2.44}$$

where

$$\boldsymbol{c}_n(A_0) = \frac{1}{2\pi}\int_0^{2\pi} \boldsymbol{f}(A_0, \tau)\, e^{-in\tau} d\phi \tag{2.45}$$

For assigned values of the amplitude A_0, the n-th coefficient of the series $\mathbf{c}_n(A_0)$ is estimated through the integral in Eq. (2.45), which can be evaluated either analytically or numerically. Equation (2.39) can be written as,

$$\omega_{0,j}^2 \mathbf{M} \frac{d^2\mathbf{u}^{(1)}}{d\tau^2} + \sum_{p,q=-1}^{+1} \mathbf{K}^{(p,q)} \mathbf{u}_{p,q}^{(1)} = \omega_{0,j}\omega_1 A_0 \mathbf{M}\mathbf{u}_{0,j}(\mathbf{k}) e^{i\tau} - \sum_{n=-\infty}^{+\infty} \boldsymbol{c}_n \, e^{in\tau} + c.c. \tag{2.46}$$

The solution $\mathbf{u}^{(1)}(\tau)$ of Eq. (2.46) can be found by superimposing the various forcing terms on the right-hand side of the equation, therefore invoking the superposition principle. For simplicity, we first consider the excitation terms in $e^{i\tau}$,

$$\omega_{0,j}^2 \mathbf{M} \frac{d^2\mathbf{u}^{(1)}}{d\tau^2} + \sum_{p,q=-1}^{+1} \mathbf{K}^{(p,q)} \mathbf{u}_{p,q}^{(1)} = \left[\omega_{0,j}\omega_1 A_0 \mathbf{M}\mathbf{u}_{0,j}(\mathbf{k}) - \boldsymbol{c}_1(A_0)\right] e^{i\tau}, \tag{2.47}$$

which can be rewritten as,

$$\omega_{0,j}^2 \mathbf{M} \frac{d^2\mathbf{u}^{(1)}}{d\tau^2} + \sum_{p,q=-1}^{+1} \mathbf{K}^{(p,q)} \mathbf{u}_{p,q}^{(1)} = \boldsymbol{f}_j e^{i\tau}, \tag{2.48}$$

where

$$\boldsymbol{f}_j = \omega_{0,j}\omega_1 A_0 \mathbf{M}\mathbf{u}_{0,j}(\mathbf{k}) - \boldsymbol{c}_1(A_0). \tag{2.49}$$

The left hand side of Eq. (2.48) is similar to the zero[th] order equation represented by Eq. (2.36). Therefore the homogenous solution of $\mathbf{u}^{(1)}(\tau)$ has the same form as a Bloch solution $\mathbf{u}^{(0)}(\tau)$ described by Eq. (2.38). Hence a "secular-Bloch" solution is assumed for $\mathbf{u}^{(1)}(\tau)$ which forms the solution to Eq. (2.48),

$$\mathbf{u}_{p,q}^{(1)}(\tau) = A_1 \mathbf{U}_0(\mathbf{k}) e^{i\tau} e^{i(p\mu_1 + q\mu_2)} + B_1 \tau \mathbf{U}_0(\mathbf{k}) e^{i\tau} e^{i(p\mu_1 + q\mu_2)} + c.c. \tag{2.50}$$

Substituting Eq. (2.50) into Eq. (2.48) leads to the following,

$$A_1\left[-\omega_{0,j}^2 \mathbf{M} + \widetilde{\mathbf{K}}(\mathbf{k})\right]\mathbf{U}_0(\mathbf{k}) e^{i\tau} + 2iB_1\omega_{0,j}^2 \mathbf{M}\mathbf{U}_0(\mathbf{k}) e^{i\tau} + B_1\tau\left[-\omega_{0,j}^2 \mathbf{M} + \widetilde{\mathbf{K}}(\mathbf{k})\right]\mathbf{U}_0(\mathbf{k}) e^{i\tau} = \boldsymbol{f}_j e^{i\tau}, \tag{2.51}$$

where $\mathbf{U_0}(\mathbf{k}) = \left[\mathbf{u}_{0,1}(\mathbf{k}),\ \mathbf{u}_{0,2}(\mathbf{k}),\ \mathbf{u}_{0,3}(\mathbf{k}), \ldots\ \mathbf{u}_{0,N}(\mathbf{k})\right]$ is the matrix of the linear wave modes. Premultiplying by $\mathbf{U}_0^{\mathrm{H}}(\mathbf{k})$ results in the following,

$$\begin{gathered} A_1\left[-\omega_{0,j}^2\mathbf{U}_0^{\mathrm{H}}(\mathbf{k})\mathbf{M}\mathbf{U}_0(\mathbf{k}) + \mathbf{U}_0^{\mathrm{H}}(\mathbf{k})\widetilde{\mathbf{K}}(\mathbf{k})\mathbf{U}_0(\mathbf{k})\right]e^{i\tau} + \\ 2iB_1\omega_{0,j}^2\mathbf{U}_0^{\mathrm{H}}(\mathbf{k})\mathbf{M}\mathbf{U}_0(\mathbf{k})e^{i\tau} + \\ B_1\tau\left[-\omega_{0,j}^2\mathbf{U}_0^{\mathrm{H}}(\mathbf{k})\mathbf{M}\mathbf{U}_0(\mathbf{k}) + \mathbf{U}_0^{\mathrm{H}}(\mathbf{k})\widetilde{\mathbf{K}}(\mathbf{k})\mathbf{U}_0(\mathbf{k})\right]e^{i\tau} = \mathbf{U}_0^{\mathrm{H}}(\mathbf{k})\boldsymbol{f}_j e^{i\tau}, \end{gathered} \tag{2.52}$$

Since $\mathbf{M}$ and $\widetilde{\mathbf{K}}(\mathbf{k})$ are identical to those defining the linear dispersion problem (Eq. (2.20)) and given that $\mathbf{U}_0(\mathbf{k})$ are the associated eigenmodes the orthogonality properties of the linear wave modes (Eqs. (2.26) and (2.27)) lead to a set of N uncoupled equations,

$$\begin{gathered} A_1\left[-\omega_{0,j}^2 m_r + k_r\right]e^{i\tau} + 2iB_1\omega_{0,j}^2 m_r e^{i\tau} + B_1\tau\left[-\omega_{0,j}^2 m_r + k_r\right]e^{i\tau} = \\ \mathbf{u}_{0,r}^{\mathrm{H}}\boldsymbol{f}_j e^{i\tau}, \quad \forall\, r = 1,2 \ldots N \end{gathered} \tag{2.53}$$

Specifically for $r = j$,

$$\begin{gathered} A_1\left[-\omega_{0,j}^2 m_j + k_j\right]e^{i\tau} + 2iB_1\omega_{0,j}^2 m_j e^{i\tau} + B_1\tau\left[-\omega_{0,j}^2 m_j + k_j\right]e^{i\tau} = \\ \mathbf{u}_{0,j}^{\mathrm{H}}\boldsymbol{f}_j e^{i\tau}. \end{gathered} \tag{2.54}$$

Substituting Eq. (2.30) into the above equation leads to the elimination of first and third terms in the left hand side of the Eq. (2.54) which gives,

$$2iB_1\omega_{0,j}^2 m_j e^{i\tau} = \mathbf{u}_{0,j}^{\mathrm{H}}\boldsymbol{f}_j e^{i\tau}, \tag{2.55}$$

which finally leads to the expression for B_1,

$$B_1 = -\frac{\mathbf{u}_{0,j}^{\mathrm{H}}\boldsymbol{f}_j}{2i\omega_{0,j}^2 m_j}. \tag{2.56}$$

Equation (2.56) implies that the "secular-Bloch" solution denoted by Eq. (2.50) satisfies Eq. (2.48). This solution grows unbounded in τ and in order to avoid the occurrence of

such unbounded solution, one needs to impose $B_1 = 0$ which leads to the solvability condition,

$$\mathbf{u}_{0,j}^{\mathrm{H}} \boldsymbol{f}_j = 0 \tag{2.57}$$

Equation (2.57) can be rewritten in extended form as,

$$\mathbf{u}_{0,j}^{\mathrm{H}}(\mathbf{k})\left[\omega_{0,j}\omega_1 A_0 \mathbf{M}\mathbf{u}_{0,j}(\mathbf{k}) - \boldsymbol{c}_1(A_0)\right] = 0, \tag{2.58}$$

which imposes a condition on the first order frequency perturbation which can be calculated as,

$$\omega_{1,j}(A_0, \mathbf{k}) = \frac{\mathbf{u}_{0,j}^{\mathrm{H}}(\mathbf{k})\mathbf{c}_1(A_0)}{\omega_{0,j}A_0\mathbf{u}_{0,j}^{\mathrm{H}}(\mathbf{k})\mathbf{M}\mathbf{u}_{0,j}(\mathbf{k})}. \tag{2.59}$$

The resulting scalar equation can be solved in terms of $\omega_{1,j}$, which defines the frequency correction for the *j*-th branch of the dispersion relation. The corresponding nonlinear dispersion branch is estimated as follows,

$$\omega_j = \omega_{0,j} + \varepsilon\omega_{1,j}(A_0, \mathbf{k}) + O(\varepsilon^2). \tag{2.60}$$

In summary, the *j*-th branch of the nonlinear system can be generally expressed as,

$$\omega_j = \omega_j(\mathbf{k}, A_0). \tag{2.61}$$

2.6 DISPERSION IN STRONGLY NONLINEAR PERIODIC STRUCTURES: HARMONIC BALANCE METHOD

A limitation to the general perturbation approach described in the previous section is that the nonlinearities are weak. Hence the systems which are governed by strongly nonlinear interactions need to resort to other approximate analytical methods to evaluate the dispersion characteristics. One such approach is a generalized harmonic balance method [53-56] adapted to wave propagation problems.

2.6.1 EQUATIONS OF MOTION

Consider a general discrete periodic lattice as detailed in the previous section (Figure 4). The periodic lattice is spanned by the lattice vectors $\mathbf{a}_1$and $\mathbf{a}_2$. The integer indices n_1 and n_2 define the location of a cell with respect to the reference cell. For a strongly nonlinear system, the parameter ε is set equal to 1. Equation of motion (Eq. (2.33)) can be rewritten with as,

$$\omega^2\mathbf{M}\frac{d^2\mathbf{u}_{n_1,n_2}}{d\tau^2} + \left[\sum_{p,q=-1,0,1}\mathbf{K}^{(p,q)}\mathbf{u}_{n_1+p,n_2+q}\right] + \boldsymbol{f}_{\boldsymbol{NL}}\left(\mathbf{u}_{n_1,n_2}, \mathbf{u}_{n_1\pm p,n_2\pm q}\right) = \boldsymbol{f}^{ext}_{n_1,n_2}(\tau) \tag{2.62}$$

As before, free wave propagation is assumed so that $\boldsymbol{f}^{ext}_{n_1,n_2}(\tau) = 0$, the linear interactions $\sum_{p,q=-1,0,1}\mathbf{K}^{(p,q)}\mathbf{u}_{n_1+p,n_2+q}$ and the nonlinear force vector $\boldsymbol{f}_{\boldsymbol{NL}}\left(\mathbf{u}_{n_1,n_2}, \mathbf{u}_{n_1\pm p,n_2\pm q}\right)$ are combined into a single term representing the total restoring force. The equations of motion for the unit cell at (n_1, n_2) are re-written as,

$$\omega^2\mathbf{M}\frac{d^2\mathbf{u}_{n_1n_2}}{d\tau^2} = \boldsymbol{f}_{\boldsymbol{NL}}\left(\mathbf{u}_{n_1n_2}, \mathbf{u}_{n_1\pm1,n_2\pm1}\right), \tag{2.63}$$

where $\boldsymbol{f}_{\boldsymbol{NL}}$ is the force interaction existing between neighboring masses. Only nearest neighbor ($\boldsymbol{u}_{n_1\pm1,n_2\pm1}$) interactions are assumed in describing the dynamics of unit cell. Depending on the lattice, the influence of the cells beyond nearest neighboring cells on the dynamics of the unit cell ($\boldsymbol{u}_{n_1n_2}$) could exist but for the present analysis to be valid, the force interaction of a unit cell is limited to its nearest neighbors.

2.6.2 HARMONIC BALANCE ANALYSIS

A wave solution is imposed by assuming the following relation for the vector of generalized coordinates,

$$\mathbf{u}_{n_1n_2} = A\left(\sum_{m=1}^{M}\left[\boldsymbol{c}_m\cos\left(m\mathbf{k}\cdot\boldsymbol{r}_{n_1n_2} - m\tau\right) + \boldsymbol{s}_m\sin(m\mathbf{k}\cdot\boldsymbol{r}_{n_1n_2} - m\tau)\right]\right) \tag{2.64}$$

where A denotes the wave amplitude, m is an integer representing the harmonic and M denotes the maximum number of harmonics used to approximate the displacement $\boldsymbol{u}_{n_1 n_2}$. Also $\boldsymbol{k}$ is the wave vector as described by Eq. (2.3), $\boldsymbol{r}_{n_1 n_2}$ is the position vector of unit cell from a reference point (Figure 4) , $\boldsymbol{c}_m = \left[c_{m1}\ c_{m2} \dots c_{mj} \dots c_{mN}\right]^{\mathrm{T}}$ and $\boldsymbol{s}_m = \left[s_{m1}\ s_{m2} \dots s_{mj} \dots s_{mN}\right]^{\mathrm{T}}$ denote m^{th}harmonic $\mathbb{R}^{N\times 1}$ normalized amplitude vectors of generalized coordinates representing degrees of freedom in unit cell. The amplitude vectors $\boldsymbol{c}_m$ and $\boldsymbol{s}_m$ are normalized such that the highest component of $[\boldsymbol{c}_m\ \boldsymbol{s}_m]^{\mathrm{T}}$ is unity,

$$max\{\boldsymbol{c}_m, \boldsymbol{s}_{\mathrm{m}}\} = 1. \tag{2.65}$$

The displacement assumption (Eq. (2.64)) represents a superposition of M travelling waves with frequencies $\omega, 2\omega \dots M\omega$ and wavevectors $\boldsymbol{k}, 2\boldsymbol{k} \dots M\boldsymbol{k}$. For $M = 1$, the solution represents a plane wave with fundamental frequency ω and wavevector $\boldsymbol{k}$ and it is equivalent to Eq. (2.20) which denotes linear solution. Hence, the $M = 1$ solution represents the fundamental wave mode supported by the nonlinear system. The response $\mathbf{u}_{n_1,n_2}$ can be rewritten in terms of the propagation constants in the following way,

$$\mathbf{u}_{n_1,n_2} = A(\textstyle\sum_{m=1}^{M}\{\boldsymbol{c}_m \cos[m(\boldsymbol{\mu}\cdot\boldsymbol{n} - \tau)] + \boldsymbol{s}_m \sin[m(\boldsymbol{\mu}\cdot\boldsymbol{n} - \tau)]\}). \tag{2.66}$$

where $\boldsymbol{\mu}\cdot\boldsymbol{n} = \mu_1 n_1 + \mu_2 n_2$.

Let $\tilde{\boldsymbol{q}}_j = \left[c_{1j}\ s_{1j}\ c_{2j}\ s_{2j} \dots\ c_{mj}\ s_{mj} \dots c_{Mj}\ s_{Mj}\right]^{\mathrm{T}}$, where c_{mj} and s_{mj} denote the m^{th} harmonic amplitude of the generalized coordinate u_j. The displacement vector can be rewritten in a compact way,

$$\mathbf{u}_{n_1,n_2} = A\mathbf{S}_{n_1 n_2}\tilde{\boldsymbol{q}}, \tag{2.67}$$

where $\tilde{\boldsymbol{q}} = [\ \tilde{\boldsymbol{q}}_1\ \ \tilde{\boldsymbol{q}}_2 \dots\ \tilde{\boldsymbol{q}}_N]^{\mathrm{T}}$ is $\mathbb{R}^{2NM\times 1}$ augmented amplitude vector and,

$$\mathbf{S}_{n_1 n_2} = \begin{bmatrix} \mathbf{C}_{n_1 n_2} & \mathbf{0} & \mathbf{0} \\ \mathbf{0} & \ddots & \mathbf{0} \\ \mathbf{0} & \mathbf{0} & \mathbf{C}_{n_1 n_2} \end{bmatrix} \tag{2.68}$$

denotes a block diagonal $\mathbb{R}^{N\times 2NM}$ transformation matrix. Each block diagonal is given by,

$$\mathbf{C}_{n_1 n_2} = \begin{bmatrix} \cos(\boldsymbol{\mu}\cdot\boldsymbol{n}-\tau) \\ \sin(\boldsymbol{\mu}\cdot\boldsymbol{n}-\tau) \\ \cos\big(2(\boldsymbol{\mu}\cdot\boldsymbol{n}-\tau)\big) \\ \sin\big(2(\boldsymbol{\mu}\cdot\boldsymbol{n}-\tau)\big) \\ \vdots \\ \cos\big(M(\boldsymbol{\mu}\cdot\boldsymbol{n}-\tau)\big) \\ \sin\big(M(\boldsymbol{\mu}\cdot\boldsymbol{n}-\tau)\big) \end{bmatrix}^T \tag{2.69}$$

Note that $\mathbf{S}_{n_1 n_2}$ is function of the propagation constants μ_1, μ_2 and of the non-dimensional time τ. Without loss of generality, the reference point can be set to $n_1 = n_2 = 0$. This implies that $\mathbf{S}_{n_1 n_2} = \mathbf{S}(\tau)$ where the subscript $n_1 n_2$ is dropped and $\mathbf{S}_{n_1\pm 1, n_2\pm 1} = \mathbf{S}(\boldsymbol{\mu},\tau)$. Substituting Eq. (2.67) into the equation of motion (Eq. (2.63)) gives,

$$\omega^2 A\mathbf{M}\frac{d^2\mathbf{S}(\tau)}{d\tau^2}\widetilde{\boldsymbol{q}} - \boldsymbol{f}_{\boldsymbol{NL}}(A,\boldsymbol{\mu},\tau,\widetilde{\boldsymbol{q}}) = \mathbf{0}, \tag{2.70}$$

where $\boldsymbol{f}_{\boldsymbol{NL}}(\mathrm{A},\boldsymbol{\mu},\tau,\widetilde{\boldsymbol{q}})$ denotes the functional dependency on the propagation vector $\boldsymbol{\mu}$ and the components of the augmented amplitude vector $\widetilde{\boldsymbol{q}}$. Equation (2.70) represents a system of coupled nonlinear differential equations in the non-dimensional time τ.

Its reduction from a differential form to algebraic form is performed through Galerkin's projection [55, 57] in the following way,

$$\int_0^{2\pi}\mathbf{S}^T(\tau)\left(\omega^2 A\mathbf{M}\frac{d^2\mathbf{S}}{d\tau^2}\widetilde{\boldsymbol{q}} - \boldsymbol{f}_{NL}(A,\boldsymbol{\mu},\tau,\widetilde{\boldsymbol{q}})\right)d\tau = \mathbf{0}. \tag{2.71}$$

The inertial force represented by the first term and the nonlinear force vector $\boldsymbol{f_{NL}}(\mathrm{A}, \boldsymbol{\mu}, \tau, \tilde{\boldsymbol{q}})$ are now transformed to be independent of non-dimensional time τ, therefore Eq. (2.71) can be written as,

$$\omega^2 A\langle \mathbf{M} \rangle \tilde{\boldsymbol{q}} - \langle \boldsymbol{f}_{NL}(A, \boldsymbol{\mu}, \tilde{\boldsymbol{q}}) \rangle = \mathbf{0}, \tag{2.72}$$

where

$$\langle \mathbf{M} \rangle = \int_0^{2\pi} \left(\mathbf{S}^T(\tau) \mathbf{M} \frac{d^2 \mathbf{S}(\tau)}{d\tau^2} \right) d\tau, \tag{2.73}$$

and

$$\langle \boldsymbol{f}_{NL}(A, \boldsymbol{\mu}, \tilde{\boldsymbol{q}}) \rangle = \int_0^{2\pi} \left(\mathbf{S}^{\mathrm{T}}(\tau) \boldsymbol{f}_{NL}(A, \boldsymbol{\mu}, \tau, \tilde{\boldsymbol{q}}) \right) \mathrm{d}\tau, \tag{2.74}$$

2.6.3 SOLUTION USING NEWTON'S METHOD

Equation (2.72) represents a set of $2NM$ nonlinear algebraic equations solved for $\tilde{\boldsymbol{q}}$ which contains the unknown coefficients $[c_{11}\, s_{11} \ldots c_{M1}\, s_{M1} \ldots c_{1N}\, s_{1N} \ldots c_{MN}\, s_{MN}]^{\mathrm{T}}$. As $\tilde{\boldsymbol{q}}$ is normalized such that one of the coefficients is equal to 1, the number of unknowns in $\tilde{\boldsymbol{q}}$ reduces to $2NM - 1$. Additional unknowns in Eq. (2.72) are the frequency of the wave ω, the wave amplitude A and the non-dimensional wave vector $\boldsymbol{\mu}$. This increases the number of unknown variables to $2NM + 1 + \dim(\boldsymbol{\mu})$ where $\dim(\boldsymbol{\mu})$ denotes the dimension of the wave vector. In the case of 2D lattice, $\dim(\boldsymbol{\mu}) = 2$.

The objective is to obtain dispersion relations which relate the frequency ω and propagation vector $\boldsymbol{\mu}$ satisfying Eq. (2.72). Hence, the procedure calls for fixing the values of the propagation vector $\boldsymbol{\mu}$ and the wave amplitude A so that the number of unknowns is reduced to $2NM$. Therefore Eq. (2.72) can be solved using any Newton-like method [58, 59] (Newton-Raphson) or any gradient-secant method to obtain frequency ω for a given propagation vector $\boldsymbol{\mu}$ and wave amplitude A. For the present study, the Newton-Raphson procedure is implemented to solve Eq. (2.72). The basic algorithm is detailed as follows:

1. Specify total number of harmonics M in the displacement approximation, the wave amplitude A and the propagation vector $\boldsymbol{\mu}$.
2. Calculate $\mathbf{S}(\tau)$ and the transformed mass matrix $\langle\mathbf{M}\rangle$.
3. Assuming that the amplitude vector $\tilde{\boldsymbol{q}}$ is normalized such that its first component is unity, then $c_{11} = 1$ and $\boldsymbol{x} = [\omega\ s_{11} \dots c_{M1}\ s_{M1} \dots c_{1N}\ s_{1N} \dots c_{MN}\ s_{MN}]^{\mathrm{T}}$ is the unknown vector to be solved. The solution to the linearized problem is a good estimate for $\boldsymbol{x}^{(0)}$ where the superscript indicates the number of iteration. The linear solution generates the frequency ω_0 and mode vector $\mathbf{u}_0$. The initial values of $s_{11}\ c_{12}\ s_{12} \dots c_{1N}\ s_{1N}$ corresponding to $M = 1$ can be determined from the linear mode vector and the rest of the variables in $\boldsymbol{x}^{(0)}$ can be set to 0. For example, for $N = 2$, let the mode vector and frequency for a specific wave-vector $\boldsymbol{\mu}$ of the linearized model be equal to $\mathbf{u}_0$ and ω_0. Then, $\left[c_{11}^{(0)}\ c_{12}^{(0)}\right] = Re(\mathbf{u}_0)$ and $\left[s_{11}^{(0)}\ s_{12}^{(0)}\right] = Im(\mathbf{u}_0)$ where Re and Im denote real and imaginary parts respectively. Therefore for $N = 2$ and $M = 2$, initial guesses of the solution can be assumed as $\boldsymbol{x}^{(0)} = [\omega_0\ s_{11}^{(0)} 0\ 0\ c_{12}^{(0)} s_{12}^{(0)}\ 0\ \ 0]^{\mathrm{T}}$.
4. Define absolute error as $\|\Delta\boldsymbol{x}\|_2 = \left\|\boldsymbol{x}^{(n)} - \boldsymbol{x}^{(n+1)}\right\|_2$ which is the Euclidean norm of the error vector Δx. This absolute error is set to a high value before the iteration begins. Depending on computational time and desired accuracy maximum allowable absolute error can be set to a fixed value denoted by $abserror_{tol}$. The value of $abserror_{tol}$ depends largely on the problem at hand. For the present problem, ω_0 which is of the order 10^3 is much larger than the rest of the unknown amplitude coefficients which are of the order 10^0, therefore for the present problem accurate results are obtained by setting $abserror_{tol} \leq 10^{-4}$.
5. Check if $\|\Delta\boldsymbol{x}\|_2 < abserror_{tol}$, if yes proceed to step 11, if no proceed to step 6.
6. Extract frequency ω and form the amplitude vector $\tilde{\boldsymbol{q}}$ from $\boldsymbol{x}^{(n)}$

7. Compute $\boldsymbol{f}\left(\boldsymbol{x}^{(n)}\right) = \omega^2 \mathrm{A}\bar{\mathbf{M}}\tilde{\boldsymbol{q}} - \langle \boldsymbol{f}_{NL}(\mathrm{A}, \boldsymbol{\mu}, \tilde{\boldsymbol{q}})\rangle$
8. Calculate Jacobian $\mathbf{J}(\boldsymbol{x}^{(n)}) = \frac{\partial \boldsymbol{f}(\boldsymbol{x}^{(n)})}{\partial \boldsymbol{x}}$ resulting in a $N \times N$ matrix. Methods to numerically compute the Jacobian matrix can be found in [60].
9. Proceed to the new solution $\boldsymbol{x}^{(n+1)} = \boldsymbol{x}^{(n)} - \left[\mathbf{J}(\boldsymbol{x}^{(n)})\right]^{-1} \boldsymbol{f}(\boldsymbol{x}^{(n)})$
10. Compute error $\boldsymbol{x}^{(n)} - \boldsymbol{x}^{(n+1)}$ and go to Step 5.
11. The solution is converged. $\boldsymbol{x}^{(n)}$ is the approximate solution to Eq. (2.72) and the frequency ω and the amplitude vector $\tilde{\boldsymbol{q}}$ can be extracted from $\boldsymbol{x}^{(n)}$.

2.7 CONCLUSIONS

The present chapter provided analytical tools to study wave propagation in periodic lattices. For a weakly nonlinear periodic structure, the perturbation approach predicts first order correction to linear dispersion relation which depends on the nonlinear interaction and the magnitude of wave amplitude. This methodology is presented in a general manner so that the approach can be applied to any nonlinear periodic structure which is discretized using Finite elements. To handle strongly nonlinear periodic structures, the harmonic balance method is presented along with the algorithm to solve for the dispersion using Newton's method. As the solution in this case does not assume any asymptotic expansion away from the linear solution, the technique becomes a powerful tool to analyze wave dispersion in strongly nonlinear systems. Analytical tools detailed in this chapter are applied to study dispersion in some example nonlinear periodic structures documented in the following chapters.

CHAPTER III

WEAKLY NONLINEAR ONE-DIMENSIONAL PERIODIC CHAINS

3.1 OVERVIEW

The present chapter documents wave propagation in nonlinear 1D periodic chain to investigate the effect of wave amplitude and nonlinearity on dispersion properties. A vast number of physical systems in scientific fields such as nano-technology, optics, crystallography, micro-mechanical systems can be modeled as one-dimensional (1D) periodic chains. Theoretical as well as experimental studies on physical systems modeled as 1D chains are for example reported in [8, 61-63]. Simplified nonlinear spring-mass models provide a convenient setting introducing nonlinearities in the structure and provide qualitative understanding of associated dispersion phenomena. Three examples exhibiting different band structures are presented and the general perturbation approach detailed in chapter 2 is applied to predict the first order effects and variations in wave propagation characteristics. Numerical estimation of propagation constants is also presented and compared with analytical predictions.

3.2 DISPERSION ANALYSIS OF EXAMPLE CHAINS

3.2.1 NONLINEAR MONO-ATOMIC CHAIN

Consider a mono-atomic chain as depicted in Figure 6. The unit cell consists of only one mass with an attached linear and nonlinear (cubic) spring.

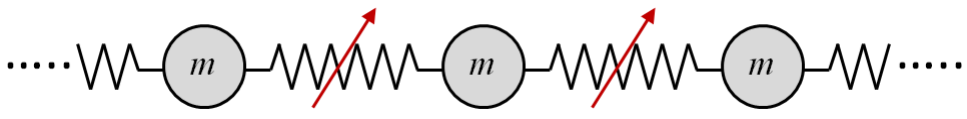

Figure 6: Nonlinear mono-atomic chain

A single degree of freedom represents the longitudinal motion of each mass. The nonlinear force interaction can be described as,

$$f = k\delta + \Gamma\delta^3 \tag{3.1}$$

where δ denotes the relative displacement between the two masses. As the system considered is one-dimensional, in relation to Eq. (2.2), $n_2 = 0$ and the 9-cell assembly reduces to the 3-cell assembly shown in Figure 7. Accordingly the notation $\mathbf{u}_{n_1,n_2}$ is changed to u_{n_1} as the generalized coordinate is a scalar value.

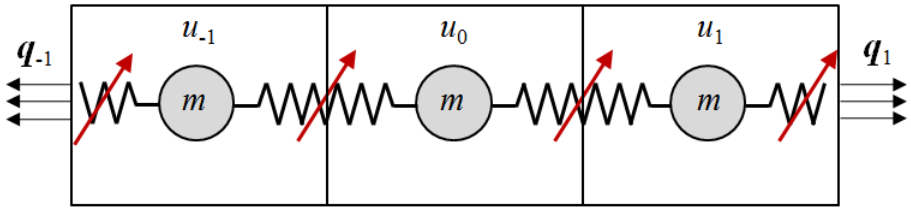

Figure 7: 3-cell assembly of nonlinear mono-atomic chain indicating internal forces on the boundary

The equation of the motion of 3-cell assembly is given by,

$$\begin{bmatrix} m & 0 & 0 \\ 0 & m & 0 \\ 0 & 0 & m \end{bmatrix} \begin{Bmatrix} \ddot{u}_{-1} \\ \ddot{u}_0 \\ \ddot{u}_1 \end{Bmatrix} + \begin{bmatrix} k & -k & 0 \\ -k & 2k & -k \\ 0 & -k & k \end{bmatrix} \begin{Bmatrix} u_{-1} \\ u_0 \\ u_1 \end{Bmatrix} + \begin{Bmatrix} f_{NL_{-1}} \\ f_{NL_0} \\ f_{NL_1} \end{Bmatrix} = \begin{Bmatrix} q_{-1} \\ 0 \\ q_1 \end{Bmatrix}. \tag{3.2}$$

Following the general outline described in chapter 2 to arrive at equations of motion for representative unit cell, the mass matrix can be identified as,

$$\mathbf{M} = m \tag{3.3}$$

The linear stiffness matrices are given by,

$$\mathbf{K}^{(p,q)} = -k \quad \forall\, p = \pm 1, q = 0, \tag{3.4}$$

$$\mathbf{K}^{(0.0)} = 2k\ . \tag{3.5}$$

Finally the nonlinear interaction is given by,

$$f_{NL} = \sum_{p=\pm1,q=0} \Gamma\left(u_{0,0} - u_{p,q}\right)^3. \tag{3.6}$$

where k and Γ are the linear and nonlinear spring coefficients.

Assuming free wave propagation, the external force on the unit cell can be neglected $\boldsymbol{f}_{n_1}^{ext}(\tau) = 0$ in Eq. (2.36), and the Bloch theorem is applied to ε^0 order equation (Eq. (2.36)) which results in the eigenvalue problem described by Eq. (2.20). The wavenumber reduced stiffness matrix (Eq. (2.20)) is given by,

$$\widetilde{\mathbf{K}}(\mathbf{k}) = 2k(1 - \cos(\mu)). \tag{3.7}$$

There exists only one branch corresponding to the above scalar $\mathbf{M}$ (mass) and $\widetilde{\mathbf{K}}(\mathbf{k})$ (stiffness) values. The following characteristic equation,

$$\omega_0^2 m - 2k(1 - \cos(\mu)) = 0, \tag{3.8}$$

is solved for the frequency leading to the linear dispersion relation

$$\omega_{0,1}(\mathbf{k}) = \sqrt{2k(1 - \cos(\mu))/m}. \tag{3.9}$$

Next step involves expressing the nonlinear force interaction in terms of Fourier series (Eq. (2.44)). The scalar term c_1 is analytically evaluated and is given by,

$$c_1 = \frac{3}{4}|A_0|^3(\Gamma\cos(2\mu) - 4\Gamma\cos(\mu) + 3\,\Gamma), \tag{3.10}$$

where A_0 denotes the wave amplitude. Since the system has a single degree of freedom the normalized wave mode described in Eq. (2.23) is reduced to $\mathrm{u}_{0,1}(\mathbf{k}) = 1$, and Eq. (2.59) results in the first order frequency correction,

$$\omega_{1,1} = 3|A_0|^2(\Gamma\cos(2\mu) - 4\Gamma\cos(\mu) + 3\,\Gamma)/4m\omega_{0,1}. \tag{3.11}$$

Hence the nonlinear dispersion relation for the one-dimensional mono-atomic chain is,

$$\omega = \omega_{0,1} + \varepsilon\left(3|A_0|^2(\Gamma\cos(2\mu) - 4\Gamma\cos(\mu) + 3\Gamma)/4m\omega_{0,1}\right) + O(\varepsilon^2). \tag{3.12}$$

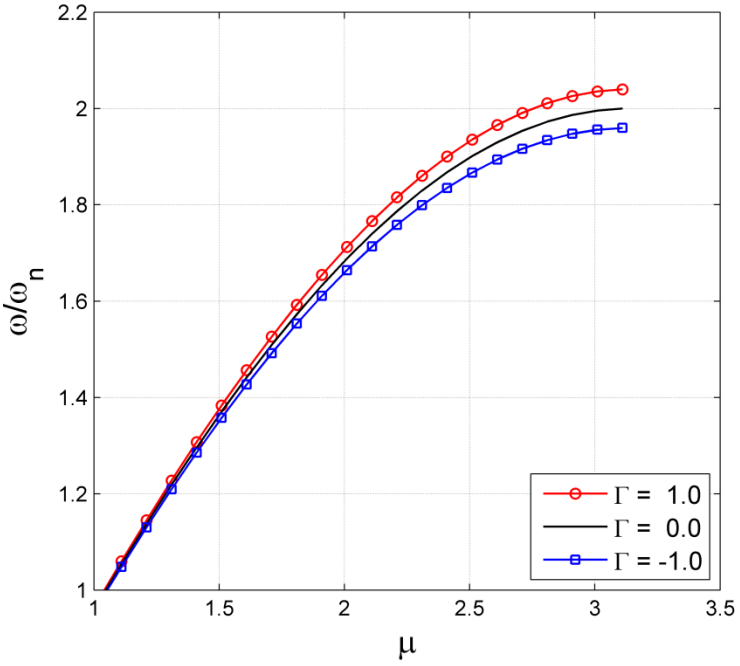

Figure 8: Dispersion behavior of nonlinear mono-atomic chain with increasing amplitude predicted by perturbation analysis

Figure 8 depicts the dispersion predicted by perturbation analysis with change in amplitude. The perturbation analysis is valid only for small wave amplitudes and the result demonstrated by Figure 8 is generated by setting the wave amplitude A to 3.0 to show a significant shift in dispersion. The frequency is non-dimensionalized with respect to the frequency $\omega_n = \sqrt{k/m}$. Squaring Eq. (3.11) and neglecting order ε^2 terms, the resulting equation can be easily solved for complex non-dimensional wavenumber in terms of wave frequency. Real part of this complex wavenumber defines propagation constant as it equals the phase shift of the two consecutive vibrating masses. The imaginary part introduces a reduction in amplitude of vibrating mass thereby introducing the attenuation in the wave profile and therefore represents the attenuation constant.

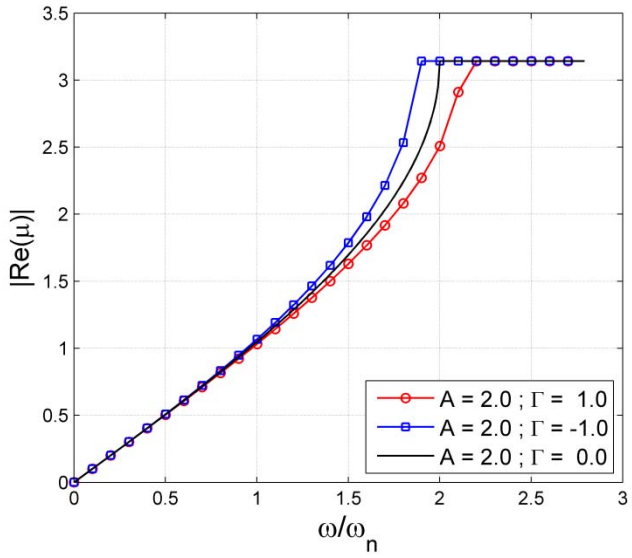

Figure 9: Propagation constant versus frequency for a nonlinear mono-atomic chain

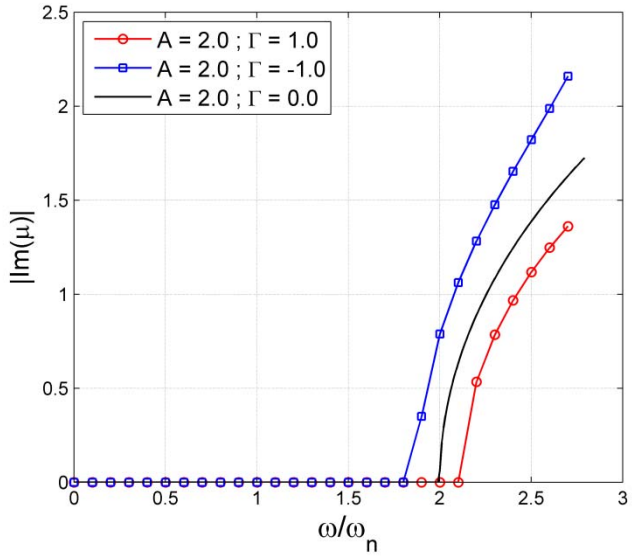

Figure 10: Attenuation constant versus frequency for nonlinear mono-atomic chain

Figure 9 and Figure 10 present the variation of propagation and attenuation constants with respect to the non-dimensional frequency. For a hard chain, the cutoff frequency increases with increase in wave amplitude and nonlinear stiffness parameter Γ, whereas the soft chain's cutoff frequency decreases with increasing wave amplitude and

nonlinear stiffness parameter Γ. For a softening chain, one can consider this cut-off frequency as a *saturation cut-off frequency*. Consider a frequency in the attenuation zone of a high amplitude wave close the cut-off frequency. As the frequency lies in the AZ, the wave amplitude decreases and this affects the bandstructure (Figure 8) resulting in an increase in cut-off frequency for a softening chain as predicted by the above analysis. Therefore as the amplitude dies down, cut-off frequency increases and the frequency of the wave enters the propagation zone (towards the edge of Brillouin zone) with saturated wave amplitude. Hence the term *saturated cut-off* frequency or *saturated bandgap* for a softening chain.

The dispersion in a weakly nonlinear system can be predicted by harmonic balance method as laid out in section 2.6. The linear and nonlinear restoring forces are lumped into one nonlinear restoring force given by,

$$\boldsymbol{f}_{\boldsymbol{NL}}\left(\mathbf{u}_{n_1 n_2}, \mathbf{u}_{n_1 \pm 1, n_2 \pm 1}\right) = \sum_{p=\pm 1, q=0} \left[k\left(u_{0,0} - u_{p,q}\right) + \Gamma\left(u_{0,0} - u_{p,q}\right)^3\right], \qquad (3.13)$$

and the solution procedure follows the transformation on differential equations to nonlinear algebraic equations using Galerkin's projection and implementing Newton's method. The comparison between the predictions by two approaches is shown in Figure 11. The harmonic balance is in excellent agreement with the result obtained from perturbation analysis. The red line in the plot indicates the hardening chain at $A = 3.0$ and the blue indicates the dispersion of a softening chain at the same amplitude.

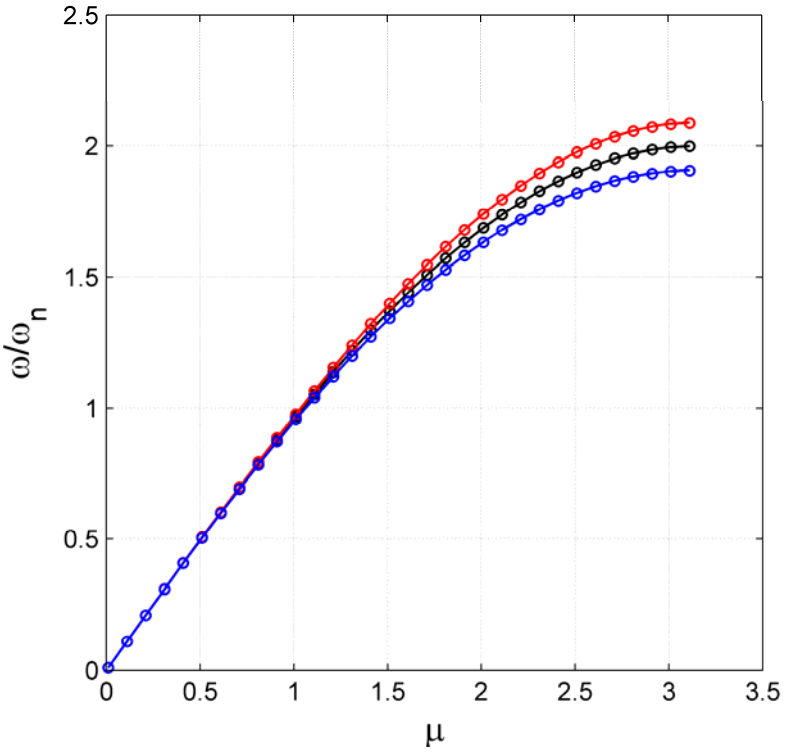

Figure 11: Dispersion predicted by — Perturbation analysis vs. ○ Harmonic balance method

3.2.2 NONLINEAR MONO-ATOMIC CHAIN ON A FOUNDATION

Consider next a mono-atomic chain with nonlinear ground-springs with a unit cell as depicted in Figure 12. Considering only longitudinal displacements, the equation of motion of a representative unit cell can be expressed as a particular case of Eq. (2.32), with $n_2 = 0$ and the mass matrix reduces to scalar quantity,

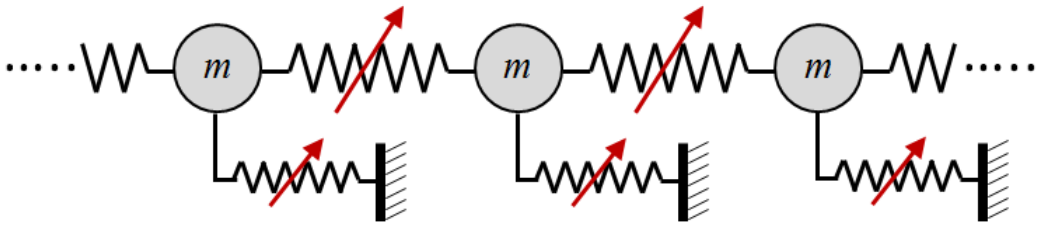

Figure 12: Nonlinear mono-atomic chain on nonlinear support

$$\mathbf{M} = m \tag{3.14}$$

The partitioned stiffness and nonlinear force vector describing the above the system are detailed below,

$$\mathbf{K}^{(p,q)} = -k \quad \forall\, p = \pm 1, q = 0, \tag{3.15}$$

$$\mathbf{K}^{(0,0)} = k(2 + \alpha), \tag{3.16}$$

and the nonlinear force interaction is described as,

$$\boldsymbol{f_{NL}} = \sum_{p=\pm 1, q=0} \Gamma\left(u_{0,0} - u_{p,q}\right)^3 + \beta\Gamma\left(u_{0,0}\right)^3, \tag{3.17}$$

where k and Γ are the linear and nonlinear spring stiffness between two adjacent masses along the chain, α denotes the ratio of linear ground stiffness to the linear inter-mass stiffness and β represents the ratio of nonlinear (cubic) ground stiffness to the nonlinear inter-mass stiffness.

Following the same procedure described in chapter 2, the two ordered equations are obtained which are in the form described by Eqs. (2.36) and (2.37). The Bloch theorem is applied to ε^0 equation resulting in an eigenvalue problem (Eq. (2.20)) with mass matrix given by Eq. ((3.14)) and reduced wavenumber stiffness matrix given by,

$$\widetilde{\mathbf{K}}(\mathbf{k}) = k(2 + \alpha - \cos(\mu)), \tag{3.18}$$

where k is the linear stiffness between the masses and α denotes the ratio of linear ground stiffness to the linear inter-mass stiffness. The solution of the eigenvalue problem (Eq. (2.20)) leads to the following linear dispersion relation,

$$\omega_{0,1}(\mathbf{k}) = \sqrt{k(2 + \alpha - \cos(\mu))/m}. \tag{3.19}$$

The nonlinear force interaction is then expressed in terms of Fourier series (Eq. (2.44)) and the term coefficient of the first harmonic c_1 is evaluated analytically,

$$c_1 = \frac{3}{4}|A_0|^3\Gamma(\cos(2\mu) - 4\cos(\mu) + 3 + \beta). \tag{3.20}$$

where β represents the ratio of nonlinear (cubic) ground stiffness to the nonlinear inter-mass stiffness. Next, the normalized wave mode can be assumed as $u_1^{(0)}(\mathbf{k}) = 1$ (single degree of freedom) and Eq. (2.59) leads to corrected frequency,

$$\omega_{1,1} = 3|A_0|^2\Gamma(\cos(2\mu) - 4\cos(\mu) + 3 + \beta)/4m\omega_{0,1}. \tag{3.21}$$

Hence, the nonlinear dispersion relation for mono-atomic chain on nonlinear support is,

$$\omega = \omega_{0,1} + \varepsilon\left(3|A_0|^2\Gamma(\cos(2\mu) - 4\cos(\mu) + 3 + \beta)/4m\omega_{0,1}\right) + O(\varepsilon^2). \tag{3.22}$$

Figure 13 shows the dispersion trend predicted by the perturbation approach (to see a significant trend the value of A is set to 3.0) with frequency normalized by $\omega_n = \sqrt{k/m}$. The system behaves similarly to the nonlinear mono-atomic chain, but acts like a pass-band filter due to the presence of a lower cutoff frequency which is parameterized by the base stiffness. Propagation and attenuation constants as functions of frequency are plotted in Figure 14 and Figure 15, while Table 1 summarizes the qualitative effect of amplitude and nonlinear stiffness parameter Γ on cutoff frequencies. As the lower cutoff frequency is dependent primarily on the ground spring stiffness and upper cutoff frequency is dependent on intermass stiffness, a hard base with soft intermass stiffness decreases the pass band with increasing amplitude.

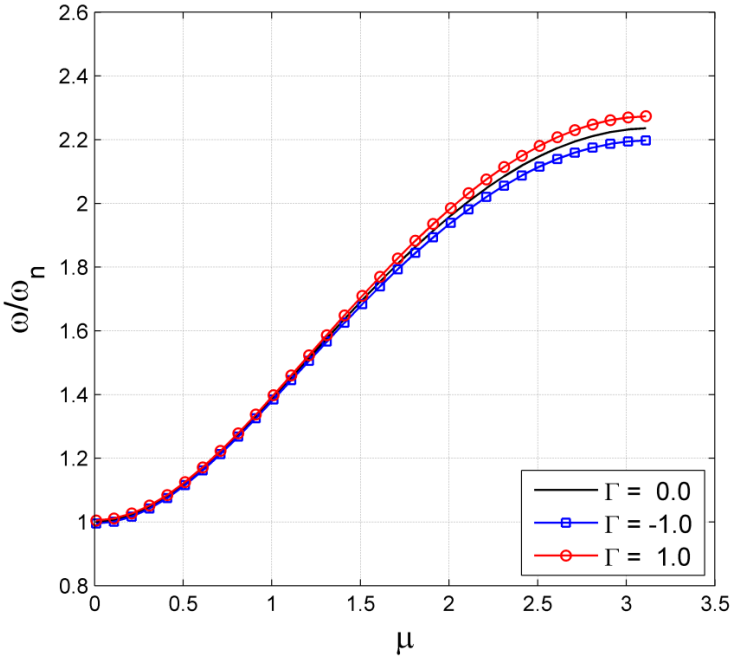

Figure 13: Dispersion of nonlinear mono-atomic chain with attached nonlinear base with increasing amplitude predicted by perturbation analysis

For a chain different permutations in ground and inter-mass stiffness are possible. Table 1 describes the direction of shift in cutoff frequencies for all such combinations.

Table 1: Effect of amplitude and nonlinearity on cutoff frequencies

Intermass	*Ground spring*	*Amplitude and nonlinear*	*Upper cutoff*	*Lower cutoff*
Hard	Hard	Increase	Increase	Increase
Soft	Soft	Increase	Decrease	Decrease
Hard	Soft	Increase	Increase	Decrease
Soft	Hard	Increase	Decrease	Increase

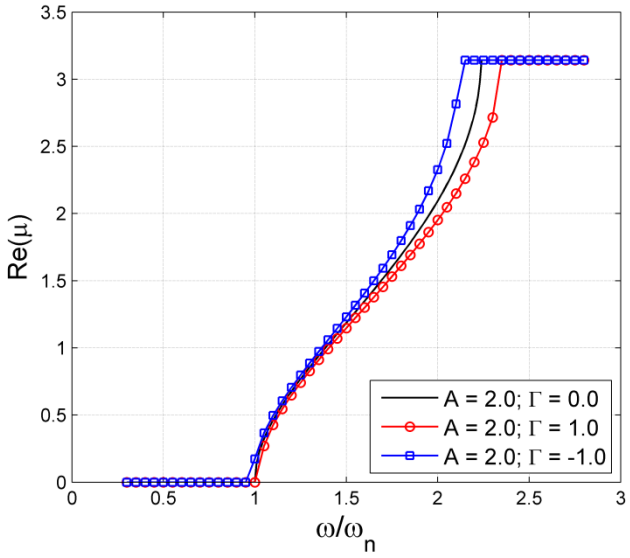

Figure 14: Propagation constant versus frequency of the wave for a nonlinear mono-atomic chain on nonlinear base

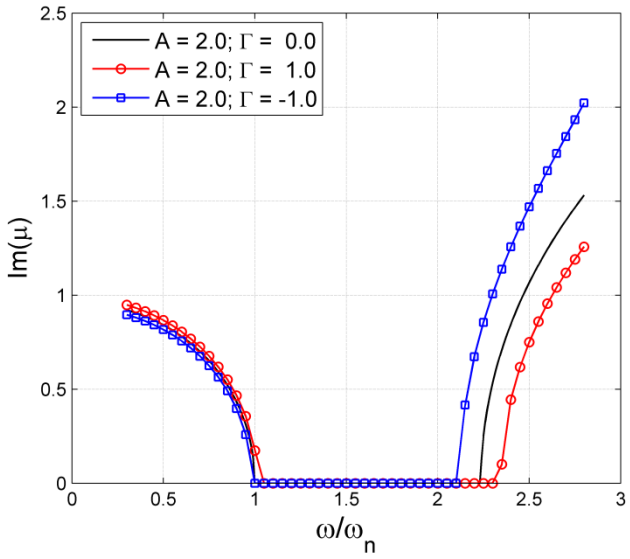

Figure 15: Attenuation constant versus frequency of the wave for a nonlinear mono-atomic chain on nonlinear base

3.2.3 DIATOMIC CHAIN

A diatomic chain consists of two different masses per unit cell, as shown in Figure 16. Linear diatomic chains behave as stop-band filters in which a centered frequency band does not permit wave propagation. The stop band exists due to the presence of two

dispersion curve branches (a lower *acoustic* branch and an upper *optical* branch) separated due to the impedance mismatch of the two spring-mass sub-systems. Note that as the plane-wave frequency approaches the acoustic cut-off frequency, the lighter masses in the chain rest with phase difference reaching $\pi/2$. Alternatively, as the frequency approaches the optical cut-off frequency, the heavier masses rest [64] as the phase difference tends to $\pi/2$. The unit cell depicted in Figure 16 contains two masses m_1 and m_2. The out of plane displacements of the two masses m_1 and m_2 define the two degrees of freedom of the unit cell.

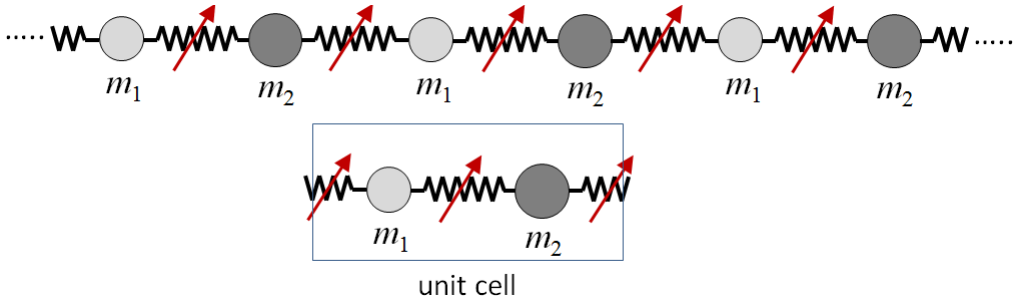

Figure 16: Schematic of a nonlinear diatomic chain depicting unit cell

The mass matrix of the unit cell is,

$$\mathbf{M} = \begin{bmatrix} m_1 & 0 \\ 0 & m_2 \end{bmatrix} \tag{3.23}$$

The partitioned stiffness matrices and nonlinear force interaction is detailed below. The linear stiffness matrices are given by,

$$\mathbf{K}^{(-1,0)} = \begin{bmatrix} 0 & -k \\ 0 & 0 \end{bmatrix}, \tag{3.24}$$

$$\mathbf{K}^{(0,0)} = \begin{bmatrix} 2k & -k \\ -k & 2k \end{bmatrix}, \tag{3.25}$$

$$\boldsymbol{K}^{(1,0)} = \begin{bmatrix} 0 & 0 \\ -k & 0 \end{bmatrix}. \tag{3.26}$$

and the nonlinear force interaction is described by,

$$\mathbf{f_{NL}} = \begin{bmatrix} \Gamma\left(\left(u_{1_{0,0}} - u_{2_{0,0}}\right)^3 + \left(u_{1_{0,0}} - u_{2_{-1,0}}\right)^{\mathbf{3}}\right) \\ \Gamma\left(\left(u_{2_{0,0}} - u_{1_{0,0}}\right)^3 + \left(u_{2_{0,0}} - u_{1_{1,0}}\right)^{\mathbf{3}}\right) \end{bmatrix} \tag{3.27}$$

where k and Γ are the linear and nonlinear spring stiffness between two adjacent masses along the chain. u_1 and u_2 denote longitudinal displacement representing the two degrees of freedom of the unit cell. The reduced wavenumber stiffness matrix is given as,

$$\widetilde{\mathbf{K}}(\mathbf{k}) = \begin{bmatrix} 2k & -k\left(1 + e^{-i\mu}\right) \\ -k\left(1 + e^{i\mu}\right) & 2k \end{bmatrix} \tag{3.28}$$

The linear modes are obtained by solving the eigenvalue problem described by Eq. (2.20) involving mass and reduced stiffness matrices defined by Eqs. (3.23) and (3.28). Next, the procedure to evaluate the first order correction to the dispersion relation follows the general procedure detailed in chapter 2. The wave modes are normalized and the vector c_1 is evaluated which is subsequently used in Eq. (2.59) to calculate the frequency correction at each wavenumber. Figure 17 plots the dispersion trend for the two modes predicted by the perturbation analysis. Frequency is normalized by the natural frequency $\omega_{n1} = \sqrt{k/m_1}$ and mass ratio $m_1/m_2 = 0.5$ is used to generate the dispersion curves shown in Figure 17. For a hard diatomic chain, the behavior of the band gap is such that the lower bound as well as the upper bound of the band gap increases for increasing amplitude. A soft diatomic chain does exactly the opposite where both the bounds decrease with increase in amplitude.

Table 2 summarizes the qualitative dispersion behavior of the diatomic chain with respect to the wave amplitude and the magnitude of the nonlinear stiffness parameter. Hence, the bandgap boundaries are shown to be affected by the nonlinearity and the magnitude of wave amplitude.

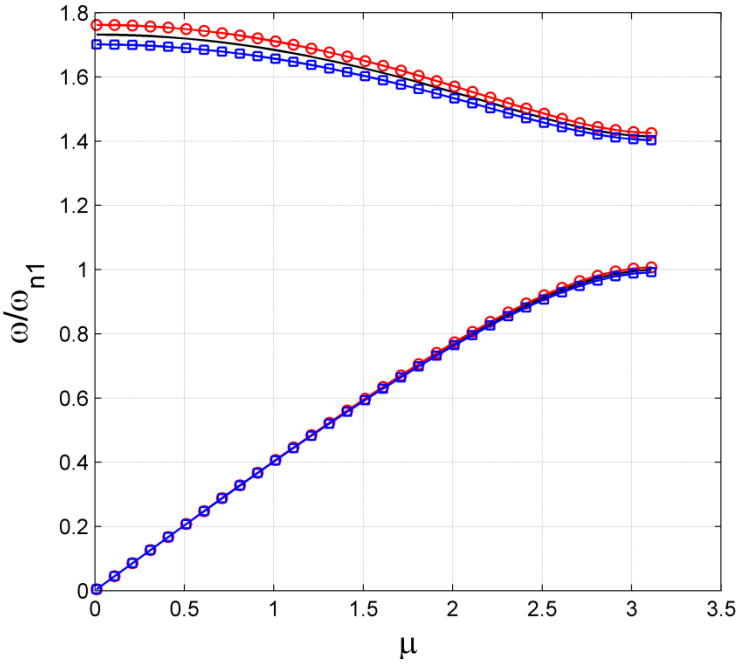

Figure 17: Dispersion trend with respect to amplitude in nonlinear diatomic chain as predicted by perturbation analysis □ $\Gamma = -1.0$, ○ $\Gamma = 1.0$, — $\Gamma = 0.0$

Table 2: Effect of amplitude and Γ on cutoff frequencies of diatomic chain

Chain	*Amplitude and Nonlinear stiffness*	*Optical Mode Upper cutoff*	*Optical Mode Lower cutoff*	*Acoustic Mode*
Hard	Increase	Increase	Increase	Increase
Soft	Increase	Decrease	Decrease	Decrease

3.3 NUMERICAL ESTIMATION OF DISPERSION

3.3.1 WAVENUMBER ESTIMATION

The analytical dispersion expressions are verified by numerical simulation of finite mass-spring chains. As stated earlier, infinite plane wave propagation is assumed in deriving the closed form dispersion relations which are detailed in the previous sections. In the

numerical simulations, a wave is generated by harmonically exciting one mass in the chain. To simulate a non-reflecting infinite plane wave, an appropriate simulation time is chosen such that waves do not reach the boundaries of the finite lattice but a steady plane wave solution is formed in the near field (close to the point of excitation). Once the appropriate simulation time is chosen, the next step involves integrating the system of nonlinear equations using MATLAB's numerical integration routine ODE45 employing 4^{th} order Runge Kutta method. Mass displacements at different instances of time in the near field (field neighboring point of excitation) are collected to calculate the propagation constant μ. More specifically, a fast Fourier transform (FFT) of each displacement time-history is computed to reveal the phase shift. The wave number is evaluated as the phase shift slope with respect to the spatial coordinate.

The procedure is explained mathematically as follows. Let the single-frequency wave function be represented by,

$$f(x,t) = f_0 e^{i(kx-\omega_0 t)}\,. \tag{3.29}$$

Introducing a change of variable,

$$\varphi = t - x/c, \tag{3.30}$$

where $c = \omega_0/k$, the complex Fourier transform of the wave function, evaluated at ω_0, can be written as,

$$F(x,\omega_0) = \int_{-\infty}^{+\infty} f(\varphi) e^{-i\omega_0\varphi} d\varphi \left(e^{-i\frac{\omega_0}{c}x}\right), \tag{3.31}$$

Evaluation of the integral leads to the following,

$$F(x,\omega_0) = \Phi(\omega_0) e^{-ikx}, \tag{3.32}$$

where $\Phi(\omega_0) = \int_{-\infty}^{+\infty} f(\varphi) \mathrm{e}^{-i\omega_0\varphi} d\varphi$. From Eq. (3.32), it can be seen that an FFT of a mass's response in time introduces a phase shift of $-kx$. Hence, for a response at a given

frequency ω_0, variation of the phase with respect to spatial variable gives the wave number.

3.3.2 NUMERICAL VALIDATION

The procedure as detailed in the previous section is applied to finite one-dimensional nonlinear lattices to estimate the wavenumber numerically. All the three cases which include mono-atomic chain, mono-atomic chain attached to a nonlinear base and nonlinear diatomic chain are considered for numerical simulation and validation. Figure 18 presents a comparison of the analytical and numerical results for small amplitude waves in a nonlinear mono-atomic chain. The numerically estimated dispersion shift is in a very good agreement with that predicted by perturbation approach. Figure 18 displays the frequency range within the irreducible Brillouin zone where the dispersion shift is significant.

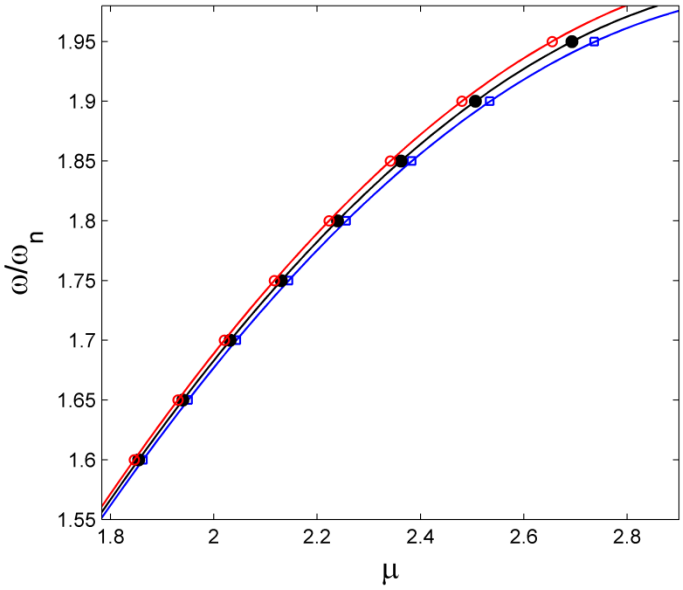

Figure 18: Numerical estimation of dispersion in nonlinear mono-atomic chain at amplitude A = 1.0 □ Numerical $\Gamma = -1.0$, ○ Numerical $\Gamma = 1.0$, ● Numerical $\Gamma = 0.0$, — Analysis

Next, a nonlinear mono-atomic chain attached to a nonlinear base is considered. Repeating the same numerical estimation approach, the wavenumbers are evaluated and compared with analytical predictions. Figure 19 demonstrates the comparison between analysis and numerical results of dispersion in nonlinear mono-atomic chain attached to a nonlinear base. For small amplitude shifts, the dispersion shifts predicted by perturbation analysis show an excellent agreement with the numerically-generated results. Next, a diatomic chain is considered. Figure 20 and Figure 21 present the numerically estimated dispersion trends for optical and acoustic modes exhibited by the considered diatomic lattice (mass ratio $\beta = 0.5$) respectively. In the small amplitude limit, the numerical results match very well with those predicted by the perturbation analysis.

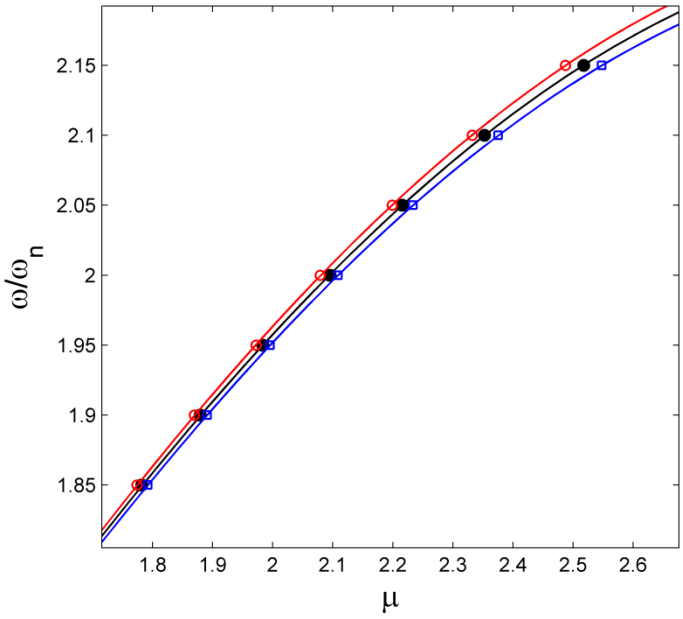

Figure 19: Numerical estimation of dispersion in nonlinear mono-atomic chain attached to a nonlinear base at amplitude $A = 1.0$, □ Numerical $\Gamma = -1.0$, ○ Numerical $\Gamma = 1.0$, ● Numerical $\Gamma = 0.0$, — Analysis

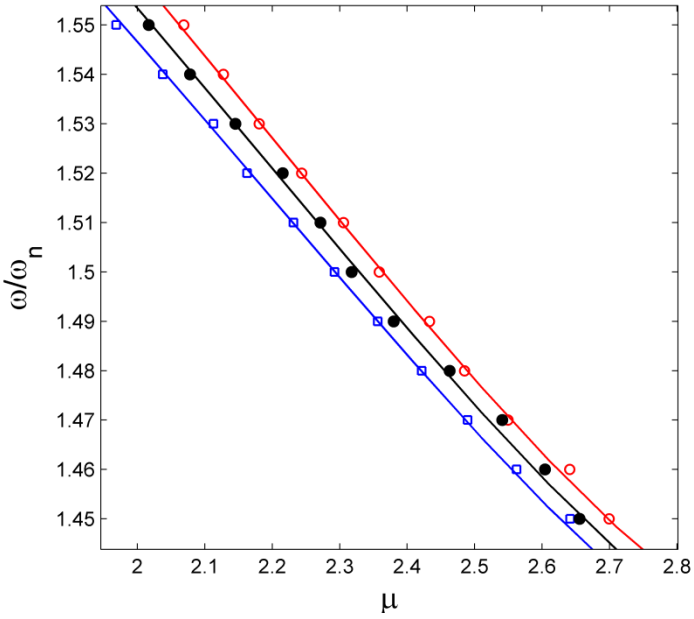

Figure 20: Numerical estimation of dispersion in optical mode of nonlinear diatomic chain at amplitude A = 1.5 , □ Numerical $\Gamma = -1.0$, ○ Numerical $\Gamma = 1.0$, ● Numerical $\Gamma = 0.0$, — Analysis

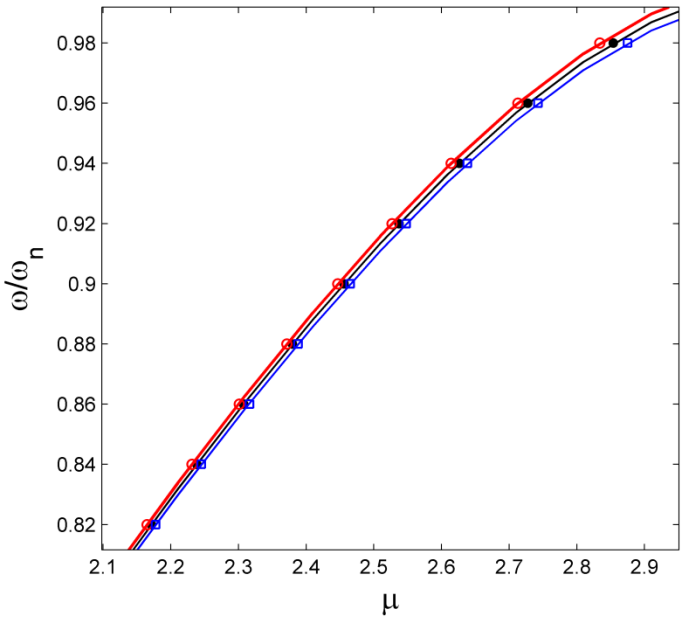

Figure 21: Numerical estimation of dispersion in acoustic mode of nonlinear diatomic chain at amplitude A = 1.5, □ Numerical $\Gamma = -1.0$, ○ Numerical $\Gamma = 1.0$, ● Numerical $\Gamma = 0.0$, — Analysis

3.4 CONCEPTUAL DEVICE DESIGN

Amplitude-dependent frequency shifts close to cut-off regions enable tunable devices based on the presented chains and unit cells. One such device is an Amplitude-dependent Frequency Isolator (ADFI) employing a nonlinear diatomic chain. The second example consists in a combination of two chains connected in series propagating waves with frequency content in a narrow band. In this example, the width of the propagated band is amplitude-dependent and hence tunable. All results presented in this section are generated using the numerical integration of the equations of motion.

3.4.1 AMPLITUDE-DEPENDENT FREQUENCY ISOLATOR

This concept describes a diatomic chain which isolates a frequency band dependent on the input signal amplitudes. The input signal consists of two frequencies close to the cut-off regions, where one is close to the lower optical cutoff, and the other is close to the acoustic cutoff frequency. Figure 22 depicts the device. The parameter space for the demonstration chain presented is given by $m = 1kg, \omega_{n1} = \sqrt{3} rads^{-1}$, mass ratio $\beta = 0.5$ and $\Gamma = 1.0$ (i.e., hardening). For the first case, with amplitude $A = 0.5$, the input signal contains frequencies $\omega = 1.5\, rads^{-1}$ (significantly-inside the acoustic propagation zone) and $\omega = 2.46\, rads^{-1}$ (just-inside the optical propagation zone).

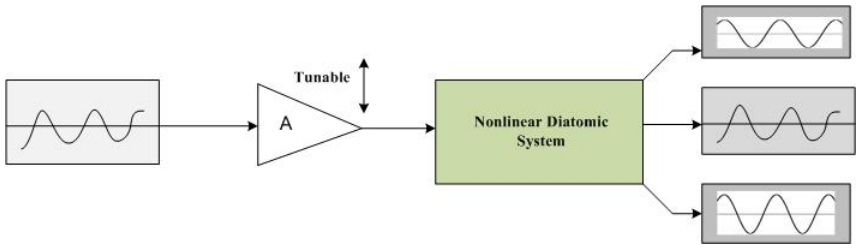

Figure 22: Schematic of an amplitude-dependent frequency isolator

Figure 23 demonstrates that at low amplitude both frequencies propagate and pass through the device. Since the chain is hardening, cut-off frequencies increase with increasing amplitude. Therefore, an increase in amplitude from $A = 0.5$ to $A = 0.75$

eliminates frequency content propagating in the optical region, while the frequency in the acoustic branch continues to propagate, as demonstrated by Figure 24.

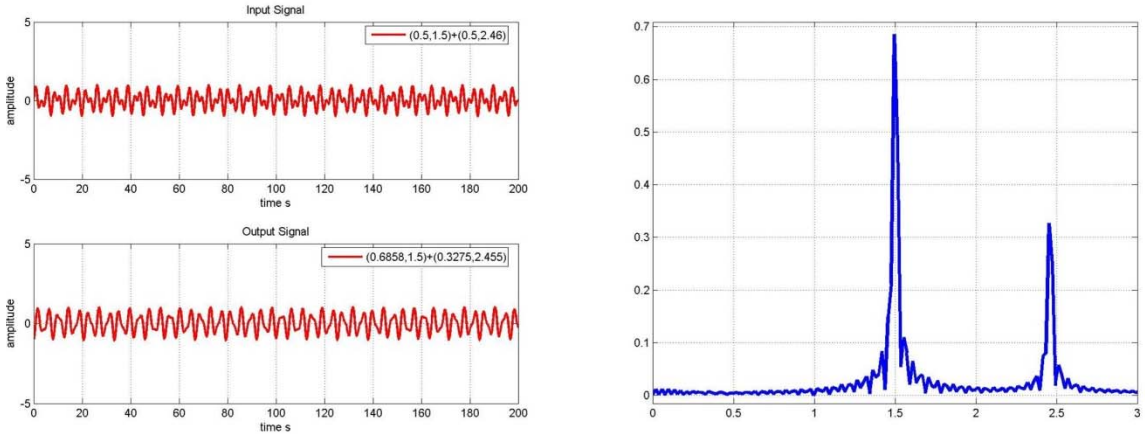

Figure 23: Input signal containing frequencies 1.50 $rads^{-1}$ and 2.46 $rads^{-1}$ at $A = 0.50$. FFT of output signal is shown on the right which depicts the existence of two input frequencies

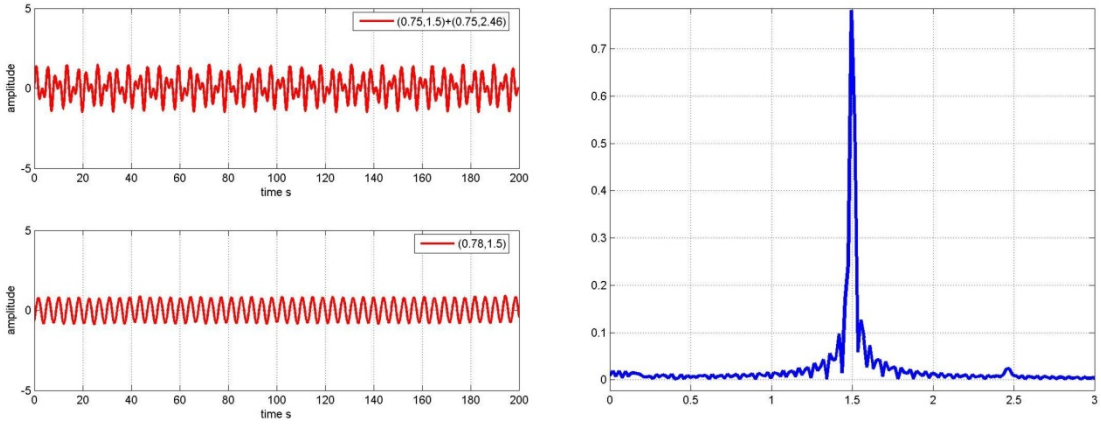

Figure 24: Input signal containing frequencies 1.50 $rads^{-1}$ and 2.46 $rads^{-1}$ at $A = 0.75$. FFT of output signal is shown on the right which depicts the elimination of high frequency content from the input signal

A second example is given for an input signal with amplitude $A = 0.70$ containing frequencies $\omega = 1.75\, rads^{-1}$ (just-inside the acoustic propagation zone) and $\omega =$

2.5 $rads^{-1}$ (significantly-inside the optical propagation zone). At this amplitude, the two frequencies pass through as shown by Figure 25.

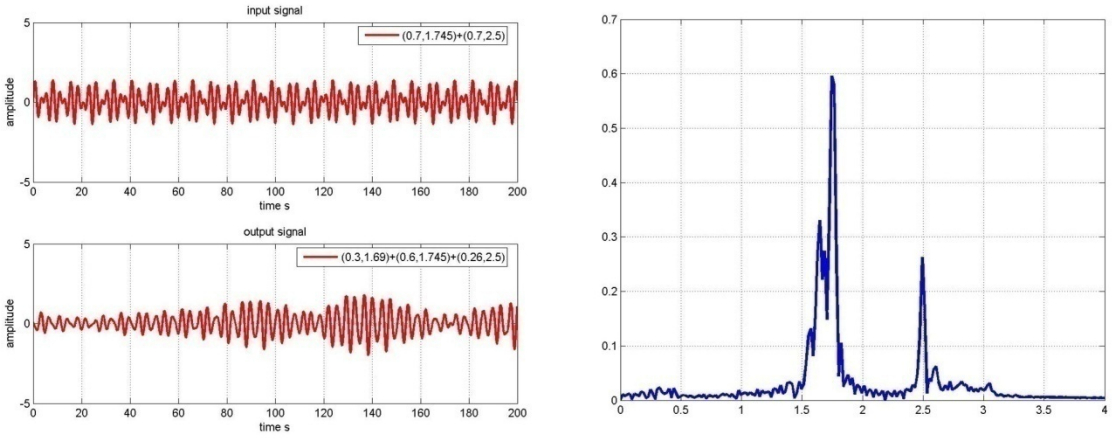

Figure 25: Input signal containing frequencies 1.75 *rads*$^{-1}$ and 2.50 *rads*$^{-1}$ at $A = 0.70$; FFT of output signal is shown on the right which depicts the existence of two input frequencies as well as a third one generated due to nonlinearity

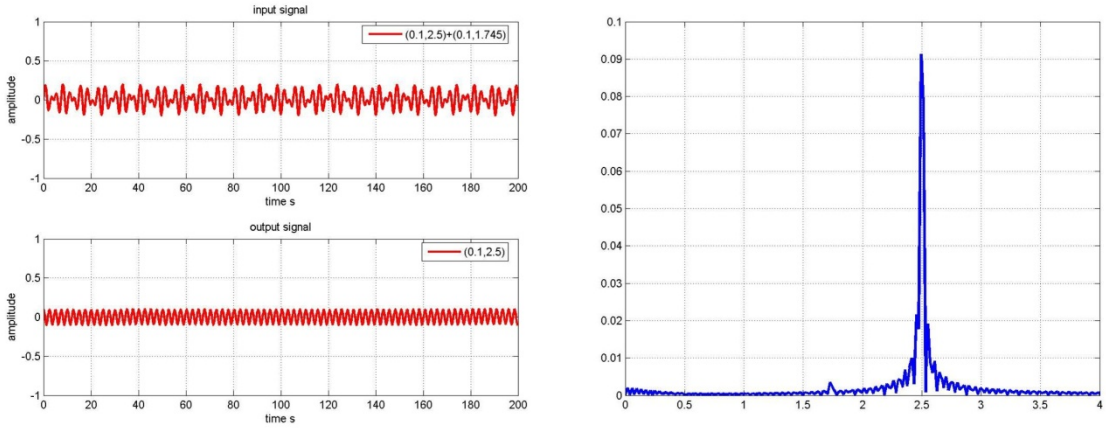

Figure 26: Input signal containing frequencies 1.75 *rads*$^{-1}$ and 2.50 *rads*$^{-1}$ at $A = 0.10$; FFT of output signal is shown on the right which depicts the elimination of lower frequency content from the actual input signal

A decrease in amplitude lowers the cutoff frequencies of the two modes in a hard chain. Hence, as the input amplitude changes from $A = 0.70$ to $A = 0.10$, the frequency

content in the acoustic stop band region is eliminated while the frequency in optical mode continues to propagate, as demonstrated by Figure 26.

3.4.2 TUNABLE NARROW-BAND PASS FILTER

This device employs two hardening chains in series: one without, and one with, grounding foundations. The combination allows the waves to propagate with frequencies limited to a very narrow bandwidth. The design of the chain with grounding foundation is such that its lower cutoff frequency is less than the cutoff frequency of the chain without foundation. This difference defines the frequency bandwidth for a wave to propagate through the designed configuration. As the amplitude increases, the cutoff frequency of the hard chain without foundation increases, thereby increasing the frequency bandwidth of the propagating wave. The bandwidth increases as the amplitude increases and decreases as the amplitude decreases. The frequency domain of this narrow band exists close to the cutoff frequency of the chain without foundation, but if a shift is desired, then material properties of the chains play a vital role. Figure 27 and Figure 28 show the schematic of the configuration and the concept respectively.

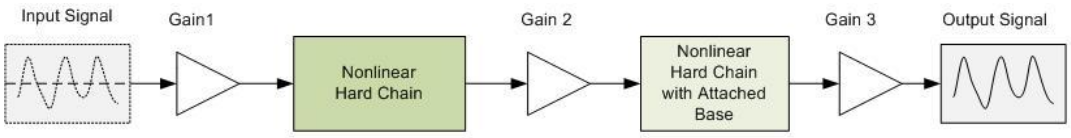

Figure 27: Schematic of tunable narrow-band pass filter

For this example, the two chains with $|\Gamma| = 1$ are considered. The input signal contains a broadband frequency content centered at the cutoff frequency ($\omega/\omega_n = 2.0$) of the hard chain without foundation. This symmetric broad band signal with a minimum leakage is generated with a *Hanning-Windowed* sinusoidal pulse. At low amplitude, the configuration lets the wave to propagate with frequency confined to a very narrow bandwidth. But as the amplitude increases, the attenuated frequency content starts to

propagate due to dispersion property of hardening chain, thereby increasing the frequency bandwidth of the propagating wave.

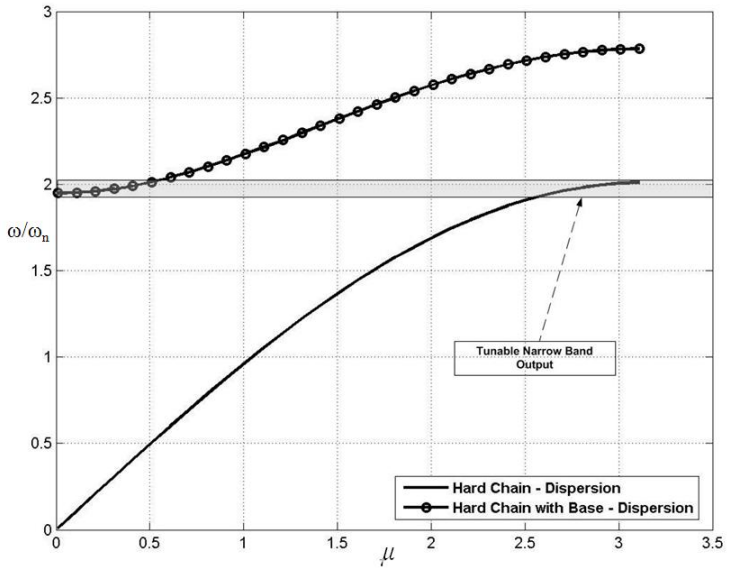

Figure 28: Schematic describing the tunable narrow band filter's output frequency regime with designed configuration

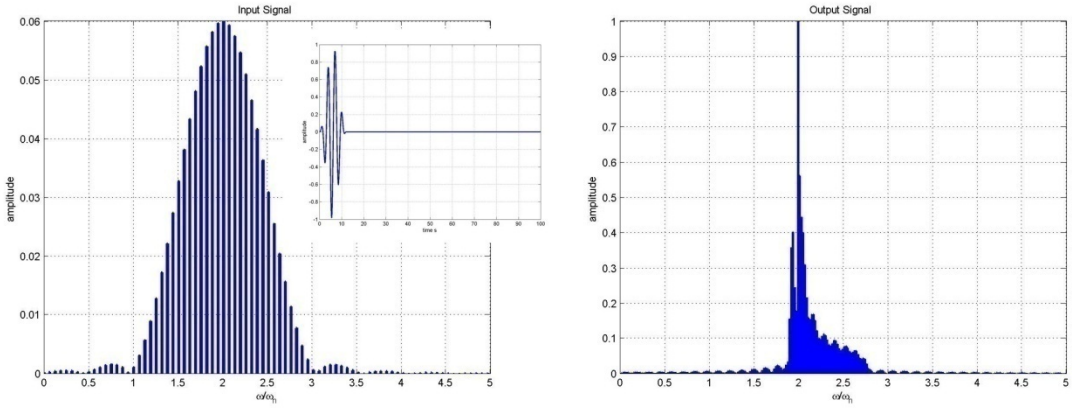

Figure 29: Input and Output signal frequency spectrum corresponding to input amplitude A = 1.0, Output signal is normalized

Figure 29 shows the input signal with peak amplitude close to 1.0 and corresponding frequency content centered at nondimensional frequency $\omega/\omega_n = 2.0$.

The corresponding output signal has a very narrow bandwidth which is shown on the right.

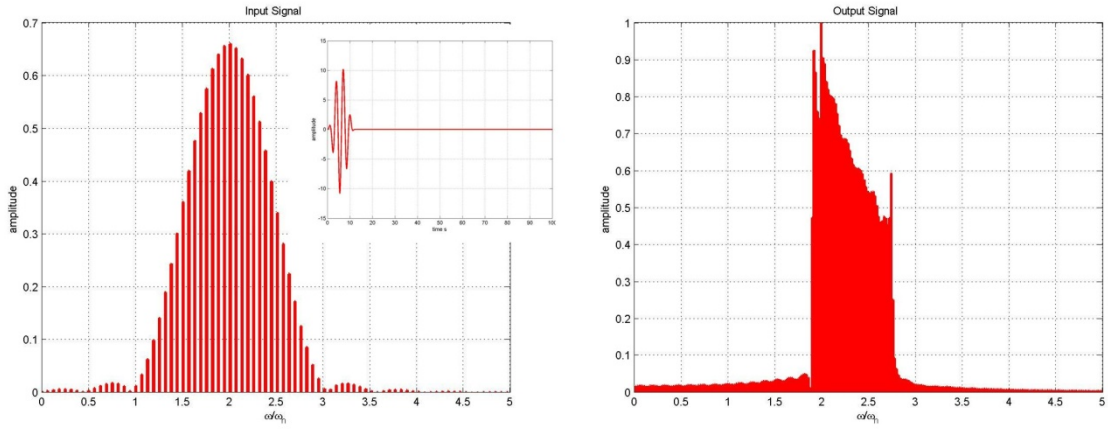

Figure 30: Input and Output signal frequency spectrum corresponding to input amplitude $A = 11.0$, Output signal is normalized

Figure 30 depicts the input signal with high amplitude with exactly same frequency content but in this case the output signal has a wider bandwidth indicating an increase in output bandwidth with increase in wave amplitude.

3.5 CONCLUSIONS

The perturbation analysis detailed in chapter 2 has been applied to predict the dispersion in one-dimensional chains modeled as finite nonlinear spring mass lattices. The dispersion predicted by approximate closed form expressions is then validated with numerical simulations. Dispersion shift due to wave amplitude and nonlinearity estimated with numerical and analytical procedures are in very good agreement. At low amplitudes, the chain systems exhibit *quasi-linear* behavior in which a single frequency plane wave propagates without introducing additional frequencies. This behavior allowed such nonlinear chains to generate amplitude-dependent frequency isolation in a signal and with a specific chain configuration produced a tunable narrow band-pass filter. Depending on the location of the frequency of the wave in such bandgap, the amplitude of the wave

propagating in a periodic chain with soft nonlinearity *saturates* to lower amplitude due to the continuous variation of the bandstructure.

CHAPTER IV

WEAKLY NONLINEAR TWO-DIMENSIONAL PERIODIC LATTICES

4.1 OVERVIEW

In general, a two-dimensional periodic lattice consists of unit cell with the cell geometry defined by two spatial coordinates. A number of physical systems are modeled as two-dimensional periodic structures. A simple bar grillage [16], stiffened shells and plates, graphene sheets at atomic level, are a few examples. A comprehensive approach to studying wave propagation in two-dimensional periodic systems is provided by Brillouin [1]. In comparison to one-dimensional periodic structures, to completely characterize the wave propagation in two-dimensional case, one of the most important parameter to be considered apart from frequency and the wavenumber is the wave direction. From the practical point of view, studying point-to-point energy transfer in a structure is important but to have a control on its direction makes it very useful. As seen in chapter 3, nonlinear periodic structures exhibit amplitude-dependent dispersion properties. Hence, the primary motivation to study wave propagation in two dimensional periodic lattices is to explore the concept of tunable wave directionality with amplitude as tuning parameter. A qualitative understanding of the effects of nonlinearity and wave amplitude on propagation characteristics and directional behavior can help design structures which focus or defocus the energy or act as tunable wave guides, etc…The present chapter discusses few example two-dimensional lattices which are modeled as spring-mass lattices. Their analysis helps the qualitative understanding of the effects of different nonlinearities on the wave dispersion properties. Dispersion in example lattices is also

estimated numerically to validate the analytical predictions and demonstrate tunable wave directional behavior.

4.2 AMPLITUDE-DEPENDENT GROUP VELOCITY

The dispersion curves obtained from the application of the general perturbation approach described in chapter 2 evaluate the wave properties of the considered nonlinear media. The dependence of dispersion on amplitude directly affects the group velocity, which suggests how the occurrence of frequencies and directions of preferential propagation may be affected by the amplitude of wave motion. The proposed perturbation approach can be used to investigate such phenomena through the straightforward evaluation of the group velocity of the nonlinear lattices under investigation. Examples of caustics generation for the class of nonlinear media considered in the present work are illustrated in the next section. Caustics are defined as frequency bands within which the response is characterized by the emergence of regions of low response ("*dead zones*") or directions along which the wave propagation is not allowed. Of note is the fact that amplitude-dependent dispersion can lead to amplitude-dependent caustics, which leads to the possibility of tuning the focusing capabilities of the medium through the modulation of the amplitude of the waves injected in the domain. For example, a lattice with isotropic linear stiffness and anisotropic nonlinear stiffness can exhibit amplitude-dependent wave directionality. This is related to the fact that at low amplitudes the nonlinear anisotropy does not affect the dynamics of the system, while as amplitude increases the nonlinearity comes into play affecting the overall isotropy of the lattice and correspondingly the energy flow patterns.

Within the perturbation approach described in this study, the group velocity corresponding to the *j*-th dispersion branch can be evaluated as,

$$\mathbf{c}_{g,j}\left(\mathbf{k}, \left|A_{0,j}\right|\right) = \boldsymbol{\nabla}\omega_{0,j}(\mathbf{k}) + \varepsilon\, \boldsymbol{\nabla}\omega_{1,j}(\mathbf{k}, \left|A_{0,j}\right|) + O(\varepsilon^2)\text{,,} \tag{4.1}$$

which explicitly indicates the dependence of the group velocity in terms of wavenumber and ampitude of wave motion.

4.3 EXAMPLE TWO-DIMENSIONAL LATTICES

4.3.1 MONO-ATOMIC LATTICE

The two-dimensional nonlinear monoatomic lattice shown in Figure 31 is modeled as an array of equal masses interconnected by springs with a linear and a cubic coefficient. Transverse (out-of-plane) displacement is the single degree of freedom describing the motion of each mass, so that the springs are assumed to act in shear with a force which is related to the relative displacements of neighboring masses [45]. The equation of motion of a representative unit cell can be expressed in a similar way to Eq. (2.33),

$$\omega^2 \mathbf{M} \frac{d^2 \mathbf{u}_{n_1,n_2}}{d\tau^2} + \left[\sum_{p,q=-1,0,1} \mathbf{K}^{(p,q)} \mathbf{u}_{n_1+p,n_2+q} \right] + \varepsilon \boldsymbol{f}_{\boldsymbol{NL}}\left(\mathbf{u}_{n_1\pm p,n_2\pm q}\right) = \mathbf{0} \tag{4.2}$$

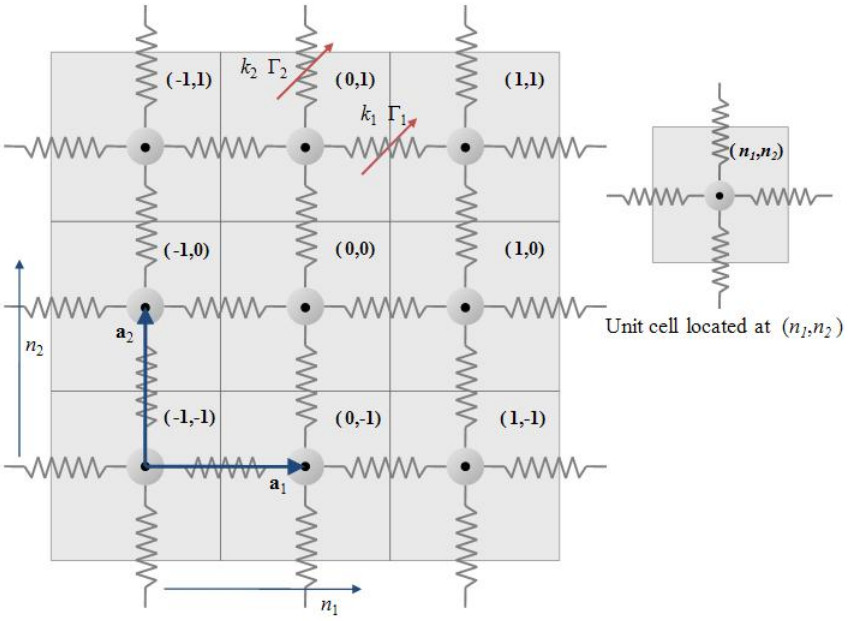

Figure 31: Mono-atomic lattice of identical masses connected by nonlinear springs

where the mass matrix reduces to a scalar quantity,

$$\mathbf{M} = m. \tag{4.3}$$

The partitioned linear stiffness matrices and the nonlinear force vector are given as,

$$\mathbf{K}^{(p,q)} = 0 \quad \forall\, p = \pm 1, q = \pm 1, \tag{4.4}$$

$$\mathbf{K}^{(p,q)} = -k_1 \quad \forall\, p = \pm 1, q = 0, \tag{4.5}$$

$$\mathbf{K}^{(p,q)} = -k_2 \quad \forall\, p = 0, q = \pm 1, \tag{4.6}$$

$$\mathbf{K}^{(0,0)} = 2(k_1 + k_2)\,, \tag{4.7}$$

and the force describing the nonlinear interaction is denoted by,

$$f_{NL} = \sum_{p=\pm 1, q=0} \Gamma_1 \left(u_{1_{0,0}} - u_{1_{p,q}}\right)^3 + \sum_{p=0, q=\pm 1} \Gamma_2 \left(u_{1_{0,0}} - u_{1_{p,q}}\right)^3, \tag{4.8}$$

where k_1 and Γ_1 are the linear and nonlinear spring stiffness between two adjacent masses along $\mathbf{a}_1$ vector respectively, k_2 and Γ_2 represent linear and nonlinear spring stiffness between two adjacent masses in $\mathbf{a}_2$ direction respectively. The direct and reciprocal lattice vectors for the present lattice are given by,

$$\mathbf{a}_1 = a\boldsymbol{i}_1, \mathbf{a_2} = a\boldsymbol{i}_2, \tag{4.9}$$

$$\mathbf{b}_1 = (1/a)\boldsymbol{i}_1,\ \mathbf{b}_2 = (1/a)\boldsymbol{i}_2, \tag{4.10}$$

where $\boldsymbol{i}_1$ and $\boldsymbol{i}_2$ denote the unit vectors along x and y axes respectively and a is the distance between the two masses which is assumed to be equal in both x and y directions. The two ordered equations in the form of Eqs. (2.36) and (2.37) are obtained through the perturbation approach. Application of Bloch theorem in ε^0 order equation results in an eigenvalue problem described by Eq. (2.20) with mass defined by Eq. (4.3), and with the following wavenumber reduced stiffness matrix (Eq. (2.19)),

$$\widetilde{\mathbf{K}}(\mathbf{k}) = 2k_1(1 - \cos(\mu_1)) + 2k_2(1 - \cos(\mu_2)) \tag{4.11}$$

where the wavevector $\mathbf{k} = \mu_1\mathbf{b_1} + \mu_2\mathbf{b_2}$. As $\mathbf{M}$ and $\widetilde{\mathrm{K}}(\mathbf{k})$ defined by Eqs. (4.3) and (4.11) are scalar quantities the resulting linear dispersion has only one branch corresponding to the single degree of freedom of the system. The linear dispersion relation is given by,

$$\omega_{0,1}(\mathbf{k}) = \sqrt{[2k_1(1-\cos(\mu_1)) + 2k_2(1-\cos(\mu_2))]/m} \tag{4.12}$$

The nonlinear force interaction is expressed in terms of Fourier series as described by Eq. (2.44). In this case, the scalar term c_1 is evaluated analytically and it is given by,

$$c_1 = \tfrac{3}{4}\left|A_{0,1}\right|^3\left(\textstyle\sum_{i=1,2}\Gamma_\mathrm{i}\cos(2\mu_\mathrm{i}) - 4\Gamma_\mathrm{i}\cos(\mu_\mathrm{i}) + 3\,\Gamma_\mathrm{i}\right), \tag{4.13}$$

The normalized wave mode reduces to $\mathrm{u}_{0,1}(\mathbf{k}) = 1$, so that from Eq. (2.59) the first order frequency correction is

$$\omega_{1,1} = 3\left|A_{0,1}\right|^2\left(\textstyle\sum_{i=1,2}\Gamma_\mathrm{i}\cos(2\mu_i) - 4\Gamma_\mathrm{i}\cos(\mu_i) + 3\,\Gamma_\mathrm{i}\right)/4m\omega_{0,1}, \tag{4.14}$$

Hence the corrected dispersion relation for nonlinear monoatomic lattice is

$$\omega = \omega_{0,1} + \varepsilon\left(3\left|A_{0,1}\right|^2\left(\textstyle\sum_{i=1,2}\Gamma_\mathrm{i}\cos(2\mu_i) - 4\Gamma_\mathrm{i}\cos(\mu_i) + 3\,\Gamma_\mathrm{i}\right)/4m\omega_{0,1}\right) + O(\varepsilon^2), \tag{4.15}$$

The wave dispersion is dependent on amplitude and degree of nonlinear stiffness in both directions. Figure 32 shows the irreducible Brillouin zone as a contour along $\mathbf{b_1}$ axis from point Γ to X, then along $\mathbf{b_2}$ axis from point X to M and then at 45° from point M back to point Γ.

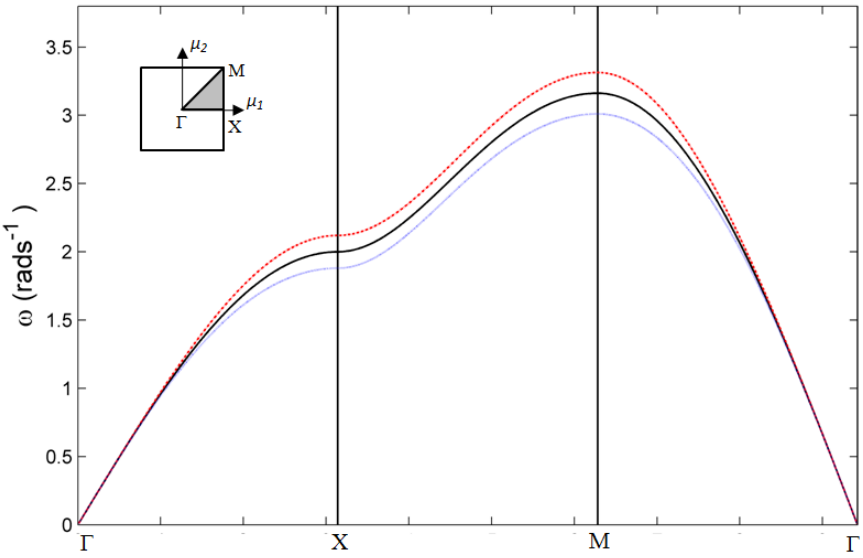

Figure 32: Band structure of the nonlinear mono-atomic lattice for $A = 2.0$

- - - - - $\Gamma_1 = \Gamma_2 = 1.0$, —— Linear ($\Gamma_1 = \Gamma_2 = 0$), ·····$\Gamma_1 = \Gamma_2 = -1.0$

The amplitude-dependent band structure of mono-atomic lattice in an irreducible Brioullin zone is also shown in Figure 32. An upward shift in the band structure for a positive Γ is associated with an increase in the wave amplitude and vice-versa. The upward shift implies that for a certain frequency there is a corresponding increase in group velocity of the wave, which is particularly noticeable at the edges of the first Brillouin zone (points X and M). These results extend to two dimensions the dispersion curves presented for a 1D mono-atomic lattice presented in chapter 3.

4.3.2 ISO-FREQUENCY CONTOURS AND GROUP VELOCITY

The discussion in previous section acknowledged the importance of the representation of the dispersion surfaces as iso-frequency contours. This section illustrates the effect of nonlinearities on the group velocity distribution, and discusses the iso-frequency contours as a tool for the analysis of directions of wave propagation within the lattice. The considered monoatomic linear lattice has parameters $m = 1\,kg, k_1 = 1\,Nm^{-1}, k_2 = 1.5\,Nm^{-1}$.

The iso-frequency contour plot of its dispersion surface is shown in Figure 33 while Figure 34 depicts the group velocity plots at frequencies $\omega = 1.65\, rads^{-1}$ and $\omega = 2.10\, rads^{-1}$, for which interesting patterns can be highlighted. In this case, the group velocity plot is obtained by computing the gradient of the dispersion relation given by Eq. (4.15) which is equivalent to evaluating normal vector at a every point on a iso-frequency contour for a specified frequency. The gradient operator $\boldsymbol{\nabla}$ in Eq. (4.1) can be taken with respect to any direction in the wavenumber domain to obtain the group velocity in that direction at specific frequency and amplitude. The angle formed between normal to the iso-frequency contour and the horizontal is denoted as θ and defines the direction of energy flow at the corresponding wavenumber pair.

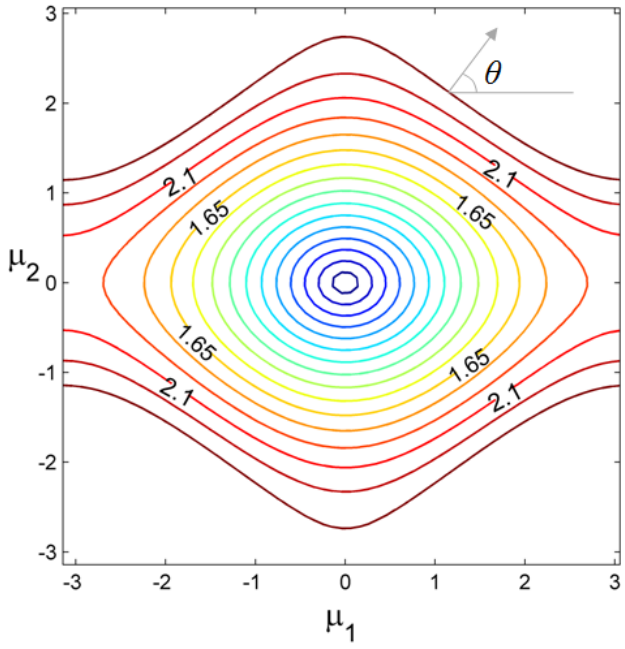

Figure 33: Dispersion iso-frequency contour plot of an anostropic mono-atomic lattice

In the contour line at $\omega = 1.65\, rads^{-1}$, the angle θ varies from 0 to $\pi/2$ as the wave vector components span the range defined by the dispersion surface at the considered frequency. This implies that waves travel in all directions as depicted in the

corresponding group velocity plot, which consists in a closed contour (red line in Figure 34). As frequency is increased to $\omega = 2.10\, rads^{-1}$, however, θ varies approximately from $\pi/3$ to $\pi/2$ which predicts the presence of an angular range between 0 to $\pi/3$ (considering only the first quadrant) where wave propagation is impeded.

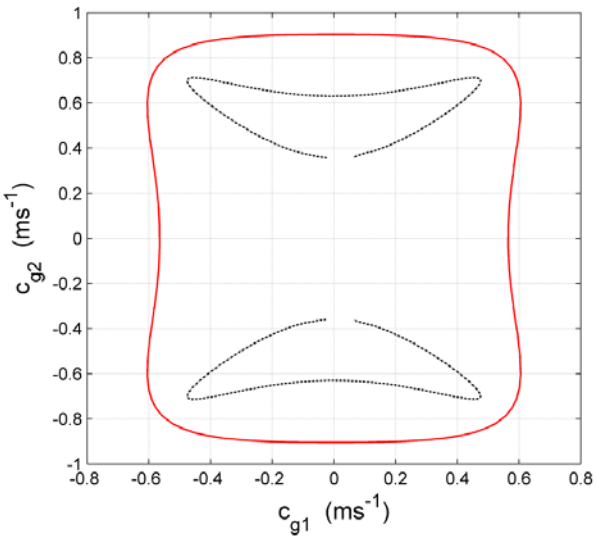

Figure 34: The group velocity plot corresponding to iso-frequency contour (Figure 33) (——— $\omega = 1.65\, rads^{-1}$, ····· $\omega = 2.10\, rads^{-1}$) The dashed line indicates the presence of caustics.

The frequency range characterized by this forbidden propagation range is termed as a '*caustic band*' [25]. The extent of the caustic band for a linear lattice depends exclusively on the properties of the lattice itself. For a nonlinear lattice, however, amplitude of wave motion is an additional parameter which affects its directional behavior. For example, consider a nonlinear lattice with parameters $m = 1\, kg$, $k_1 = 1.0\, Nm^{-1}$, $k_2 = 1.0\, Nm^{-1}$ and $\Gamma_1 = -3.0\, Nm^{-3}, \Gamma_2 = 0.0\, Nm^{-3}$. The iso-frequency contour plot at $\omega = 1.75\, rads^{-1}$ for three different amplitudes ($A = 0.1$, $A = 1.0$ and $A = 2.0$) along with the corresponding group velocity plots is presented in Figure 35 and Figure 36 respectively. It is observed that depending on the lattice stiffness configuration, an increase in amplitude causes a *stretching* of the iso-frequency contour

along the $\mathbf{a}_1$ axis. This *stretching* of the contour forces the wave frequency to enter the caustic band which is initially absent at lower amplitudes.

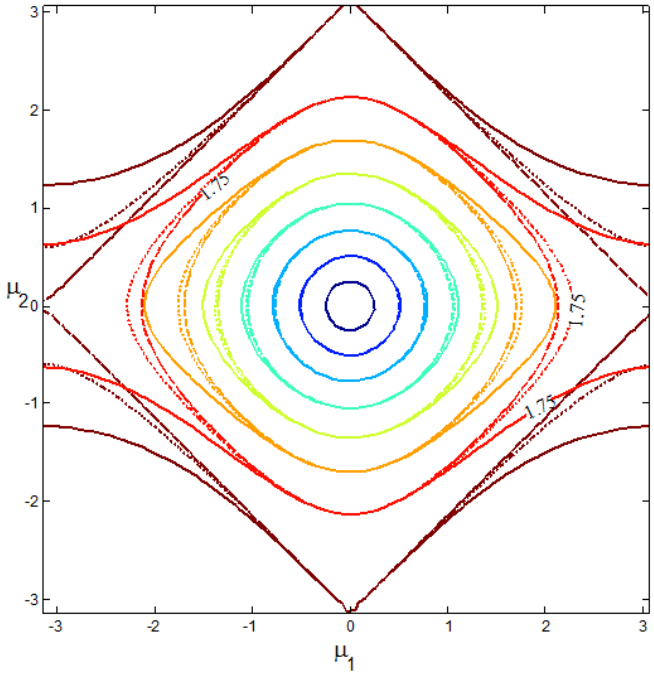

Figure 35: Dispersion iso-frequency contours for a nonlinear lattice with nonlinearity in the $\mathbf{a}_1$ direction show noticeable stretching in one direction as amplitude increases

(- - - - - - A = 0.1, ····· A = 1.0, ——— A = 2.0)

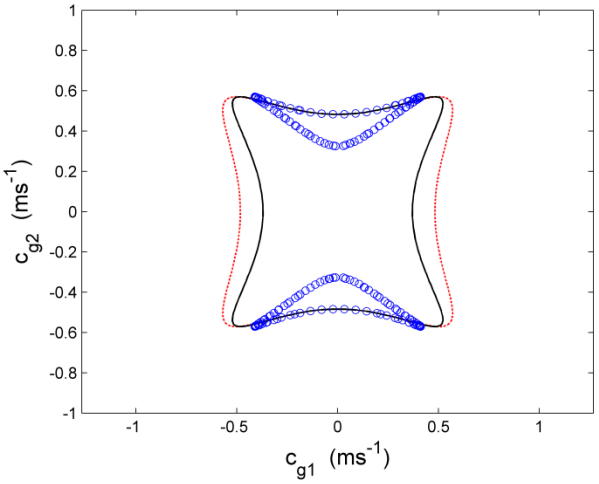

Figure 36: Group velocity corresponding to Figure 35 at frequency 1.75 *rads*$^{-1}$ and varying amplitude. (····· A = 0.1, ——— A = 1.0, ○ A = 2.0)

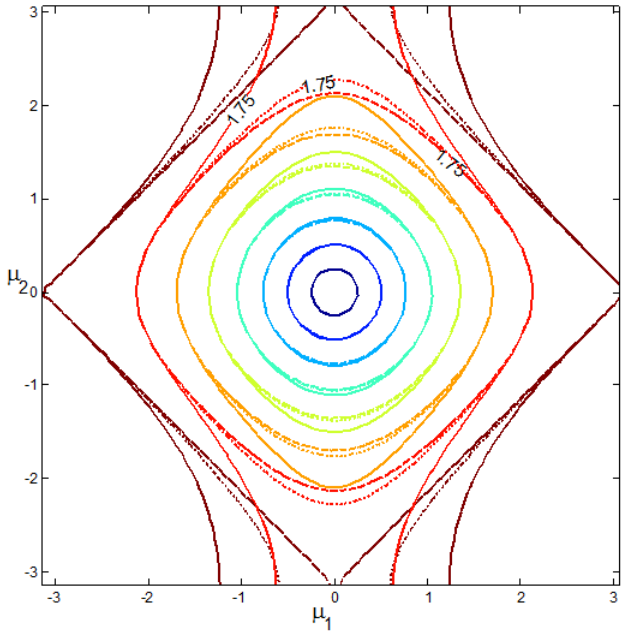

Figure 37: Dispersion iso-frequency contours for a nonlinear lattice with soft nonlinearity in the $\mathbf{a}_2$ direction show noticeable stretching in one direction as amplitude increases (- - - - - A = 0.1, ····· A = 1.0, ——— A = 2.0)

Figure 37 shows change in nonlinear stiffness parameters with $\Gamma_1 = 0.0\ Nm^{-3}, \Gamma_2 = -3.0\ Nm^{-3}$ introduces contour stretching along $\mathbf{a}_2$ axis.

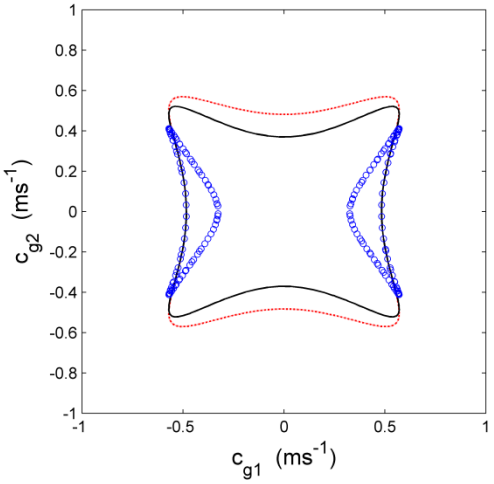

Figure 38: Group velocity corresponding to Figure 37 nonlinear mono-atomic lattice

This implies that as amplitude increases, waves attenuate along $\mathbf{a}_2$ direction. This is clearly depicted in the corresponding group velocity plot of Figure 38, which shows a marked decrease in wave group velocity in the $\mathbf{a}_2$ direction with increasing amplitude until two closed curves correspond to the absence of a velocity component in the x_2 direction.

4.3.3 DIATOMIC LATTICE

The direct lattice space depicted in Figure 39 contains two masses m_1 and m_2. Let the displacement of the mass m_1 be u_1 and that of mass m_2 be u_2, where u_1 and u_2 denote out of plane displacements of two masses defining the two degrees of freedom of the unit cell. The mass matrix of the unit cell is,

$$\mathbf{M} = \begin{bmatrix} m_1 & 0 \\ 0 & m_2 \end{bmatrix}, \tag{4.16}$$

and the partitioned stiffness matrices are given by,

$$\mathbf{K}^{(p,q)} = \begin{bmatrix} 0 & 0 \\ 0 & 0 \end{bmatrix} \ \forall\ (p,q) = [(1,1),(-1,-1)], \tag{4.17}$$

$$\mathbf{K}^{(p,q)} = \begin{bmatrix} 0 & -k_2 \\ 0 & 0 \end{bmatrix} \ \forall\ (p,q) = [(-1,1),(0,-1)], \tag{4.18}$$

$$\mathbf{K}^{(p,q)} = \begin{bmatrix} 0 & 0 \\ -k_2 & 0 \end{bmatrix} \forall (p,q) = [(0,1),(1,-1)], \tag{4.19}$$

$$\mathbf{K}^{(-1,0)} = \begin{bmatrix} 0 & -k_1 \\ 0 & 0 \end{bmatrix}, \tag{4.20}$$

$$\mathbf{K}^{(1,0)} = \begin{bmatrix} 0 & 0 \\ -k_1 & 0 \end{bmatrix}, \tag{4.21}$$

$$\mathbf{K}^{(0,0)} = \begin{bmatrix} 2(k_1+k_2) & -k_1 \\ -k_1 & 2(k_1+k_2) \end{bmatrix}, \tag{4.22}$$

and the force describing the nonlinear interaction is denoted by,

$$f_{NL}(1) = \Gamma_1 \begin{pmatrix} \left(u_{1_{0,0}} - u_{2_{0,0}}\right)^3 \\ +\left(u_{1_{0,0}} - u_{2_{-1,0}}\right)^3 \end{pmatrix} + \Gamma_2 \begin{pmatrix} \left(u_{1_{0,0}} - u_{2_{-1,1}}\right)^3 \\ +\left(u_{1_{0,0}} - u_{2_{0,-1}}\right)^3 \end{pmatrix}, \tag{4.23}$$

$$f_{NL}(2) = \Gamma_1 \begin{pmatrix} \left(u_{2_{0,0}} - u_{1_{0,0}}\right)^3 \\ +\left(u_{2_{0,0}} - u_{1_{1,0}}\right)^3 \end{pmatrix} + \Gamma_2 \begin{pmatrix} \left(u_{2_{0,0}} - u_{1_{0,1}}\right)^3 \\ +\left(u_{2_{0,0}} - u_{1_{1,-1}}\right)^3 \end{pmatrix}, \tag{4.24}$$

where $\boldsymbol{f_{NL}} = [f_{NL}(1) \quad f_{NL}(2)]^{\mathrm{T}}$, k_1 and Γ_1 are the linear and nonlinear spring stiffness between two adjacent masses along $\mathbf{a}_1$ vector respectively, k_2 and Γ_2 represent linear and nonlinear spring stiffness between two adjacent masses in $\mathbf{a}_2$ direction respectively.

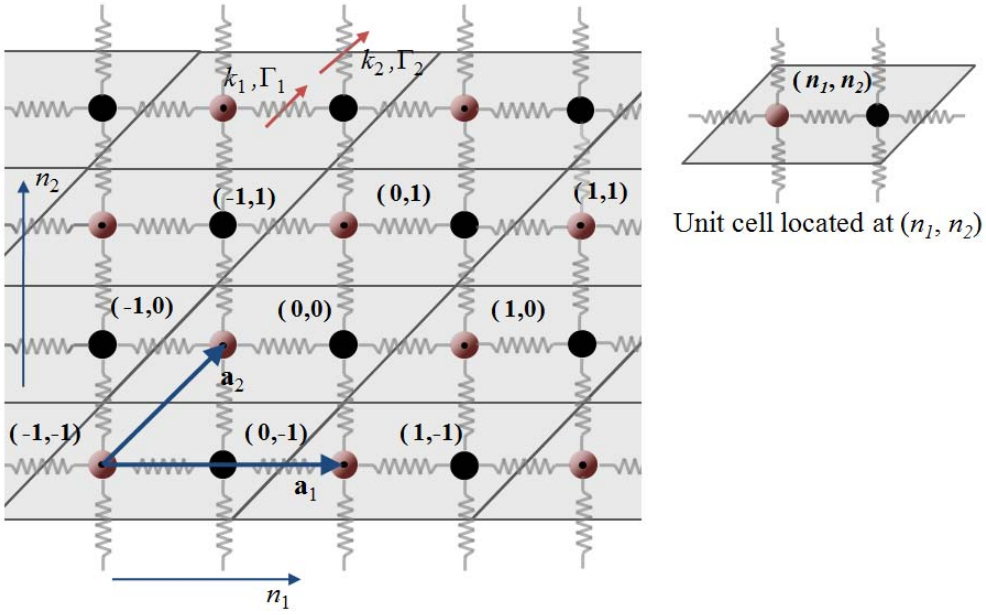

Figure 39: Nonlinear diatomic lattice

u_1 and u_2 denote out of plane displacements which represent two degrees of freedom of the unit cell. For the present lattice, the direct and reciprocal lattice vectors are given by,

$$\mathbf{a}_1 = a\boldsymbol{i_1}, \ \mathbf{a}_2 = (a/2)\boldsymbol{i}_1 + (a/2)\boldsymbol{i}_2\,, \tag{4.25}$$

$$\mathbf{b}_1 = (1/a)\boldsymbol{i}_1 - (1/a)\boldsymbol{i}_2,\ \mathbf{b}_2 = (2/a)\boldsymbol{i}_2, \tag{4.26}$$

where $\boldsymbol{i}_1$ and $\boldsymbol{i}_2$ denote the unit vectors along x and y axes respectively and a is the distance between the unit cells along $\mathbf{a}_1$. Employing the Bloch wave analysis the wavenumber reduced stiffness matrix can be expressed as,

$$\widetilde{\mathbf{K}}(\mathbf{k}) = \begin{bmatrix} 2(k_1 + k_2) & \mathrm{G} \\ \overline{\mathrm{G}} & 2(k_1 + k_2) \end{bmatrix}, \tag{4.27}$$

where,

$$\mathrm{G} = -k_1\left(1 + e^{-i\mu_1}\right) - k_2\left(e^{-i\mu_2} + e^{-i(\mu_1 - \mu_2)}\right), \tag{4.28}$$

and $\overline{\mathrm{G}}$ denotes the complex conjugate of G while k_1 and k_2 are the linear spring stiffness values between two adjacent masses along $\mathbf{a}_1$ and $\mathbf{a}_2$ vector respectively.

The procedure outlined in the previous section in this case predicts two wave modes: a lower frequency mode (acoustic) and high frequency mode, respectively term "acoustic" and "optical" modes. Depending on the mass and stiffness parameters, a gap between the corresponding two branches identifies a range of frequencies (bandgaps) where waves do not propagate in any direction on the plane of the lattice. Figure 40 shows the band diagram of the considered diatomic lattice and the associated irreducible Brillouin zone. The diagram is computed at different wave amplitudes, which shows how the two branches shift as a result of amplitude changes. Such shift corresponds to a change in the band gap frequency range, and therefore ultimately affects the frequencies at which the lattice behaves as a stop band mechanical filter. This example illustrates how amplitude may be exploited as a tuning parameter to control the ability of a given nonlinear periodic domain to impede or permit the propagation of mechanical waves at specified frequencies.

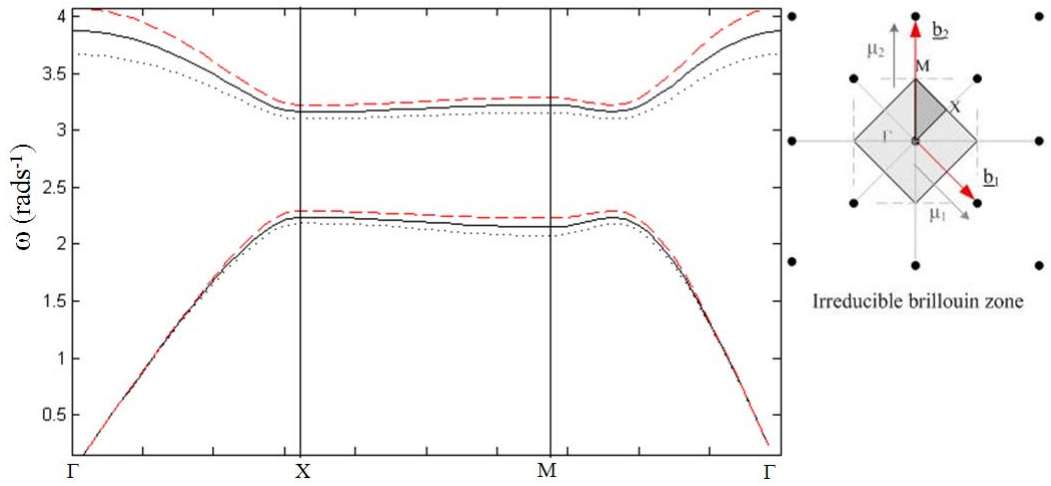

Figure 40: Amplitude-dependent band diagram of the nonlinear diatomic lattice $m_1 = 2.0$ kg, $m_2 = 1.0$ kg, $k_1 = 1.0$ Nm^{-1}, $k_2 = 1.5$ Nm^{-1}, A = 2.0

- - - - - $\Gamma_1 = \Gamma_2 = 1.0$ (hard), —— Linear ($\Gamma_1 = \Gamma_2 = 0$), ·····$\Gamma_1 = \Gamma_2 = -1.0$ (soft)

4.3.4 LATTICE WITH INCLUSION

The nonlinear lattice with inclusion is shown in Figure 41.

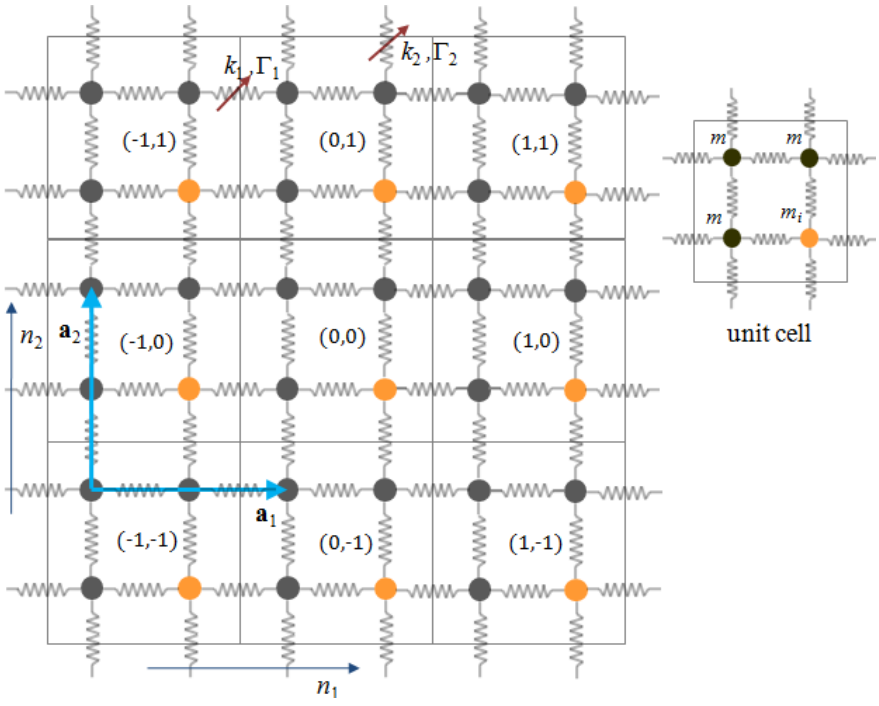

Figure 41: Lattice with an inclusion

The mass matrix is given by,

$$\mathbf{M} = \begin{bmatrix} m_i & 0 & 0 & 0 \\ 0 & m & 0 & 0 \\ 0 & 0 & m & 0 \\ 0 & 0 & 0 & m \end{bmatrix}, \tag{4.29}$$

where m_i denotes the inclusion mass and m denotes the mass neighboring the inclusion mass. The linear partitioned stiffness matrices are given by,

$$\mathbf{K}^{(p,q)} = \begin{bmatrix} 0 & 0 & 0 & 0 \\ 0 & 0 & 0 & 0 \\ 0 & 0 & 0 & 0 \\ 0 & 0 & 0 & 0 \end{bmatrix} \; \forall \, p = \pm 1, q = \pm 1, \tag{4.30}$$

$$\mathbf{K}^{(0,1)} = \begin{bmatrix} 0 & 0 & 0 & 0 \\ 0 & 0 & 0 & 0 \\ 0 & -k_2 & 0 & 0 \\ -k_2 & 0 & 0 & 0 \end{bmatrix}, \tag{4.31}$$

$$\mathbf{K}^{(0,-1)} = \begin{bmatrix} 0 & 0 & 0 & -k_2 \\ 0 & 0 & -k_2 & 0 \\ 0 & 0 & 0 & 0 \\ 0 & 0 & 0 & 0 \end{bmatrix}, \tag{4.32}$$

$$\mathbf{K}^{(1,0)} = \begin{bmatrix} 0 & 0 & 0 & 0 \\ -k_1 & 0 & 0 & 0 \\ 0 & 0 & 0 & -k_1 \\ 0 & 0 & 0 & 0 \end{bmatrix}, \tag{4.33}$$

$$\mathbf{K}^{(-1,0)} = \begin{bmatrix} 0 & -k_1 & 0 & 0 \\ 0 & 0 & 0 & 0 \\ 0 & 0 & 0 & 0 \\ 0 & 0 & -k_1 & 0 \end{bmatrix}, \tag{4.34}$$

$$\mathbf{K}^{(0,0)} = \begin{bmatrix} 2(k_1 + k_2) & -k_1 & 0 & -k_2 \\ -k_1 & 2(k_1 + k_2) & -k_2 & 0 \\ 0 & -k_2 & 2(k_1 + k_2) & -k_1 \\ -k_2 & 0 & -k_1 & 2(k_1 + k_2) \end{bmatrix}. \tag{4.35}$$

The nonlinear force interaction among the masses in the unit cell can be written as:

$$\boldsymbol{f_{NL}} =$$

$$\begin{bmatrix} \sum_{p=0,-1,q=0} \Gamma_1 \left(u_{1_{0,0}} - u_{2_{p,q}}\right)^3 + \sum_{p=0,q=0,-1} \Gamma_2 \left(u_{1_{0,0}} - u_{4_{p,q)}}\right)^3 \\ \sum_{p=0,1,q=0} \Gamma_1 \left(u_{2_{0,0}} - u_{1_{p,q}}\right)^3 + \sum_{p=0,q=0,-1} \Gamma_2 \left(u_{2_{0,0}} - u_{3_{p,q}}\right)^3 \\ \sum_{p=0,1,q=0} \Gamma_1 \left(u_{3_{0,0}} - u_{4_{p,q}}\right)^3 + \sum_{p=0,q=0,1} \Gamma_2 \left(u_{3_{0,0}} - u_{2_{p,q)}}\right)^3 \\ \sum_{p=0,-1,q=0} \Gamma_1 \left(u_{4_{0,0}} - u_{3_{p,q}}\right)^3 + \sum_{p=0,q=0,1} \Gamma_2 \left(u_{4_{0,0}} - u_{1_{p,q}}\right)^3 \end{bmatrix}, \tag{4.36}$$

where k_1 and Γ_1 are the linear and nonlinear spring stiffness between two adjacent masses along $\mathbf{a}_1$ vector respectively, k_2 and Γ_2 represent linear and nonlinear spring stiffness between two adjacent masses in $\mathbf{a}_2$ direction respectively. Displacement of the inclusion mass m_i be u_1 and that of the neighboring masses each of mass m be u_2, u_3 and u_4. The direct and reciprocal lattice vectors are given as,

$$\boldsymbol{a}_1 = 2a\boldsymbol{i}_1,\ \boldsymbol{a}_2 = 2a\boldsymbol{i}_2, \tag{4.37}$$

$$\mathbf{b}_1 = (1/2a)\boldsymbol{i}_1,\ \mathbf{b}_2 = (1/2a)\boldsymbol{i}_2, \tag{4.38}$$

where $\boldsymbol{i}_1$ and $\boldsymbol{i}_2$ denote the unit vectors along x and y axes respectively and a is the distance between the two consecutive masses which is assumed to be equal in both x and y directions. The reduced wavenumber stiffness matrix can be expressed as,

$$\widetilde{\mathbf{K}}(\mathbf{k}) = \begin{bmatrix} 2(k_1+k_2) & -k_1\left(1+e^{-i\mu_1}\right) & 0 & -k_2\left(1+e^{-i\mu_2}\right) \\ -k_1\left(1+e^{i\mu_1}\right) & 2(k_1+k_2) & -k_2\left(1+e^{-i\mu_2}\right) & 0 \\ 0 & -k_2\left(1+e^{i\mu_2}\right) & 2(k_1+k_2) & -k_1\left(1+e^{i\mu_1}\right) \\ -k_2\left(1+e^{i\mu_2}\right) & 0 & -k_1\left(1+e^{-i\mu_1}\right) & 2(k_1+k_2) \end{bmatrix} \tag{4.39}$$

The unit cell of the lattice contains 4 masses which leads to four dispersion branches. This case is considered to show the applicability of the approach to a more complex

system, where the matrix formulation of the linear eigenvalue problem and of the correction process related to the perturbation approach can be conveniently applied.

The coefficient $\boldsymbol{c_1}$ in Eq. (2.44) determines the frequency correction for each mode depending on the magnitude of the wave amplitude. Its effect on the dispersion relations in shown in Figure 42 which confirms the shifting trend previously highlighted for simpler lattices, as it affects each branch as well as the bandgap frequency range generated by the presence of the mass inclusion. The results of Figure 42 also show how a hardening lattice shifts the band structure upwards, whereas the softening lattice shifts the dispersion curves downward with increase in amplitude.

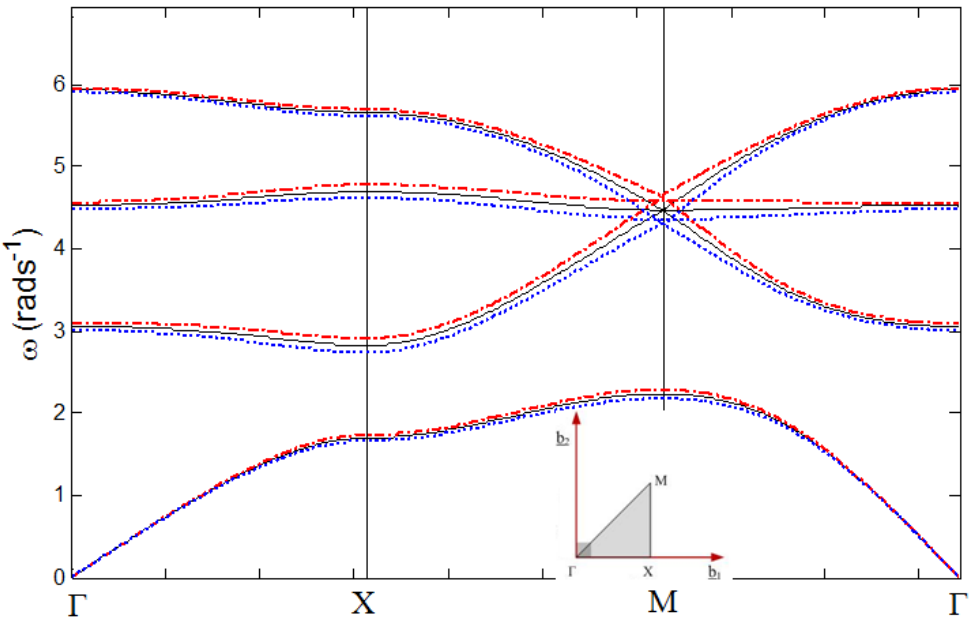

Figure 42: Band diagram for nonlinear lattices with inclusion m_i = 4.0 kg, m = 1.0 kg, k_1 = 1.0 Nm^{-1}, k_2 = 1.5 Nm^{-1}, A = 2.0

- - - - - $\Gamma_1 = \Gamma_2 = 2.0$ (hard), —— Linear ($\Gamma_1 = \Gamma_2 = 0$), ····· $\Gamma_1 = \Gamma_2 = -2.0$ (soft)

4.4 ESTIMATION OF DISPERSION THROUGH NUMERICAL INTEGRATION

The predictions of the dispersion analysis and the associated perturbation relations are validated by computing the response of selected lattice configurations when excited at various frequencies and amplitudes. The excitation is first designed to inject a plane wave in the domain propagating in different directions, which allows the estimation of the wavenumber variation in terms of direction of propagation and amplitude of the input. This is achieved by applying a distributed excitation at one edge of a finite lattice. In addition, the response to a point harmonic force is evaluated to visualize the occurrence of response directionality and the presence of amplitude-dependent caustics as predicted by the perturbation analysis.

4.4.1 NUMERICAL ESTIMATION OF DISPERSION

The aforementioned amplitude-dependent wave dispersion properties are validated through the analysis of the results of the numerical integration of the equations of motion for finite lattices. The selected configuration considers a 61x61 assembly of unit cells of the monoatomic lattice described in previous section. The numerical integration of the equations of motion of the resulting assembly are performed using a conventional Runge-Kutta scheme available in Matlab©. The lattice is free at all edges and it is excited by imposing the harmonic motion of the masses of the bottom horizontal edge. The imposed displacement can be expressed as

$$(\boldsymbol{r}_{n_1,0},\mathrm{t}) = A_0 e^{-i\omega_0 t} e^{i\,\mathbf{k_0}\cdot\boldsymbol{r}_{0,n_1}} = A_0 e^{-i\omega_0 t} e^{i\,n_1\mu_{1,0}}, \tag{4.40}$$

where $\mathbf{k_0} = \mu_{1,0}\mathbf{b}_1 + \mu_{2,0}\mathbf{b}_2$, and A_0 defines the amplitude of the imposed displacement. In this case, the lattice geometry is such that $\mathbf{a}_1 = \mathbf{b}_1 = \boldsymbol{i}_1$ and $\mathbf{a}_2 = \mathbf{b}_2 = \boldsymbol{i}_2$, under the assumption that the distance between each mass is equal to 1. The imposed displacement distribution can be considered as the result of a plane wave incident on the bottom edge

of the domain at an angle α (Figure 43). The wavenumber of the incident wave can be expressed as

$$\mathbf{k_0} = \mu_0(\cos\alpha\,\mathbf{i}_1 + \sin\alpha\,\mathbf{i}_2), \tag{4.41}$$

so that in Eq. (4.40) $\mu_{1,0} = \mu_0 \cos\alpha$. Equation (4.40) also implies that each mass on the bottom edge of the domain is excited by displacements of equal amplitude and of phase relation which depends on the wavenumber and angle of incidence of the wave. Simulations for different input frequencies ω_0 and wavenumber $\mu_{1,0}$ are performed to evaluate the wavenumber content of the wave generated in the lattice by an input in the form of Eq. (4.12). Imposing the input frequency ω_0 corresponds to selecting a particular isofrequency contour on the dispersion surface of the lattice (Figure 33). The objective is to evaluate the wavenumber component $\mu_{2,0}$ corresponding to an assigned value of $\mu_{1,0}$, which vary in the range defined by the corresponding iso-frequency contour.

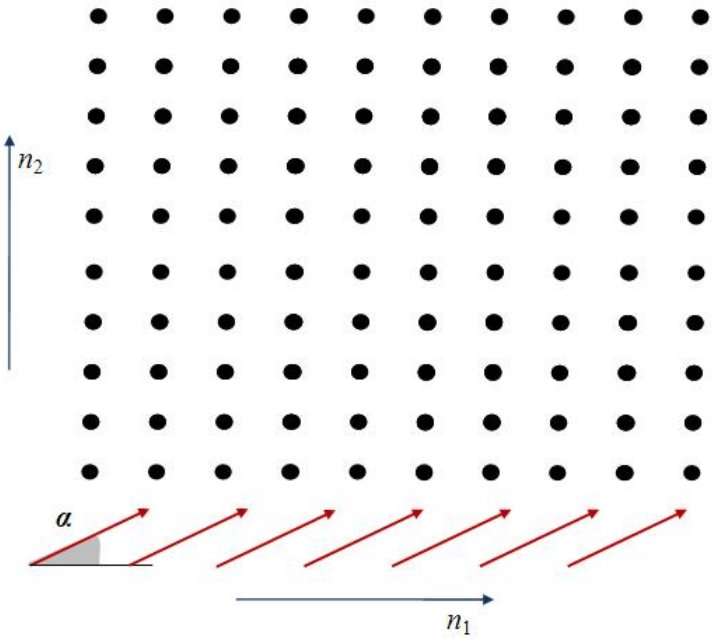

Figure 43: Schematic of a finite monoatomic lattice and incident wave at angle $\boldsymbol{\alpha}$

As indicated above, the equations of motion of the finite lattice are numerically integrated to obtain the time response of the system $u(n_1, n_2, t)$. In general, the lattice response can be expressed as a propagating plane wave in the following form

$$u(n_1, n_2, t) = u(t - \mathbf{k_0} \cdot \boldsymbol{r}_{n_1,n_2}) \tag{4.42}$$

The evaluation of the wavenumber content of the computed response is based on the Fourier Transform of Eq. (4.42), which gives,

$$U(n_1, n_2, \omega) = \int_{-\infty}^{+\infty} u(t - \boldsymbol{k_0} \cdot \boldsymbol{r}_{n_1,n_2})\, e^{-i\omega t} dt \tag{4.43}$$

$$U(n_1, n_2, \omega) = \mathrm{U}(\omega) \mathrm{e}^{-\mathrm{i}\, \mathbf{k_0} \cdot \mathbf{r}_{n_1,n_2}} = \mathrm{U}(\omega)\ \mathrm{e}^{i\,(n_1\mu_{1,0} + n_2\mu_{2,0})}. \tag{4.44}$$

Specifically, the Fourier Transform of the response is evaluated at the frequency of the imposed displacement ω_0. Of interest is the phase of the obtained quantity which can be expressed as

$$\angle U(n_1, n_2, \omega_0) = n_1\mu_{1,0} + n_2\mu_{2,0}. \tag{4.45}$$

From the phase of the computed response at ω_0, one can estimate the wavenumber components by evaluating the relative phase of masses aligned along given directions. Given that the procedure imposes the wavenumber $\mu_{1,0}$, the wavenumber $\mu_{2,0}$ can be estimated from the phase variation of the response in the direction x_1, i.e. for a specified value of n_1, along which the phase of the response varies linearly.

The process is applied by computing the response for assigned values of frequency and wavenumber in one direction, as well as for increasing forcing amplitudes so that the effect of nonlinearities on dispersion contours can be estimated. The results of these investigations are shown in Figure 44 which depicts the amplitude-dependent iso-frequency contour for a lattice with parameters $m = 1\ kg$, $k_1 = 1.5\ Nm^{-1}$, $k_2 =$

$1.0\ Nm^{-1}$ and $\Gamma_1 = 1.0\ Nm^{-3}$, $\Gamma_2 = -1.0\ Nm^{-3}$ excited at $\omega_0 = 1.60\ rads^{-1}$. The dots represent the numerically estimated wavenumbers, while the continuous lines correspond to the predictions from the dispersion analysis. Excellent agreement between analytical and numerical results is obtained for the considered amplitude values.

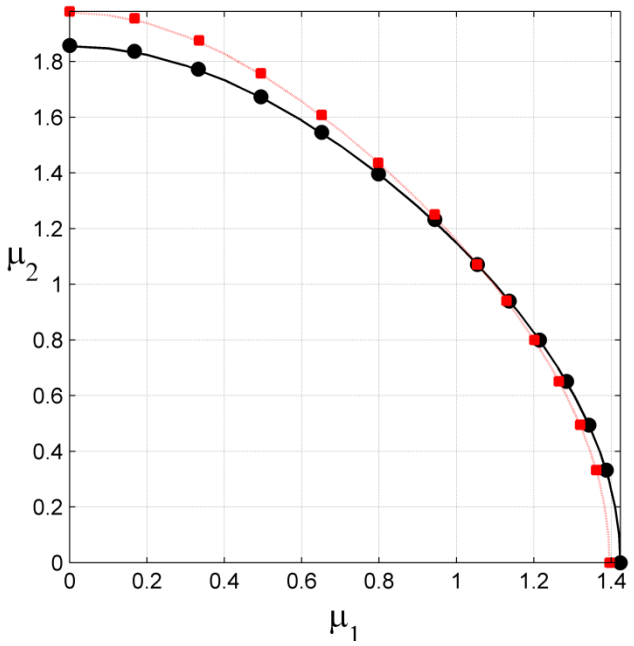

Figure 44: Comparison of dispersion iso-frequency contours and numerically estimated wavenumbers at ω_0 = 1.60 $rads^{-1}$ and two values of amplitude.

——— A = 0.1 (Perturbation Analysis), ● A = 0.1 (Numerical Estimation),

····· A = 2.0 (Perturbation Analysis), ■ A = 2.0 (Numerical Estimation)

Figure 45 shows the results for excitation at $\omega_0 = 1.90\ rads^{-1}$, and illustrates the emergence of a caustic-like behavior as amplitude increases. Of note is the fact that the procedure fails to identify the correct dispersion in the caustic region, as highlighted by the circled dots in Figure 45. This is due to the fact that the wave is significantly attenuated in the '2' direction, and its evanescent behavior cannot be described as in Eq. (4.40) and evaluated through the procedure outlined above.

4.4.2 POINT HARMONIC RESPONSE OF A FINITE LATTICE

The response of the system to a point harmonic excitation with the excitation point located on the edge of the lattice is investigated. Previous sections showed that the trend predicted by the perturbation analysis is verified by the numerical simulations for valid wave amplitudes. Although small amplitude numerical response is important to verify the trends predicted by analytical methods, high amplitude response can lead to better understanding of the system behavior. High amplitude response can determine whether the system continues to follow the trend to generate "dead zones" at specific frequencies.

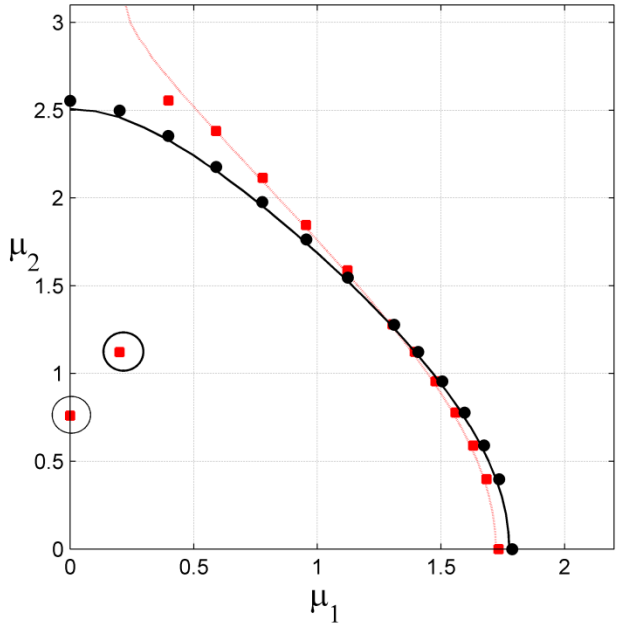

Figure 45: Comparison of dispersion is-frequency contours and numerically estimated wavenumbers at $\omega_0 = 1.90\ rads^{-1}$ and two different amplitudes. Outliers in high amplitude curve indicate evanescent waves in forbidden propagation direction.

——— A = 0.1 (Perturbation Analysis), ● A = 0.1 (Numerical Estimation),

····· A = 2.0 (Perturbation Analysis), ■ A = 2.0 (Numerical Estimation)

The present case emulates a number of different practical scenarios such as a simulating a protective material around sensitive equipment with local excitation imposed from an external source. This implies that the excitation is imposed on the surface

boundary of the material and the wave propagation is perpendicular to the surface. If it is imagined that the source is on the opposite face of the structure from the excitation point, it is desired to check whether waves at certain frequencies with low amplitude can reach the source or steer away as amplitude increases. The computed numerical responses illustrate the property of amplitude-dependent wave directionality in a nonlinear two dimensional periodic structure.

A nonlinear lattice with parameters $m = 1\,kg$, $k_1 = 1.00\,Nm^{-1}$, $k_2 = 1.00\,Nm^{-1}$ and $\Gamma_1 = -3.0\,Nm^{-3}$, $\Gamma_2 = 0.0\,Nm^{-3}$ is considered. The structure's linear stiffness is symmetric but the nonlinear stiffness is highly asymmetric. The edge is excited at a frequency $\omega_0 = 1.40\,rads^{-1}$, which is well within the pass band of the structure. Three different cases are considered. First, point harmonic excitation amplitude $A = 3.0$ is considered. Figure 46 shows the displacement of each mass at an instant of time as the wave reaches the boundary of the considered lattice.

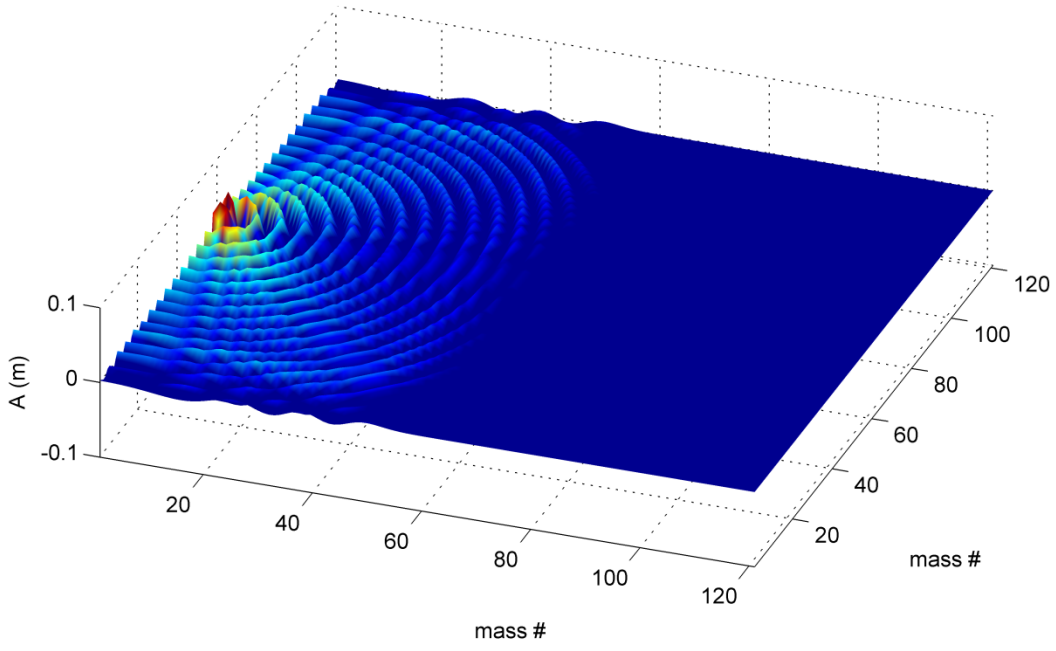

Figure 46: Response of point harmonic excitation amplitude $A = 3.0$

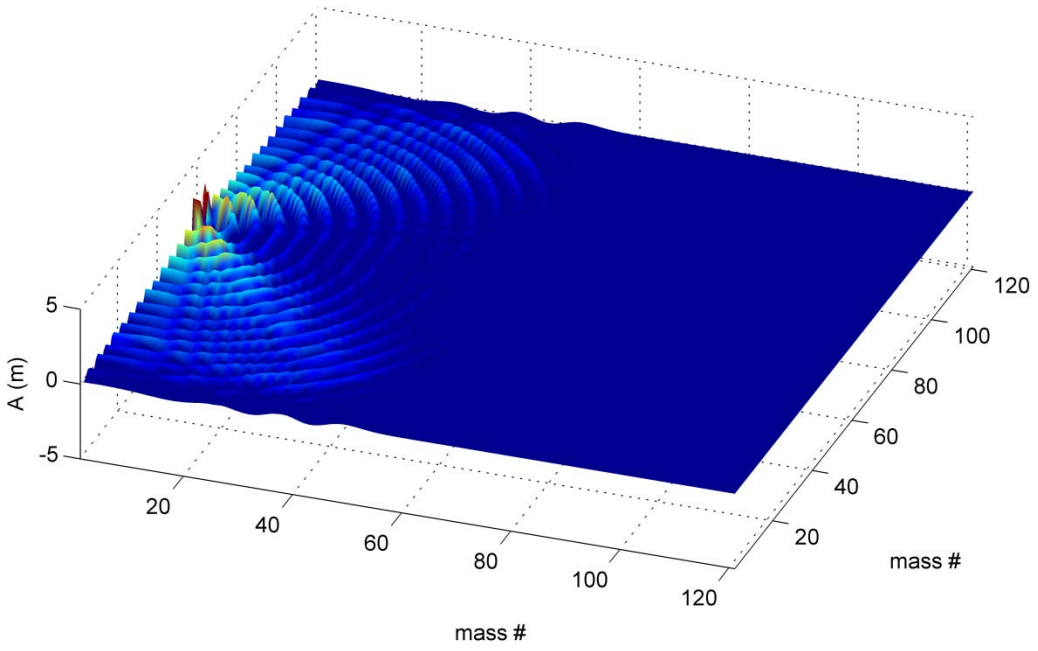

Figure 47: Response of point harmonic excitation amplitude $A = 4.5$

The second and third cases involve the response computed for amplitudes $A = 4.5$, $A = 4.75$ as shown in Figure 47 and Figure 48 respectively.

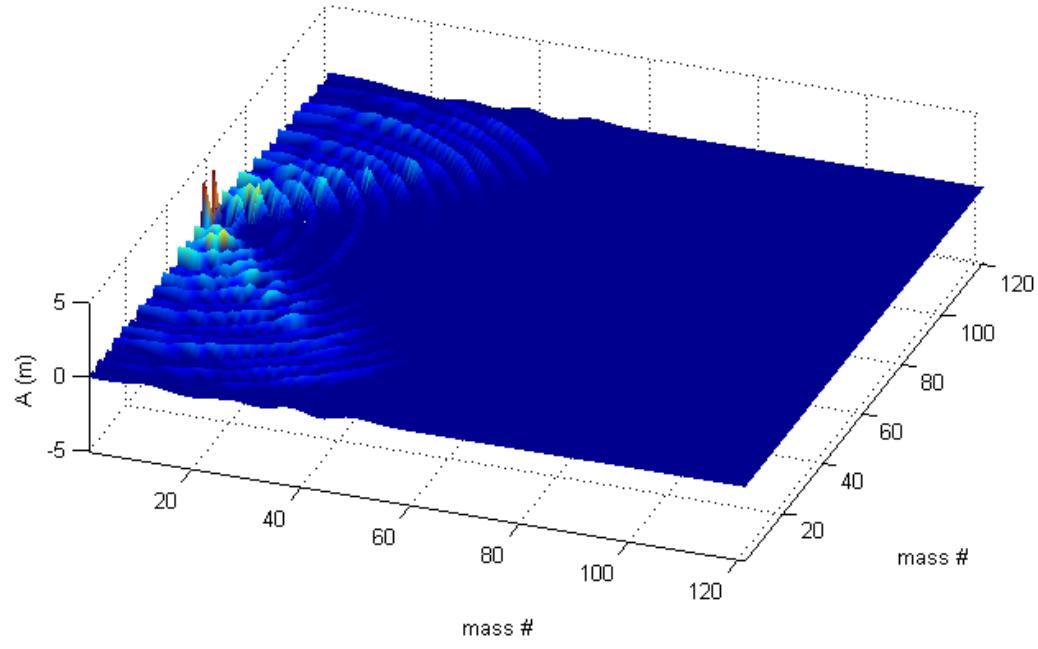

Figure 48: Response of point harmonic excitation amplitude $A = 4.75$

The results clearly indicate the wave directivity in the nonlinear periodic medium. At low amplitude, the wave travels in all directions, while as amplitude increases, the response is characterized by the emergence of very low response regions, or "dead zones", along the $\mathbf{a}_1$ direction. Hence, at the certain frequency for specific excitation amplitude, the waves propagate in all directions through the structure and at the same frequency the structure inhibits the energy flow along $\mathbf{a_1}$ direction with increase in the excitation amplitude.

4.5 CONCLUSIONS

A nonlinear periodic structure subject to plane wave excitation is studied and results for response to a point harmonic excitation are presented. Closed form expressions for dispersion relations are obtained using perturbation analysis applied to a discrete lattice model. Amplitude-dependent dispersion trends predicted by perturbation analysis are validated by the numerical response of a finite mass-spring lattice. It is observed that the two-dimensional nonlinear periodic structure exhibits amplitude-dependent wave directionality and band gap behavior. Depending on the stiffness configuration, wave directional behavior is shown to be dependent on the linear and nonlinear stiffness arrangement leading to tunable wave transmission properties. The spring-mass lattices have provided a convenient setting allowing the perturbation approach to study the first order effects of nonlinearity on the wave dispersion in periodic structures. The next chapter illustrates that the same perturbation approach can be applied to study the dispersion in a complex nonlinear periodic media whose domain has been discretized using Finite element method. This applicability of the method makes it a powerful tool to analyze first order nonlinear effects on wave propagation characteristics exhibited by periodic structures.

CHAPTER V

DISPERSION IN A COMPLEX NONLINEAR PERIODIC STRUCTURE

5.1 OVERVIEW

Due to their convenient setting for introducing nonlinearities, spring-mass models are considered in the previous chapters to demonstrate the application of perturbation theory to estimate the dispersion. Using the same perturbation theory, the present chapter illustrates the study of dispersion in a weakly nonlinear periodic structure discretized through the Finite Element method. A two-dimensional membrane under tension supported by a weakly nonlinear elastic foundation is considered. First, a brief introduction and the motivations for considering membrane structures are detailed followed by the equations of motion capturing the dynamics of the unit periodic element. The dispersion analysis first illustrates the linear modes demonstrating the band structure. Finally, the nonlinear behavior is evaluated using perturbation theory to demonstrate amplitude-dependent dispersion characteristics.

5.2 MOTIVATION

Ranging from simple percussion instruments such as drums, to acoustic devices such as speakers, elastic membranes play a major role in everyday applications. However the primary motivation to consider this problem comes from a recent advancement of transducer technology which led to membrane based *capacitive micro-machined ultrasonic transducers* (CMUT). CMUTs are essentially metallic membranes on flexible supports which vibrate due to alternating current to generate ultrasonic waves [65]. In the

sensing mode, the pressure waves generate vibrations in the membrane which induces a measurable change in capacitance. These micro electro-mechanical systems are used in various applications such as low frequency sonar applications [66], photo-acoustic imaging in which the body absorbs electromagnetic waves and emits ultrasonic waves which are then used to map the internal structure of the body [67]. In most cases, CMUT elements are arranged in 1D or 2D periodic array arrangements to act as effective sensing devices (Figure 49).

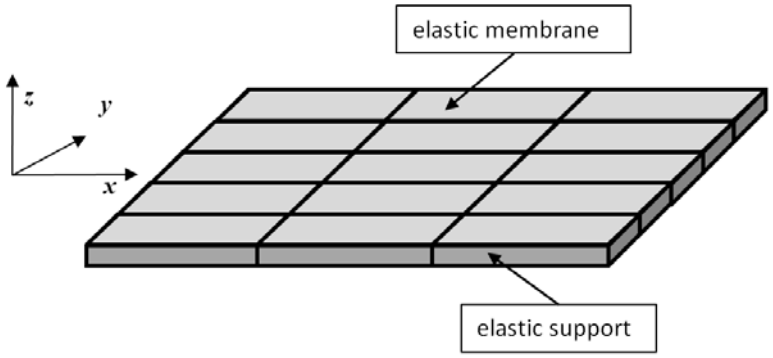

Figure 49: Schematic of a 2D membrane array

The performance of CMUT array is primarily dependent on the reduction of *acoustic crosstalk* [68, 69] among the components of the array. Hence, modeling wave propagation in such arrays to minimize crosstalk (coupling among components) could help enhance the performance and the design of CMUTs. For large membrane displacement, the dynamics of the CMUT element are nonlinear [70] and the whole array can be modeled as a two dimensional nonlinear periodic structure with each element modeled as elastic membranes supported by nonlinear springs. A number of designs exist for membrane elements ranging from square to piston type arrangements. The magnitude of nonlinearity present depends on the dimensions and the material composition of the membrane and its elastic support. For example, one design employs a rectangular membrane supported by cantilevered electrodes whose dynamics are inherently nonlinear. The nonlinearity can also exist due to the elastic plate dynamics in the

presence of an electrostatic field in the vacuum or air gap under each membrane unit. The motivation provided by CMUTs suggested the considered configuration, which is studied next using the developed perturbation analysis.

5.3 EQUATIONS OF MOTION

Consider an elastic membrane under constant tension with the boundary of the element on a flexible support. A schematic of such element is shown in Figure 50.

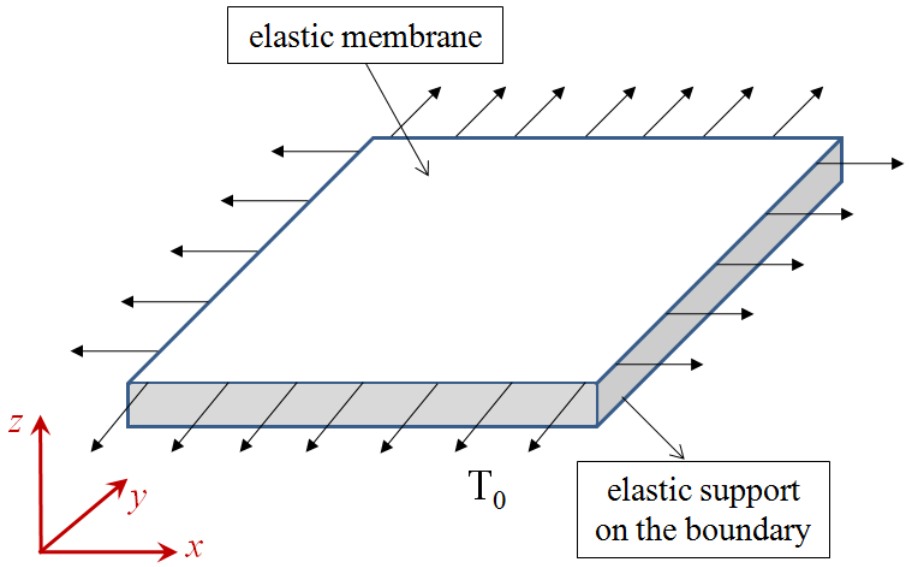

Figure 50: Schematic of periodic element - membrane on elastic support

The following assumptions are considered while deriving the governing equations of motion.

1. The membrane is homogenous implying that the mass of the membrane per unit area (ρ) is constant
2. The membrane is perfectly flexible and offers no resistance to bending
3. The tension per unit length caused by stretching the membrane is same at all points and in all directions and is assumed not to change during the motion.

4. Deflection $u(x, y, t)$ of the membrane is small compared to the size of the membrane

The equations of motion governing the dynamics of a membrane are,

$$\ddot{u} = c^2 \nabla^2 u + f_0 , \tag{5.1}$$

where $u = u(x, y, t)$, $\ddot{u} = \frac{\partial^2 u}{\partial t^2}$, $c = \sqrt{\frac{T_0}{\rho}}$,T_0 denotes the tension per unit area, ∇^2 is the Laplacian operator and f_0 is the external force per unit area.

5.4 FINITE ELEMENT DISCRETIZATION

The weak form of equations of motion for a membrane element is obtained by multiplying the equation of motion with appropriate weighting function and integrating over the domain.

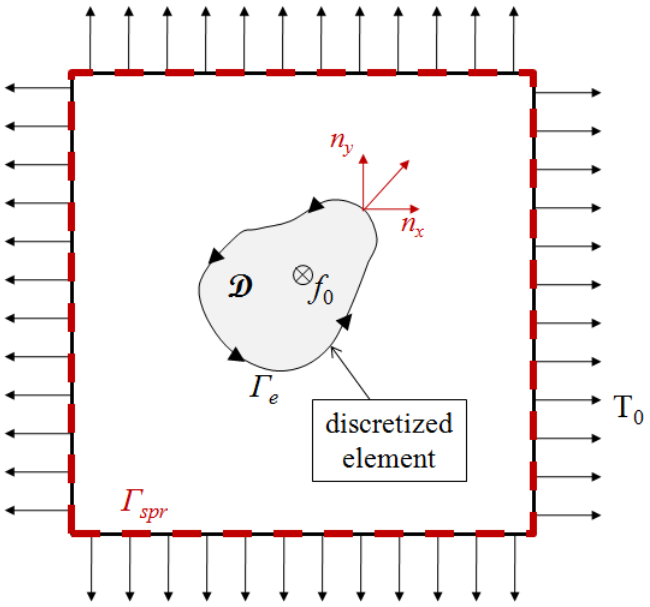

Figure 51: Discretized element within elastically supported membrane

. Let $w = w(x, y, t)$ be a suitable weighting function, then the weak form is expressed as,

$$\iint_{\mathcal{D}} w\,(c^2\boldsymbol{\nabla}^2 u - \frac{\partial^2 u}{\partial t^2} + f_0)\;dx\,dy = 0, \tag{5.2}$$

where $\mathcal{D}$ defines the domain of the element as shown in Figure 51 . Next, a change of variables $a_1 = \frac{\partial u}{\partial x}$ and $a_2 = \frac{\partial u}{\partial y}$ is introduced transforming Eq. (5.2) which is given as,

$$\iint_{\mathcal{D}} w\left(c^2\left(\frac{\partial a_1}{\partial x} + \frac{\partial a_2}{\partial y}\right) - \frac{\partial^2 u}{\partial t^2} + f_0\right)dxdy = 0. \tag{5.3}$$

Next using the product rule of differentiation, it can be easily shown that,

$$w\frac{\partial a_1}{\partial x} = -a_1\frac{\partial w}{\partial x} + \frac{\partial (wa_1)}{\partial x}. \tag{5.4}$$

Substituting Eq. (5.4) into Eq. (5.3), the weighted integral can be written as,

$$\iint_{\mathcal{D}}\left(c^2\left(-a_1\frac{\partial w}{\partial x} + \frac{\partial (wa_1)}{\partial x} - a_2\frac{\partial w}{\partial y} + \frac{\partial (wa_2)}{\partial y}\right) - w\frac{\partial^2 u}{\partial t^2} + wf_0\right)dxdy = 0\,, \tag{5.5}$$

Applying Green's theorem to the above equation, Eq. (5.5) can be rewritten as,

$$\iint_{\mathcal{D}}\left(-c^2\left(a_1\frac{\partial w}{\partial x} + a_2\frac{\partial w}{\partial y}\right) - w\frac{\partial^2 u}{\partial t^2} + wf_0\right)dxdy + \oint_{\Gamma_e} c^2 w(a_1 n_x - a_2 n_y)ds = 0\,, \tag{5.6}$$

where Γ_{e} denotes the contour of the boundary of the discretized element as shown in Figure 51, n_x and n_y are the components of the normal vector at point (x, y) on the contour. The positive direction of the normal is outward facing with elemental arc length ds moving counterclockwise. The coefficient of w in the integrand of the line integral can be realized as a generalized constraint force q_n ,

$$q_n \equiv c^2(a_1 n_x - a_2 n_y). \tag{5.7}$$

Using the following notation and expanding a_1 and a_2 ,

$$\mathcal{B}(w,u) = \iint_{\mathcal{D}} \left(-c^2 \left(\frac{\partial u}{\partial x}\frac{\partial w}{\partial x} + \frac{\partial u}{\partial y}\frac{\partial w}{\partial y}\right) - w\frac{\partial^2 u}{\partial t^2} + wf_0\right) dxdy, \tag{5.8}$$

$$l(w) = \oint_{\Gamma_e} wq_n ds, \tag{5.9}$$

so that the weak form can be expressed as,

$$\mathcal{B}(w,u) = l(w). \tag{5.10}$$

The finite element model for the membrane element is developed by expressing $u(x,y)$ in terms of nodal displacements as,

$$u(x,y) = \sum_{j=1}^{N} u_j^e \psi_j^e(x,y), \tag{5.11}$$

where $\psi_j^e(x,y)$ denotes the j^{th} shape function. Substituting Eq. (5.11) into weak form Eq. (5.10) and expanding leads to,

$$0 = \iint_{\mathcal{D}} \left(-c^2 \left(\frac{\partial w}{\partial x}\sum_{j=1}^{N} u_j^e \frac{\partial \psi_j^e}{\partial x} + \frac{\partial w}{\partial y}\sum_{j=1}^{N} u_j^e \frac{\partial \psi_j^e}{\partial y}\right) - w\sum_{j=1}^{N} \frac{\partial^2 u_j^e}{\partial t^2}\psi_j^e + wf_0\right) dxdy + \oint_{\Gamma_e} wq_n ds\,. \tag{5.12}$$

The i^{th} algebraic equation is obtained by choosing the weighting function as one of the interpolation functions $w = \psi_i^e(x,y)$ which gives,

$$\sum_{j=1}^{N} -\left(\iint_{\mathcal{D}} c^2 \left(\frac{\partial \psi_i^e}{\partial x}\frac{\partial \psi_j^e}{\partial x} + \frac{\partial \psi_i^e}{\partial y}\frac{\partial \psi_j^e}{\partial y}\right) dxdy\right) u_j^e - \sum_{j=1}^{N}\left(\iint_{\mathcal{D}} \psi_i^e \psi_j^e dxdy\right)\ddot{u}_j^e + \iint_{\mathcal{D}} \psi_i^e f_0 dxdy + \oint_{\Gamma_e} \psi_i^e q_n ds = 0. \tag{5.13}$$

Equation (5.13) which can be rewritten in a compact form,

$$\sum_{j=1}^{N} \mathrm{K}_{ij}^{e} u_j^e + \sum_{j=1}^{N} \mathrm{M}_{ij}^{e} \ddot{u}_j^e = f_i^e + q_i^e, \ \forall\, i = 1,2 \ldots N, \tag{5.14}$$

where,

$$\mathrm{K}_{ij}^{e} = \iint_{\mathcal{D}} c^2 \left(\frac{\partial \psi_i^e}{\partial x} \frac{\partial \psi_j^e}{\partial x} + \frac{\partial \psi_i^e}{\partial y} \frac{\partial \psi_j^e}{\partial y} \right) dxdy, \tag{5.15}$$

$$\mathrm{M}_{ij}^{e} = \iint_{\mathcal{D}} \psi_i^e \psi_j^e dxdy, \tag{5.16}$$

the external load vector,

$$f_i^e = \iint_{\mathcal{D}} \psi_i^e f_0 dxdy, \tag{5.17}$$

and the internal force constraint,

$$q_i^e = \oint_{\Gamma_e} \psi_i^e q_n ds\,. \tag{5.18}$$

From here on, the notation bold face capital letters indicate matrices and lower case bold face indicate vectors. To further simplify, let $\mathbf{H} = [\psi_1^e\ \psi_2^e\ \psi_3^e \ldots \psi_N^e]$ denote the matrix of shape functions and let the derivatives of the shape functions be expressed as,

$$\mathbf{B} = \begin{bmatrix} \frac{\partial \psi_1^e}{\partial x} & \frac{\partial \psi_2^e}{\partial x} \ldots \frac{\partial \psi_N^e}{\partial x} \\ \frac{\partial \psi_1^e}{\partial y} & \frac{\partial \psi_2^e}{\partial y} \ldots \frac{\partial \psi_N^e}{\partial y} \end{bmatrix}. \tag{5.19}$$

Hence, the stiffness and mass matrices along with the force vector can be conveniently expressed in matrix form,

$$\mathbf{K}^e = \iint_{\mathcal{D}} c^2 \mathbf{B}^{\mathbf{T}} \mathbf{B}\, dxdy, \tag{5.20}$$

$$\mathbf{M}^e = \iint_{\mathcal{D}} \mathbf{H}^{\mathbf{T}} \mathbf{H}\, dxdy, \tag{5.21}$$

and

$$\boldsymbol{f}^e = \iint_{\mathcal{D}} \mathbf{H}^{\mathrm{T}} f_0 dxdy. \tag{5.22}$$

$$\boldsymbol{q}^{\boldsymbol{e}} = \oint_{\Gamma_e} \boldsymbol{H}^T q_n ds. \tag{5.23}$$

For the present case, the external flexible support can be modeled as the external force applied to the system on the boundaries of the membrane element,

$$f_0 = k_s u(x,y)|_{\Gamma_{spr}} + \varepsilon \Gamma_s u^3(x,y)|_{\Gamma_{spr}}, \tag{5.24}$$

where $u(x,y)|_{\Gamma_{spr}}$ in the above equation is the displacement of the membrane along the boundary of the membrane element which is denoted by a dashed line in Figure 51, k_s is the equivalent linear stiffness, Γ_s denotes the equivalent cubic stiffness and ε is small parameter ensuring the weak nonlinear interaction.

5.5 ORDERED EQUATIONS OF MOTION

The equations of motion (Eq. (5.14)) for a discretized finite element can be written in a matrix form using Eqs. (5.20) - (5.22),

$$\mathbf{M}^e \ddot{\mathbf{u}}^e + \mathbf{K}^e \mathbf{u}^e = \boldsymbol{f}^e + \boldsymbol{q}^e, \tag{5.25}$$

where $\mathbf{u}^e = [u_1^e \; u_2^e \; u_3^e \; \ldots u_N^e]^{\mathrm{T}}$ denotes the vector of elemental nodal displacements. The external force vector consists of linear and nonlinear components as described by Eq. (5.24). Substituting Eq. (5.24) into Eq. (5.22), $\boldsymbol{f}^e$ can be expressed as,

$$\boldsymbol{f}^e = k_s \iint_{\mathcal{D}} \mathbf{H}^{\mathrm{T}} u(x,y)|_{\Gamma_{spr}} \, dxdy + \varepsilon \Gamma_s \iint_{\mathcal{D}} \mathbf{H}^{\mathrm{T}} u^3(x,y)|_{\Gamma_{spr}} \, dxdy. \tag{5.26}$$

To be consistent with the notation introduced in chapter 2, the internal constraint force denoted by $\boldsymbol{q}^e$ is replaced by $\boldsymbol{f}_{int}^e$. Introducing change in variable $\tau = \omega t$ and substituting Eq. (5.26) into Eq. (5.25), the equation of motion for the finite element,

$$\omega^2 \mathbf{M}^e \frac{d^2\mathbf{u}^e}{d\tau^2} + \mathbf{K}^e\mathbf{u}^e = \boldsymbol{f}_L^e + \varepsilon \boldsymbol{f}_{NL}^e + \boldsymbol{f}_{\boldsymbol{int}}^e. \tag{5.27}$$

The linear force component in comparison with Eq. (5.26) can be expressed in the following manner by replacing the displacement field $u(x, y)$ in terms of nodal displacements $\mathbf{u}^e$ using Eq. (5.11),

$$\boldsymbol{f}_L^e(\mathbf{u}^e) = k_s \iint_{\mathcal{D}} \mathbf{H}^{\mathbf{T}}\mathbf{H}|_{\Gamma_{\boldsymbol{spr}}}\, dxdy\, \mathbf{u}^e, \tag{5.28}$$

and the nonlinear force is given by,

$$\boldsymbol{f}_{NL}^e(\mathbf{u}^e) = \Gamma_s \iint_{\boldsymbol{\mathcal{D}}} \mathbf{H}^{\mathbf{T}}(\mathbf{H}\mathbf{u}^e)^{\mathbf{3}}\big|_{\Gamma_{spr}}\, dxdy. \tag{5.29}$$

Next, the following asymptotic expansion of the displacement and the frequency ω (Eqs. (2.34) and (2.35)) is considered,

$$\mathbf{u}^{\mathrm{e}} = \mathbf{u}^{(\mathbf{0})e} + \varepsilon \mathbf{u}^{(\mathbf{1})e} + O(\varepsilon^2), \tag{5.30}$$

$$\omega = \omega_0 + \varepsilon\omega_1 + O(\varepsilon^2)\ . \tag{5.31}$$

Substituting Eqs. ((5.30) and (5.31)) into Eq. (5.26) leads to the following ordered equations,

$$\varepsilon^0 \colon \omega_0^2 \mathbf{M}^e \frac{d^2\mathbf{u}^{(0)e}}{d\tau^2} + \mathbf{K}^e\mathbf{u}^{(0)e} = \boldsymbol{f}_L^e\left(\mathbf{u}^{(0)e}\right) + \boldsymbol{f}_{int}^e. \tag{5.32}$$

$$\varepsilon^1 \colon \omega_0^2 \mathbf{M}^e \frac{d^2\mathbf{u}^{(1)e}}{d\tau^2} + \mathbf{K}^e\mathbf{u}^{(1)e} = -2\omega_0\omega_1 \mathbf{M}^e \frac{d^2\mathbf{u}^{(0)e}}{d\tau^2} + \boldsymbol{f}_{NL}^e\left(\mathbf{u}^{(0)e}\right). \tag{5.33}$$

Note that the nonlinear forcing occurs at first order equation expressed in terms of the linear solution $\mathbf{u}^{(0)\boldsymbol{e}}$. Equations ((5.32), (5.33)) are defined for a finite element within the membrane element. Therefore obtaining the equations of motion for entire periodic

element requires the assembly of finite elements which is performed by introducing the following transformation relating the local coordinates to the global coordinates

$$\mathbf{u}^e = \mathbf{A}_e \mathbf{u}. \tag{5.34}$$

Using Eq. (5.34) the ordered equations of motion can be expressed as,

$$\varepsilon^0: \omega_0^2 \mathbf{M} \frac{d^2\mathbf{u}^{(0)}}{d\tau^2} + \mathbf{K}\mathbf{u}^{(0)} = \boldsymbol{f}_L\left(\mathbf{u}^{(0)}\right) + \boldsymbol{f}_{int}. \tag{5.35}$$

$$\varepsilon^1: \omega_0^2 \mathbf{M} \frac{d^2\mathbf{u}^{(1)}}{d\tau^2} + \mathbf{K}\mathbf{u}^{(1)} = -2\omega_0\omega_1 \mathbf{M} \frac{d^2\mathbf{u}^{(0)}}{d\tau^2} + \boldsymbol{f}_{NL}\left(\mathbf{u}^{(0)}\right). \tag{5.36}$$

where,

$$\mathbf{M} = \sum_{\mathbf{1}}^{\boldsymbol{N_{el}}} \mathbf{A}_e^{\mathrm{T}} \mathbf{M}^e \mathbf{A}_e, \tag{5.37}$$

$$\mathbf{K} = \sum_{\mathbf{1}}^{\boldsymbol{N_{el}}} \mathbf{A}_e^{\mathrm{T}} \mathbf{K}^e \mathbf{A}_e, \tag{5.38}$$

$$\boldsymbol{f}_L\left(\mathbf{u}^{(0)}\right) = \sum_{\mathbf{1}}^{\boldsymbol{N_{el}}} \mathbf{A}_e^{\mathrm{T}} \boldsymbol{f}_L^e\left(\mathbf{u}^{(0)e}\right), \tag{5.39}$$

$$\boldsymbol{f}_{NL}\left(\mathbf{u}^{(0)}\right) = \sum_{\mathbf{1}}^{\boldsymbol{N_{el}}} \mathbf{A}_e^{\mathrm{T}} \boldsymbol{f}_{NL}^e\left(\mathbf{u}^{(0)e}\right). \tag{5.40}$$

where N_{el} is the total number of finite elements in the membrane periodic element.

1.1 LINEAR PERIODIC MEMBRANE MODEL

The perturbation approach as described in chapter 2 requires the solution of linear problem given by Eq. (5.35). The present section details the linear solution of the periodic structure formed by membrane elements under elastic support. Figure 52 demonstrates the finite element model of the periodic element. The ε^0 equation as described by Eq. (5.35) captures the linear dynamics of the membrane structure whose periodic elements are elastically supported at the boundaries. The linear force vector $\boldsymbol{f}_L\left(\mathbf{u}^{(0)}\right)$ contributes to the overall elemental stiffness of the membrane periodic element.

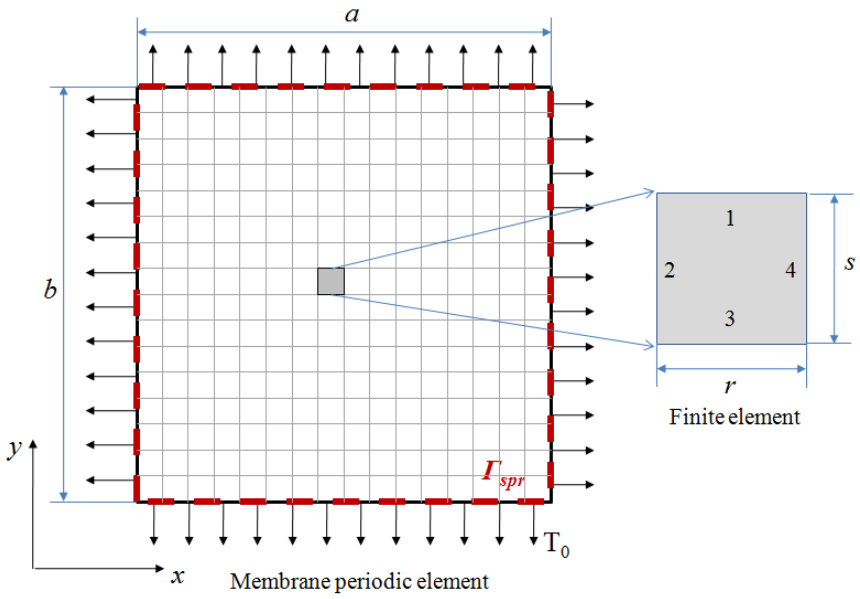

Figure 52: Schematic showing discretized periodic element of membrane structure. The elastic support is present on the boundary of the element indicated by a dashed line.

For example, if the elastic support is present on side 1 of the finite element, the equivalent stiffness matrix can be evaluated using Eq. (5.28),

$$\boldsymbol{f}_L^e(\mathbf{u}^e) = k_s \iint_{\mathcal{D}} \mathbf{H}^{\mathbf{T}}(x,y)\mathbf{H}(x,y)\delta(y-s)\,dxdy\mathbf{u}^e = k_s \int_0^r \mathbf{H}^{\mathbf{T}}(x,s)\mathbf{H}(x,s)\,dx\mathbf{u}^e = \mathbf{K}_{spr}^{(1)}\mathbf{u}^e, \tag{5.41}$$

therefore the equivalent stiffness due to elastic support which is present on the top boundary of the finite element can be expressed as,

$$\mathbf{K}_{spr}^{(1)} = k_s \int_0^r \mathbf{H}^{\mathrm{T}}(x,s)\mathbf{H}(x,s)\,dx, \tag{5.42}$$

Similarly, equivalent stiffness matrices for spring elements on the rest of the boundary can be expressed as,

$$\mathbf{K}_{spr}^{(2)} = k_s\left(\int_0^s \mathbf{H}^{\mathrm{T}}(0,y)\mathbf{H}(0,y)dy\right), \tag{5.43}$$

$$\mathbf{K}_{spr}^{(3)} = k_s\left(\int_0^r \mathbf{H}^{\mathrm{T}}(x,0)\mathbf{H}(x,0)dx\right), \tag{5.44}$$

$$\mathbf{K}_{spr}^{(4)} = k_s\left(\int_0^s \mathbf{H}^{\mathrm{T}}(r,y)\mathbf{H}(r,y)dy\right), \tag{5.45}$$

Hence, if n sides of a finite element are connected to the Γ_{spr}, then modified stiffness matrix can be given as,

$$\mathbf{K}_{mod}^{e} = \mathbf{K}^{\mathrm{e}} + \sum_{i=1}^{n} \mathbf{K}_{spr}^{(\mathrm{i})}, \tag{5.46}$$

where $\mathbf{K}^{e}$ is given by Eq. (5.20) and $\mathbf{K}_{spr}^{(\mathrm{i})}$ is given by either of the Eqs. ((5.42) - (5.45)).

The modified elemental stiffness (Eq. (5.20)) and mass matrices (Eq. (5.21)) are assembled over the finite element domain which comprises of 9-periodic elements as shown in Figure 53 to obtain global stiffness and mass matrices as this formulation leads to the elimination of internal forces for the reference element (refer chapter 2).

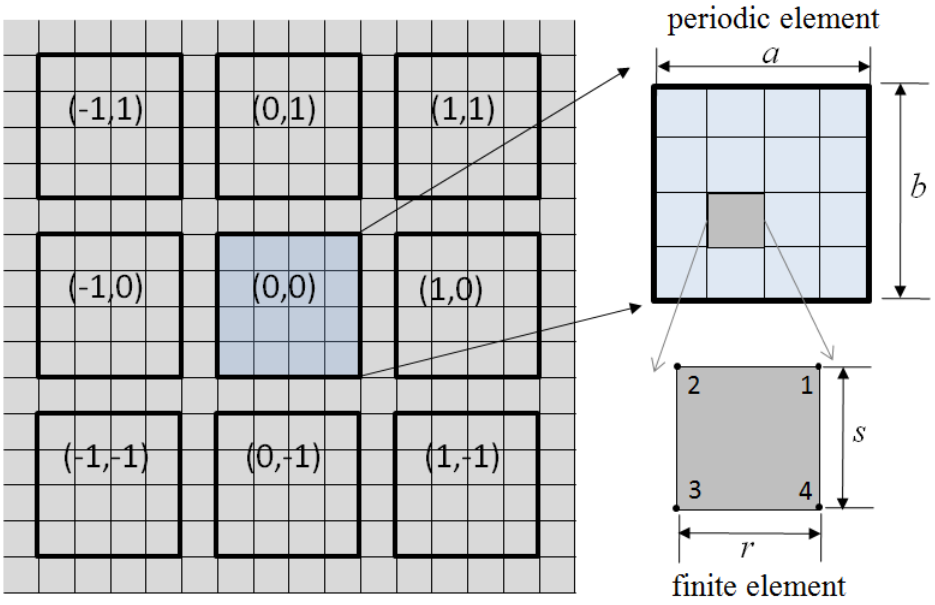

Figure 53: A schematic showing 9-periodic cells of a membrane under flexible support. The dark squares indicate the presence of elastic support which is also the boundary of periodic element

Using Bloch analysis, the linear wave modes are obtained by solving the eigenvalue problem similar to Eq. (2.20). Consider a membrane element with the following parameters,$\mathrm{T}_0 = 1\mathrm{Nm}^{-2}$, $\rho = 1\ \mathrm{kgm}^{-3}$, the linear elastic support on the boundary $k_s = 1\mathrm{Nm}^{-1}$, the dimensions of the unit cell $a = \mathrm{b} = 1\mathrm{m}$. 4-node rectangular elements are considered for the finite element model of the periodic membrane model. The geometry of the membrane element for the present analysis is a square and hence rectangular elements provide a convenient setting to generate finite element mesh. The shape of the finite element does not affect the solution in the present case as the structure is regular and continuous. But the accuracy of the solution obtained with a discretized structure depends on the mesh density, the finer the mesh the more accurate the solution is. For example, Figure 54 and Figure 55 depict the convergence of first two wave modes in an irreducible Brillouin zone as the number of finite elements within the unit cell denoted by N_{el} increases from 4 (coarse mesh) to 81 (fine mesh).

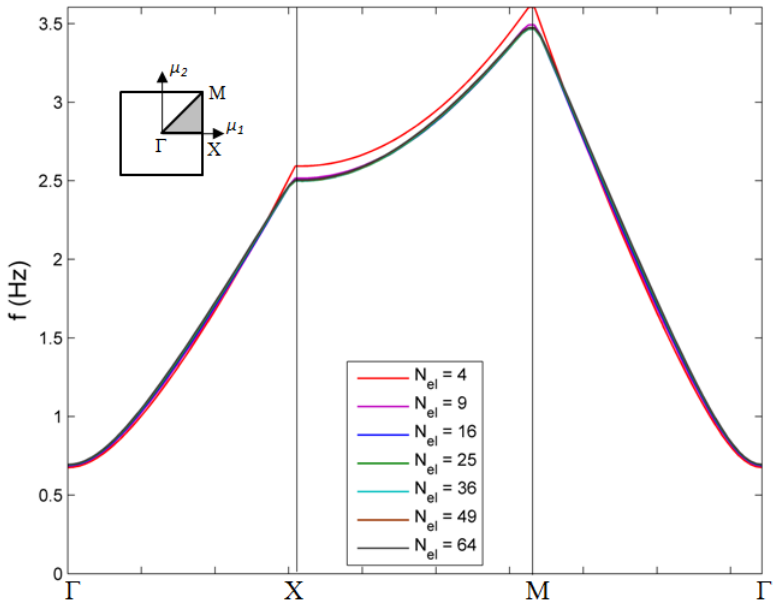

Figure 54: Convergence of the first linear wave mode with increasing mesh density

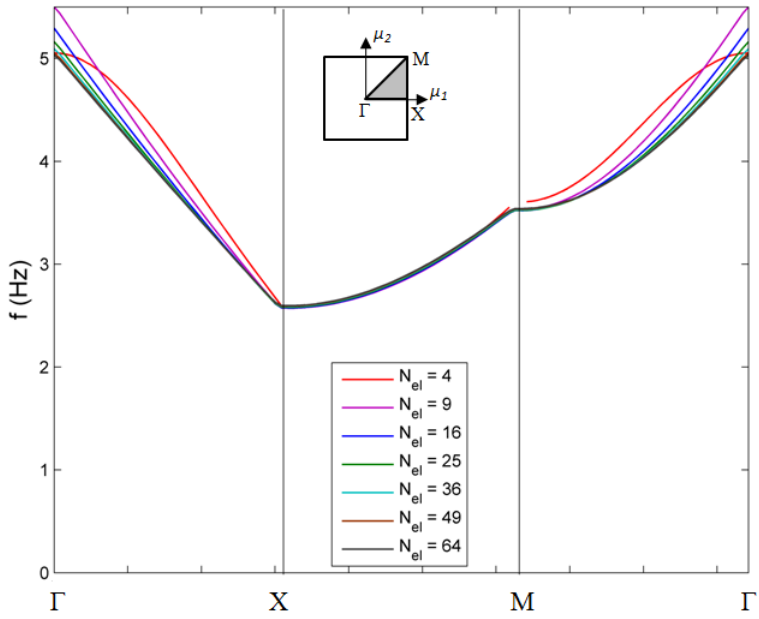

Figure 55: Convergence of the second linear wave mode with increasing mesh density

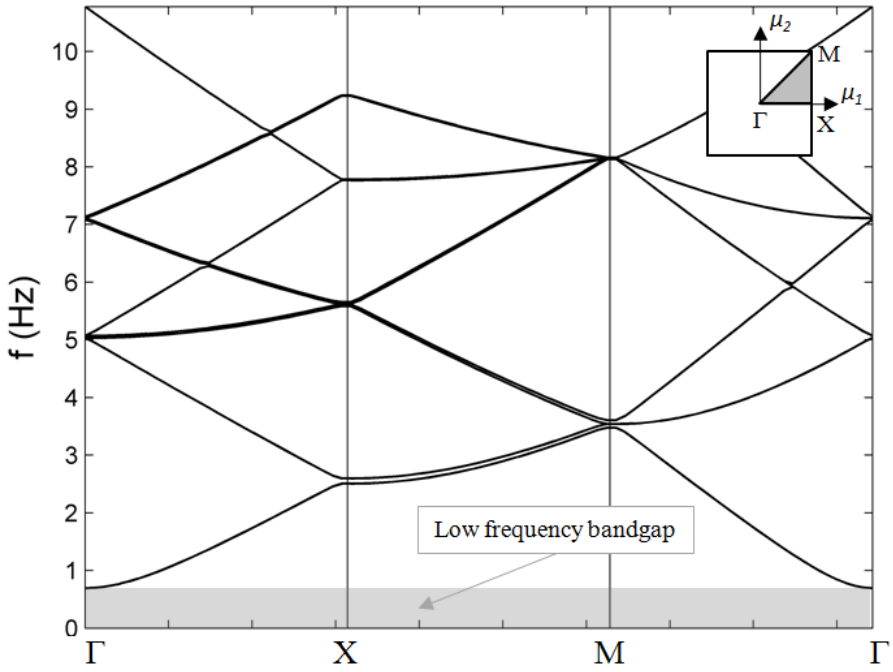

Figure 56: Linear wave modes for $k_s/T_0 = 0.5$ depicting a low frequency bandgap

From the above convergence study of the first two wave modes it is concluded that the wave modes can be captured accurately with 4-node rectangular elements with N_{el} set to 64. Two cases are considered, one with very low k_s/T_0 value indicating a weak

elastic support in comparison to the tension in the membrane, second with a high k_s/T_0 value indicating a strong elastic support. The first case considers the parameters $\mathrm{T}_0 = 1.0\ \mathrm{Nm}^{-1}$,$\rho = 1.0\ \mathrm{kgm}^{-3}$ and $k_s = 0.5\ \mathrm{Nm}^{-1}$ with $N_{el} = 64$. The band diagram for this as depicted by Figure 56 shows a low frequency bandgap whose width is determined by the magnitude of elastic support. This configuration does not allow any other bandgaps as shown by Figure 56. Second case considers the following configuration: parameters $\mathrm{T}_0 = 0.5\ \mathrm{Nm}^{-1}$, $\rho = 1.0\ \mathrm{kgm}^{-3}$ and $k_s = 5\ \mathrm{Nm}^{-1}$. Figure 57 shows the bandstructure for the considered configuration. The first bandgap occurs at low frequency and the large bandwidth is associated with the high $k_s/\mathrm{T}_0 = 10$ ratio considered for this configuration. Higher the ratio of k_s/T_0 the wider is the low frequency bandgap as the bounding frequency is determined by the magnitude of elastic support.

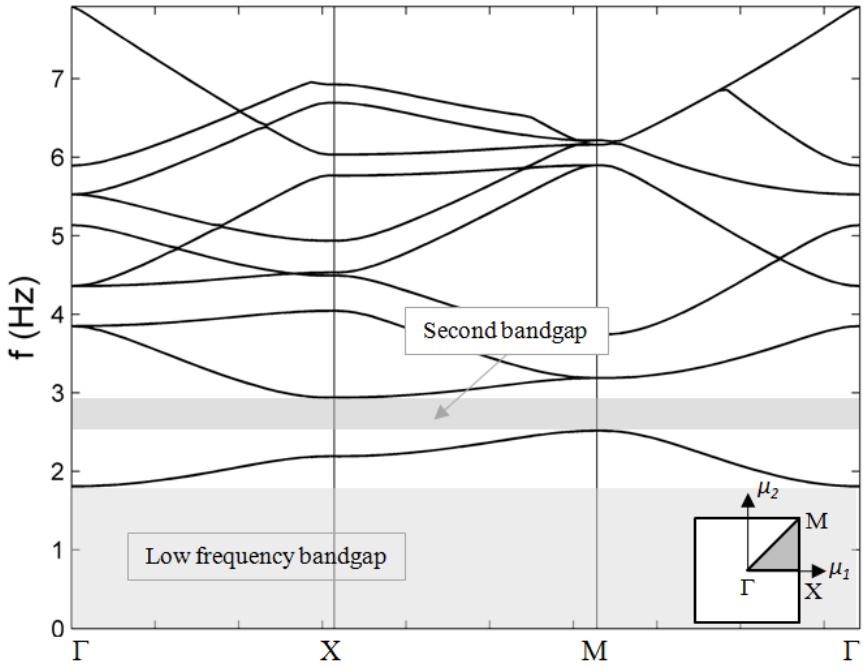

Figure 57: Linear wave modes for membrane configuration with $k_s/T_0 = 10$ depicting a large low frequency bandgap and second bandgap between first and second modes

As depicted in Figure 57 a second bandgap exists between the first and second wave mode for this configuration and for the frequencies beyond the second wave mode the

considered structure does not exhibit any bandgaps. The ratio of the stiffness of the ground support to the stiffness of the membrane is quite important in this problem as it directly affects the bandstructure of the periodic structure. Figure depicts that as the ratio k_s/T_0 increases, the bandgaps beyond the second mode emerge and the one can realize that the first mode appears to be a resonant mode as the slope of the curve remains close to zero along the irreducible Brillouin contour.

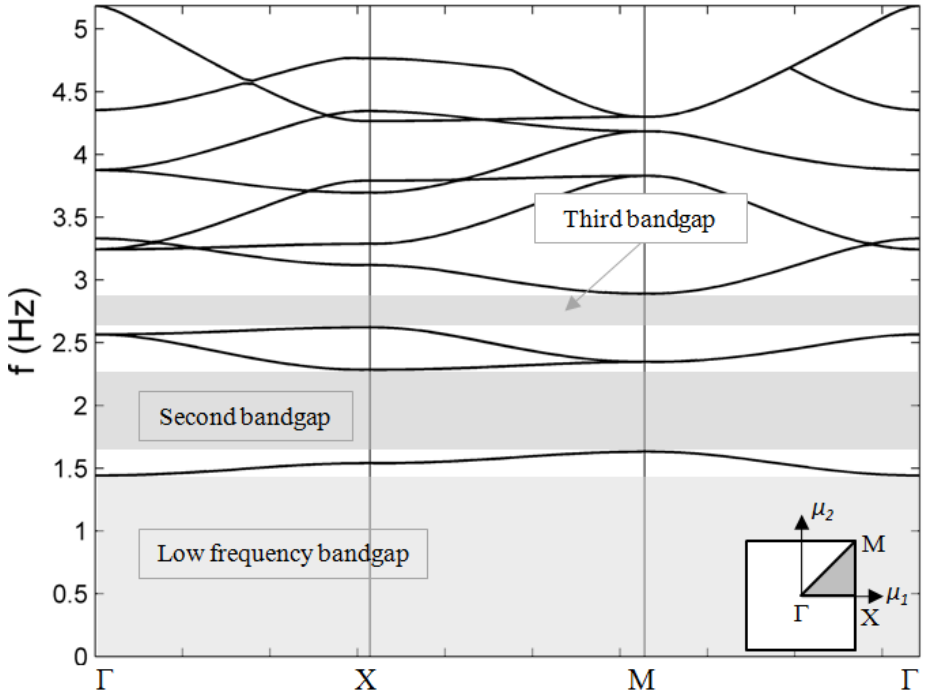

Figure 58: Linear wave modes for membrane configuration with $k_s/T_0 = 25$ depicting the emergence of a third bandgap. Increase in the ratio k_s/T_0 directly affects the bandstructure and the number of bandgaps

5.6 NONLINEAR PERIODIC MEMBRANE MODEL

The boundary of the membrane element is now assumed to be supported by a nonlinear flexible foundation (Figure 53). Note that the nonlinear component is of the order ε in comparison with the linear component as depicted by Eq. (5.27). The ordered equations obtained in section 5.5 given by Eqs. (5.35) and (5.36) reveal that the nonlinear forcing

only appears at the ε^1 order equation and is a function of the linear solution $\mathbf{u}^{(0)e}$. From the perturbation approach outlined in chapter 2, the first step to obtain the first order correction to the dispersion relation requires obtaining the correction coefficient $\boldsymbol{c_1}$ which is evaluated by substituting the linear wave solution into the nonlinear force vector $\boldsymbol{f}_{NL}^{e}\left(\mathbf{u}^{(0)e}\right)$ and obtaining the fundamental harmonic component. Therefore the first step is to analytically express the generalized nonlinear force vector in terms of the linear nodal displacements which are obtained from the ε^0 equation. The next step requires evaluating $\boldsymbol{c}_1$ to obtain the first order nonlinear dispersion relation. The two steps are detailed in the following sections for the periodic membrane problem.

5.6.1 GENERALIZED NONLINEAR FORCE VECTOR

Due to the ordered equations, the nonlinear forcing appears at ε^1 order and nonlinear force is expressed in terms of linear solution. Considering the cubic nonlinearity, the perturbation approach requires the generalized nonlinear force vector which is given by Eq. (5.29) now be expressed in terms of the linear solution $\mathbf{u}^{(0)\boldsymbol{e}}$,

$$\boldsymbol{f}_{NL}^{e}\left(\mathbf{u}^{(0)e}\right) = \Gamma_{\mathrm{s}} \iint_{\mathcal{D}} \mathbf{H}^{\mathrm{T}}\left(\mathbf{H}\mathbf{u}^{(0)e}\right)^{3}\Big|_{\Gamma_{spr}} dxdy. \tag{5.47}$$

Since the nonlinear force is present only on the boundary of the periodic element, generalized force vectors are zero for all the finite elements not connected to the boundary of the periodic element. For all the elements connected to the boundary, Eq. (5.47) can be used to analytically determine the expressions for the generalized nonlinear force vector. As the linear problem utilized four node rectangular elements with linear interpolation functions the same follows to express the nonlinear force vector.

Analytical expressions for the nonlinear force vector are derived in the following manner. Assuming that the finite element's left boundary is on the nonlinear flexible support the $\boldsymbol{f}_{NL}^{e}\left(\mathbf{u}^{(0)e}\right)$ given by Eq. (5.47) can be expressed as,

$$\boldsymbol{f}_{NL}^{e}\left(\mathbf{u}^{(0)e}\right) = \Gamma_s \iint_{\mathcal{D}} \mathbf{H}^{\mathrm{T}}(x,y)\left(\mathbf{H}(x,y)\,\mathbf{u}^{(0)e}\right)^3 \delta(x)\,dxdy = \Gamma_s \int_0^s \mathbf{H}^{\mathrm{T}}(0,y)\left(\mathbf{H}(0,y)\,\mathbf{u}^{(0)e}\right)^3 dy \tag{5.48}$$

The shape function matrix **H** for a four node element can be given as,

$$\mathbf{H} = \left[\left(\frac{xy}{rs}\right), \quad \left(\frac{y}{s} - \frac{xy}{rs}\right), \quad \left(\frac{xy}{rs} - \frac{y}{s} - \frac{x}{r} + 1\right), \quad \left(\frac{x}{r} - \frac{xy}{rs}\right)\right], \tag{5.49}$$

where r and s denote the width and height of the finite element (Figure 52). Therefore,

$$\mathbf{H}(0,y)\mathbf{u}^{(0)e} = \begin{bmatrix} 0 & \frac{y}{s} & 1-\frac{y}{s} & 0 \end{bmatrix} \begin{Bmatrix} \mathrm{u}_1^{(0)} \\ \mathrm{u}_2^{(0)} \\ \mathrm{u}_3^{(0)} \\ \mathrm{u}_4^{(0)} \end{Bmatrix} = \mathrm{u}_3^{(0)} + \frac{(\mathrm{u}_2^{(0)} - \mathrm{u}_3^{(0)})y}{s}. \tag{5.50}$$

Hence, Eq. (5.48) can be rewritten by substituting Eq. (5.50),

$$\boldsymbol{f}_{NL}^{e}\left(\mathbf{u}^{(0)e}\right) = \Gamma_s \int_0^s \mathbf{H}^{\mathrm{T}}(0,y)\left(\mathrm{u}_3^{(0)} + \frac{(\mathrm{u}_2^{(0)} - \mathrm{u}_3^{(0)})y}{s}\right)^3 dy, \tag{5.51}$$

Therefore for the finite element connected to the left boundary of the periodic element, the generalized nonlinear force vector can be expressed as,

$$\boldsymbol{f}_{NL}^{e}\left(\mathbf{u}^{(0)e}\right) = \Gamma_s \begin{bmatrix} 0 \\ s\left(4\mathrm{u}_2^{(0)^3} + 3\mathrm{u}_2^{(0)^2}\mathrm{u}_3^{(0)} + 2\mathrm{u}_2^{(0)}\mathrm{u}_3^{(0)^2} + \mathrm{u}_3^{(0)^3}\right)/20 \\ s\left(\mathrm{u}_2^{(0)^3} + 2\mathrm{u}_2^{(0)^2}\mathrm{u}_3^{(0)} + 3\mathrm{u}_2^{(0)}\mathrm{u}_3^{(0)^2} + 4\mathrm{u}_3^{(0)^3}\right)/20 \\ 0 \end{bmatrix}. \tag{5.52}$$

Similarly, the generalized nonlinear force vector can be expressed for each finite element forming the whole periodic element. The generalized nonlinear force vector for the elements connected to the right boundary of the periodic element is given as,

$$\boldsymbol{f}_{NL}^{e}(\,\mathbf{u}^{(0)e}) = \Gamma_s \begin{bmatrix} s\left(4u_1^{(0)^3} + 3u_1^{(0)^2}u_4^{(0)} + 2u_1^{(0)}\,u_4^{(0)^2} + u_4^{(0)^3}\right)/20 \\ 0 \\ 0 \\ s\left(u_1^{(0)^3} + 2u_1^{(0)^2}u_4^{(0)} + 3u_1^{(0)}\,u_4^{(0)^2} + 4u_4^{(0)^3}\right)/20 \end{bmatrix}. \quad (5.53)$$

Similarly for the finite element connected to the top boundary of the periodic element,

$$\boldsymbol{f}_{NL}^{e}(\,\mathbf{u}^{(0)e}) = \Gamma_s \begin{bmatrix} r\left(4u_1^{(0)^3} + 3u_1^{(0)^2}u_2^{(0)} + 2u_1^{(0)}\,u_2^{(0)^2} + u_2^{(0)^3}\right)/20 \\ r\left(u_1^{(0)^3} + 2u_1^{(0)^2}u_2^{(0)} + 3u_1^{(0)}\,u_2^{(0)^2} + 4u_2^{(0)^3}\right)/20 \\ 0 \\ 0 \end{bmatrix}. \quad (5.54)$$

And for the finite element connected to the bottom boundary of the periodic element,

$$\boldsymbol{f}_{NL}^{e}(\,\mathbf{u}^{(0)e}) = \Gamma_s \begin{bmatrix} 0 \\ 0 \\ r\left(4u_3^{(0)^3} + 3u_3^{(0)^2}u_4^{(0)} + 2u_3^{(0)}\,u_4^{(0)^2} + u_4^{(0)^3}\right)/20 \\ r\left(u_3^{(0)^3} + 2u_3^{(0)^2}u_4^{(0)} + 3u_3^{(0)}\,u_4^{(0)^2} + 4u_4^{(0)^3}\right)/20 \end{bmatrix}. \quad (5.55)$$

5.6.2 CORRECTION COEFFICIENT C_1

After the elemental nonlinear force vectors are obtained, the next step requires the computation of the correction coefficient $\boldsymbol{c_1}$. Let us assume that the normalized linear wave modes to this problem are obtained from solving the eigenvalue problem similar to Eq. (2.20). Following the procedure outlined in chapter 2, it is shown that the nonlinear force vector is a periodic function which can be expressed in Fourier series described by Eq. (2.44). The coefficient $\boldsymbol{c_1}$ defines the amplitude of the fundamental harmonic and the evaluation of this term facilitates the estimation of the first order correction to the dispersion. The present section describes in detail the computation of coefficient $\boldsymbol{c_1}$ for the membrane problem.

For j^{th} mode the linear solution can be expressed as,

$$\mathbf{u}^{(0)}(\tau) = A_0 \mathbf{u}_{0,j} e^{i\tau} + c.c, \tag{5.56}$$

where $\mathbf{u}_{0,j}$ defines the normalized complex mode shape vector. Using Eq. (2.45), the amplitude of the fundamental harmonic can be given as,

$$\boldsymbol{c}_{1,j} = \frac{1}{2\pi} \int_0^{2\pi} \boldsymbol{f}_{NL}\left(A_0, \mathbf{u}_{0,j}, \tau\right) e^{-i\tau} d\tau \tag{5.57}$$

Substituting Eq. (5.40) into Eq. (5.57) and assuming that the j^{th} mode linear solution for the element $\mathbf{u}^{(0)e}(\tau) = A_{0,j} \mathbf{u}_{0,j}^{e} \cos(\phi)$, the coefficient $\boldsymbol{c}_1$ can be expressed as,

$$\boldsymbol{c}_{1,j} = \tfrac{1}{2\pi} \textstyle\int_0^{2\pi} \sum_1^{N_{el}} \mathbf{A}_e^{\mathrm{T}} \boldsymbol{f}_{NL}^{e}\left(A_0, \mathbf{u}_{0,j}, \tau\right) e^{-i\tau} d\tau, \tag{5.58}$$

The above equation implies that each elemental nonlinear force vector is evaluated by substituting the normalized linear mode values in place of nodal displacements. Taking the summation out of the integration, Eq. (5.58) can be expressed as,

$$\boldsymbol{c}_{1,j} = \textstyle\sum_1^{N_{el}} \mathbf{A}_e^{\mathrm{T}} \left(\tfrac{1}{2\pi} \int_0^{2\pi} \boldsymbol{f}_{NL}^{e}\left(A_0, \mathbf{u}_{0,j}, \tau\right) e^{-i\tau} d\tau \right). \tag{5.59}$$

5.7 DISPERSION USING PERTURBATION APPROACH

The present section details the application of perturbation approach to obtain dispersion in two-dimensional membrane on weakly nonlinear flexible support. All the elements required for the perturbation analysis are obtained in the previous sections which includes the generalized nonlinear force vector expressed in terms of nodal displacements and the estimation of the coefficient $\boldsymbol{c}_1$. A step-by-step procedure of the application of perturbation analysis is detailed below:

1) Consider a discretized domain of a 9-periodic element structure as shown in Figure 53. Obtain the global mass $\mathbf{M}_g$ and global stiffness $\mathbf{K}_g$ matrices. The linear part of the stiffness on the boundary of periodic element is included in $\mathbf{K}_g$ using

Eq. (5.46). The present analysis assumed 64 4-node rectangular finite elements per unit cell.

2) Next step requires the partitioning of the global mass and stiffness matrices to obtain $\mathbf{M}^{(p,q)}$ and $\mathbf{K}^{(p,q)}$. From these matrices, the eigenvalue problem defined by Eq. (2.20) is solved to obtain linear dispersion including linear mode shapes $\mathbf{u}_{0,j}(\mathbf{k})$.
3) Now the normalized linear mode shape for the j^{th} mode $\mathbf{u}_{0,j}(\mathbf{k})$ is substituted into elemental nonlinear force vector described by Eqs. (5.52) - (5.55) and using Eq. (5.56) the correction coefficient $\boldsymbol{c}_1$ for the j^{th} mode is obtained.
4) Once $\boldsymbol{c}_{1,j}$ is obtained, the first order correction to the wave frequency can be computed using Eq. (2.59) and Eq. (2.60) evaluates the corrected frequency for the j^{th} mode.

5.8 AMPLITUDE-DEPENDENT DISPERSION

The dispersion in the two-dimensional membrane on a nonlinear foundation is analyzed through band diagrams which are now amplitude dependent. The first case considers the parameters $\mathrm{T} = 1.0\ \mathrm{Nm}^{-1}$,$\rho = 1.0\ \mathrm{kgm}^{-3}$, $k_s = 0.5\ \mathrm{Nm}^{-1}$, $\Gamma_s = -2\ \mathrm{Nm}^{-3}$ and the small parameter $\varepsilon = 0.1$. The small parameter ε is introduced in the asymptotic expansion of frequency and displacement given by Eqs. (5.29, 5.30). Although the magnitude of cubic nonlinearity appears to be large in comparison with k_s the overall system is still weakly nonlinear due to the stiffness of the membrane. The band diagram is demonstrated in Figure 59 in which the first 10 modes are displayed at two different wave amplitudes $A = 0.1$ and $A = 2.0$. The low wave amplitude $A = 0.1$ bandstructure is similar to the linear bandstructure for the present configuration displayed by Figure 56. As the wave amplitude increases, the nonlinear dynamics come into play affecting the overall bandstructure.

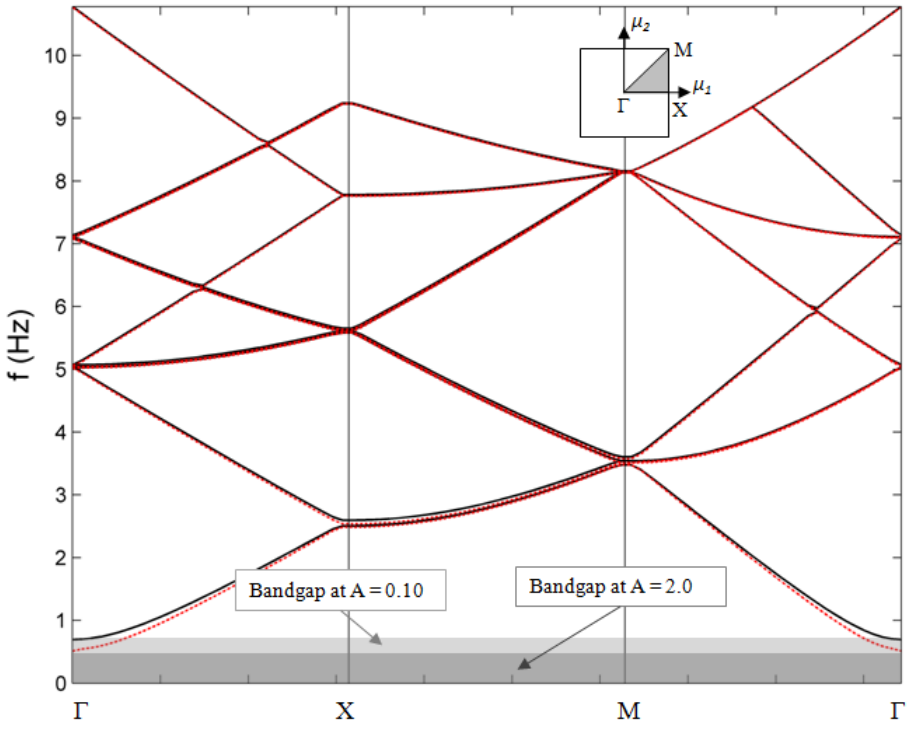

Figure 59: Band diagram of membrane on nonlinear support at two different amplitudes — A = 0.10 and ····· A = 2.0 demonstrating the shift in low frequency bandgap

The present case assumes a soft nonlinear foundation which generates a downward shift of the dispersion curves as the wave amplitude increases. This result is similar to that of the amplitude dependent dispersion predicted in soft nonlinear spring mass models. Of important note is the shift in low frequency bandgap whose width is primarily governed by the elastic ground support. Due to soft nonlinear foundation, the low frequency bandgap is decreased significantly (approximately 40%) by increase in amplitude varies from $A = 0.10$ to $A = 2.00$. This implies that the low frequency wave propagation can be controlled with variation in wave amplitude.

5.9 CONCLUSIONS

The dispersion in a periodic structure employing elastically supported membrane elements has been analyzed using perturbation approach outlined in chapter 2. Weak form of governing equations of motion is derived and a finite element model is

developed. The dispersion behavior is observed to be affected by the ratio of support stiffness to membrane tension. With the nonlinear model and at low k_s/T_0 ratio, there exists a strong dependence of the low frequency bandgap on the wave amplitude. But as the ratio increases, the band diagram modifies in two ways; the first being the upward shift of the first mode depending on the support stiffness and the second being the appearance of the bandgap between the first and the second mode. For this case, i.e. high k_s/T_0 ratio, the first mode does not appear to have significant dependence on the amplitude but the bandgap between the first and second mode appears to weaken with increase in wave amplitude.

Overall, the effect of amplitude and nonlinearity on the plane wave dispersion in complex nonlinear periodic structure is captured by perturbation analysis. Finally the analysis demonstrated the applicability of perturbation approach to evaluate the dispersion in complex weakly nonlinear periodic structure with aid of Finite element formulation.

CHAPTER VI

STRONGLY NONLINEAR PERIODIC STRUCTURES

6.1 OVERVIEW

The present chapter documents the plane wave propagation characteristics in strongly nonlinear systems. A plane wave can be injected into the structure through point harmonic forcing or by directly imposing a specific wavelength (wavenumber) into the structure. The latter is analogous to how a plane wave is injected into a piezoelectric substrate by an inter-digital-transducer (IDT) in a surface acoustic wave device [71] (Figure 60). One of the examples of strongly nonlinear periodic systems is granular media. The contact dynamics which govern the motion of each granule makes the system strongly nonlinear. For granular chains composed of metallic beads, the magnitude of nonlinearity can be tuned in accordance with the initial pre-compression [42].

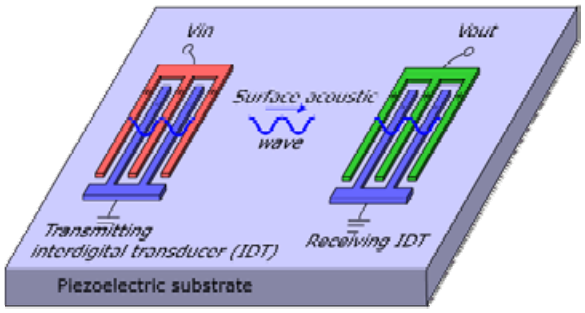

Figure 60: A schematic of SAW device injecting plane wave [71]

The focus is on the analysis of plane wave propagation in pre-compressed chain with wave amplitudes comparable to the initial pre-compressive displacement of the beads. Such strongly nonlinear granular chains under pre-compression allow acoustic waves with strong amplitude dependent dispersive properties that could potentially lead to tunable acoustic applications with wave amplitude as tuning parameter.

Effect of weak nonlinearities on the dispersion of periodic systems as predicted by the general perturbation analysis has been presented in previous chapters. Due to the weak nonlinearity, the solution is expressed as a perturbation from the linear solution and the effects are observed to be prominent with a large variation in wave amplitude. As mentioned earlier, nonlinear periodic systems exhibit very rich and interesting dynamics such as solitary wave propagation and localization phenomenon [40, 72]. One example of a strongly nonlinear periodic media is a granular material in which the contact forces are of Hertzian type. Granular media are of significant practical importance as they have been considered for shock wave mitigators, for example in explosive test environments [73, 74]. The nonlinearity in the granular chain stems from the geometry of the granules. Although the strain in the granule is within the elastic limit, the geometry of the granule determines the nonlinearity of the interaction. Typically, such interaction is modeled using Hertz contact force law which has been experimentally validated by Coste and Gilles [75] who studied acoustic wave and solitary wave propagation in chains comprised of spherical beads made of different materials.

Nesterenko et al. [41] first revealed the existence of solitary waves that propagate without separation of granules under zero pre-compression. Uncompressed granular chains possess no linear restoring forces, hence cannot support any travelling wave which leads to the characterization of such media as *sonic vacuum*. Granular chains under zero pre-compression support strongly nonlinear waves and some of the analytical and experimental results can be found in recent literature [76-84]. For example, Herbold et al. [85] demonstrate tunability of the solitary wave speed in one-dimensional chain of beads for varying pre-compression and wave amplitude. A more detailed analytical study on uncompressed chain of beads has been reported by Starosvetsky and Vakakis [86]. With energy arguments, the authors analyze one, two, three and four bead finite chains with applied periodic boundary conditions. A two bead cyclic chain is observed to exhibit only standing waves with out-of-phase mode. As the number of granules increases the authors

report the existence of a family of travelling waves with the help of nonlinear modes revealed by Poincare' maps. As $N \to \infty$ in an N-bead cyclic chain, the solution tends to a solitary wave as reported by Nesterenko [41]. Also, the authors report localized standing waves leading to the concept of "energy trapping". Nesterenko and Herbold [87] report the generation of quasi-periodic strain waves in compressed granular chains with two different amplitudes as the harmonic forcing amplitude reaches the initial pre-compression. Numerical simulations impose a single harmonic force excitation at the boundary which leads to the modulation of excitation frequency as the force is transmitted through the chain. Such modulation depends on the ratio of excitation frequency and the characteristic cut-off frequency which depends on the stiffness of contacting spheres and initial static pre-compressive force. Based on the force-time envelope modulation observed in single harmonic excitation, authors then construct a special composite force function which is essentially a summation of different harmonic force functions. Such a composite force applied at the boundary generates a force-time envelope in the chain that does not appear to change its shape, thus indicating a strongly nonlinear periodic wave.

The next section details the application of harmonic balance method presented in chapter 2 section 2.6 to predict the plane wave dispersion in strongly nonlinear granular chains.

6.2 MONO-ATOMIC GRANULAR CHAIN

6.2.1 MODEL DESCRIPTION

A mono-atomic chain consists of a unit cell whose dynamic behavior is described by a single degree of freedom. A schematic of the mono-atomic chain formed by spherical beads is shown in Figure 61. The chain is initially pre-compressed with a static force F_0 acting on both ends which compresses the chain by δ_0 (compression in each sphere). For the present analysis, the mono-atomic chain is modeled with the following assumptions:

a) The contact force is modeled by Hertzian contact law which implies that the strain in each bead does not exceed the elastic limit
b) Although implied by Hertz law, no dissipation due to frictional forces is assumed
c) Plane wave amplitudes are such that the beads do not separate or there is no loss of contact

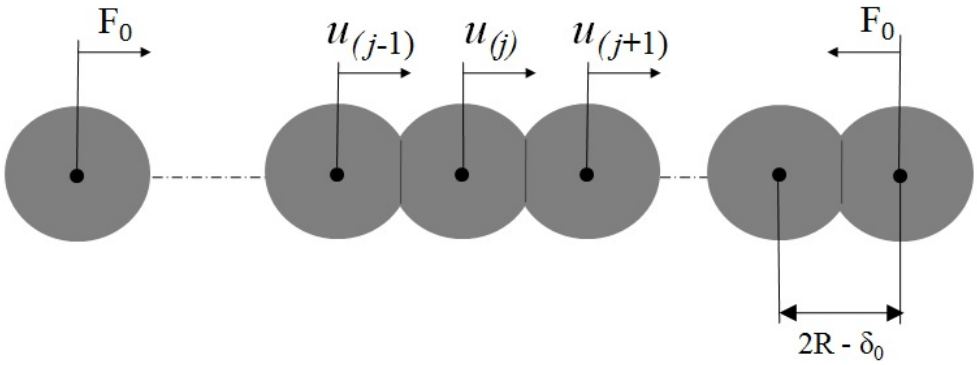

Figure 61: Schematic of a mono-atomic chain [88]

6.2.2 EQUATIONS OF MOTION

The index notation for a general 2D periodic structure as detailed in chapter 2 section 2.2 is slightly modified. For the present 1D granular chain, $n_2 = 0$, the index n_1 which defines the number of mass from the reference mass is replaced by j. Assuming the Hertz contact law, the equations of motion for the j^{th} mass can be written as,

$$\frac{d^2u_j}{dt^2} = \Gamma\left(\eta_j^+\right)^{3/2} - \Gamma\left(\eta_{j+1}^+\right)^{3/2} \tag{6.1}$$

$$\eta_j = \delta_0 - \left(u_j - u_{j-1}\right) \tag{6.2}$$

where

$$\Gamma = \frac{E(2R)^{1/2}}{3(1-v^2)m} \tag{6.3}$$

where the following notation is adopted;

$$\eta^{+} = \begin{cases} \eta \ \forall \ \eta \geq 0 \\ 0 \ \forall \ \eta < 0 \end{cases}. \tag{6.4}$$

Also E denotes the elastic modulus, R and m are respectively the radius and the mass of the sphere and υ is Poisson's ratio. In the next section, the dispersion analysis of a mono-atomic chain is predicted first by perturbation analysis with the assumption that the relative displacement between the masses is much smaller than the initial pre-compression ($\delta_0 \gg u_j - u_{j-1}$). With this assumption, the nonlinear force can be expanded into asymptotic series that allows the application of perturbation analysis. The motivation to perform perturbation analysis is to qualitatively determine the variation of the bandstructure as the wave amplitude varies. Next, the trend predicted by the perturbation analysis is confirmed by other analytical methods applicable to strongly nonlinear problems such as He's method [89, 90] as described later in this section along with the generalized harmonic balance method described in chapter 2 section 2.6.

6.2.3 ESTIMATION OF DISPERSION THROUGH PERTURBATION ANALYSIS

A more general approach of the perturbation procedure is detailed in chapters 3 and 4 wherein various one and two-dimensional unit cell configurations are examined and closed-form dispersion relations are obtained. Eq. (6.1) is transformed by Taylor series expansion more suitable for perturbation analysis. It is assumed that

$$\frac{|u_{j-1} - u_j|}{\delta_0} \ll 1. \tag{6.5}$$

The Taylor series expansion truncated to three terms gives,

$$\ddot{u}_j = \alpha\left(u_{j-1} + u_{j+1} - 2u_j\right) + \beta\left(\left(u_{j-1} - u_j\right)^2 - \left(u_j - u_{j+1}\right)^2\right) + \gamma\left(\left(u_{j-1} - u_j\right)^3 - \left(u_j - u_{j+1}\right)^3\right) + O\left(\left(u_j\right)^4 \ldots\right) \tag{6.6}$$

where,

$$\alpha = \frac{3}{2}\Gamma\delta_0^{1/2}, \beta = \frac{3}{8}\Gamma\delta_0^{-1/2}, \gamma = -\frac{1}{16}\Gamma\delta_0^{-3/2}. \tag{6.7}$$

Introducing non-dimensional time $\tau = \omega t$ and substituting the following displacement and frequency expansions about the linear solution into Eq. (6.6),

$$\omega = \omega_0 + \varepsilon\omega_1 + \varepsilon^2\omega_2 + O(\varepsilon^3), \tag{6.8}$$

$$u_j = \varepsilon u_j^{(0)} + \varepsilon^2 u_j^{(1)} + \varepsilon^3 u_j^{(2)} + O(\varepsilon^4), \tag{6.9}$$

leads to following ordered equations:

$$\varepsilon^1: \omega_0^2 \frac{d^2u_j^{(0)}}{d\tau^2} + \alpha\left(2u_j^{(0)} - u_{j-1}^{(0)} - u_{j+1}^{(0)}\right) = 0, \tag{6.10}$$

$$\varepsilon^2: \omega_0^2 \frac{d^2u_j^{(1)}}{d\tau^2} + \alpha\left(2u_j^{(1)} - u_{j-1}^{(1)} - u_{j+1}^{(1)}\right) = -2\omega_0\omega_1 \frac{d^2u_j^{(0)}}{d\tau^2} + \beta\left(u_{j+1}^{(0)} + u_{j-1}^{(0)} - 2u_j^{(0)}\right)\left(u_{j-1}^{(0)} - u_{j+1}^{(0)}\right), \tag{6.11}$$

$$\varepsilon^3: \omega_0^2 \frac{d^2u_j^{(2)}}{d\tau^2} + \alpha\left(2u_j^{(2)} - u_{j-1}^{(2)} - u_{j+1}^{(2)}\right) = -2\omega_0\omega_1 \frac{d^2u_j^{(1)}}{d\tau^2} - (\omega_1^2 + 2\omega_0\omega_2)\frac{d^2u_j^{(0)}}{d\tau^2} + \beta\left(u_{j+1}^{(0)} + u_{j-1}^{(0)} - 2u_j^{(0)}\right)\left(u_{j-1}^{(1)} - u_{j+1}^{(1)}\right) + \beta\left(u_{j+1}^{(1)} + u_{j-1}^{(1)} - 2u_j^{(1)}\right)\left(u_{j-1}^{(0)} - u_{j+1}^{(0)}\right) + \gamma\left(\left(u_{j-1}^{(0)} - u_j^{(0)}\right)^3 - \left(u_j^{(0)} - u_{j+1}^{(0)}\right)^3\right), \tag{6.12}$$

Next, a plane wave solution is imposed to yield the following generator solutions,

$$u_j^{(0)} = \frac{A}{2} e^{i\mu j} e^{i\tau} + c.c., \tag{6.13}$$

$$u_{j\pm1}^{(0)} = \frac{A}{2} e^{i\mu(j\pm1)} e^{i\tau} + c.c., \tag{6.14}$$

where $c.c.$ denotes complex conjugate of the preceding terms, A is the wave amplitude and μ defines the nondimensional wavenumber. The linear dispersion relation is obtained by substituting Eq. (6.13) into Eq. (6.10),

$$\omega_0 = \sqrt{2\alpha\big(1 - cos(\mu)\big)}. \tag{6.15}$$

The updated ε^2 order equation after substitution of Eq. (6.13) is given by,

$$\varepsilon^2 \colon \omega_0^2 \frac{d^2 u_j^{(1)}}{d\tau^2} + \alpha\Big(2u_j^{(1)} - u_{j-1}^{(1)} - u_{j+1}^{(1)}\Big) = c_1 e^{i\mu j} e^{i\tau} + c_2 e^{i2\mu j} e^{i2\tau} + c.c., \tag{6.16}$$

where *c.c.* denotes complex conjugate of all the preceding terms and the coefficient c_1 and c_2 are given by,

$$c_1 = 2\omega_0\omega_1,\ c_2 = i\left(\frac{\beta \mathrm{A}^2}{2}(\sin(2\mu) - 2\sin(\mu))\right), \tag{6.17}$$

The homogenous part of Eq. (6.16) is similar to Eq. (6.10) and it can be shown that all the terms in the forcing function (i.e. RHS of Eq. (6.16)) with spatial-temporal form of $e^{i\mu j} e^{i\tau}$ yield an unbounded solution for $u_j^{(1)}$ and therefore need to be eliminated (secular). To eliminate the secular term the coefficient $c_1 = 0$ and hence from Eq. (6.17), $2\omega_0\omega_1 = 0$. As $\omega_0 \neq 0\ \forall\ \mu$, the solution to $2\omega_0\omega_1 = 0$ leads to the first order correction of frequency $\omega_1 = 0$. But the remaining forcing in Eq. (6.16) always occurs at

$e^{i2\mu j}e^{i2\tau}$ and hence a particular solution for $u_j^{(1)}$ is found at this order for a subsequent substitution in the next ordered equation to find second order correction to the frequency.

$$u_j^{(1)} = \mathrm{A}_1 e^{i\mu j}e^{i\tau} + \mathrm{B}_1 e^{i2\mu j}e^{i2\tau} + c.c., \tag{6.18}$$

where,

$$\mathrm{B}_1 = \frac{-c_2}{4\omega_0^2+\omega_s^2}, \tag{6.19}$$

$$\omega_s = \sqrt{2\alpha(cos(2\mu)-1)}, \tag{6.20}$$

By substituting Eq. (6.18)and Eq. (6.13) into Eq. (6.12), the following equation results,

$$\omega_0^2\frac{d^2u_j^{(2)}}{d\tau^2} + \alpha\left(2u_j^{(2)} - u_{j-1}^{(2)} - u_{j+1}^{(2)}\right) = d_1e^{i\mu j}e^{i\tau} + d_3e^{i3\mu j}e^{i3\tau} + c.c. \tag{6.21}$$

The linear kernel of Eq. (6.21) is similar to Eq. (6.10). Also the forcing term $e^{i\mu j}e^{i\tau}$ yields an unbounded solution for $u_j^{(2)}$therefore d_1 is set to zero which yields an expression for frequency correction at second order.

The closed form expression for frequency correction at second order in terms of linear and nonlinear parameters is given by,

$$\omega_2 = \frac{\mathrm{A}^2\left((3\gamma\alpha-2\beta^2)(\cos(\mu))^2-6\gamma\alpha\cos(\mu)+2\beta^2+3\gamma\alpha\right)}{2\alpha\omega_0}, \tag{6.22}$$

Hence, the frequency of the wave is a function of wave amplitude A and of the non-dimensional wavenumber μ which is expressed as $\omega = \omega_0 + \varepsilon^2\omega_2$, where ω_0 and ω_2 are given by Eq. (6.15) and Eq. (6.21) respectively. From Eq. (6.6), it is observed that the nonlinearity is present in quadratic and in the cubic form. The quadratic nonlinearity is hardening indicating an increase in cut-off frequency with increase in the amplitude while

the cubic is softening implying that the cut-off frequency decreases with increase in the amplitude. From the results detailed in the previous chapters that the hardening stiffness increases the cutoff frequencies while the softening decreases the cutoff frequencies with increasing wave amplitude. Figure 62 depicts the dispersion trend predicted by perturbation analysis with change in amplitude for a generic Hertzian-modeled periodic chain with parameters $E = 68.9$ GPa, $R = 9.5025\,mm$, $\nu = 0.35$, $m = 9.73\,g$ and $\mathrm{F}_0 = 20$ N.

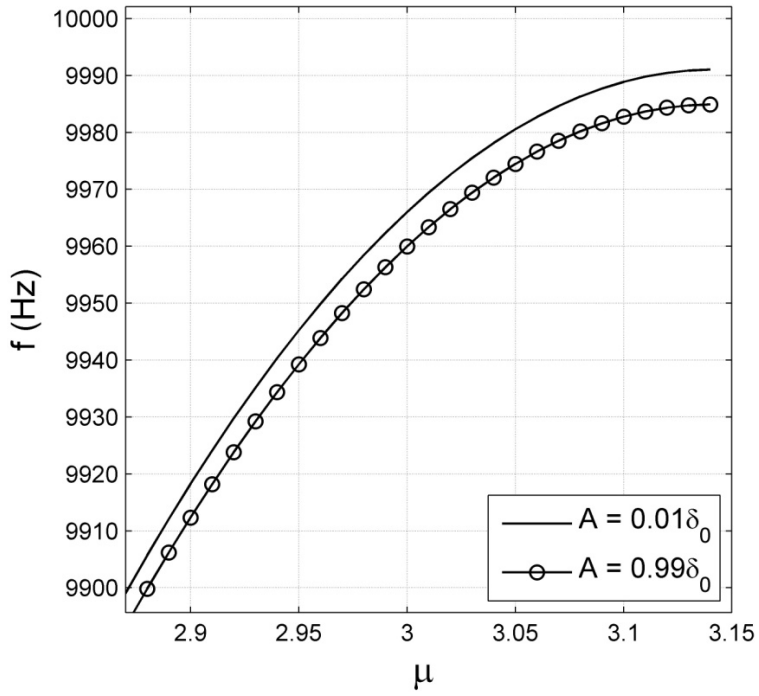

Figure 62: Dispersion in mono-chain predicted by perturbation analysis

The result demonstrates the effect of cubic nonlinearity on dispersion. The figure qualitatively reveals the downward shift in cut-off frequency as the wave amplitude increases due to the soft cubic nonlinearity.

6.2.4 DISPERSION THROUGH HARMONIC BALANCE

The chain under consideration has the following parameters, $E = 68.9$ GPa, $R = 9.5025\,mm$, $\nu = 0.35$, $m = 9.73\,g$ and $\mathrm{F}_0 = 20$ N. Following the harmonic balance

method (HB method) detailed in chapter 2 section 2.6, consider the following M harmonic displacement approximation for u_j,

$$u_j = \mathrm{A}\left(\sum_{m=1}^{M} c_m \cos(m\mu j - m\tau)\right). \tag{6.23}$$

In comparison with Eqs. (2.2) and (2.3), $\boldsymbol{k} \cdot \boldsymbol{r}_{n_1 n_2}$ is replaced by μj where μ is the propagation constant and j is the cell index (note that notation n_1 has been changed to j). Also the sine component $s_m = 0$ and the reason for this assumption is that the unit cell contains a single mass represented by a single degree of freedom and the relative phase which exists between the neighboring cells in a plane wave can be completely captured by the approximation given by Eq. (6.23).

The above approximation leads to the following $\mathbb{R}^{1\times M}$ transformation matrix with reference to cell $j = 0$,

$$\mathbf{S}_j = \mathbf{S}(\tau) = [\cos(\tau) \quad \cos(2\tau) \ldots \cos((M-1)\tau) \quad \cos(M\tau)]. \tag{6.24}$$

Therefore the transformation matrices for adjacent cells can be given as,

$$\mathbf{S}_{j\pm1} = \mathbf{S}(\pm\mu, \tau) = [\cos(\pm\mu - \tau) \quad \cos(2(\pm\mu - \tau)) \ldots \cos(M(\pm\mu - \tau))] \tag{6.25}$$

The amplitude vector $\tilde{\boldsymbol{q}}$ can be given as,

$$\tilde{\boldsymbol{q}} = [1 \quad c_2 \quad c_3 \ldots c_{M-1} \quad c_M]^{\mathrm{T}}, \tag{6.26}$$

In the above equation, the amplitude vector is normalized with first component c_1 representing the fundamental mode or the first harmonic. Substituting the displacement approximation $u_j = \mathrm{A}\mathbf{S}(\tau)\tilde{\boldsymbol{q}}$ and $u_{j\pm1} = \mathrm{A}\mathbf{S}(\mu, \tau)\tilde{\boldsymbol{q}}$ into Eq. (6.1) and applying the Galerkin's projection, the equations of motion in differential form are reduced to a set of nonlinear algebraic equations:

$$\omega^2\langle\mathbf{M}\rangle\mathrm{A} + \langle\boldsymbol{f}_{NL}(\mu,\mathrm{A})\rangle = 0, \tag{6.27}$$

The transformed mass matrix takes the following form,

$$\langle\mathbf{M}\rangle = \pi(diag[1 \quad 2^2 \quad 3^2 \quad \dots \quad M^2\,]), \tag{6.28}$$

where $diag$ denotes a diagonal matrix. The transformed nonlinear force is a $\mathbb{R}^{M\times 1}$ vector and the m^{th} component can be given as,

$$\langle\boldsymbol{f}_{NL}(\mu,\mathrm{A})\rangle_m = \Gamma\mathrm{A}^{3/2}\int_0^{2\pi}\cos(m\tau)\left[(\xi^+)^{3/2} - (\eta^+)^{3/2}\right]d\tau, \tag{6.29}$$

where,

$$\xi = \left(\mathbf{S}(-\mu,\tau)\tilde{\boldsymbol{q}} - \mathbf{S}(\tau)\tilde{\boldsymbol{q}} + \hat{\delta}_0\right), \tag{6.30}$$

$$\eta = \left(\mathbf{S}(\tau)\tilde{\boldsymbol{q}} - \mathbf{S}(\mu,\tau)\tilde{\boldsymbol{q}} + \hat{\delta}_0\right), \tag{6.31}$$

$$\xi^+,\eta^+ = \begin{cases} \xi,\eta\ \forall\ \xi^+ \geq 0, \eta^+ \geq 0 \\ 0,0\ \forall\ \xi^+ < 0, \eta^+ < 0 \end{cases}, \tag{6.32}$$

Also in Eq. (6.30) and (6.31), $\hat{\delta}_0 = \delta_0/\mathrm{A}$. Equation (6.29) can be solved for frequency ω at fixed value of propagation constant μ by any numerical iteration scheme. For the present study, Newton-Raphson iteration [58] scheme is employed and the algorithm for the present problem is detailed in the previous section. The amplitude dependent dispersion exhibited by the strongly nonlinear one-dimensional periodic chain modeled on Hertzian contact law is shown in Figure 63. The result is obtained by considering single harmonic approximation $M = 1$. The result demonstrates the variation in bandstructure with wave amplitude. As wave amplitude increases, the cut-off frequency decreases which indicates a softening effect. Figure 64 displays the dispersion predicted by the harmonic balance method for $M = 1, 3$ and 7.

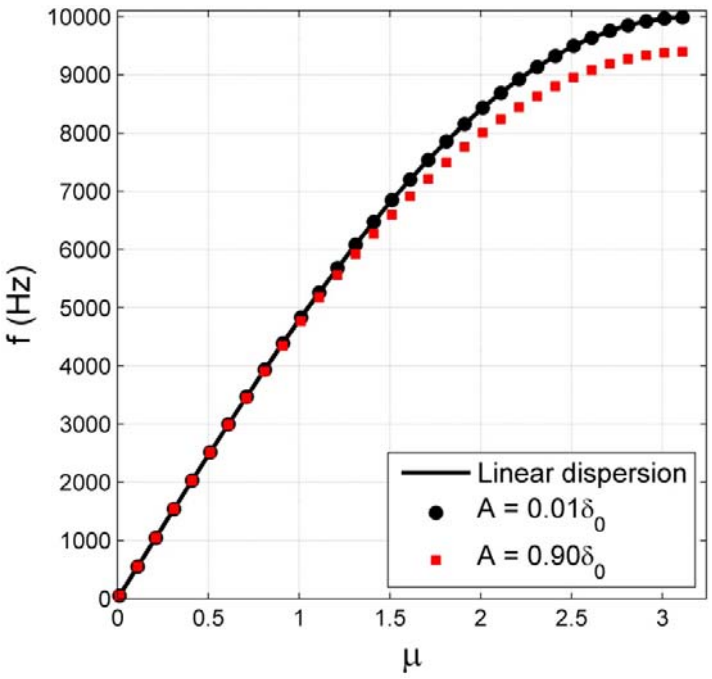

Figure 63: Dispersion of mono-chain predicted by GHB method ($M = 1$)

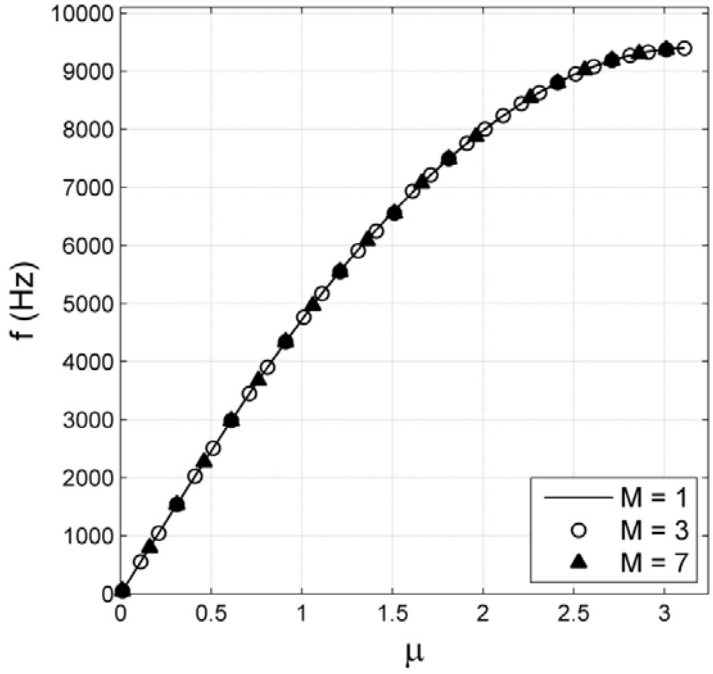

Figure 64: Dispersion predicted by GHB method for increasing harmonics at $A = 0.90\delta_0$

The result depicts the negligible shift (maximum of 0.5%) in dispersion curve predicted by $M = 1$ and 7 harmonic approximations. As defined in section 2.6.3 the

absolute error tolerance for the present analysis is set to 10^{-4} for all the harmonic approximations.

6.2.5 DISPERSION PREDICTION THROUGH HE'S MODIFIED PERTURBATION ANALYSIS

The dispersion shift predicted by closed form analytical expressions derived using perturbation analysis is valid for $A \ll \delta_0$. For analysis purposes, the wave propagation in one-dimensional periodic chains which are governing strongly nonlinear interactions can be studied by the modified-perturbation analysis or He's method [91-95]. This approximate method can only be applied to single degree of freedom systems and He's method cannot be extended to higher dimensional problems. The reason lies in the zeroth order equation which in a higher dimensional problem cannot identify the linear modes required to identify secular terms at next order. For a single degree of freedom system, the mode is defined by just a scalar constant, hence first order equation is capable of generating secular terms which can be eliminated to solve for frequency. The equation of motion for the unit cell of a mono-atomic chain can be modified as follows:

$$\frac{d^2u_j}{dt^2} + 0u_j = pf_{NL}(u_j, u_{j\pm1}), \tag{6.33}$$

where $f_{NL}(u_j, u_{j\pm1})$ is given by right hand side of Eq. (6.1) with $p = 1$. The above equation implies that there is a zero linear restoring force. He's method specifically assumes that there exists a periodic solution and the frequency can be expressed in a series form [93],

$$0 = \omega^2 + p\omega_1 + p^2\omega_2 + \cdots, \tag{6.34}$$

Next, the solution u_j is also assumed to have the following form,

$$u_j = u_j^{(0)} + pu_j^{(1)} + p^2u_j^{(2)} + \cdots, \tag{6.35}$$

Substituting Eqs. (6.34) and (6.35) into the equation of motion described by Eq. (6.33) leads to the following ordered equations,

$$\frac{d^2u_j^{(0)}}{dt^2} + \omega^2 u_j^{(0)} = 0, \tag{6.36}$$

$$\frac{d^2u_j^{(1)}}{dt^2} + \omega^2 u_j^{(1)} + \omega_1 u_j^{(0)} = f_{NL}\left(u_j^{(0)}, u_{j\pm1}^{(0)}\right), \tag{6.37}$$

where the nonlinear restoring force is assumed to be function of $u_j^{(0)}$. The solution of Eq. (6.36) can be expressed as $u_j^{(0)} = \mathrm{A}\cos(\omega \mathrm{t})$. Assuming a plane wave propagation (single harmonic) $u_{j\pm1}^{(0)} = \mathrm{A}\cos(\pm\mu - \omega \mathrm{t})$, Eq. (6.37) can be written as,

$$\frac{d^2u_j^{(1)}}{dt^2} + \omega^2 u_j^{(1)} = -\omega_1 \mathrm{A}\cos(\omega \mathrm{t}) + f_{NL}\left(\mathrm{A}\cos(\omega \mathrm{t}), \mathrm{A}\cos(\pm\mu - \omega \mathrm{t})\right), \tag{6.38}$$

Since f_{NL} is periodic in t, $f_{NL}\left(\mathrm{A}\cos(\omega \mathrm{t}), \mathrm{A}\cos(\pm\mu - \omega \mathrm{t})\right)$ can be expressed as Fourier series:

$$f_{NL}\left(\mathrm{A}\cos(\omega \mathrm{t}), \mathrm{A}\cos(\pm\mu - \omega \mathrm{t})\right) = \sum_{m=1}^{M} c_m \cos(m\omega \mathrm{t}), \tag{6.39}$$

where,

$$c_m = \frac{\omega}{2\pi}\int_{-\pi/\omega}^{\pi/\omega} \cos(m\omega \mathrm{t}) f_{NL}\left(\mathrm{A}\cos(\omega \mathrm{t}), \mathrm{A}\cos(\pm\mu - \omega \mathrm{t})\right) d\mathrm{t}, \tag{6.40}$$

The nonlinear force is a function on only cosine functions therefore the sine terms are not included in Eq. (6.39).

Next, the forcing at first harmonic is examined, Eq. (6.38) can be written as,

$$\frac{d^2u_j^{(1)}}{dt^2} + \omega^2 u_j^{(1)} = (-\omega_1 \mathrm{A} + c_1)\cos(\omega \mathrm{t}), \tag{6.41}$$

the solution of which can force the solution $u_j^{(1)}$ unbounded. Hence, setting $-\omega_1 \mathrm{A} + c_1 = 0$ leads to $\omega_1 = c_1/\mathrm{A}$. From Eq. (6.34), the frequency ω can be evaluated as,

$$\omega = \sqrt{-pc_1/\mathrm{A}}, \tag{6.42}$$

Therefore the dispersion at a specific wave amplitude A is evaluated by varying μ from 0 to π and computing the frequency ω using Eq. (6.42). To obtain c_1, a change of variable $\tau = \omega t$ is introduced, transforming Eq. (6.40) to

$$c_m = \frac{1}{2\pi}\int_{-\pi}^{\pi} \cos(m\tau)\mathrm{f_{NL}}\big(\mathrm{A}\cos(\tau), \mathrm{A}\cos(\pm\mu - \tau)\big)\, d\tau, \tag{6.43}$$

The coefficient c_1 can be found through the integration Eq. (6.43) using any numerical integration scheme for a specific propagation constant μ .

Next, the dispersion in a granular chain with same parameters as discussed in the previous section is considered. The cut-off frequency defined by ω_c corresponding to $\mu = \pi$ is evaluated for a specific wave amplitude A using He's method as described earlier. The variation in the cut-off frequency with wave amplitude A is defined as

$$\boldsymbol{\Delta}\omega_c = 100 \times (\omega_c - \omega_c^L)/\omega_c^L, \tag{6.44}$$

where ω_c^L denotes the cut-off frequency of linear model. Figure 65 shows the plot of $\boldsymbol{\Delta}\omega_c$ with wave amplitude predicted by He's method and the generalized harmonic balance method. The amplitude-dependent cut-off frequency as predicted by He's method is in excellent agreement with that predicted by the harmonic balance method.

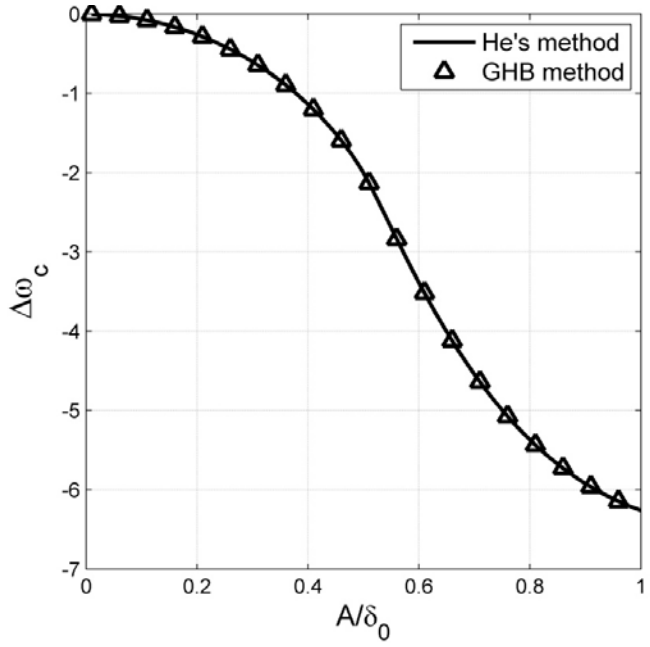

Figure 65: Variation in cut-off frequency with wave amplitude (GHB and He's method)

At low A/δ_0, $\boldsymbol{\Delta}\omega_c$ is close to zero indicating that the linear model predicts dispersion very well at amplitudes much lower than the initial pre-compression. As the amplitude increases to the level of pre-compression, linear model fails and approximately 6% reduction in cut-off frequency is predicted.

6.2.6 NUMERICAL ESTIMATION OF DISPERSION

The variation in band structure predicted by the generalized harmonic balance is validated through numerical simulation of the dynamic response of finite granular chains. Previously, a point harmonic excitation in the chain is assumed to a generate plane wave in the finite chain. Depending on excitation amplitude and frequency, point harmonic forcing generates solitary and quasi-periodic waves [87] in pre-compressed granular chains. Therefore a different approach is taken to impose a plane wave into the compressed granular chain. Consider a finite chain of N masses with a predetermined initial displacement and velocity imposed on each mass. The dynamics of each mass governed by the differential equation (Eq. (6.1)) can be formulated as an initial-value problem:

$$\begin{bmatrix}\dot{u}_j \\ \dot{v}_j\end{bmatrix} = \begin{bmatrix} v_j \\ \Gamma\left(\eta_j^+\right)^{3/2} - \Gamma\left(\eta_{j+1}^+\right)^{3/2}\end{bmatrix}, \tag{6.45}$$

$$\begin{bmatrix}u_j \\ v_j\end{bmatrix}_{(t=0)} = \begin{bmatrix}\mathrm{A}\cos(\mu j) \\ \mathrm{A}\,\omega\sin(\mu j)\end{bmatrix}, \tag{6.46}$$

where overdot represents the $\frac{d}{dt}$, η_j^+ is a function of u_j as defined by Eqs. (6.2) - (6.4) and ω is the wave frequency corresponding to the propagation constant μ which is analytically determined from linearized model of the Hertzian chain. The initial-value problem can be solved numerically using 4th order Runge-Kutta method. The initial conditions set a plane wave into the system propagating to the right or left depending on the sign of initial velocity v_j. With the initial conditions specified by Eq. (6.46), the chain of masses is then simulated for a minimum time of 4T where T is the time period of oscillation $\mathrm{T} = 2\pi/\omega$.

As the plane wave is set into the system, due to the finiteness, the reflections at the both ends of the chain start to distort the plane wave profile. This plane wave profile at $\mathrm{t} = 5\mathrm{T}$ in a chain composed of 800 masses is displayed by Fi. Estimation of frequency and wavenumber is calculated for the undistorted wave profile. For the present system consisting of 800 masses, with a simulation time of 5T the wave profile over 200 masses at the center of chain is used to compute frequency and wavenumber. The fast Fourier transform in space and time estimates the wavenumber and the wave frequency respectively following the same procedure as described in chapter 3 section 3.3. Figure 67 demonstrates the numerically estimated dispersion and its variation with wave amplitude in comparison with analytical predictions.

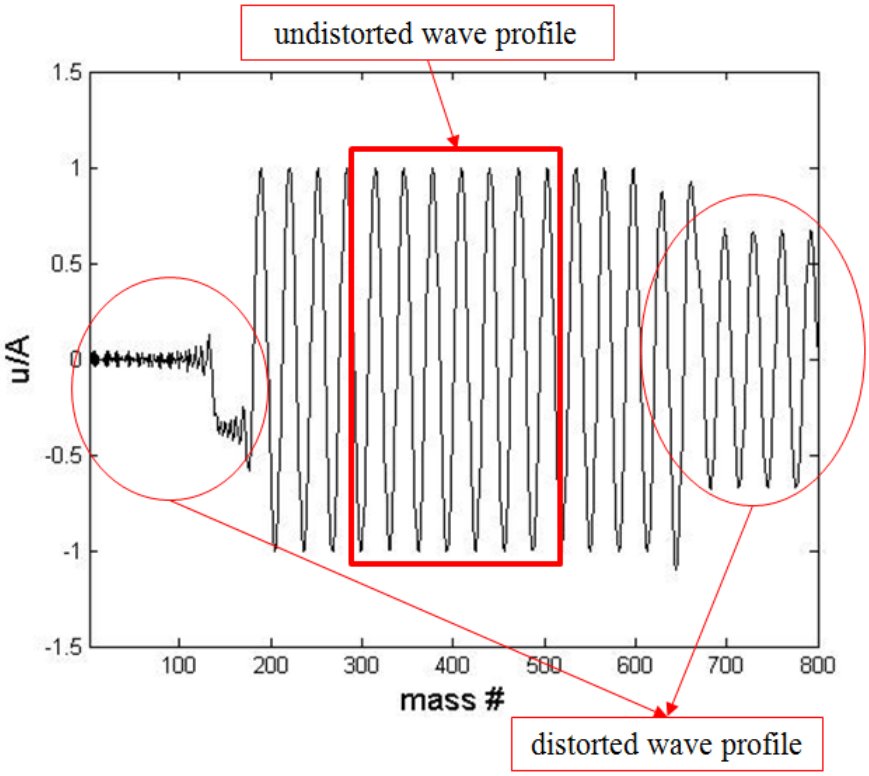

Figure 66: Plane wave in a granular chain of 800 masses at time t = 5T and f = 6 kHz indicating the distorted and undistorted wave profiles

The numerical results are in excellent agreement with the analysis indicating the softening effect which is reduction in cut-off frequency for the increase in wave amplitude. The dispersion shown in Figure 67 is valid if the modeling assumptions are not violated. The vital assumption which needs to hold for the above result to be valid is the limitation on the strain values in the spheres.

High strain values beyond the elastic limit permanently deform the sphere locally and Hertz theory could then become invalid. Therefore it is important to monitor the axial strain in the spheres, which can be computed by,

$$\varepsilon = 100 \times \left(\frac{\delta_0 + u_{j-1} - u_{j+1}}{2R}\right). \tag{6.47}$$

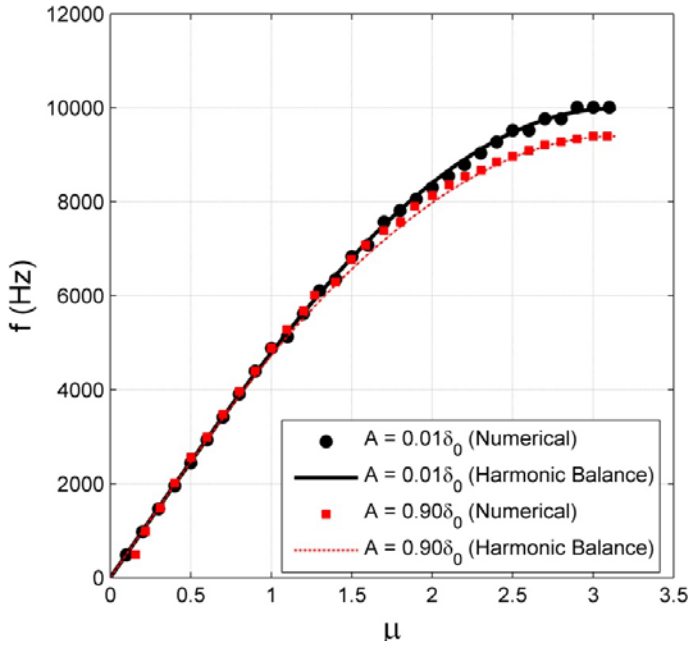

Figure 67: Dispersion of nonlinear mono-chain (Numerical vs Harmonic balance)

Maximum allowable percentage strain for Aluminum T-6061 sphere can be computed by $\varepsilon_{al} = 100 \times \left(\sigma_{yield}/E\right) = 0.40$. As long as magnitude of ε is below ε_{al} the spheres can be considered to be within the elastic limit.

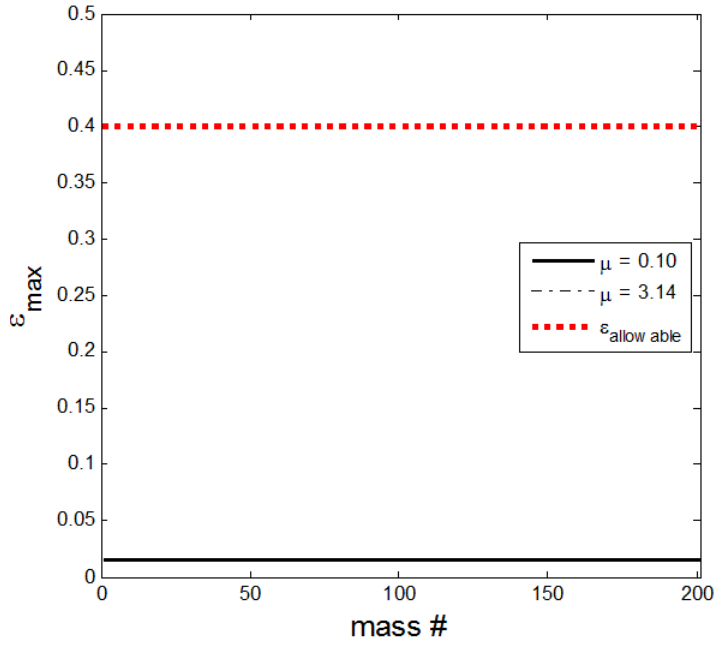

Figure 68: Maximum axial compressive strain at wave amplitude $A = 0.10\delta_0$

Figure 68 displays the maximum ε of each sphere for wave amplitude $A = 0.10\delta_0$ at wavenumbers $\mu = 0.10$ and $\mu = \pi$. Figure 69 shows the maximum ε at wave amplitude $A = 0.90\delta_0$. At high wave amplitudes also, the maximum strain value is well within the allowable elastic strain.

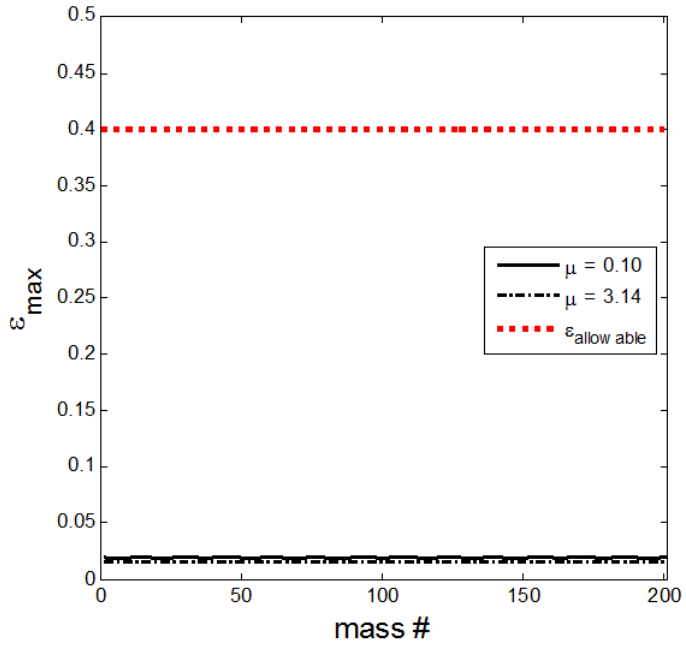

Figure 69: Maximum axial compressive strain at wave amplitude $A = 0.90\delta_0$

6.3 DIATOMIC GRANULAR CHAIN

6.3.1 MODEL DESCRIPTION AND EQUATIONS OF MOTION

The unit cell consists of two different masses m_1 and m_2. The force interaction model which is assumed for a mono-atomic chain is also assumed valid for the diatomic chain. Assumptions such as uniform initial pre-compression and elastic deformation of the spheres with Hertzian force law are also applicable to this problem. Physical model of the chain is depicted by a schematic as shown by Figure 70.

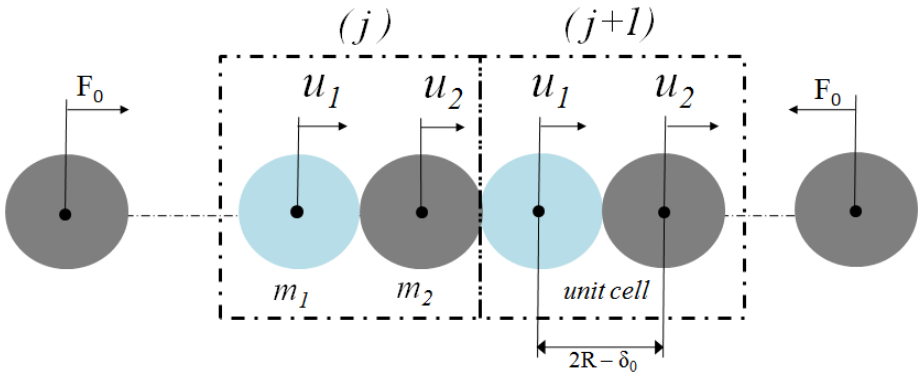

Figure 70: Schematic of a diatomic chain

The equations of motion can be written in format described by Eq. (2.33) and as the system is still one-dimensional ($n_2 = 0$), the index n_1 defining the unit cell from the reference cell is replaced by j. Finally, the mass matrix and the nonlinear restoring force vector corresponding to Eq. (2.33) for the diatomic chain considered are given as,

$$\mathbf{M} = \begin{bmatrix} m_1 & 0 \\ 0 & m_2 \end{bmatrix}, \tag{6.48}$$

$$\boldsymbol{f}_{NL} = \begin{bmatrix} \Gamma(\xi_j^+)^{3/2} - \Gamma(\eta^+)^{3/2} \\ \Gamma(\eta^+)^{3/2} - \Gamma(\xi_{j+1}^+)^{3/2} \end{bmatrix}, \tag{6.49}$$

where $\xi_j = \delta_0 - \left(u_1^j - u_2^{j-1}\right)$, $\eta = \delta_0 - \left(u_1^j - u_2^j\right)$ and the following notation is adopted:

$$\xi_j^+ = \begin{cases} \xi_j \; \forall \; \xi_j \geq 0 \\ 0 \; \forall \; \xi_j < 0 \end{cases}, \; \eta^+ = \begin{cases} \eta \; \forall \; \eta \geq 0 \\ 0 \; \forall \; \eta < 0 \end{cases}, \tag{6.50}$$

$$\Gamma = \frac{4E_1E_2(1/R_2+1/R_1)^{-1/2}}{3[E_2(1-\nu_1^2)+E_1(1-\nu_2^2)]}. \tag{6.51}$$

In the equations above, E_1 and E_2 , and ν_1 and ν_2 are the elastic moduli and Poisson's ratio for mass m_1 and m_2 respectively, while R_1 and R_2 represent the radii of the contact of spheres. Also $\boldsymbol{u}_j = \begin{bmatrix} u_1^j & u_2^j \end{bmatrix}^{\mathrm{T}}$ is the displacement vector of unit cell.

6.3.2 DISPERSION THROUGH PERTURBATION ANALYSIS

The diatomic chain can be considered as an extension of the mono-atomic problem by an extra degree of freedom associated with the unit cell. By assuming small displacements (very low wave amplitude) in comparison with the initial pre-compression, Taylor series expansion leads to a weakly nonlinear model. The linear solution yields two wave modes, high frequency mode termed as optical mode and a low frequency mode termed as acoustic mode. The same procedure as detailed in section 6.2.3 is followed which leads to the frequency correction at the order of ε^2. Although the computation is not detailed here due to the lengthy expressions obtained for a second order correction, one can easily derive them using any symbolic mathematics software such as MAPLE©.

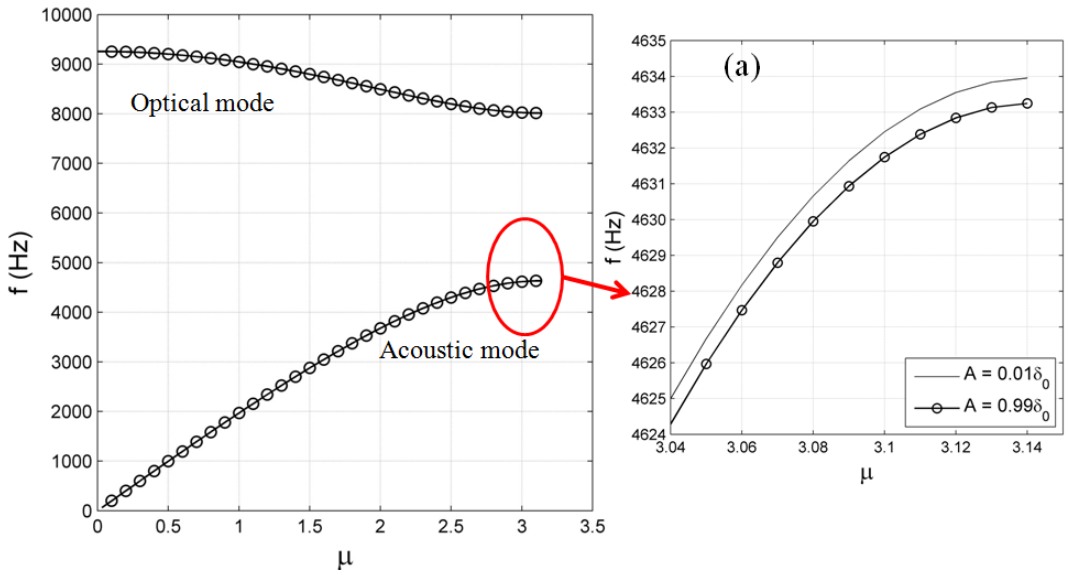

Figure 71: Acoustic mode as predicted by perturbation analysis

Figure 71 demonstrates the qualitative trend of the variation in acoustic mode due to the change in wave amplitude as predicted by the perturbation analysis. For very low amplitude variation, the perturbation analysis theoretically predicts changes in the band structure that are so small that they do not practically shift the overall dispersion. A slight downward shift indicating softening effect of interaction is revealed in the calculations. Figure 71 qualitatively shows the dispersion trend for the acoustic mode estimated by

perturbation analysis with low and high amplitude dispersion curves. Similarly, Figure 72 shows the dispersion trend for the optical mode estimated by perturbation analysis with low and high amplitude dispersion curves.

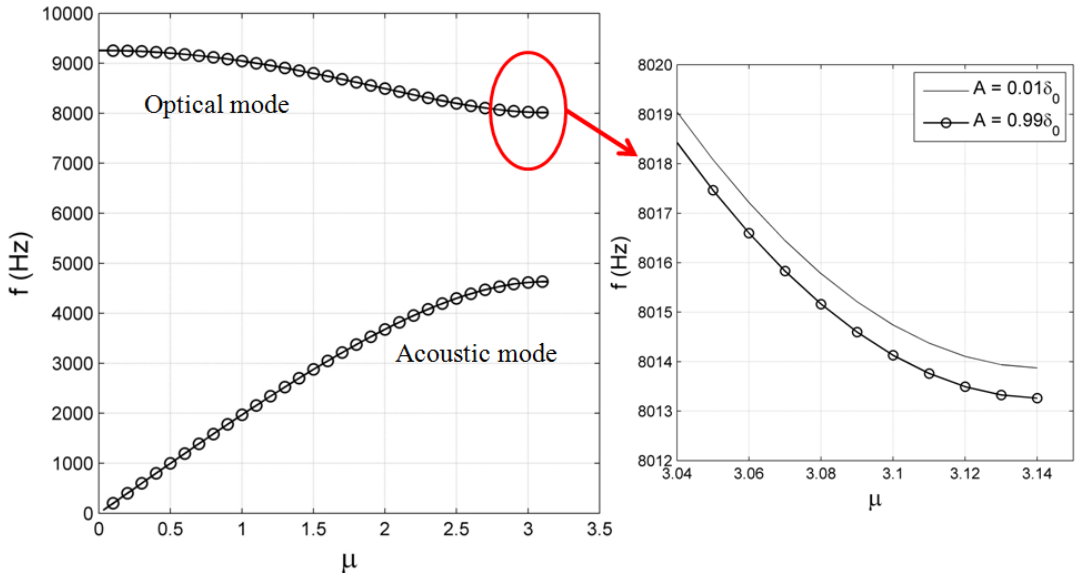

Figure 72: Optical mode as predicted by perturbation analysis

6.3.3 DISPERSION THROUGH GHB METHOD

The dispersion in a strongly nonlinear diatomic system is now estimated using the generalized harmonic balance approach as described in section 2 of this chapter. A chain consisting of Aluminum and Stainless steel spheres is considered with parameters $E_{al} = 68.9$ GPa, $E_{ss} = 193$ Gpa, $R_{al} = R_{ss} = 9.5025\, mm, \nu_{al} = 0.35,$ $\nu_{ss} = 0.3,$ $m_{al} = 9.73\, g, m_{ss} = 29.10\, g$ and an initial pre-compressive force $\mathrm{F}_0 = 20$ N. Following the HB method detailed in section 2.6, consider the following M harmonic displacement approximation for $\boldsymbol{u}_j$,

$$\boldsymbol{u}_j = \mathrm{A}\left(\sum_{m=1}^{M}[\boldsymbol{c}_m \cos(m\mu j - m\tau) + \boldsymbol{s}_m \sin(m\mu j - m\tau)]\right). \tag{6.52}$$

In comparison with Eq. (2.64), $\boldsymbol{k}\cdot\boldsymbol{r}_{n_1n_2}$ is replaced by μj where μ is the propagation constant, j denotes the cell index and $\boldsymbol{u}_j = \begin{bmatrix} u_1^j & u_2^j \end{bmatrix}^{\mathrm{T}}$. The above approximation leads to the following $\mathbb{R}^{2\times 4M}$ transformation matrix with reference cell index $j = 0$,

$$\mathbf{S}_{(j)} = \mathbf{S}(\tau) = \begin{bmatrix} \mathbf{C}(\tau)_{1\times 2M} & \mathbf{O}_{1\times 2M} \\ \mathbf{O}_{1\times 2M} & \mathbf{C}(\tau)_{1\times 2M} \end{bmatrix}. \tag{6.53}$$

where $\mathbf{C}(\tau) = [\cos(\tau) \quad \sin(\tau) \quad \cos(2\tau) \quad \sin(2\tau) \ldots \cos(M\tau) \quad \sin(M\tau)]$ and $\mathbf{O} = [0\ 0\ \ldots\ 0]$ is a row vector of zeros.

The transformation matrices for adjacent cells can be given as,

$$\mathbf{S}_{(j\pm 1)} = \mathbf{S}(\pm\mu - \tau) = \begin{bmatrix} [\mathbf{C}(\pm\mu - \tau)]_{1\times 2M} & [\mathbf{O}]_{1\times 2M} \\ [\mathbf{O}]_{1\times 2M} & [\mathbf{C}(\pm\mu - \tau)]_{1\times 2M} \end{bmatrix}. \tag{6.54}$$

The amplitude vector $\tilde{\boldsymbol{q}} \in \mathbb{R}^{4M\times 1}$ can be expressed as,

$$\tilde{\boldsymbol{q}} = [c_{11} \quad s_{11} \quad c_{21} \quad s_{21} \ldots c_{M1} \quad s_{M1} \quad c_{12} \quad s_{12} \quad c_{22} \quad s_{22} \quad \ldots \quad c_{M2} \quad s_{M2}]^{\mathrm{T}}. \tag{6.55}$$

In the above equation, the values for c_{11}, s_{11}, c_{12} and s_{12} can be determined from the normalized mode vector of the linear model at a particular frequency and the rest of the coefficients can be initially assumed zero. Substituting the displacement approximation $\boldsymbol{u}_j = \mathrm{A}\mathbf{S}(\tau)\tilde{\boldsymbol{q}}$ and $\boldsymbol{u}_{j\pm 1} = \mathrm{A}\mathbf{S}(\mu,\tau)\tilde{\boldsymbol{q}}$ into Eq. (2.63) using Eqs. (6.53) and (6.54) and applying the Galerkin's projection, transformed mass matrix yields the following,

$$\bar{\mathbf{M}} = \pi \begin{bmatrix} \mathbf{D}_1 & 0 & 0 & 0 \\ 0 & \mathbf{D}_2 & 0 & 0 \\ 0 & 0 & \ddots & 0 \\ 0 & 0 & 0 & \mathbf{D}_M \end{bmatrix}_{4M\times 4M}. \tag{6.56}$$

where $\mathbf{D}_m = m^2 diag[m_1 \quad m_2 \quad m_1 \quad m_2]$, $m = 1,2 \ldots M$ is a $\mathbb{R}^{2\times 2}$ diagonal matrix. For example, a single harmonic approximation $M = 1$ would lead to the following transformed mass matrix,

$$\bar{\mathbf{M}} = \pi diag([m_1 \quad m_2 \quad m_1 \quad m_2]). \tag{6.57}$$

Using Eqs. (6.49) - (6.51), the transformed nonlinear force vector takes the following form,

$$\langle \boldsymbol{f}_{NL}(\mu, \mathrm{A}) \rangle = \Gamma \mathrm{A}^{3/2} \int_0^{2\pi} \mathbf{S}^{\mathrm{T}} \left[f_{NL}\left(\mu, \tau, \hat{\delta}_0\right) \right] d\tau, \tag{6.58}$$

where $\hat{\delta}_0 = \delta_0/\mathrm{A}$. At wave amplitudes much lower than the initial pre-compression $\mathrm{A} \ll \delta_0$, the dispersion predicted by the harmonic balance should match the linear dispersion which is demonstrated by Figure 73.

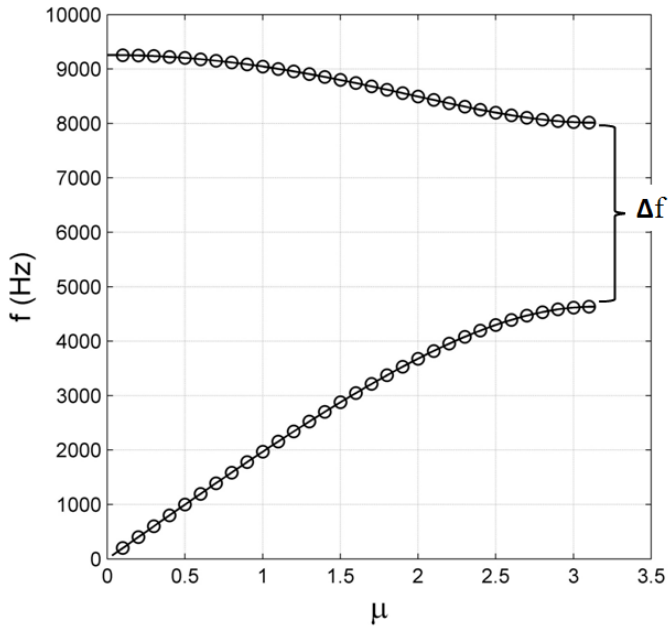

Figure 73: Dispersion of diatomic chain for $\mathrm{A} \ll \delta_0$ ○ GHB — Linear

As demonstrated in the previous section, for a mono-atomic chain there is negligible difference in dispersion predicted with the displacement approximation for $M = 1$ and $M = 7$ harmonics (Figure 64). Therefore the present case considers the harmonic

balance approach with single harmonic approximation ($M = 1$). The dispersion shift with variation in wave amplitude is demonstrated in Figure 74.

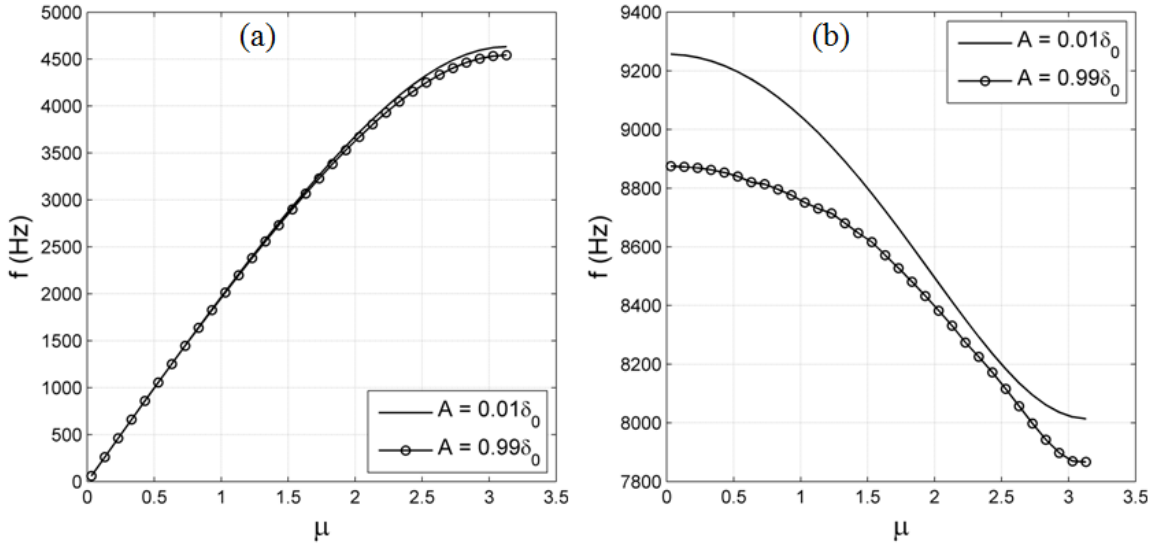

Figure 74: Dispersion in diatomic chain by GHB ($M = 1$) (a) Acoustic mode (b) Optical mode

The effect of wave amplitude shifts the dispersion curves downward demonstrating the softening effect of the nonlinear interaction. Let $\mathbf{\Delta}$f denote the bandgap of the considered diatomic chain as shown in Figure 73 and f_c denote the center frequency of the bandgap. The center frequency for the present diatomic chain can be calculated as $f_c = f_{ac} + \mathbf{\Delta}f/2 = f_{oc} - \mathbf{\Delta}f/2$, where f_{ac} and f_{oc} are the cut-off frequencies of the acoustic and optical mode respectively. To study the amplitude dependent dispersion it is important to examine the variation of the two parameters $\mathbf{\Delta}$f and the center frequency f_c which determine the width and the location of the bandgap. Also the shift in band edge frequency, which is the upper cut-off frequency in the optical mode (at $\mu = 0$) denoted as f_{edge} is also examined. Figure 75 displays the variation of $\mathbf{\Delta}$f, f_c and f_{edge} in terms of percentage shift. The result depicts the narrowing of bandwidth by 2% and a

downward shift of 2% and 4% in center frequency and the band-edge frequency respectively as the amplitude A varies from $0.01\delta_0$ to $0.99\delta_0$.

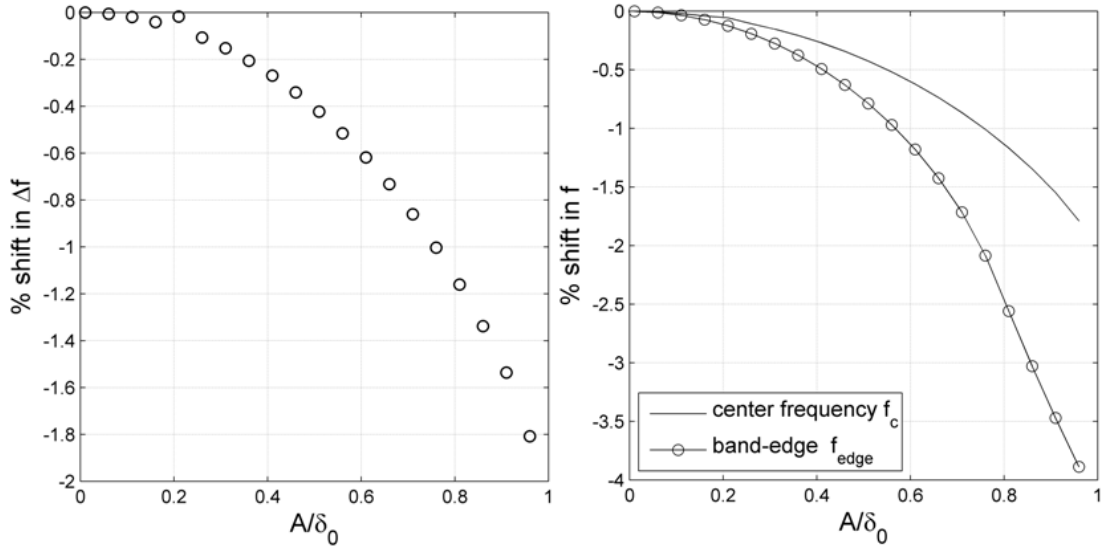

Figure 75: Percentage shift in bandwidth, center frequency and band-edge frequency

6.3.4 NUMERICAL ESTIMATION OF DISPERSION

The dispersion trend predicted by the generalized harmonic balance is numerically validated by simulating a finite diatomic chain of $N = 800$ masses. A plane wave is imposed in the lattice by setting up an initial value problem with initial displacement and velocity defined as,

$$\frac{d\boldsymbol{u}_j}{dt} = \boldsymbol{v}_j \, , \frac{d\boldsymbol{v}_j}{dt} = \mathbf{M}^{-1}\boldsymbol{f}_{NL} \; \forall \, j = 1,2 \ldots N, \tag{6.59}$$

$$\boldsymbol{u}_j(\mathrm{t} = 0) = \mathrm{A}\tilde{\boldsymbol{u}}_j \cos(\mu j + \phi), \tag{6.60}$$

$$\boldsymbol{v}_j(\mathrm{t} = 0) = \mathrm{A}\omega\tilde{\boldsymbol{u}}_j \sin(\mu j + \phi), \tag{6.61}$$

where $\mathbf{M}$ and $\boldsymbol{f}_{NL}$ are given by Eqs. (6.48) and (6.49), the normalized mode vector $\tilde{\boldsymbol{u}}_j \in \mathbb{R}^{2\times 1}$, phase difference ϕ and the frequency ω are obtained by solving the dispersion in the linearized diatomic chain model. As explained for the case of the mono-atomic chain,

the travelling wave is reflected at the boundaries of the finite chain where it is distorted. For the present case, the simulation is run for a minimum of $5T$ (five cycles) where $T = 2\pi/\omega$. For the present system consisting of 800 masses, with a simulation time of 5T the undistorted wave profile over 200 masses at the center of chain is considered (refer to Figure 66). The fast Fourier transform in space and time computes the wavenumber and frequency of the plane wave. The numerically calculated amplitude dependent dispersion agrees well with that predicted by the harmonic balance method which is depicted in Figure 76.

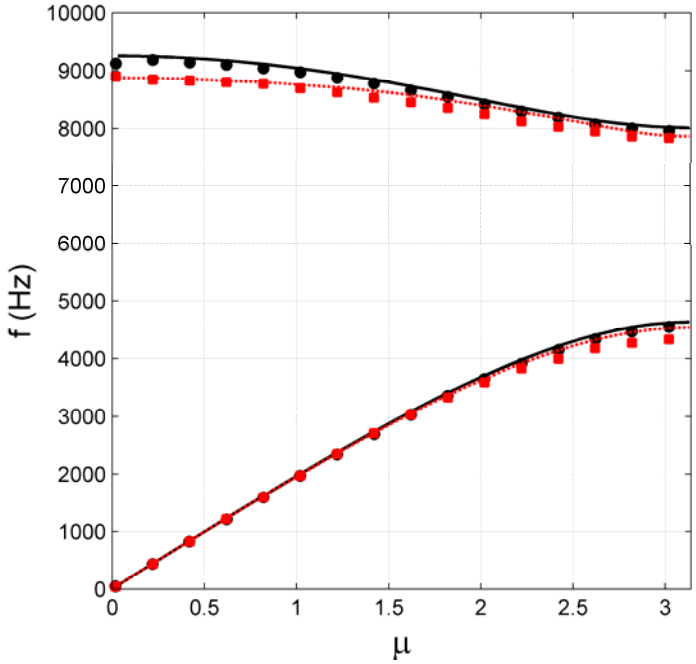

Figure 76: Dispersion in diatomic chain - numerical vs. harmonic Balance ─ Analytical ($A = 0.01\delta_0$) ····· Analytical ($A = 0.90\delta_0$) ● Numerical ($A = 0.01\delta_0$) ■ Numerical ($A = 0.90\delta_0$)

6.4 TWO-DIMENSIONAL HEXAGONAL GRANULAR PACKING

The present example is an extension of the one-dimensional granular chain to a two-dimensional setting where the spheres or beads are arranged in hexagonal packing to form a lattice structure. As mentioned in the previous chapter, an important propagation

characteristic of a travelling wave in two dimensional media is its directional behavior. The motivation to study two dimensional strongly nonlinear lattices comes from the fact that such highly nonlinear systems could exhibit high degree of variation in directional behavior based on wave amplitude. The study of plane waves and their propagation characteristics in strongly nonlinear media such as granular packing is important as it serves as a first step towards the understanding of such complex systems. Gilles and Coste [96] experimentally studied low frequency acoustic wave propagation in a two dimensional hexagonally packed granular media. The authors demonstrate that at high pre-compression the acoustic wave velocities are in agreement with the force scaling based on Hertzian interaction. But as the pre-compressive stress lowers the acoustic wave propagation is no longer in agreement with Hertzian behavior due to loss of contact which in turn creates a random disorder in the system which distorts the acoustic signal. The paper quantifies the boundary of static pre-compression required to achieve a homogenous lattice (defined as the lattice with each bead of same size and shape) where the acoustic wave propagation can be modeled based on linear theory. For example, for a lattice of stainless steel spheres a high static pre-compression of 800 N is necessary to model it as a regular triangular lattice for linear wave propagation problem.

In the one-dimensional case, as detailed in the previous section, low pre-compressive granular chains exhibit complex wave phenomena such as solitary waves. As the piling dimensionality of the structure increases from one-dimension to two or three dimensions, the complexity of the nonlinear dynamics gets even more intricate with wave directionality as an additional wave propagation characteristic. The present study restricts to acoustic plane wave propagation with initial pre-compression and aims to explore the variation in propagation characteristics as the wave amplitude changes. Since the dynamics governing the displacement of the particles is highly nonlinear it is expected that the wave dispersion and energy flow are amplitude dependent.

6.4.1 MODEL DESCRIPTION AND EQUATIONS OF MOTION

Figure 77 shows the two-dimensional hexagonal packing of spheres where each sphere within the lattice is in contact with surrounding six spheres. A static pre-compressive force is applied to the boundary of the lattice which introduces the initial pre-compression in each sphere along the lines joining the center of the spheres to the point of contact. The contact force is again modeled using Hertz contact theory. The assumption implies that the spheres are frictionless, fully elastic and the strain deformation is very small in comparison with the radius of the sphere. The model also assumes that the lattice is uniform and homogeneous with no disorder or impurity.

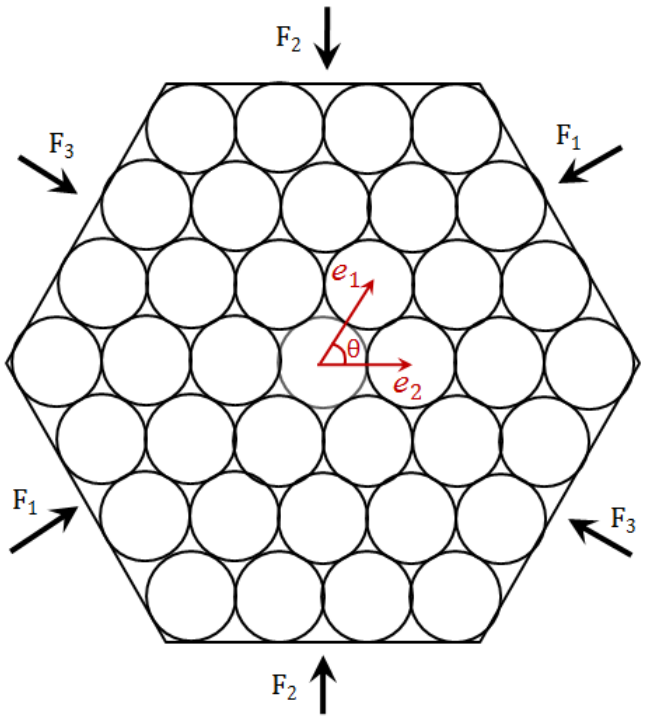

Figure 77: Schematic of hexagonal packed spheres

The unit cell consists of a single mass with two degrees of freedom u_1 and u_2 representing the in-plane displacement. The direct lattice vectors which describe the periodicity of the lattice are denoted by $\boldsymbol{e_1}$ and $\boldsymbol{e_2}$. Let θ denote the angle between the two lattice vectors and let n_1 and n_2 denote the cell index along $\boldsymbol{e_1}$ and $\boldsymbol{e_2}$ respectively.

Let δ_{01}, δ_{02} and δ_{03} denote the initial pre-compressions of the sphere along lines joining the center of spheres and point of contact represented by $\boldsymbol{e}_1$, $\boldsymbol{e}_2$ and $\boldsymbol{e}_3 = \boldsymbol{e}_2 - \boldsymbol{e}_1$ (Figure 78). The physical space is spanned by the unit vectors denoted by $\boldsymbol{i}_1$ and $\boldsymbol{i}_2$.

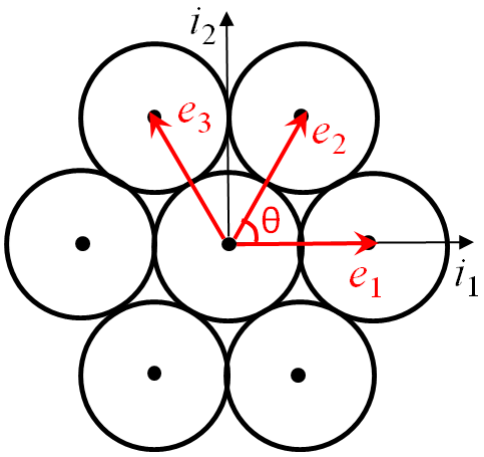

Figure 78: Unit cell in HCP lattice with vectors denoting lines of contact $\boldsymbol{e}_1$, $\boldsymbol{e}_2$ and $\boldsymbol{e}_3$

Let the unit vectors along the lines joining the centers and point of contact be denoted by $\hat{\boldsymbol{e}}_j = \boldsymbol{e}_j / |\boldsymbol{e}_j| \quad \forall\, j = 1,2,3$ and let the position of unit cell be represented by an index vector defined as $\boldsymbol{n} = n_1\boldsymbol{e}_1 + n_2\boldsymbol{e}_2$. The governing equations of motion for the unit cell can be written as,

$$\frac{d^2 u_{k(n_1,n_2)}}{dt^2} = \Gamma \sum_{j=1}^{3} \left(\left(\alpha_j^+\right)^{3/2} - \left(\beta_j^+\right)^{3/2} \right) \boldsymbol{e}_j \cdot \boldsymbol{i}_k \quad \forall\, k = 1,2. \tag{6.62}$$

and

$$\alpha_j^+ = \begin{cases} \alpha_j \;\forall\; \alpha_j \geq 0 \\ 0 \;\forall\; \alpha_j < 0 \end{cases}, \; \beta_j^+ = \begin{cases} \beta_j \;\forall\; \beta_j \geq 0 \\ 0 \;\forall\; \beta_j < 0 \end{cases}, \tag{6.63}$$

where,

$$\alpha_j = \left(\sum_{k=1}^{2} \left[u_{k\left((\boldsymbol{n}-\boldsymbol{e}_j)\cdot\boldsymbol{e}_1, (\boldsymbol{n}-\boldsymbol{e}_j)\cdot\boldsymbol{e}_2\right)} - u_{k(n_1,n_2)} \right] \boldsymbol{i}_k \cdot \hat{\boldsymbol{e}}_j \right) - \delta_{0j}, \tag{6.64}$$

$$\beta_j = \left(\sum_{k=1}^{2}\left[u_{k(\boldsymbol{n}\cdot\boldsymbol{a}_1,\boldsymbol{n}\cdot\boldsymbol{a}_2)} - u_{k\left((\boldsymbol{n}+\boldsymbol{e}_j)\cdot\boldsymbol{a}_1,(\boldsymbol{n}+\boldsymbol{e}_j)\cdot\boldsymbol{a}_2\right)}\right]\boldsymbol{i}_k \cdot \hat{\boldsymbol{e}}_j\right) - \delta_{0j}, \tag{6.65}$$

$$\Gamma = \frac{E(2R)^{1/2}}{3(1-\nu^2)m}, \tag{6.66}$$

where E denotes elastic modulus, R denotes the radius of the sphere, ν is Poisson's ratio. For a hexagonally packed lattice the angle between the lattice vectors $\theta = 60°$.

6.4.2 LINEARIZED MODEL

The present section details the linearized model of the described nonlinear system. The linearization is valid as long as the magnitude of the relative displacements of the beads is much lower than the initial pre-compression. The model is useful for the analysis in two ways: 1) it captures the lattice dispersion for low wave amplitudes, and 2) it serves as a reference to compare harmonic balance results generated for low wave amplitudes.

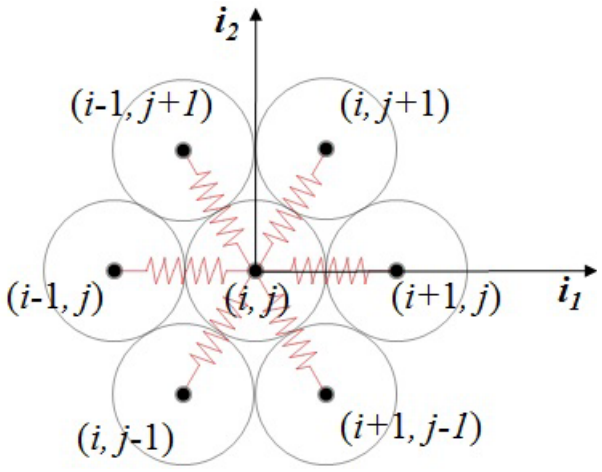

Figure 79: Schematic of a linear model of hexagonal packed spheres

In fact such simplified linear discrete models of structures have been used in the literature to predict dispersion and response analysis and understand the effect of elastic/bulk properties on wave propagation characteristics [97]. The system can be modeled as a hexagonal spring mass lattice with each spring denoting the stiffness along the line

joining the center of spheres and point of contact as shown in Figure 79. The lattice vectors and the reciprocal basis vectors expressed in Cartesian frame are given by,

$$\boldsymbol{e}_1 = a\boldsymbol{i}_1;\ \boldsymbol{e}_2 = \frac{a}{2}\boldsymbol{i}_1 + \frac{\sqrt{3}a}{2}\boldsymbol{i}_2, \tag{6.67}$$

$$\boldsymbol{b}_1 = \frac{1}{a}\boldsymbol{i}_1 - \frac{1}{\sqrt{3}a}\boldsymbol{i}_2;\ \boldsymbol{b}_2 = \frac{2}{\sqrt{3}a}\boldsymbol{i}_2, \tag{6.68}$$

where $a = 2R$ is distance between the centers of spheres which is assumed to be same along all the lines of contact for an isotropic pre-compressed lattice ($\delta_{01} = \delta_{02} = \delta_{03}$).

6.4.3 LINEAR DISPERSION ANALYSIS

Bloch theorem is invoked to solve the linear dispersion problem. The equations of motion reduce to an eigenvalue problem (Eq. (6.69)) from which the frequency and the corresponding mode-shape can be evaluated for a specific wavenumber pair (μ_1, μ_2).

$$\left[\widetilde{\mathbf{M}}^{-1}\widetilde{\mathbf{K}}\right]\boldsymbol{u} = \omega^2\boldsymbol{u}, \tag{6.69}$$

where,

$$\widetilde{\mathbf{M}} = \begin{bmatrix}1 & 0\\ 0 & 1\end{bmatrix}, \widetilde{\mathbf{K}} = \begin{bmatrix}K_1 & K_2\\ K_3 & K_4\end{bmatrix}, \tag{6.70}$$

$$K_1 = 2\sum_{j=1}^{3}\left[k_j \cos^2\big((j-1)\theta\big)\Big(1 - \cos\big(\boldsymbol{\mu}\cdot\boldsymbol{e}_j\big)\Big)\right], \tag{6.71}$$

$$\mathrm{K}_2 = \mathrm{K}_3 = 2\sum_{\mathrm{j}=2}^{3}\left[k_j \cos\big((j-1)\theta\big)\sin\big((j-1)\theta\big)\big(1 - \cos\big(\boldsymbol{\mu}\cdot\boldsymbol{e}_j\big)\big)\right], \tag{6.72}$$

$$K_4 = 2\sin^2\theta\sum_{j=2}^{3}\left[k_j\big(1 - \cos\big(\boldsymbol{\mu}\cdot\boldsymbol{e}_j\big)\big)\right], \tag{6.73}$$

$$k_i = \frac{3\Gamma\,(\delta_{0i})^{1/2}}{2}, \tag{6.74}$$

and $\theta = 60°$. In the next subsections, the necessary tools such as iso-frequency contours and group velocity plots are utilized to analyze the plane wave dispersion in a systematic way. Next, the results generated by using the linear model and that obtained by applying generalized harmonic balance approach at very low wave amplitudes are compared and analyzed. Chapter 4, section 4.3.2 introduced the concept of iso-frequency contours and group velocity plots as tools to analyze the dispersion in two dimensional periodic structures. This section presents the iso-frequency contour analysis pertaining to the hexagonal packing of spheres. From Eq. (6.69), the eigenvalue problem can be solved for frequency once the propagation constants μ_1 and μ_2 are fixed. In general, the dispersion relation can be written as,

$$\omega = f(\mu_1, \mu_2). \tag{6.75}$$

The relation can be represented by a three-dimensional surface and the number of surfaces generated in the wavenumber domain (first Brillouin zone) depends on the dimension of the eigenvalue problem described, and is equal to the degrees of freedom. Each surface describes the dispersion of the wave corresponding to the mode of propagation through the structure. From an analysis point of view, such surfaces are not convenient to analyze and therefore a contour plot of the dispersion, also known as *iso-frequency contour,* can be useful in such cases. Each line on the *iso-frequency contour* denotes a frequency and any point on that same line represents the pair (μ_1, μ_2) that satisfies the dispersion relation. As the study limits to plane wave propagation without attenuation, $(\mu_1, \mu_2) \in \mathbb{R}$ and they are measured along the reciprocal lattice vectors $\boldsymbol{b}_1$and $\boldsymbol{b}_2$. An intuitive interpretation of the results can be achieved by representing the components of the wave vector in the physical space denoted by ξ_1 and ξ_2 along $\boldsymbol{i}_1$and $\boldsymbol{i}_2$ respectively,

$$\boldsymbol{\mu} = \xi_1 \boldsymbol{i}_1 + \xi_2 \boldsymbol{i}_2, \tag{6.76}$$

where,

$$\xi_j = \boldsymbol{\mu} \cdot \boldsymbol{i}_j \ \ \forall\, j = 1,2. \tag{6.77}$$

Therefore, $\xi_1 = \mu_1$ and $\xi_2 = \left(\frac{2}{\sqrt{3}}\mu_2 - \frac{1}{\sqrt{3}}\mu_1\right)$, this transformation is now used to represent the iso-contour plots in physical space. Figure 80 and Figure 81 denote iso-frequency contours for the two modes of propagation respectively.

Following plots are the results of analysis performed on hexagonal packing of aluminum spheres with the parameters $E = 68.9$ GPa, $R = 9.5025\ mm$, $\nu = 0.35$, $m = 9.73\ g$ and isotropic pre-compressive force $\mathrm{F_{01}} = \mathrm{F_{02}} = \mathrm{F_{03}} = 20$ N.

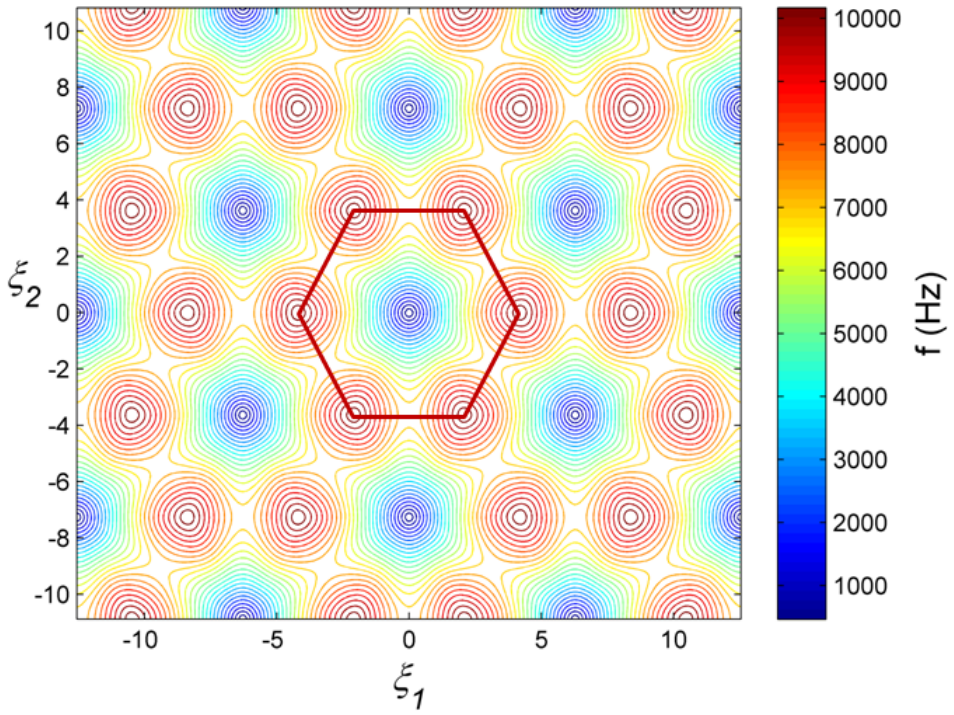

Figure 80: Iso-frequency contour of first mode representing first Brillouin zone

Figure 80 denotes first mode and it is easily observed that the dispersion surface is periodic in the two dimensional wavenumber domain. The first Brillouin zone is

identified by the red hexagonal domain in the figure. The same domain can also be realized in mode 2 which is detailed in Figure 81.

A detailed discussion on band structures of lattices is presented in section 4.3.2. For the present lattice, there are two degrees of freedom and hence the band diagram consists of two branches as shown in Figure 82. Examining the low-frequency range, the discrete structure supports wave modes equivalent to pressure and shear modes exhibited by a continuous structure. Specifically, the low phase velocity curve relates to the shear or transverse wave and higher velocity curve is analogous to the pressure or longitudinal wave. From the band diagram of the lattice, it is evident that beyond frequency 10.5 kHz, the propagation of the waves occurs only through pressure mode.

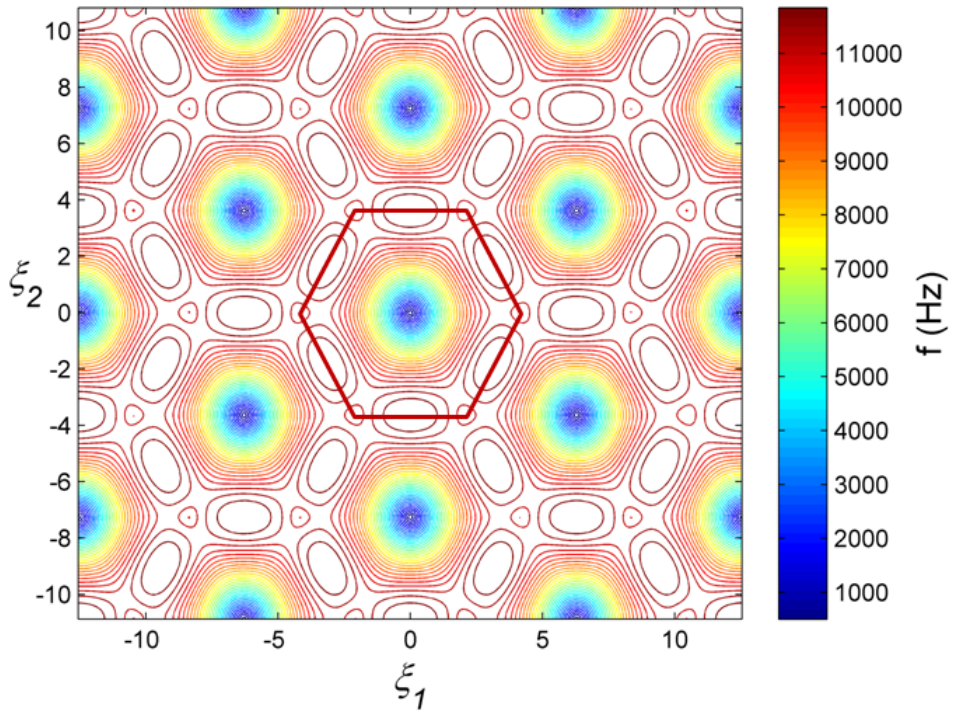

Figure 81: Iso-frequency contour of second mode representing first Brillouin zone

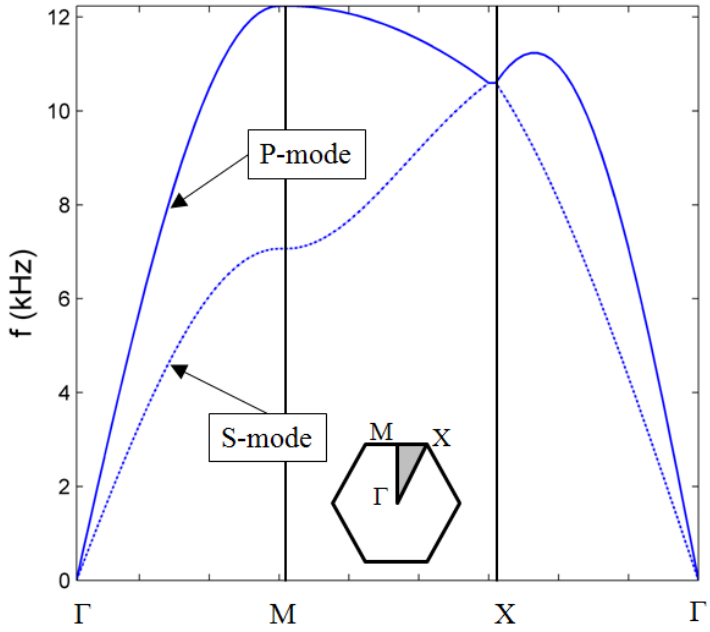

Figure 82: Band structure of the lattice of hexagonally packed spheres

6.4.4 GROUP VELOCITY PLOTS

Group velocity as a tool to evaluate the wave directional behavior has been introduced in detail in section 4.3.2. Each line on the iso-frequency contour denotes a frequency and any point on that same line represents the pair (μ_1, μ_2) or (ξ_1, ξ_2) that satisfies the dispersion relation. The normal at each point on the iso-frequency line represents the gradient of the frequency with respect to the wavevector which is equal to the group or the energy velocity of the wave directed along the normal.

This section presents group velocity plots generated at specific frequencies using the linearized model (Eq. (6.69)). These group velocity plots are then compared with those obtained from the generalized harmonic balance method applied to the nonlinear problem. To simulate the linear model, the effect of wave amplitude should be negligible which is accomplished by assuming the wave amplitudes much lower than the initial pre-compression. The lattice under discussion exhibits complex group velocity patterns at

high wave frequencies where the shear mode ceases to exist and the propagation only happens through the pressure/longitudinal mode.

Consider the generalized harmonic balance approach described in the chapter 2 to solve the dispersion in a two dimensional hexagonally packed granular lattice. The displacement approximation is given as,

$$\boldsymbol{u}_j = \mathrm{A}\left(\sum_{m=1}^{M}[\boldsymbol{c}_m \cos(m\mu j - m\tau)]\right), \tag{6.78}$$

where $\boldsymbol{c}_m = [c_{m1} \quad c_{m2}]^{\mathrm{T}}$ as the degrees of freedom for the unit cell $N = 2$. The degrees of freedom u_1 and u_2 denote the projections of the in-plane displacement of the single bead along $\boldsymbol{i}_1$ and $\boldsymbol{i}_2$ axes. The above approximation leads to the following $\mathbb{R}^{2\times 2M}$ transformation matrix with reference cell index $j = 0$,

$$\mathbf{S}_j = \mathbf{S}(\tau) = \begin{bmatrix} \mathbf{C}(\tau)_{1\times M} & \mathbf{O}_{1\times M} \\ \mathbf{O}_{1\times M} & \mathbf{C}(\tau)_{1\times M} \end{bmatrix}, \tag{6.79}$$

Therefore the transformation matrices for adjacent cells can be given as,

$$\mathbf{S}_{j\pm 1} = \mathbf{S}(\pm\mu - \tau) = \begin{bmatrix} \mathbf{C}(\pm\mu - \tau)_{1\times M} & \mathbf{O}_{1\times M} \\ \mathbf{O}_{1\times M} & \mathbf{C}(\pm\mu - \tau)_{1\times M} \end{bmatrix}. \tag{6.80}$$

The amplitude vector $\widetilde{\boldsymbol{q}} \in \mathbb{R}^{2M\times 1}$ can be given as,

$$\widetilde{\boldsymbol{q}} = [c_{11} \quad c_{21} \quad \cdots \quad c_{M1} \quad c_{12} \quad c_{22} \quad \cdots \quad c_{M2}]^{\mathrm{T}}. \tag{6.81}$$

In the above equation, the values for c_{11} and c_{12} can be determined from the normalized mode vector of linear model at a particular frequency and the rest of the coefficients can be initially assumed zero. Substituting the displacement approximation $\boldsymbol{u}_j = \mathrm{A}\mathbf{S}(\tau)\widetilde{\boldsymbol{q}}$ and $\boldsymbol{u}_{j\pm 1} = \mathrm{A}\mathbf{S}(\mu, \tau)\widetilde{\boldsymbol{q}}$ into Eq. (6.62) and applying the Galerkin's projection, the transformed mass matrix takes the following form,

$$\bar{\mathbf{M}} = \pi \begin{bmatrix} \mathbf{D}_1 & 0 & 0 & 0 \\ 0 & \mathbf{D}_2 & 0 & 0 \\ 0 & 0 & \ddots & 0 \\ 0 & 0 & 0 & \mathbf{D}_M \end{bmatrix}_{2M \times 2M}, \tag{6.82}$$

where $\mathbf{D}_m = m^2 \mathbf{I}_2 \; \forall \; m = 1,2 \ldots M$ and $\mathbf{I}_2$ is an $\mathbb{R}^{2\times 2}$ identity matrix. For example, single harmonic approximation $M = 1$ would lead to the following transformed mass matrix,

$$\bar{\mathbf{M}} = \pi \begin{bmatrix} 1 & 0 \\ 0 & 1 \end{bmatrix}, \tag{6.83}$$

Using Eqs. (6.79) **-** (6.81), transformed nonlinear force vector takes the following form,

$$\langle \boldsymbol{f}_{NL}(\mu, \mathrm{A}) \rangle = \Gamma \mathrm{A}^{3/2} \int_0^{2\pi} \mathbf{S}^{\mathrm{T}} \left[\boldsymbol{f}_{NL}\left(\mu, \tau, \hat{\delta}_0\right) \right] d\tau, \tag{6.84}$$

where $\hat{\delta}_0 = \delta_0/\mathrm{A}$ and $\boldsymbol{f}_{NL}\left(\mu, \tau, \hat{\delta}_0\right)$ in the above equation is given by right hand side of Eq.(6.62). The projection of nonlinear force function onto first harmonic and integration over one cycle (Eq. (6.84)) is numerically evaluated using adaptive Gauss-Kronrod quadrature algorithm [98]. For a specific wavenumber pair (μ_1, μ_2) or (ξ_1, ξ_2) , the frequency is computed by solving the nonlinear algebraic equations using Newton-Raphson's scheme as described in chapter 2. The initial guess plays a very important role in convergence of the solution when applying Newton's method. If the initial guess is far away from the actual solution, Newton Raphson procedure could converge to either of the modes, at times invalidating the magnitude constraint on the vector of normalized amplitude coefficients $\boldsymbol{c}_m$. Therefore for the present problem, the initial guess for the unknown vector can be written as,

$$\boldsymbol{x}^{(0)} = [\omega \; c_{21} \; c_{31} \ldots c_{M1} \ldots c_{1N} \; c_{2N} \ldots c_{MN}]^{\mathrm{T}}, \tag{6.85}$$

where the values of ω and $[c_{12}\ c_{13}\ \dots c_{1N}]$ can be set to the frequency and normalized mode shape vector obtained from the linear model. The rest of the variables are defined as,

$$\boldsymbol{x}^{(0)} \setminus [\omega\ c_{12}\ c_{13}\ \dots c_{1N}] = 0. \tag{6.86}$$

In the above case, the normalized mode vector is such that $c_{11} = 1$. For the other modes, any coefficient in $[c_{11}\ c_{12}\ c_{13}\ \dots c_{1N}]$ could be equal to 1.

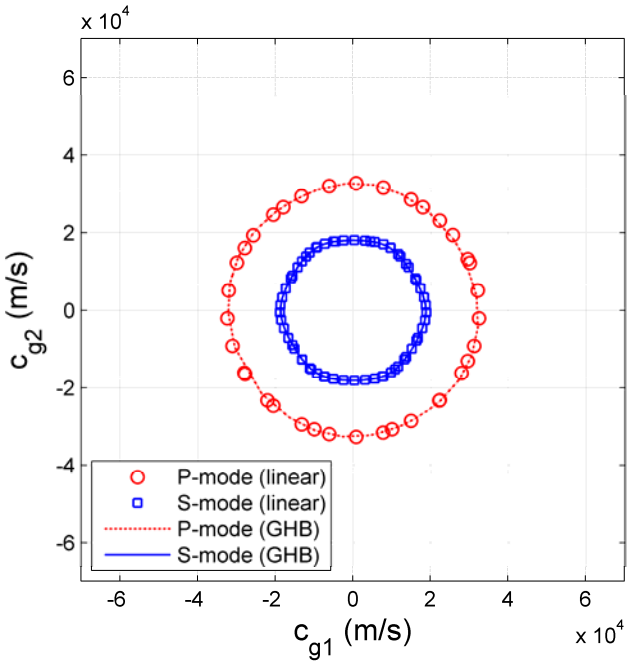

Figure 83: Group velocity plot of HCP granular lattice at A $= 0.01\delta_0$ and $f = 2.4$ kHz

At very low wave amplitudes, the dispersion predicted by the harmonic balance method and that obtained from the linearized model are in excellent agreement. Figure 83 - Figure 85 reveal the previous statement by displaying the group velocity plots at various frequencies. The group velocity vector $\boldsymbol{c_g}$ is expressed in physical space by the following relation,

$$\mathbf{c_g}(\boldsymbol{\mu}) = \boldsymbol{\nabla}\omega(\boldsymbol{\mu}) = \begin{Bmatrix} d\omega/d\xi_1 \\ d\omega/d\xi_2 \end{Bmatrix}. \tag{6.87}$$

where $\boldsymbol{\mu}$ in the above equation is given by Eq. (6.76) .

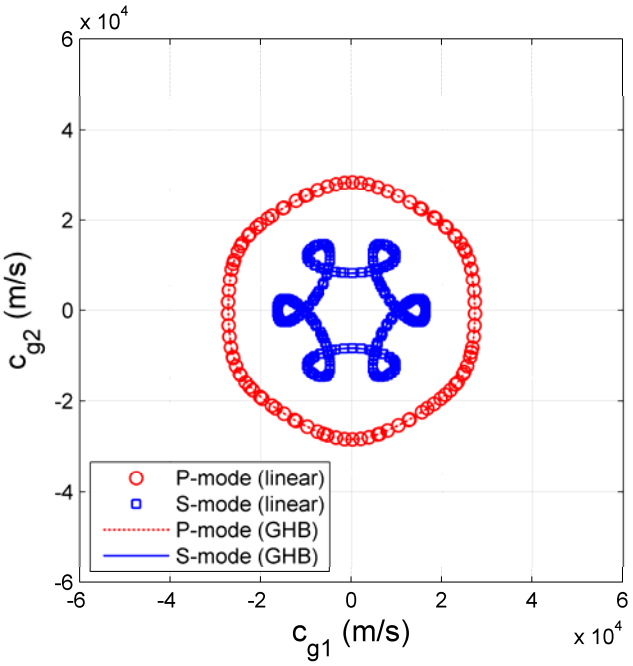

Figure 84: Group velocity plot of HCP granular lattice at A $= 0.01\delta_0$ and $f = 6.4$ kHz

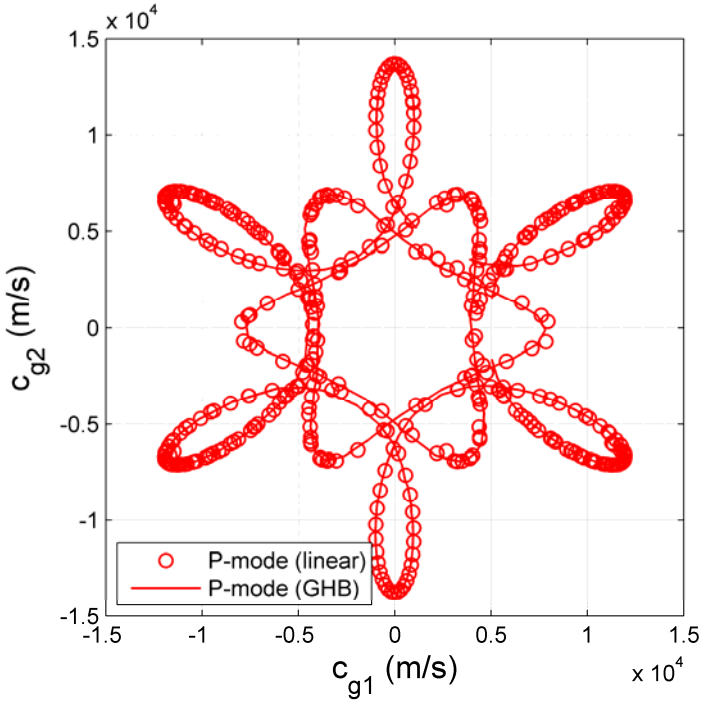

Figure 85: Group velocity plot of HCP granular lattice at A $= 0.01\delta_0$ and $f = 11.1$ kHz

6.4.5 NONLINEAR MODEL: AMPLITUDE DEPENDENT DISPERSION

The previous section demonstrated the application of generalized harmonic balance method at very low wave amplitudes. The amplitude dependent dispersion is studied by examining the variation of iso-frequency contours and the corresponding group velocity plots. Such a qualitative analysis could be very useful in design studies in a sense that the lattice can be tailored to obtain the desired response characteristics. Due to the generation of complex wave patterns such as solitary waves at high excitation amplitudes in the present example, the study limits the variation of the wave amplitudes to the order of initial pre-compression. The variation of S-mode iso-frequency contour for a lattice with initial pre-compressive force $F_{01} = F_{02} = F_{03} = 20\ N$ is shown in Figure 86.

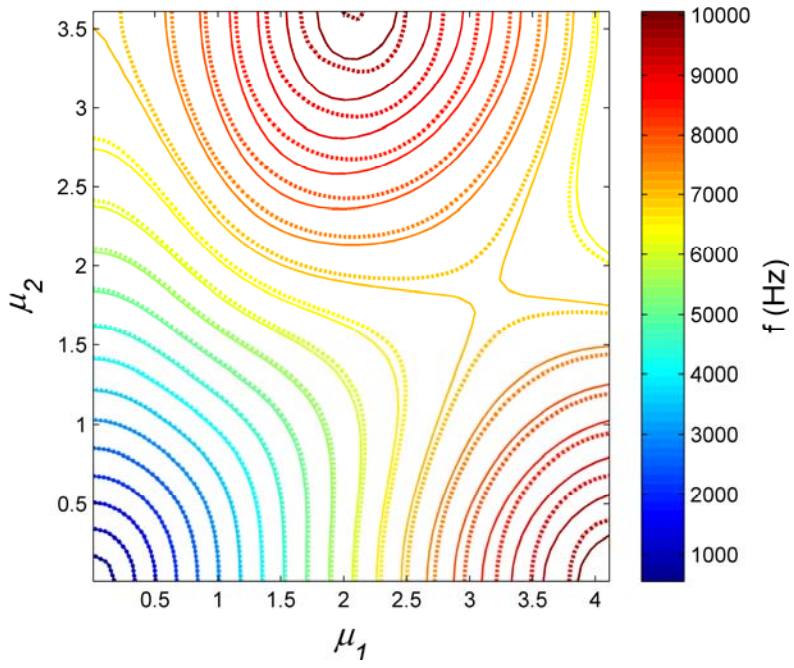

Figure 86: S-mode iso-frequency contour — $A = 0.01\delta_0$ ····· $A = 0.90\delta_0$

In a similar way, variation of P-mode iso-frequency contour with change in wave amplitude is detailed in Figure 87. Both modes at low wave frequency range, the change in amplitude tends to move the contours outwards. This indicates a shallower cone

looking at a three dimensional surface of the dispersion which indicates the reduction in group velocity or energy flow as the wave amplitude increases. This is in agreement with the one-dimensional case where the dispersion curve exhibits a softening effect.

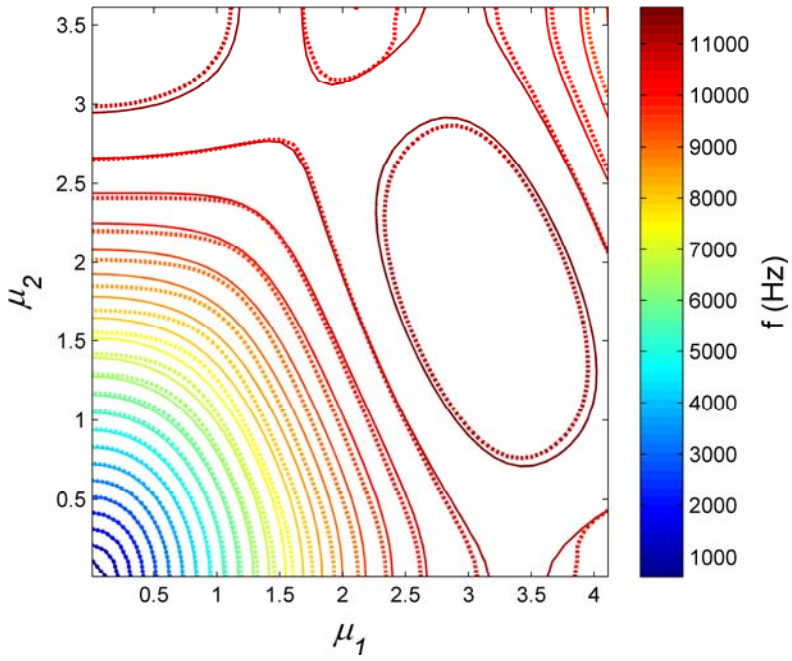

Figure 87: P-mode iso-frequency contour —A = $0.01\delta_0$ ····· A = $0.90\delta_0$

Iso-frequency contours are useful in identifying caustic frequency bands (definition in chapter 4.3.2) and associated amplitude effects. If the variation in energy flow has to be examined at a specific frequency, group velocity plots are convenient to interpret. For example, at frequency $\omega = 5$ kHz , the variation in group velocity with wave amplitude is shown in Figure 88. The results demonstrates that for the S-mode, the variation in energy flow with increase in amplitude is negligible as the plots almost overlap but for the P-mode there is a slight reduction in group velocity and as the frequency increases to $\omega = 11.10$ kHz where the propagation mode is only P-mode, the reduction in group velocity is significant. It is interesting to note the complex pattern displayed by group velocity plot at $\omega = 11.10$ kHz . The six-lobed figure reveals that the magnitude of group velocity at angles $\pm 30^{\circ}, \pm 90^{\circ}$ from the horizontal is comparatively larger than all the other directions. These directions can be considered as preferential directions of the plane

wave or spherical wave emanating from a point source travelling at wave frequency 11.10 kHz . This beaming phenomenon is further validated numerically which is explained in later section. The harmonic balance predicts that the amplitude effect on the dispersion at this frequency is two folded: 1) Loss in preferential directional behavior and 2) significant reduction in group velocity as demonstrated by Figure 88.

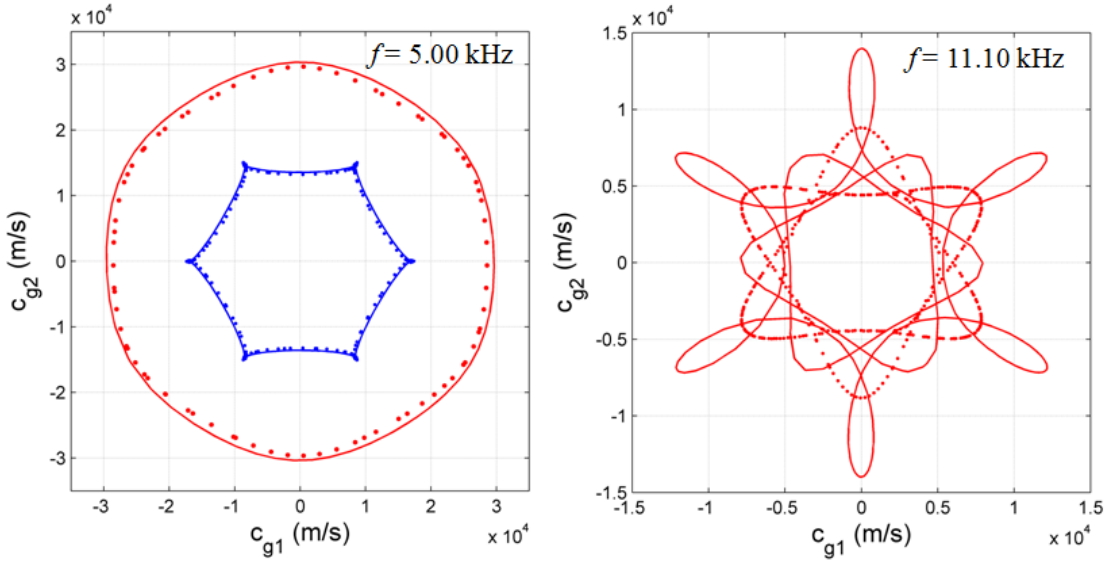

Figure 88: Variation in group velocity plot for a two dimensional hexagonal granular packing with change in wave amplitude — $A = 0.01\delta_0$ ····· $A = 0.90\delta_0$

6.4.6 NUMERICAL ESTIMATION OF DISPERSION

The variation of dispersion with amplitude predicted by harmonic balance is validated by numerical simulations of a finite lattice. Similar to the one-dimensional case, a plane wave is imposed on the two-dimensional lattice and the variation of an iso-frequency contour is observed for a specific frequency. The numerical simulations consider a finite 41×41 lattice with free boundary. The procedure to examine the variation of an iso-frequency contour begins with specifying the wave frequency at ω_0. To examine the contour, the wave vector $\boldsymbol{\mu}$ must satisfy the dispersion relation at the wave frequency ω_0. Therefore, (ξ_1, ξ_2) pairs satisfying the dispersion at ω_0 are determined using the

harmonic balance method. To excite p-mode or s-mode at specific frequency ω_0 and wave vector (ξ_1, ξ_2) , knowledge of the mode-shape is necessary. The mode-shape vector can be obtained from the linear dispersion solution or from the harmonic balance method. The normalized amplitude coefficients $\tilde{\boldsymbol{u}} = [c_{11}\ \ c_{12}]$ which represent the fundamental mode can be extracted from the converged solution obtained using harmonic balance method. A plane wave is imposed into the lattice by setting up an initial value problem in which the equations of motion and initial conditions for each mass in the lattice are given by,

$$\frac{d\boldsymbol{u}_j}{dt} = \boldsymbol{v}_j\ , \frac{d\boldsymbol{v}_j}{dt} = \mathbf{M}^{-1}\boldsymbol{f}_{NL}, \tag{6.88}$$

$$\boldsymbol{u}_{s_1,s_2}(t=0) = \mathrm{A}\tilde{\boldsymbol{u}}\cos(\xi_1 s_1 + \xi_2 s_2), \tag{6.89}$$

$$\boldsymbol{v}_{s_1,s_2}(t=0) = \mathrm{A}\omega\tilde{\boldsymbol{u}}\cos(\xi_1 s_1 + \xi_2 s_2). \tag{6.90}$$

In the above equations, $\boldsymbol{u} = [u_1 \quad u_2]^{\mathrm{T}}$ where u_1 and u_2 denote the projections of in-plane displacement of each mass along $\boldsymbol{i}_1$and $\boldsymbol{i}_2$ axes respectively, s_1 and s_2 denote mass index along $\boldsymbol{i}_1$and $\boldsymbol{i}_2$ axes respectively, and $\tilde{\boldsymbol{u}}$ denotes the normalized mode shape vector defining the propagation mode. The frequency ω in the velocity condition can be a frequency close to ω_0 or equal to ω_0.The perturbation in this initial condition does not affect the final solution as the numerical integration of equations of motion determines the frequency of vibration of the masses. The procedure for the numerical evaluation of the iso-frequency contour is detailed below:

1) Specify the frequency ω_0 and obtain all the (ξ_1, ξ_2) pairs satisfying the dispersion at wave amplitude A using the harmonic balance approach.
2) Extract the normalized mode shape vector $\tilde{\boldsymbol{u}}$ for each (ξ_1, ξ_2) pair

3) Impose a plane wave into the system by setting up the initial value problem described by Eqs. (6.88) - (6.90)

4) Due to the finite lattice, the reflections from the boundaries start to distort the plane wave profile. For simulation time of 5T where $T = 2\pi/\omega$ and considering a 41×41 lattice, the wave profile over a sub-lattice of 31×31 from the center are used to compute propagation constants and frequency.

5) Fourier Transform in space along $\boldsymbol{i}_1$ and $\boldsymbol{i}_2$ and in time generates the propagation constants and frequency of the wave.

Figure 89 shows the configuration corresponding to the considered simulations. The figure shows a 41×41 lattice in which a plane wave is setup. For a simulated time of $0.15\ ms$ the reflections from the boundary do not distort the plane wave profile of a 30×30 sub-lattice.

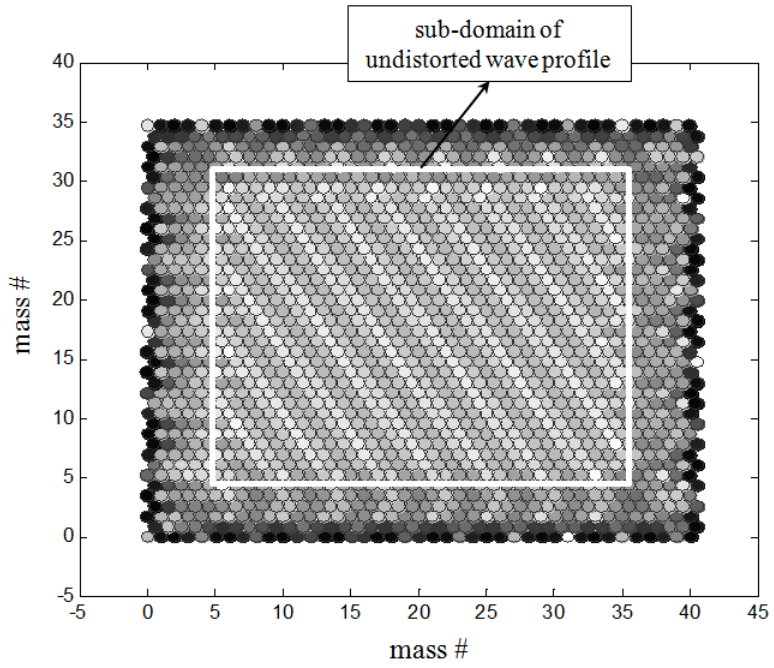

Figure 89: Schematic of 41×41 lattice with plane wave imposed illustrating a sub-domain of 30X30 mass lattice

Figure 88 reveals that with the change in amplitude, the variation in iso-frequency contours of S-mode is very small in comparison with the variation in P-mode. Hence, the numerical results are generated for an iso-frequency contour of a P-mode. Figure 90 displays the variation of the iso-frequency contour for the P-mode at frequency $f = 7.96$ kHz.

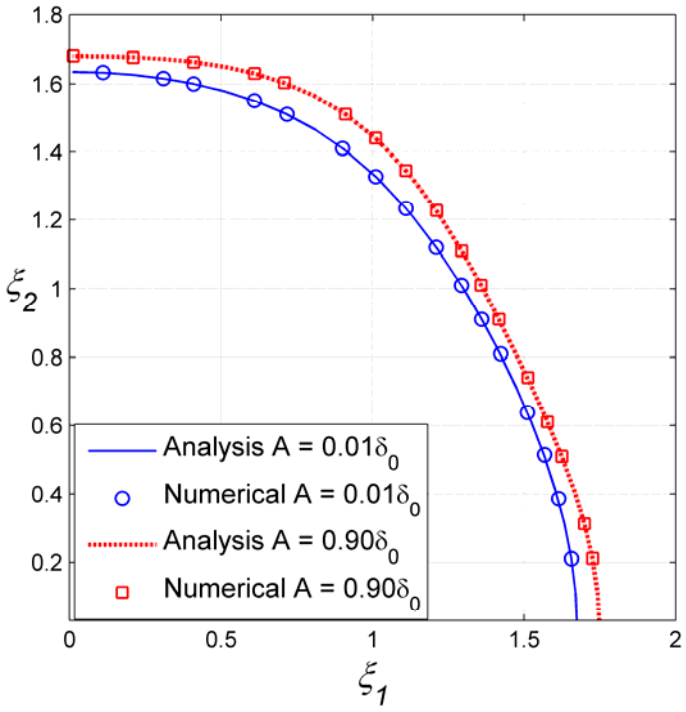

Figure 90: Variation of p-mode iso-frequency contour (Numerics vs Harmonic balance)

The numerical results are in excellent agreement with the analytical predictions of the generalized harmonic balance. The contour moves outward indicating a decreased slope at each point on the dispersion surface. This in turn leads to the decrease in group velocity with increase in amplitude indicated in Figure 88.

6.4.7 ACOUSTIC WAVE BEAMING

Group velocity plots as mentioned before are indicators of the energy flow in the lattice. This present section demonstrates the response of the isotropically pre-compressed hexagonal lattice of Aluminum spheres ($F_{01} = F_{02} = F_{03} = 20N$) to point harmonic

excitation of the lattice at two specific frequencies 1) where the wave propagates in all directions and 2) where acoustic wave beaming phenomenon is expected. First, consider the frequency excitation at $f = 7.95$ kHz, the corresponding group velocity plot (Figure 91) shows the propagation of P- and S-mode in all directions.

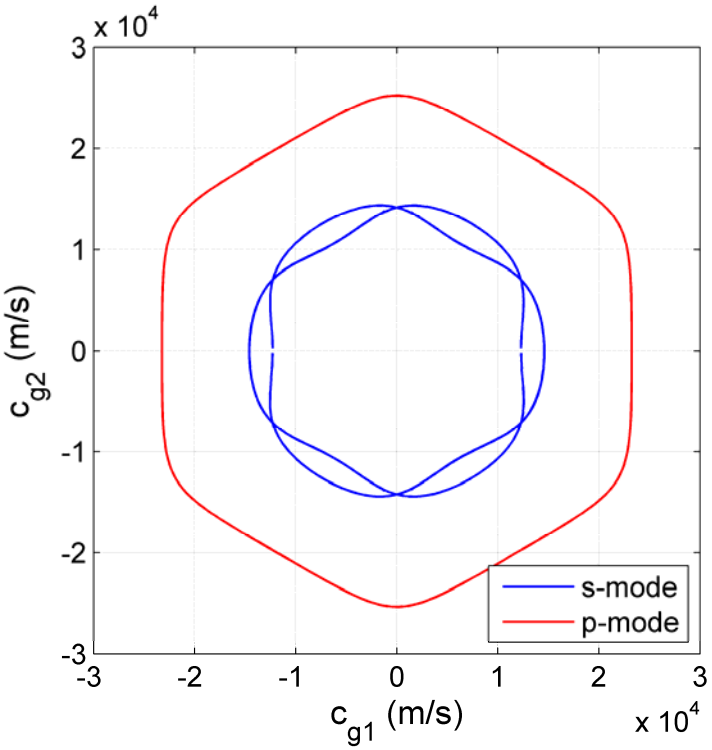

Figure 91: Group velocity plot of HCP lattice at A $= 0.01\delta_0$ and $f = 7.95$ kHz

As the figure suggests, there exists slight anisotropy in the propagation implying that the group velocities are not exactly equal in all directions. The displacement of the excitation mass $u_{ex}(t) = \text{Asin}(\omega t)$ sets up the harmonic excitation in the lattice and the response is demonstrated by the snapshot of actual displacement of each mass in the lattice at a time when the wave reaches the boundaries. In this case, the wave travels in all directions as shown in Figure 92.

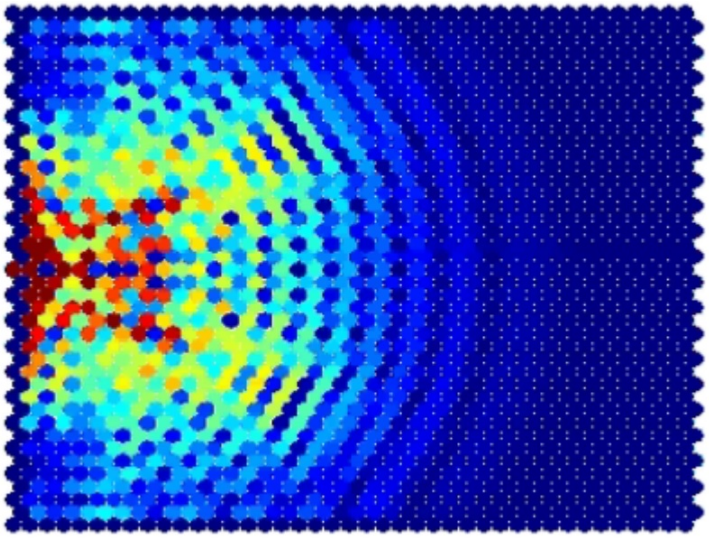

Figure 92: Numerical response of 41×41 lattice to harmonic excitation at frequency $f = 7.95$ kHz

The same lattice exhibits beaming as predicted by the group velocity of frequency 11.10 kHz as shown in Figure 82. The plot of Figure 93 indicates that the magnitude of energy-flow velocity along $\theta = \pm\pi/6, \pm\pi/2, \pm 5\pi/6$ is large in comparison to the other directions. The statement implies that the resistance along these directions to the wave travel is considerably less in comparison to other directions. Figure 94 demonstrates the numerical response of a 41×41 pre-compressed lattice at amplitude $A = 0.01\delta_0$ to a point harmonic excitation at the left edge of the lattice at frequency $\omega =$ 11.10 KHz. As the lattice is highly nonlinear, it is expected that this energy flow is dependent on excitation amplitude. Analytically, Figure 88 demonstrates that the lattice gradually loses its beaming capability as the amplitude increases since the magnitude of energy flow velocity appears to decrease in the preferential directions without affecting much the rest of orientation.

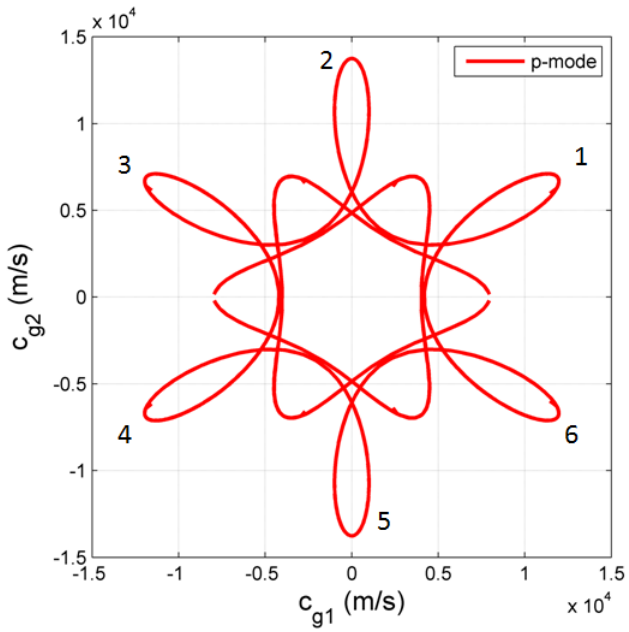

Figure 93: Group velocity plot at f = 11.10 kHz indicating the six preferential directions marked by points 1, 2…6

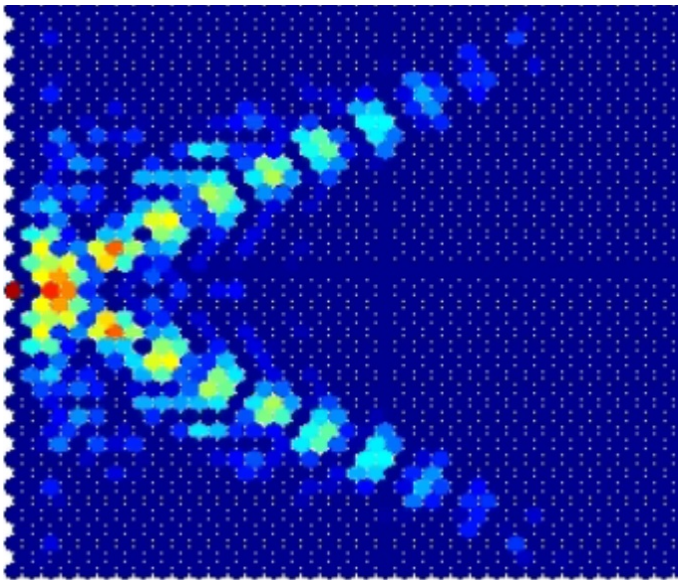

Figure 94: Snapshot of bead displacement at to point harmonic excitation at frequency $f = 11.10$ kHz

6.5 NOTE ON PLANE WAVE SIMULATION

One method to generate a plane wave is point harmonic excitation of system. In general, linear dynamical systems generate wave frequencies equal to the excitation frequency. In the present example of the granular chain, the force interaction is highly nonlinear and asymmetric with respect to the relative displacement. The asymmetry arises due to contact interaction of the spheres and nonlinearity due to the geometry of the interaction. Such a chain where the elements of the system could have intermittent zero restoring force is capable of exhibiting very rich and interesting dynamics such as supporting solitary waves. In the case of strongly nonlinear systems, a single harmonic excitation could generate multiple harmonic waves within the system. Relative amplitude of the excitation frequency content in the propagating wave depends on the frequency of excitation and the magnitude of initial pre-compression. For a zero pre-compression, the propagation is through the Nesterenko solitary wave as shown in Figure 95. Figure 95a shows the grain velocity plot of the masses with point harmonic forcing at frequency $f = 1\,\text{kHz}$ and amplitude $\text{A} = 10^{-8}\,m$ which is comparable to previously observed magnitudes of displacement. The plot indicates that the disturbance is localized to 4-5 particles and the particles before the disturbance are in equilibrium (zero velocity).

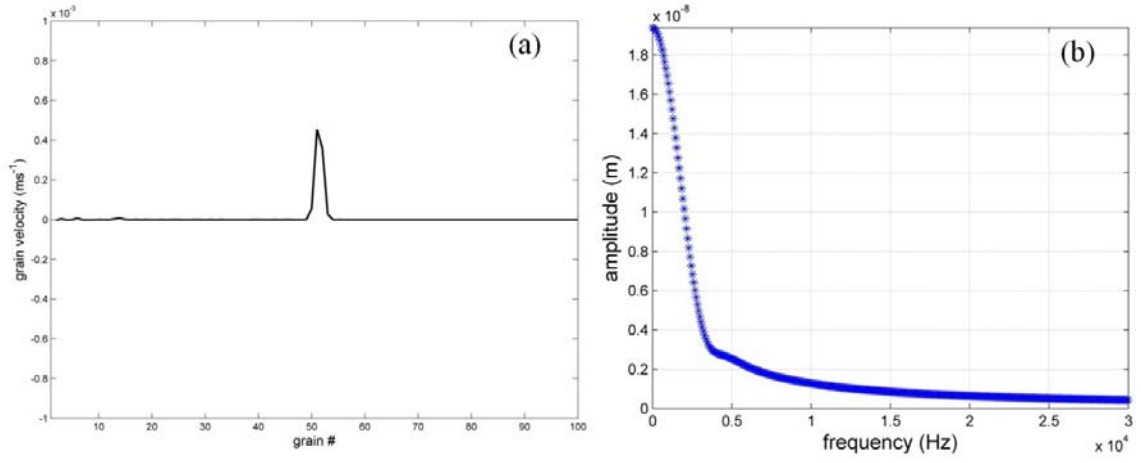

Figure 95: (a) Solitary wave in zero pre-compressed chain (b) Frequency spectrum of bead displacement

Figure 95b displays the frequency spectrum of the particle displacement (bead # 30) from the point of excitation. This is similar to frequency spectrum of a step function as the low frequency content indicates zero oscillation after a finite particle displacement.

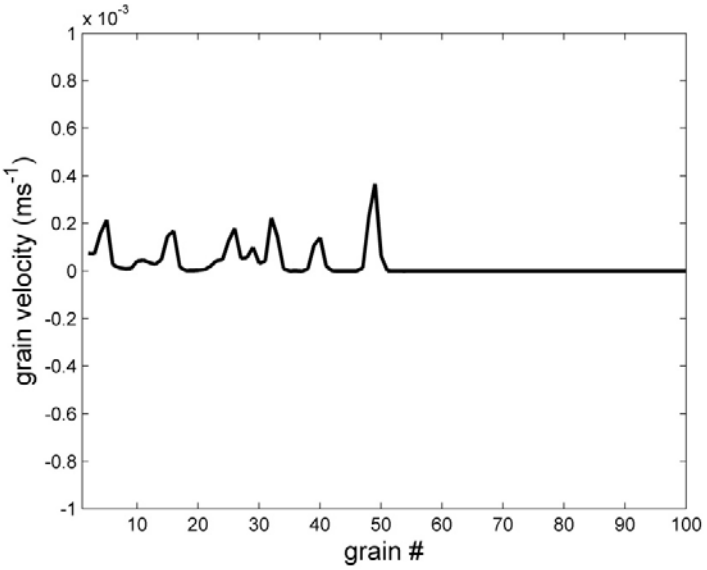

Figure 96: Train of solitary waves in granular chain

To emphasize the complex dynamics exhibited by these uncompressed granular media one more case is presented with a higher frequency excitation. The increase in frequency leads to a *train of solitary waves* rather than a single solitary wave which is indicated in Figure 96.

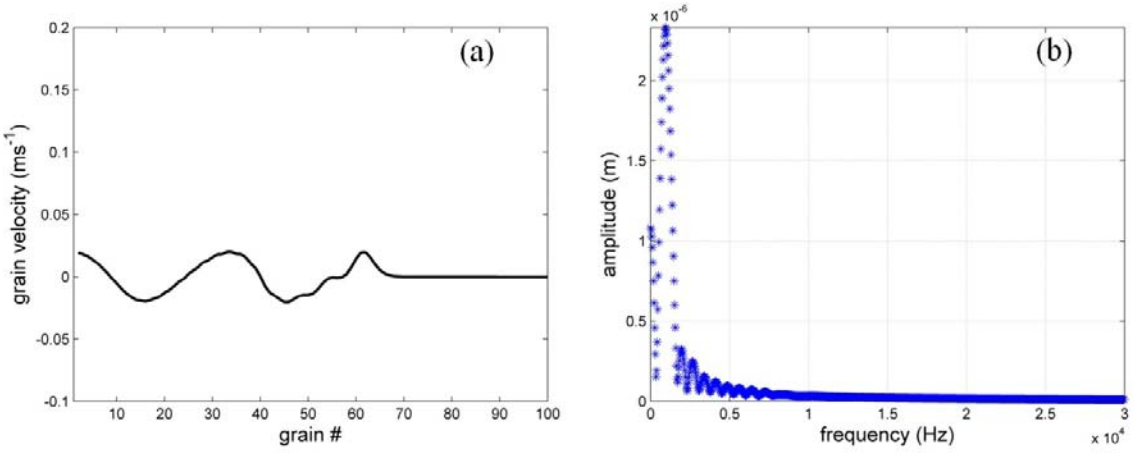

Figure 97: Periodic wave trailing a leading solitary wave at $A = 0.01\delta_0$

With a pre-compressed chain at amplitudes which are low compared to the initial pre-compression δ_0 , the wave form is a quasi-periodic. But as the wave amplitude increases to the order of δ_0 , the wave form has a complex structure as shown by Figure 97-Figure 99. At low frequency $\omega = 1$ kHz, Figure 97 shows a leading solitary wave along with a trailing solitary wave which is depicted in the frequency spectrum plot.

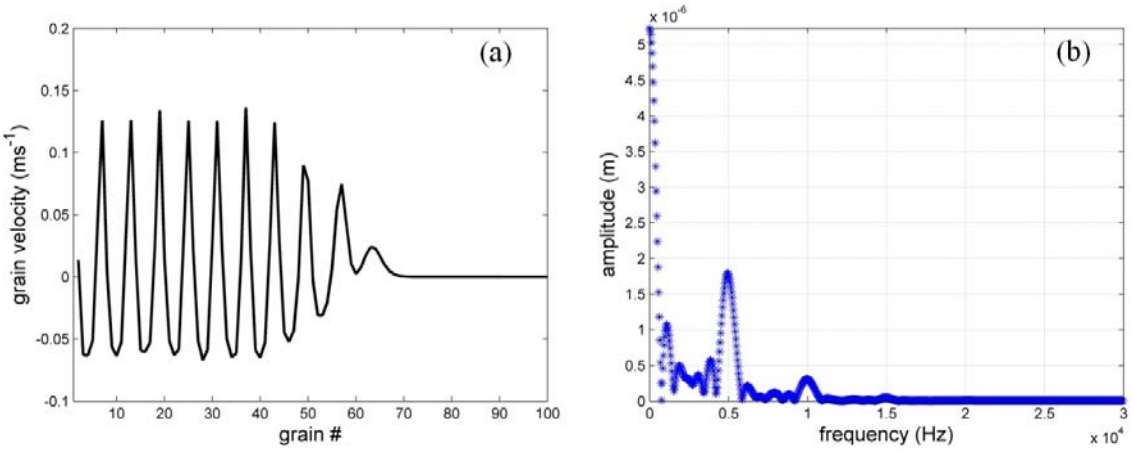

Figure 98: (a) Grain velocity vs time (b) Frequency spectrum at A = 0.50δ_0 (bead # 50) indicating the transmission of solitary wave and trailing periodic wave

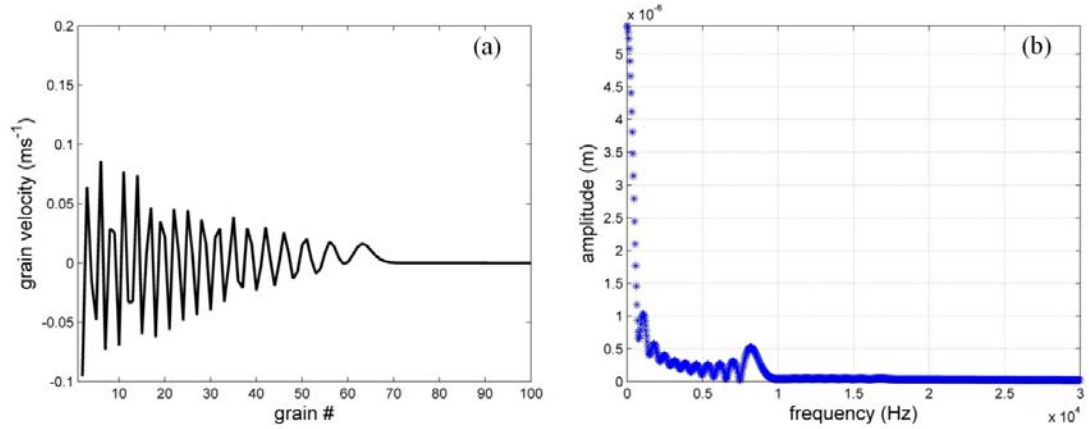

Figure 99: (a) Grain velocity vs time (b) Frequency spectrum at A = 0.99δ_0 (bead # 50 from excitation source) indicating the propagation is mainly through solitary wave

As the frequency increases, the magnitude of amplitude of the solitary wave increases compared to that of the trailing harmonic wave which is depicted Figure 98. As the

frequency approaches the edge of the Brillouin zone, the harmonic wave decays significantly and the propagating wave is just solitary as depicted by Figure 99.

6.6 CONCLUSIONS

A generalized harmonic balance method is presented to predict wave dispersion in strongly nonlinear periodic lattices. For weakly nonlinear system, perturbation analysis led to qualitative understanding of the effects of wave amplitude on dispersion solution. Analytical estimation of dispersion is numerically validated through time-domain integration of equations of motion. Limitations and the scope of validity with the analysis as well as numerical models have been detailed. In the two dimensional case, amplitude dependent *iso-frequency contours* and *group-velocity plots* are analyzed to predict energy flow in the lattice. At a certain frequency, it is shown that the lattice exhibits acoustic wave beaming phenomenon.

Scope for the further work involves analyzing the lattices with asymmetric pre-compression ($\delta_{01} \neq \delta_{02} = \delta_{03}$) which could lead to caustic frequency bands. Such caustic bands if strongly dependent on the wave amplitude would lead to tunable energy directionality. On the other hand, zero pre-compressed lattices could support solitary wave solutions. Tunability in transmission properties of solitary waves in two dimensional lattices can be the subject of the future work. This could potentially lead to a number of enhance applications such as tunable stress redirecting mechanical structures.

CHAPTER VII

CONCLUDING REMARKS

7.1 SUMMARY

The research presented in this work investigated the effect of nonlinearities and wave amplitude on plane wave dispersion characteristics in periodic structures. Wave filtering properties of periodic structures enable them to act as mechanical band-pass filters, vibration isolators, wave guides and resonators. The periodicity and structural design of the periodic element can be tailored to achieve the required filtering properties. In the recent past, documents in the literature report tunable filtering properties of periodic structures which depend on modifying geometry or the properties of the material using external sources such as electro-magnetic forces. In nonlinear systems, amplitude of excitation and degree of nonlinearity play a vital role in the system response. Therefore the major motivation for the research was to investigate the influence of nonlinearity as well as wave amplitude on a periodic structure's dispersion properties and tunable filtering capabilities.

A perturbation approach is formulated which predicts amplitude dependent dispersion in *weakly* nonlinear periodic structures whose general domain can be discretized through a Finite Element formulation. The analysis is first applied to spring-mass models which provide a convenient setting to introduce nonlinearities and qualitatively capture the wave propagation properties. The amplitude dependent wave characteristics led to the design of some conceptual tunable acoustic devices. To demonstrate the generality of the formulated perturbation approach, dispersion properties of a complex weakly nonlinear periodic structure e.g. membrane on nonlinear elastic support are also explored. The perturbation approach however limits the analysis to low

wave amplitudes as the solution is assumed to be a perturbation from the linear solution. Therefore the dispersion analysis in periodic structures with *strong* nonlinear interactions should resort to other analytical methods.

Next, the research documented a harmonic balance method to predict dispersion in strongly nonlinear periodic lattices. Due to the geometry of interaction, the granular media can be considered as an example of strongly nonlinear periodic structure. The harmonic balance method is applied to one-dimensional granular chains and two-dimensional hexagonally packed media to predict the dispersion and the variation of propagation characteristics due to the wave amplitude. For all the configurations, the predicted analytical results are numerically validated by simulating wave propagation in finite dimensional nonlinear lattices.

7.2 RESEARCH CONTRIBUTIONS

The research presented in this thesis provides the following original contributions:

- ◊ An asymptotic approach to analyze the wave propagation in discrete weakly nonlinear periodic structures which allows for a solution of higher-order dispersion relationships
- ◊ A novel perturbation methodology which handles an infinite set of difference equations eliminating the need to replace the discrete setting with continuous one;
- ◊ Prediction of amplitude-dependent bandgaps and tunable wave directional behavior in two-dimensional nonlinear periodic structures;
- ◊ Demonstrating significant shift in cut-off frequencies with respect to the wave amplitude exhibited by strongly nonlinear granular chains using harmonic balance method;
- ◊ Acoustic wave beaming phenomenon in two-dimensional hexagonal granular packing;

7.3 RECOMMENDATIONS FOR FUTURE WORK

7.3.1 NONLINEAR DISPERSION THROUGH MESH PERIODICITY

A number of materials such as plastics, rubber (nonmetals), embedded-matrix structures, alloys, polymer networks etc… exhibit nonlinear elastic properties. A number of reports have been dedicated to study the wave transmission properties in materials with nonlinear elastic behavior. For example, wave propagation in structures with complex geometries employing nonlinear constitutive laws with cellular automata approach [99] is documented by Autrusson T.B. [100].

Future work seeks to estimate dispersion in physically non-periodic media by applying the general perturbation approach using mesh-periodicity (Figure 100). A finite element discretized model leads to element-wise periodic structure. A generic nonlinear constitutive law can be written as,

$$\sigma = C\epsilon + g(\epsilon), \tag{7.1}$$

where $g(\epsilon)$ denotes nonlinear stress-strain relationship. For example, a quadratic nonlinearity assumes the following,

$$g(\epsilon) = \frac{1}{2}\epsilon^{T} D\epsilon, \tag{7.2}$$

Application of such law would lead to equations of motion for discretized model which are of the form,

$$\boldsymbol{M\ddot{u}} + \boldsymbol{Ku} + \boldsymbol{f}_{NL}(\boldsymbol{u}) = \boldsymbol{f}_{ext}, \tag{7.3}$$

where $\boldsymbol{M}$ denotes mass matrix, $\boldsymbol{K}$ is linear stiffness matrix, $\boldsymbol{f}_{NL}$ denotes nonlinear force vector, $\boldsymbol{f}_{ext}$ describes external forcing and $\boldsymbol{u}$ is vector describing the nodal displacement field. At this point, if each element is similar to one another, mesh-periodicity can be applied approximate the dispersion using general perturbation approach. This element wise similarity would limit the application of the analysis to uniform, homogenous structures such as beams, plates, etc… The procedure provides a novel methodology to

estimate dispersion in such nonlinear media although limited to simple structures as mentioned above.

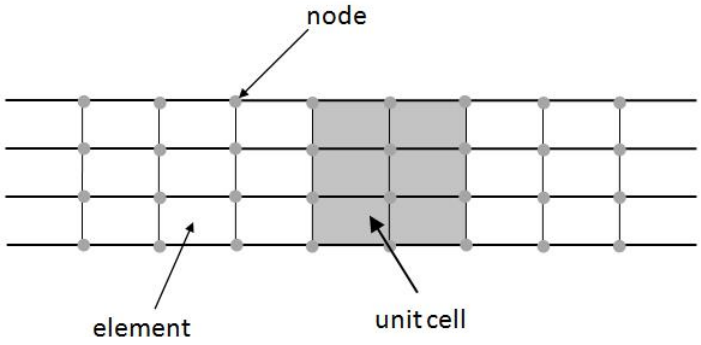

Figure 100: Meshing introduces periodicity if each element is similar to one another and the unit cell as shown can be considered as a periodic element

7.3.2 EXPERIMENTAL INVESTIGATION OF AMPLITUDE-DEPENDENT DISPERSION

The present research provided the analytical and numerical analysis of the dispersion properties in nonlinear periodic structures. The tools provided aid in designing a periodic structure which exhibits the desired tunable dispersion characteristics. Experimental evidence of amplitude-dependent dispersion could lead to potential practical applications. Therefore, future work can be devoted to designing experimental setups which can capture the amplitude-dependent wave dispersion as documented in the thesis along with other nonlinear phenomena such as wave localization and soliton propagation.

7.3.3 SOLITARY WAVE PROPAGATION IN 2D GRANULAR MEDIA

Dispersion analysis in nonlinear periodic structures revealed tunable wave directional behavior. The present work reports the effects of nonlinearities on plane wave propagation characteristics. Strongly nonlinear media support complex wave patterns such as solitary waves. In essentially nonlinear media, the disturbance propagates through the generation of solitary wave which in general is highly stable implying that the profile is robust to the perturbations. Study of such waves in two- and three- dimensional

strongly nonlinear mechanical structures and their directional behavior has not been explored much. Hence, future work can focus on the analysis of tunable directional behavior of solitary waves in essentially nonlinear periodic structures such as two- or three-dimensional granular media which could potentially lead to shock or energy re-directive materials.

7.3.4 RESPONSE OF NONLINEAR LATTICE TO INITIAL CONDITIONS

The study on strongly nonlinear lattices depicted the existence of complex wave solutions and wave propagation characteristics. For example, a complex group velocity pattern is predicted for a high frequency wave in a two-dimensional hexagonally packed granular media as shown by Figure 93. Apart from the preferential wave directional behavior, the plot also indicates multiple group velocities for the same wave frequency along different directions. The above statement implies that multiple wave vectors satisfy the dispersion relation at the same frequency and the harmonic response of a lattice can be a combination of these solutions. As a part of the future work, one can investigate the effect of initial conditions on the wave solutions supported by the nonlinear lattice. Does the plane wave support only one of the possible solutions? For a plane wave propagating along a specific direction, does it support single wavenumber or multiple wavenumbers or does it always get attracted to one of the solutions? Such issues can be further explored by studying the stability analysis of such solutions.

7.3.5 NONLINEAR WAVE-WAVE INTERACTIONS

The present research focused on the nonlinear effects on a single plane wave propagating through a periodic structure. Multiple-wave propagation in nonlinear periodic media can be investigated to explore the nonlinear wave interactions. As one wave affects the propagation characteristics of the other wave nonlinearly one can explore interesting energy flow patterns and amplitude dependent nonlinear responses in periodic media.

REFERENCES

[1] BRILLOUIN, L., Wave propagation in periodic structures, Dover, (1946)

[2] MARTINEZ-SALA, R., SANCHO, J., SANCHEZ, J.V., GOMEZ, V., LLINARES, J. and MESEGUER, F. "Sound attenuation by sculpture," Nature, vol. 378, pp 241-241, 1995.

[3] RAYLEIGH "XVII.On the maintenance of vibrations by forces of double frequency, and on the propagation of waves through a medium endowed with a periodic structure," Philosophical Magazine Series 5, vol. 24, pp 145 - 159, 1887.

[4] MEAD, D.J. "Wave propagation in continous periodic structures: Research contributions from southampton 1964-1995," Journal of Sound and Vibration, vol. 190, pp 495-524, 1996.

[5] ELACHI, C. "Waves in active and passive periodic structures: A review," Proceedings of the IEEE, vol. 64, pp 1666-1698, 1976.

[6] MOVCHAN, A., MOVCHAN, N. and HAQ, S. "Localised vibration modes and stop bands for continuous and discrete periodic structures," Materials Science and Engineering: A, vol. 431, pp 175-183, 2006.

[7] JENSEN, J.S. and SIGMUND, O., Phononic Band Gap Structures as Optimal Designs, Springer Netherlands, 113 (2004)

[8] GRY, L. and GONTHER, C. "Dynamic modeling of railway track: A periodic model based on generalized beam formulation," Journal of Sound and Vibration, vol. 199, pp 531-558, 1995.

[9] PARMLEY, S., ZOBRIST, T., CLOUGH, T., PEREZ-MILLER, A., MAKELA, M. and YU, R. "Phononic band structure in a mass chain," Applied Physics Letters, vol. 67, pp 777-779, 1995.

[10] DIEZ, A., KAKARANTZAS, G., BIRKS, T.A. and RUSSELL, P.S.J. "Acoustic stop-bands in periodically microtapered optical fibers," Applied Physics Letters, vol. 76, pp 3481-3483, 2000.

[11] GRIFFITHS, D.J. and STEINKE, C.A. "Waves in locally periodic media," American Journal of Physics, vol. 69, pp 137-154, 2001.

[12] LANGLET, P., HLADKY-HENNION, A.-C. and DECARPIGNY, J.-N. "Analysis of the propagation of plane acoustic waves in passive periodic materials using the finite element method," The Journal of the Acoustical Society of America, vol. 98, pp 2792-2800, 1995.

[13] AXMANN, W. and KUCHMENT, P. "An efficient finite element method for computing spectra of photonic and acoustic band-gap materials. I. scalar case," J. Comput. Phys., vol. 150, pp 468-481, 1999.

[14] MACE, B. and MANCONI, E. "Modelling wave propagation in two-dimensional structures using finite element analysis," Journal of Sound and Vibration, vol. 318, pp 884-902, 2008.

[15] MEAD, D.J. and PARTHAN, S. "Free wave propagation in two-dimensional periodic plates," Journal of Sound and Vibration, vol. 64, pp 325-348, 1979.

[16] MEAD, D.J., D.C., Z. and N.S., B. "Free vibration of an orthogonally stiffened flat plate," Journal of Sound and Vibration, vol. 127, pp 19-48, 1988.

[17] POULTON, C.G., MOVCHAN, A.B., MCPHEDRAN, R.C., NICOROVICI, N.A. and ANTIPOV, Y.A. "Eigenvalue problems for doubly periodic elastic structures and phononic band gaps," Proceedings of the Royal Society of London. Series A: Mathematical, Physical and Engineering Sciences, vol. 456, pp 2543-2559, 2000.

[18] SUZUKI, T. and YU, P.K.L. "Complex elastic wave band structures in three-dimensional periodic elastic media," Journal of the Mechanics and Physics of Solids, vol. 46, pp 115-138, 1998.

[19] LIU, Z., ZHANG, X., MAO, Y., ZHU, Y.Y., YANG, Z., CHAN, C.T. and SHENG, P. "Locally Resonant Sonic Materials," Science, vol. 289, pp 1734-1736, 2000.

[20] VASSEUR, J.O. and ET AL. "Experimental evidence for the existence of absolute acoustic band gaps in two-dimensional periodic composite media," Journal of Physics: Condensed Matter, vol. 10, p 6051, 1998.

[21] RUZZENE, M., SCARPA, F. and F., S. "Wave beaming effects in two-dimensional cellular structures," Smart materials and structures, vol. 12, pp 363-372, 2003.

[22] PHANI, A.S., WOODHOUSE, J. and FLECK, N.A. "Wave propagation in two-dimensional periodic lattices," The Journal of the Acoustical Society of America, vol. 119, p 1995, 2006.

[23] RUZZENE, M. and TSOPELAS, P. "Control of wave propagation in sandwich plate rows with perioidc honeycomb core," Journal of Engineering Mechanics, vol. 129, pp 975-986, 2003.

[24] KOHRS, T. and PETERSSON, B.A.T. "Wave beaming and wave propagation in light weight plates with truss-like cores," Journal of Sound and Vibration, vol. 321, pp 137-165, 2009.

[25] LANGLEY, R.S. "The response of two-dimensional periodic structures to point harmonic forcing," Journal of Sound and Vibration, vol. 197, pp 447-469, 1996.

[26] JENSEN, J.S. "Phononic band gaps and vibrations in one- and two-dimensional mass-spring structures," Journal of Sound and Vibration, vol. 266, pp 1053-1078, 2003.

[27] LANGLEY, R.S., BARDELL, N.S. and RUIVO, H.M. "The response of two-dimensional periodic structures to harmonic point loading: A theoretical and experimental study of a beam grillage," Journal of Sound and Vibration, vol. 207, pp 521-535, 1997.

[28] NAYFEH, A. and MOOK, D., Nonlinear Oscillations, Wiley, (1996)

[29] VAKAKIS, A.F. and KING, M.E. "Nonlinear wave transmission in a monocoupled elastic periodic system," Journal of Acoustical Society of America, vol. 98, pp 1534-1546, 1995.

[30] R.M., R. "The normal modes of nonlinear n-degree-of-freedom systems," Transactions of the ASME. Journal of Applied Mechanics, vol. 29, pp 7-14, 1962.

[31] PIERRE, C., JIANG, D. and SHAW, S. "Nonlinear normal modes and their application in structural dynamics," Mathematical Problems in Engineering, vol. 2006, pp 1-16, 2006.

[32] VAKAKIS, A.F. "Nonlinear normal modes (NNMs) and their applications in vibration theory: An overview," Mechanical Systems and Signal Processing, vol. 11, pp 3-22, 1997.

[33] CHAKRABORTY, G. and MALIK, A.K. "Dynamics of weakly non-linear periodic chain," International Journal of Non-Linear Mechanics, vol. 36, pp 375-389, 2001.

[34] ROMEO, F. and REGA, G. "Wave propagation properties in oscillatory chains with cubic nonlinearities via nonlinear map approach," Chaos, Solitons & Fractals, vol. 27, pp 606-617, 2006.

[35] VAKAKIS, A.F. and GEORGIOU, I.T. "An invariant manifold approach for studying waves in a one-dimensional array of non-linear oscillators," International Journal of Non-Linear Mechanics, vol. 31, pp 871-886, 1996.

[36] VAKAKIS, A., NAYFEH, T. and KING, M. "A Multiple-Scales Analysis of Nonlinear, Localized Modes in a Cyclic Periodic System," Journal of Applied Mechanics, vol. 60, pp 388-397, 1993.

[37] LAZAROV, B.S. and JENSEN, J.S. "Low-frequency bandgaps in chains with attached non-linear oscillators," International Journal of Non-Linear Mechanics, vol. 42, pp 1186-1193, 2007.

[38] BULLOUGH, R.K. and CAUDREY, P.J., Solitons, Springer, (1980)

[39] SIEVERS, A.J. and TAKENO, S. "Intrinsic localized modes in anharmonic crystals," Physical Review Letters, vol. 61,1988.

[40] VAKAKIS, A.F., KING, M.E. and PEARLSTEIN, A.J. "Forced Localization in a periodic chain of non-linear oscillators," International Journal of Non-Linear Mechanics, vol. 29, pp 429-447, 1994.

[41] NESTERENKO, V.F. "New wave dynamics in granular state," Journal of Applied Mechanics and Technical Physics, vol. 24,1983.

[42] DARAIO, C., NESTERENKO, V., HERBOLD, E. and JIN, S. "Tunability of solitary wave properties in one-dimensional strongly nonlinear phononic crystals," Physical Review E, vol. 73, p 026610, 2006.

[43] ACEVES, A. "Localization and trapping of light in one- and two-dimensional nonlinear periodic structures," Wave Motion, vol. 45, pp 48-58, 2007.

[44] FENG, B. and KAWAHARA, T. "Discrete breathers in two-dimensional nonlinear lattices," Wave Motion, vol. 45, pp 68-82, 2007.

[45] SREELATHA, K.S. and BABU JOSEPH, K. "Wave propagation through a 2D lattice," Chaos, Solitons & Fractals, vol. 11, pp 711-719, 2000.

[46] DUAN, W.-S., SHI, Y.-R., ZHANG, L., LIN, M.-M. and LV, K.-P. "Coupled nonlinear waves in two-dimensional lattice," Chaos, Solitons & Fractals, vol. 23, pp 957-962, 2005.

[47] GOFFAUX, C. and VIGNERON, J.P. "Theoretical study of a tunable phononic band gap system," Physical Review B, vol. 64, p 075118, 2001.

[48] YEH, J.-Y. "Control analysis of the tunable phononic crystal with electrorheological material," Physica B: Condensed Matter, vol. 400, pp 137-144, 2007.

[49] ROBILLARD, J.F., MATAR, O.B., VASSEUR, J.O., DEYMIER, P.A., STIPPINGER, M., HLADKY-HENNION, A.C., PENNEC, Y. and DJAFARI-ROUHANI, B. "Tunable magnetoelastic phononic crystals," Applied Physics Letters, vol. 95, pp 124104-124103, 2009.

[50] GONELLA, S. and RUZZENE, M. "Analysis of in-plane wave propagation in hexagonal and re-entrant lattices," Journal of Sound and Vibration, vol. 312, pp 125-139, 2008.

[51] SPADONI, A., RUZZENE, M., GONELLA, S. and SCARPA, F. "Phononic properties of hexagonal chiral lattices," Wave Motion, vol. 46, pp 435-450, 2009.

[52] WOLFE, J.P., Imaging Phonons: Acoustic wave propagation in solids, Cambridge University Press, (1998)

[53] COOPER and K. "Generalized harmonic balance/numerical method for determining analytical approximations to the periodic solutions of the x4/3 potential," Journal of Sound and Vibration, vol. 250, pp 951-954, 2002.

[54] MARATHE, A. and CHATTERJEE, A. "Wave attenuation in nonlinear periodic structures using harmonic balance and multiple scales," Journal of Sound and Vibration, vol. 289, pp 871-888, 2006.

[55] GUSKOV, M., SINOU, J.-J. and THOUVEREZ, F. "Multi-dimensional harmonic balance applied to rotor dynamics," Mechanics Research Communications, vol. 35, pp 537-545, 2008.

[56] BELÉNDEZ, A., GIMENO, E., ALVAREZ, M.L. and MÉNDEZ, D.I. "Nonlinear oscillator with discontinuity by generalized harmonic balance method," Computers & Mathematics with Applications, vol. 58, pp 2117-2123, 2009.

[57] BOBYLEV, N.A., BURMAN, Y.M. and KOROVIN, S.K., Approximation Procedures in Nonlinear Oscillation Theory, 2 (1994)

[58] HOUSEHOLDER, A.S., Principles of numerical analysis, McGraw-Hill, (1953)

[59] ORTEGA, J.M. and RHEINBOLDT, W.C., Iterative solution of nonlinear equations in several variables, SIAM, (2000)

[60] C.T., K., Solving nonlinear equations with newton's method, Fundamentals of algorithms 1, SIAM, (2003)

[61] SHENG, X. and LI, M.H. "Propagation constants of railway tracks as a periodic structure," Journal of Sound and Vibration, vol. 299, pp 1114-1123, 2007.

[62] STEPHEN, N.G. "On the vibration of one-dimensional periodic structures," Journal of Sound and Vibration, vol. 227, pp 1133-1142, 1999.

[63] TSO, Y.K. and HANSEN, C.H. "The transmission of vibration through a coupled periodic structure," Journal of Sound and Vibration, vol. 215, pp 63-79, 1998.

[64] GEORGIEVA, A., KRIECHERBAUER, T. and VENAKIDES, S. "Wave propagation and resonance in one-dimensional nonlinear discrete periodic medium," SIAM Journal of Applied Mathematics, vol. 60, pp 272-294, 1999.

[65] ORALKAN, O. "Capacitive Micromachined Ultrasonic Transducers: Next generation arrays for acoustic imaging?," IEEE T. Ultrason. Ferr., vol. 49, pp 1596-1610, 2002.

[66] HUANG, Y., ERGUN, A.S., HAEGGSTROM, E. and KHURI-YAKUB, B.T., "Fabrication of Capacitive Micromachined Ultrasonic Transducers (CMUTs) using wafer bonding technology for low frequency (10 kHz-150 kHz) sonar applications", OCEANS '02 MTS/IEEE 2002.

[67] WYGANT, I.O., ZHUANG, X.K., P.S. , YEH, D.T., ORALKAN, O. and KHURI-YAKUB, B.T., "Photoacoustic imaging using a two-dimensional CMUT array", Ultrasonic Symposium IEEE, 2005.

[68] BAYRAM, B., KUPNIK, M., YARALIOGLU, G., ORALKAN, O., LIN, D., ZHUANG, X., ERGUN, A., SARIOGLY, A., WONG, S. and KHURI-YAKUB, B.T. "Characterization of cross-coupling in capacitive micromachined ultrasonic transducers," Proc. IEEE Ultrasonics Symposium pp 601-604, 2006.

[69] BAYRAM, B., KUPNIK, M., YARALIOGLU, G., ORALKAN, O., LIN, D., ZHUANG, X., ERGUN, A., SARIOGLY, A., WONG, S. and KHURI-YAKUB, B.T. "Finite element modeling and experimental characterization of crosstalk in 1-D CMUT arrays," IEEE Transactions of Ultrasonics, Ferroelect., Freq. Contr.2006.

[70] IRA, O., WYGANT and KUPNIK, M. "Analytically calculating membrane displacement and the equivalent circuit model of a circular CMUT cell," IEEE Int. Ultrason. Sym. Proc. pp 2111-2114, 2008.

[71] DEPARTMENT OF APPLIED PHYSICS, H., http://tfy.tkk.fi/optics/research/m1.php, (Accessed 2010)

[72] VAKAKIS, A.F. and KING, M.E. "Resonant oscillations of a weakly coupled, nonlinear layered system," Acta. Mech., vol. 128, pp 69-80, 1998.

[73] NESTERENKO, V.F. "Shock (Blast) Mitigation by "Soft" Condensed Matter " MRS Symp. Proc., vol. 759, pp MM4.3.1-MM4.3.12, 2003.

[74] DARAIO, C., NESTERENKO, V.F., HERBOLD, E. and JIN, S. "Energy trapping and shock disintegration in a composite granular medium," Physical Review Letters, vol. 96,2006.

[75] COSTE, C. and GILLES, B. "On the validity of Hertz contact law for granular material acoustics," The European Physical Journal B - Condensed Matter and Complex Systems, vol. 7, pp 155-168, 1999.

[76] COSTE, C. "Sound propagation in a constrained lattice of beads: High-frequency behavior and dispersion relation," Physical Review E, vol. 77, p 021302, 2008.

[77] COSTE, C., FALCON, E. and FAUVE, S. "Solitary waves in a chain of beads under Hertz contact," Physical Review E, vol. 56, p 6104, 1997.

[78] COSTE, C. and GILLES, B. "Sound propagation in a lattice of elastic beads: Time of flight, dispersion relation and time-frequency analysis," Physics Procedia, vol. 3, pp 433-441, 2010.

[79] DARAIO, C., NESTERENKO, V.F., HERBOLD, E.B. and JIN, S. "Strongly nonlinear waves in a chain of Teflon beads," Physical Review E, vol. 72, p 016603, 2005.

[80] HERBOLD, E.B. and NESTERENKO, V.F. "Shock wave structure in a strongly nonlinear lattice with viscous dissipation," Physical Review E, vol. 75, p 021304, 2007.

[81] NESTERENKO, V.F., DARAIO, C., HERBOLD, E.B. and JIN, S. "Anomalous Wave Reflection at the Interface of Two Strongly Nonlinear Granular Media," Physical Review Letters, vol. 95, p 158702, 2005.

[82] BOECHLER, N., THEOCHARIS, G., JOB, S., KEVREKIDIS, P.G., PORTER, M.A. and DARAIO, C. "Discrete Breathers in One-Dimensional Diatomic Granular Crystals," Physical Review Letters, vol. 104, p 244302, 2010.

[83] CHATTERJEE, A. "Asymptotic solution for solitary waves in a chain of elastic spheres," Physical Review E, vol. 59, p 5912, 1999.

[84] SEN, S., HONG, J., BANG, J., AVALOS, E. and DONEY, R. "Solitary waves in the granular chain," Physics Reports, vol. 462, pp 21-66, 2008.

[85] HERBOLD, E.B., KIM, J., NESTERENKO, V.F., WANG, S. and DARAIO, C. "Tunable frequency band-gap and pulse propagation in a strongly nonlinear diatomic chain," Acta. Mech., vol. DOI 10.1007/s00707, pp 0163-0166, 2009.

[86] STAROSVETSKY, Y. and VAKAKIS, A.F. "Traveling waves and localized modes in one-dimensional homogenous granular chains with no pre-compression," Physical Review E2010.

[87] NESTERENKO, V.F. and HERBOLD, E.B. "Periodic waves in a Hertzian chain," Physics Procedia, vol. 3, pp 457-463, 2010.

[88] NESTERENKO, V.F., Dynamics of Heterogeneous Materials, Springer-Verlag, (2001)

[89] YILDIRIM, A. "Determination of periodic solutions for nonlinear oscillators with fractional powers by He's modified Lindstedt-Poincaré method," Meccanica, vol. 45, pp 1-6, 2009.

[90] HE, J.-H. "Modified Lindstedt-Poincare methods for some strongly non-linear oscillations Part II: a new transformation," International Journal of Non-Linear Mechanics, vol. 37, pp 315-320, 2000.

[91] HE, J.-H. "Modified Lindstedt-Poincare methods for some strongly non-linear oscillations: Part I: expansion of a constant," International Journal of Non-Linear Mechanics, vol. 37, pp 309-314, 2002.

[92] HE, J.-H. "Modified Lindstedt-Poincare methods for some strongly non-linear oscillations: Part II: a new transformation," International Journal of Non-Linear Mechanics, vol. 37, pp 315-320, 2002.

[93] LIAO, S. "A short communication on Dr. He's modified Lindstedt–Poincaré method," Nonlinear Dynamics, vol. 49, pp 317-318, 2006.

[94] CHEUNG, Y.K., CHEN, S.H. and LAU, S.L. "A modified Lindstedt-Poincaré method for certain strongly non-linear oscillators," International Journal of Non-Linear Mechanics, vol. 26, pp 367-378, 1991.

[95] CHEN, S.H. and CHEUNG, Y.K. "A MODIFIED LINDSTEDT-POINCARE METHOD FOR A STRONGLY NON-LINEAR TWO DEGREE-OF-FREEDOM SYSTEM," Journal of Sound and Vibration, vol. 193, pp 751-762, 1996.

[96] GILLES, B. and COSTE, C. "Low-Frequency Behavior of Beads Constrained on a Lattice," Physical Review Letters, vol. 90, p 174302, 2003.

[97] SUIKER, A.S.J., METRIKINE, A.V. and DE BORST, R. "Comparison of wave propagation characteristics of the Cosserat continuum model and corresponding discrete models," International Journal of Solids and Structures, vol. 38, pp 1563-1583, 2001.

[98] SHAMPINE, L.F. "Vectorized adaptive quadrature in MATLAB," Journal of Computational and Applied Mathematics, vol. 211, pp 131-140, 2008.

[99] LEAMY, M.J. "Application of cellular automata modeling to seismic elastodynamics," International Journal of Solids and Structures, vol. 45, pp 4835-4849, 2008.

[100] AUTRUSSON, T.B., Nonlinear ultrasonic guided waves for quantitative life prediction of structures with complex geometries, Georgia Institute of Technology, (2009)